UNIVERSITE DE NEUCHATEL FACULTE DES SCIENCES

NEW MULTIFUNCTIONAL LIGANDS FOR THE CATALYTIC CARBONYLATION OF METHANOL

THESE PRESENTEE A LA FACULTE DES SCIENCES PAR

CHRISTOPHE THOMAS

CHIMISTE DIPLOME DE L'UNIVERSITE LOUIS PASTEUR DE STRASBOURG

INSTITUT DE CHIMIE DE L'UNIVERSITE DE NEUCHATEL

14 MAI 2002

UNIVERSITE DE NEUCHATEL FACULTE DES SCIENCES

NEW MULTIFUNCTIONAL LIGANDS FOR THE CATALYTIC CARBONYLATION OF METHANOL

THESE PRESENTEE A LA FACULTE DES SCIENCES PAR

CHRISTOPHE THOMAS

CHIMISTE DIPLOME DE L'UNIVERSITE LOUIS PASTEUR DE STRASBOURG

INSTITUT DE CHIMIE DE L'UNIVERSITE DE NEUCHATEL

14 MAI 2002

IMPRIMATUR POUR LA THESE

New Multifunctional Ligands for the Catalytic Carbonylation of Methanol

de M. Christophe Thomas

UNIVERSITE DE NEUCHATEL

FACULTE DES SCIENCES

La Faculté des sciences de l'Université de Neuchâtel sur le rapport des membres du jury,

MM. G. Süss-Fink (directeur de thèse), T. Ward et L. Gade (Strasbourg F)

autorise l'impression de la présente thèse.

Neuchâtel, le 16 mai 2002

Le doyen.

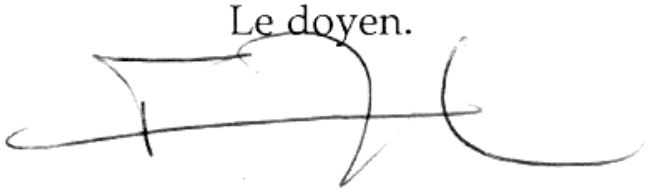

F. Zwahlen

A ma mère

A Tatiana

A mon père

La science ne consiste pas seulement à savoir ce qu'on doit ou peut faire, mais aussi à savoir ce qu'on pourrait faire quand bien même on ne doit pas le faire.

Umberto Eco (*Le nom de la rose*)

Tout le talent d'écrire ne consiste après tout que dans le choix des mots.

Gustave Flaubert (*Extrait d'une Lettre à Louise Colet 22 juillet 1852*)

Remerciements

Les travaux décrits dans cette thèse ont été réalisés au laboratoire de Chimie Organométallique et de Catalyse Homogène de l'Université de Neuchâtel sous la direction du Professeur Georg Süss-Fink. Je tiens à le remercier sincèrement de m'avoir accueilli dans son groupe et de m'avoir fait partager son enthousiasme pour la recherche. J'aimerais également lui exprimer ma profonde gratitude pour le soutien qu'il m'a apporté, tant par ses qualités humaines que scientifiques.

J'aimerais également remercier les Professeurs Thomas Ward et Lutz Gade d'avoir accepté de juger ce manuscrit et de m'avoir fait part de leurs remarques éclairées et pertinentes.

Je remercie sincèrement les Docteurs Régis Gauvin, Frédéric Chérioux et Bruno Therrien d'avoir relu ce manuscrit avec attention. Il est bien connu que Monsieur Therrien est efficace dans son travail mais je sais également maintenant que Messieurs Gauvin et Chérioux sont redoutables dans leurs appréciations.

J'adresse également un grand merci à Monsieur David Schwab qui a reussi à me supporter pendant sa deuxième année d'apprentissage et qui m'a permis d'avancer plus rapidement et dans la bonne humeur.

Il va sans dire que je remercie aussi les membres du groupe Süss-Fink grâce auxquels il a régné une ambiance conviviale et chaleureuse au laboratoire (en particulier Laurent, Amel, Frédéric, Ludovic et Bruno) et mes collègues de l'Institut (Blaise, Sandrine, Olivier, Sébastien, Philippe, Michaël et Gilles).

J’adresse mes remerciements aux personnes responsables des services d’analyses RX, RMN et MS de l’Institut de Chimie de Neuchâtel (à savoir le Docteur Bruno Therrien, le Docteur Armelle Michel, le Professeur Helen Stoeckli-Evans, le Docteur Antonia Neels et Monsieur Heinz Bursian), au Professeur T. Jenny et à Monsieur F. Nydegger du Département de Chimie Organique de Fribourg et au Docteur Hansjörg Eder responsable du Service de Microanalyse de Genève.

Je remercie l'Université de Neuchâtel et le Fonds National Suisse de la Recherche Scientifique qui ont soutenu financièrement ce projet.

Enfin je remercie tout particulièrement mes amis et mes proches dont le soutien a été plus qu'une aide pendant toutes ces années. A ce titre j'ai une pensée particulière pour ma "belle-famille", mes parents et surtout Tatiana.

Table of Contents

Chapter 1

Introduction

Organometallic chemistry, which involves metal complexes containing direct metal-to-carbon bonds, has grown since the early 1950s at an almost exponential rate, mostly owing to the development of an impressive array of highly sophisticated apparatus of which in particular NMR and single-crystal X-ray equipments have been invaluable.[1] Theoretical studies of the bonding in metal compounds and of the course of reaction pathways have not only contributed to new knowledge, but also to the purposeful design of complexes and their use in stoichiometric and catalytic reactions.

Although fortunate surprises do occur frequently, our theoretical knowledge has increased to a level where we have a deep insight into the steric and electronic properties of ligands and of their complexes. Therefore, we are now, to a certain extent, able to design ligands and to control reactions occurring on metal centers in complexes.

As this thesis is concerned with the preparation and properties of new transition-metal complexes containing new multifunctional ligands involved in the carbonylation of methanol, we will discuss in this introduction some historical aspects of carbonylation reactions and some recent developments in the carbonylation of methanol. Finally, we will present the scope and the aims of this thesis.

1.1 Historical Aspects of Carbonylation Reactions

Homogeneous carbonylation catalysis is concerned with the transition-metal-assisted addition of carbon monoxide to organic compounds and involves a carbon-carbon coupling process to give higher molecular weight carbonyl-containing products. Carbonylation chemistry was pioneered by Otto Roelen (Ruhrchemie) and Walther Reppe (IG Farben, later BASF) in the late 1930s.[2] Since then it has developed into the highest volume and most important industrial process based on homogeneous catalysis.

The first thirty years of industrial carbonylation catalysis implied the use of simple metal carbonyl catalysts, high reaction temperatures and pressures, and only low product selectivities. Significant cost advantages resulted from the use of carbon monoxide (derived from natural gas) and of low-priced methanol (from synthesis gas) as feedstocks. A first methanol-to-acetic acid carbonylation process was commercialized in 1960 by BASF. It used an iodide-promoted cobalt catalyst, and required very high pressures (600 atm) as well as high temperatures (230°C), but gave acetic acid in *ca.* 90% selectivity.[2]

The situation changed in the mid-sixties with the discovery that organophosphine-substituted rhodium and palladium complexes are active catalysts for carbonylation reactions under milder reaction conditions. The serendipitous discovery of $Rh(PPh_3)_3Cl$ by Osborn and Wilkinson,[3,4] which was used as a catalyst for the hydroformylation of alkenes but also for the hydrogenation of alkenes,[5] has stimulated a tremendous amount of fundamental and applied research in this area.

1.2 Recents Developments in the Carbonylation of Methanol

A major advance came in 1966 with the discovery of rhodium-iodide catalysts for the carbonylation of methanol by Monsanto, which led to the start-up of the first commercial unit in 1970. The advantages over the cobalt-catalyzed BASF process consist in significantly milder conditions (30-60 atm pressure and 150-200°C), allowing substantial savings in construction costs and hence in capital expenditure, and in higher selectivity for acetic acid, making further savings on both running and capital costs. The disadvantage of using rhodium, a costly precious metal, is counter-balanced by lower operating costs, especially as milder reaction conditions decrease the corrosion risk due to the aggressive reaction medium (acetic acid, iodic acid).[6]

$$CH_3OH + CO \xrightarrow{[Rh(CO)_2I_2]^-} CH_3COOH$$

In 1986, the ownership of the Monsanto technology was acquired by BP Chemicals who further developed the process and licensed it around the world. In 1996, a new catalytic process for the carbonylation of methanol to acetic acid named Cativa™ was announced by BP Chemicals; this process is based on a catalyst system composed of iridium complexes with ruthenium activators.[6]

1.3 Scope and Aims of this Work

The research of our group has focused on the build-up of metal clusters, in particular, mixed-metal carbonyl clusters for the carbonylation of methanol. The cluster anions $[Ru_3Ir(CO)_{13}]^-$ and $[Os_3Ir(CO)_{13}]^-$, which were prepared for this process, are indeed catalytically active, but unstable under the reaction conditions,

which has been confirmed by the isolation of the fragmentation products $Ir_4(CO)_{12}$ and $[N(PPh_3)_2][M(CO)_3I_3]$ (M = Ru, Os).[7-9]

In this context, we were interested in the behavior of other types of complexes stabilized by multifunctional ligands. Therefore, it was the aim of this thesis to synthesize new multifunctional ligands, to study their coordination properties and to exploit their catalytic potential for the carbonylation of methanol.

Chapter 2

The Catalytic Carbonylation of Methanol: State of the Art

Carbonylation catalysis encompasses a large and important area of chemistry. The majority of carbonylation reactions is carried out in homogeneous phase, because homogeneous catalysts generally give higher rates and selectivities than heterogeneous systems.

Apart from the carbonylation of methanol, we can quote other catalytic carbonylation reactions: The hydroformylation of olefins to give aldehydes and alcohols, which is the most important homogeneous catalytic process on the industrial scale,[2] the synthesis of ketones from olefins and the synthesis of lactones and lactams from olefins or halide-containing alcohols.[10] The production of carboxylic acids, carboxylic esters and acyl halides from methanol is the second most important industrial homogeneous catalytic process.[11,12]

2.1 Chemicals from Methanol and Carbon Monoxide

Methanol is a versatile, readily available C_1 compound obtained from synthesis gas. Large-scale industrial methanol production from CO/H_2 started up in 1925 by BASF using a ZnO/Cr_2O_3 catalyst.[13,6] At present, methanol still is produced almost exclusively from synthesis gas (a mixture of H_2, CO and some CO_2) in a gas-phase reaction over copper-based catalysts such as $Cu/ZnO/Al_2O_3$ or $Cu/ZnO/Cr_2O_3$ at temperatures ranging from 200 to 270°C and pressures from 50 to 100 bar, according to Eq. 1.

$$CO + 2\,H_2 \longrightarrow CH_3OH \qquad (1)$$

The present methanol production capacity has been reported to be 21 million tons/years, while the actual demand is only in the range of 12 million tons/years.[6] This overcapacity is mainly due to the set-up of new plants, where surplus natural gas is available at a very low price.[14] The ready supply as well as the low raw material costs will keep the price of methanol down in the near future. This will stimulate the demand of methanol and will help to introduce new methanol-based processes for motor fuels as well as for basic organic chemicals.[15]

The present industrial uses of methanol include the production of formaldehyde, methyl esters, methyl amines and methyl halides. In addition, methanol and its derivatives find an increasing interest as substrates for carbonylation and dehydration reactions, which are summarized in Scheme 1.

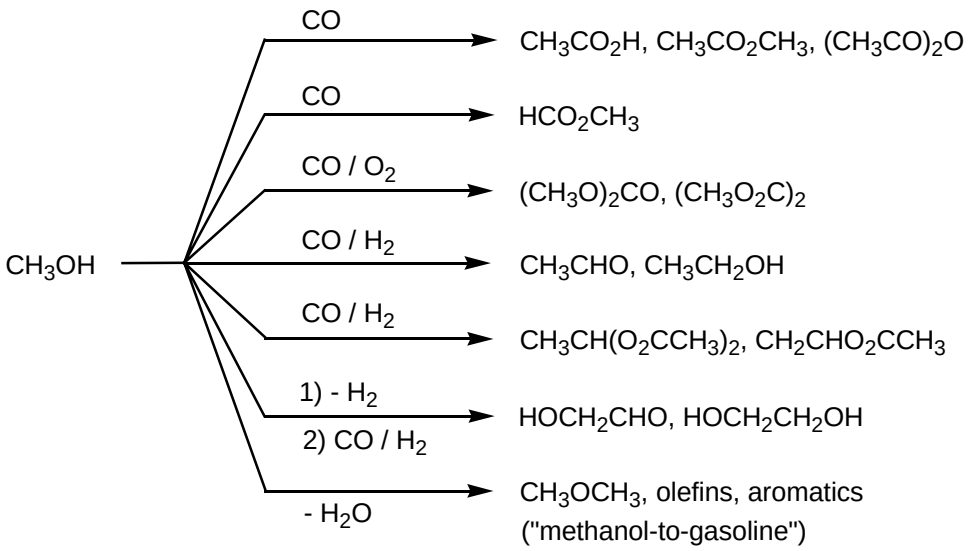

Scheme 1: Summary of industrial methanol conversion reactions

Some of these processes have already been used for the commercialization of acetic acid, acetic anhydride, or methyl formate. In addition there is a variety of carbon monoxide-based reactions which convert methanol mainly into C_2 oxygenated compounds. These can potentially replace ethylene-based routes, e.g. in the case of ethanol, acetaldehyde, vinyl acetate, and ethylene glycol. With methanol from cheap natural gas becoming available in the near future, these processes, although uneconomic today, might become industrially attractive.

2.2 The Transition Metal Catalyzed Carbonylation of Methanol

While the base-catalyzed carbonylation of methanol yields methyl formate, a versatile intermediate for formic acid and formamide synthesis, the transition metal catalyzed carbonylation of methanol involves C-C coupling, giving acetic acid derivatives as C_2 oxygenates.

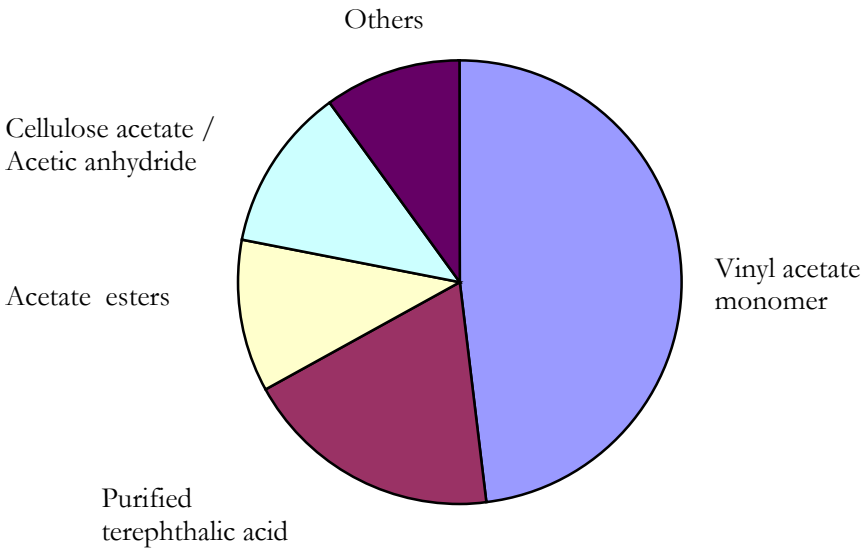

Figure 1: Use of acetic acid

As shown in Figure 1, acetic acid is used primarily as a raw material for vinyl acetate monomer (VAM) and acetic anhydride synthesis, and as a solvent for purified terephthalic acid (PTA) production.[16]

Acetic acid is an important industrial commodity chemical, with a world demand of about 6 million tons per year and many industrial uses. Novel acetic acid processes and catalysts have been introduced, commercialized, and improved continuously since the 1950s. The objective of the development of new acetic acid processes has been to reduce raw material consumption, energy requirements, and investment costs. At present, industrial processes for the production of acetic acid are dominated by methanol carbonylation and the oxidation of acetaldehyde or of hydrocarbons such as ethylene, *n*-butane, and naphtha.

Table 1: Industrial routes to acetic acid

Method	Catalyst	Conditions	Yield
Methanol Carbonylation	Rhodium or Iridium complexes	180-220 °C 30-40 bar	99%
Acetaldehyde Oxidation	Manganese or cobalt acetate	50-60 °C 1 bar	95%
Ethylene Direct Oxidation	Palladium/copper/ heteropolyacid	150-160 °C 80 bar	87%
Hydrocarbon Oxidation	Manganese or cobalt acetate	150-230 °C 50-60 bar	50% (*n*-butane) 40% (naphtha)

Originally, acetic acid was produced by aerobic fermentation of ethanol, which is still the major process for the production of vinegar. The first major commercial process for the production of synthetic acetic acid was based on the oxidation of acetaldehyde. In an early process for the conversion of acetylene to acetaldehyde, introduced in 1916 in Germany and used in China until recently, an organo-mercury compound was used as the catalyst. The toxicity of the mercury catalyst resulted in significant environmental pollution, and consequently, the process was essentially replaced by alternative routes. As the petrochemical industry developed in the 1950s, the raw material for the production of acetaldehyde shifted from acetylene to ethylene. Other processes for the production of acetic acid, introduced in the 1950s and 1960s, were based on the oxidation of *n*-butane or naphtha. The major producers of acetic acid *via* direct oxidation of hydrocarbons were Celanese (*via n*-butane) and BP (*via* naphtha). However, these reactions also produce significant amounts of oxidation by-products, and their separation can be very complex and expensive.[17-20]

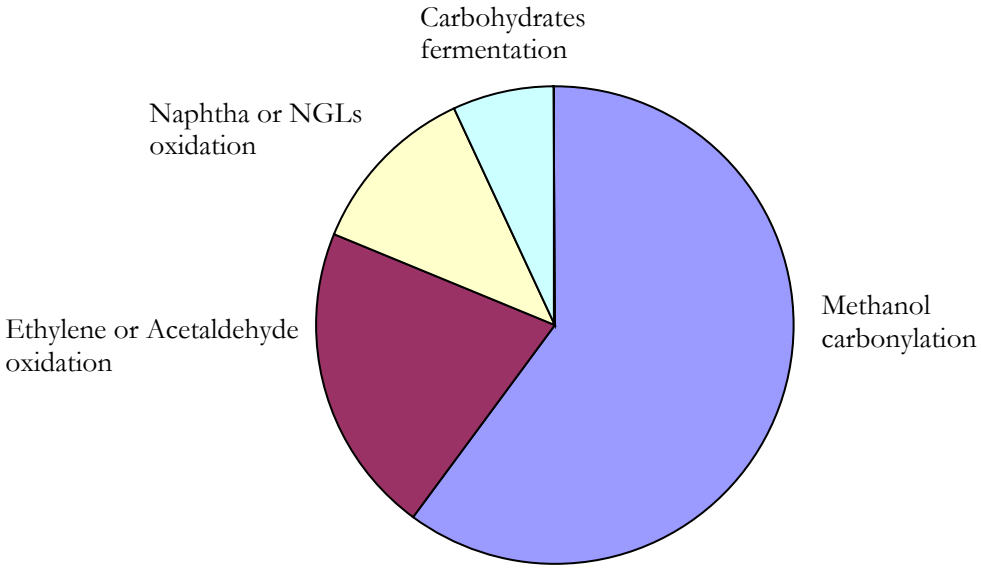

Figure 2: Acetic acid process routes

Nowadays, approximately 60 per cent of the total world acetic acid manufacturing capacity is covered by the carbonylation of methanol. From the industrial point of view, one of the major achievements of applied homogeneous catalysis has been the introduction of methanol-to-acetic-acid processes *via* the carbonylation of methanol, which are not only highly selective, but also allow the use of methanol as a cheaper feedstock as compared to ethylene. The carbonylation of methanol is catalysed by Group VIII transition metal complexes, especially by rhodium, iridium, cobalt, and nickel.[21-25]

$$CH_3OH + CO \longrightarrow CH_3COOH \qquad (2)$$

$$CH_3COOH + CH_3OH \longrightarrow CH_3COOCH_3 + H_2O \qquad (3)$$

All methanol carbonylation processes need iodine compounds as essential co-catalysts, the reaction proceeding *via* methyl iodide, which alkylates the transition metal involved. Apart from acetic acid, the carbonylation of methanol (Eq. 2) gives also rise to the formation of methyl acetate, according to Eq. 3. In some carbonylation processes (Cativa™), methyl acetate is also used as a solvent. The cobalt-catalysed BASF process was introduced in the late 1950s, and the rhodium-based Monsanto process followed in the early seventies. As it is evident from Table 2,[26-28] rhodium catalysts operate at very mild conditions and with very high selectivities, as compared to cobalt or nickel catalysts. It is therefore not surprising that most commercial plants now use the rhodium-based Monsanto process. Meanwhile, the worldwide capacity for acetic acid from methanol is well over 1 000 000 tons/years and is expected to increase further.[16]

Table 2: Acetic acid production by carbonylation of methanol

Catalyst	Temperature (°C)	Pressure (bar)	Selectivity (%)
Rh_2O_3/HI	175	1-15	99
$Co(OAc)_2/CoI_2$	250	680	90
$Ni(CO)_4$/MeI/LiOH	180	70	84

Typical side reactions of the methanol carbonylation to acetic acid (Eq. 2) are the formation of methyl acetate, methyl formate, dimethyl ether and the water-gas shift reaction, the formation of methyl acetate (Eq. 3) being the most important one. These reactions are equilibria, which can be controlled by reaction conditions, catalyst metals, ligands, promoters, and solvents.

2.2.1 Cobalt Catalysts

Cobalt catalysts were used in the classical BASF process. The lower activity of Co catalysts as compared to rhodium catalysts requires a high catalyst concentration of about 0.1 M. The selectivity reaches 90%, based on methanol. By-products are methane, acetaldehyde, ethanol and ethers. $HCo(CO)_4$ is supposed to be the active species, and it is formed according to Eq. 4 and 5.[27]

$$2\,CoI_2 + 2\,H_2O + 10\,CO \longrightarrow Co_2(CO)_8 + 4\,HI + 2\,CO_2 \quad (4)$$

$$Co_2(CO)_8 + H_2O + CO \longrightarrow 2\,HCo(CO)_4 + CO_2 \quad (5)$$

The assumption of hydrido cobalt carbonyl as the active species is in agreement with the observation that small amounts of H_2 enhance the catalytic activity. The mechanism proposed is shown in Scheme 2.[27]

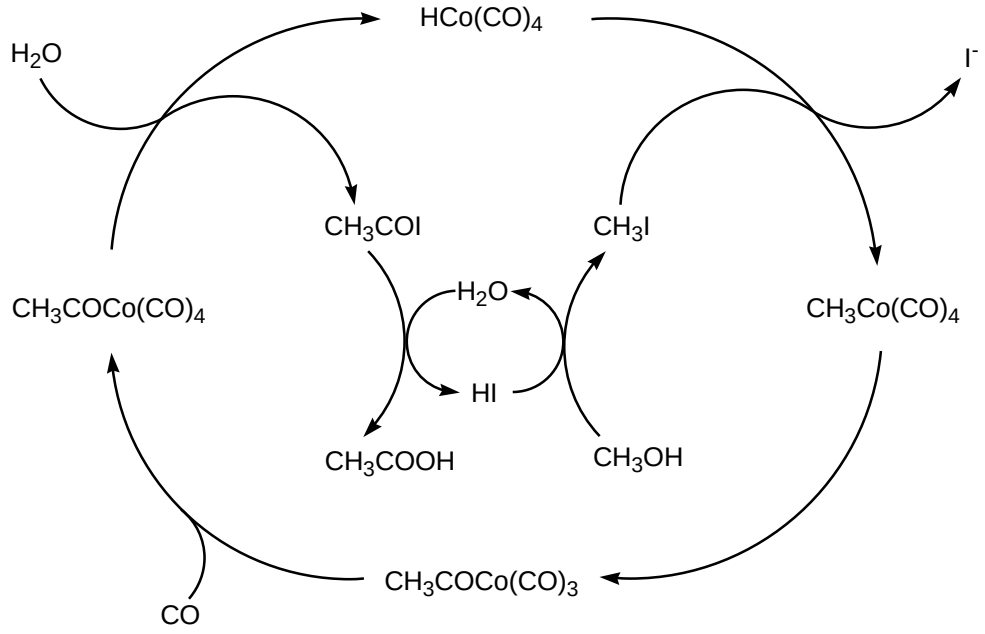

Scheme 2: Catalytic cycle of the cobalt-catalyzed methanol carbonylation (BASF process)

The role of iodine is not restricted to the formation of alkyl iodides, which act as alkylating agents, but also includes the cleavage of the acyl intermediate *via* the formation of acetyl iodide.[29] Given that, in this process, the rate depends on the carbon monoxide pressure, high pressures of 600-700 bar are required for good conversion. Slightly lower pressures are possible in the presence of Ru, Ir, Pd, Pt, or Cu salts as activators.[30,31] Cobalt catalysts can also be used for the carbonylation of higher alcohols, such as benzyl alcohol.[32]

2.2.2 Nickel Catalysts

Nickel carbonyl, as well as a variety of nickel compounds, is also catalytically active for the carbonylation of methanol in the presence of iodine. $Ni(CO)_4$ is formed from NiI_2 according to Eq. 6.[33]

$$NiI_2 + H_2O + 5\,CO \longrightarrow Ni(CO)_4 + 2\,HI + CO_2 \qquad (6)$$

The hydrogen iodide formed in Eq. 6 is used to transform the alcohol into an alkyl halide, which adds oxidatively to nickel, as described in Scheme 3.[34] The resulting acetyl iodide is hydrolyzed either by water or alcohols. Usually nickel catalysts require rather high pressure and temperature conditions.[35] However, with high methyl iodide concentrations, carbonylation occurs already under milder conditions.[28] If the molar ratio of CH_3I to CH_3OH is at least 1 : 10, pressures as low as 35 bar can be applied at 150°C, using $Ni(OAc)_2 \cdot 4H_2O$ and Ph_4Sn as catalyst system.[36] Vapor phase carbonylation of methanol using supported nickel metal catalysts has also been reported.[37]

The activity of nickel catalyst systems can be increased, and the volatility of nickel carbonyl compounds can be lowered by the introduction of stabilizers such as phosphines, alkali metals, tin, and molybdenum.[38-42] The active catalysts are thought to be Ni(0) complexes. In the case of phosphine-containing nickel catalysts, 14-electron species such as $Ni(PR_3)_2$ are considered as catalysts, in addition to $Ni(CO)_4$ observed in all cases; the concentration of the latter species is reduced by strongly coordinating ligands or enhanced by weakly coordinating ligands.[42]

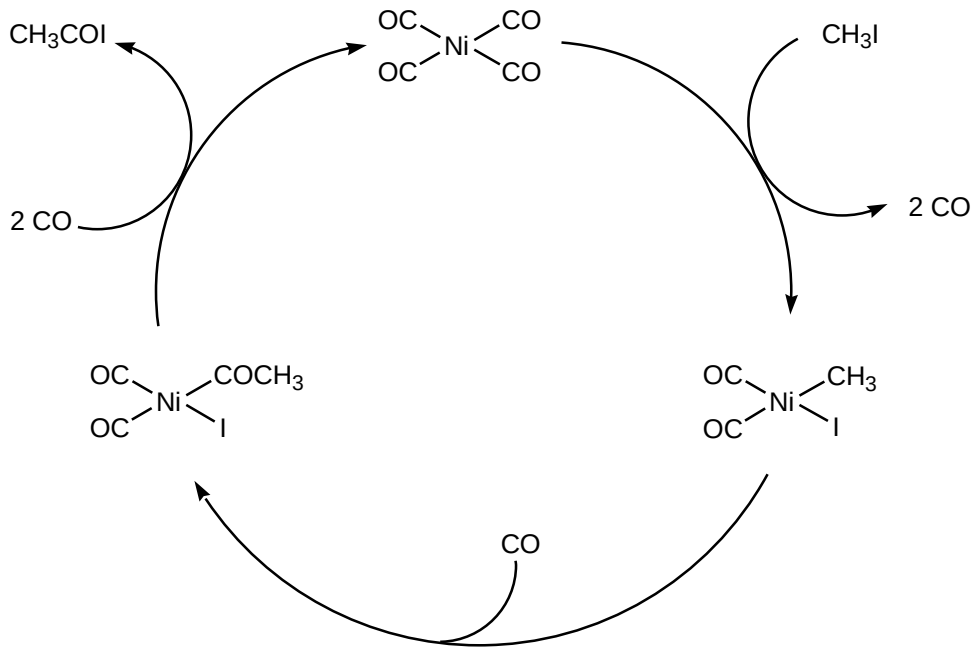

Scheme 3: Catalytic cycle of the nickel-catalyzed methanol carbonylation

Recent work on nickel catalyst systems shows that reaction rates and selectivities can approach those achieved in the rhodium catalyst system. Although nickel catalysts have the advantage of being much cheaper than rhodium and are easy to stabilize at low water concentrations, no commercialization has been achieved to date, since $Ni(CO)_4$ is a very toxic and volatile compound.

2.2.3 The Rhodium-Based Monsanto Catalyst

The production of acetic acid by the Monsanto process is based on a rhodium catalyst and operates at a pressure of 30 to 60 bar and at temperatures of 150 to 200°C. The process gives selectivity of over 99 per cent based on methanol. The catalytic cycle of this classic example of a homogeneous catalytic reaction consists of six steps (Scheme 4).[43] The cycle includes several of the main reaction types known in organometallic chemistry,[44] such as oxidative addition, ligand

migration, CO insertion, and reductive elimination. These types of elementary steps have been examined separately in a number of experimental and theoretical studies.[45-48] Systematic studies including a detailed inspection of full catalytic cycles are much rarer.[49-51] The catalytic cycle of methanol carbonylation was proposed[43] on the base of selected data on structures of reactants and intermediates which have been identified by X-ray crystallography,[25] infrared and NMR spectroscopy (Scheme 4).[52]

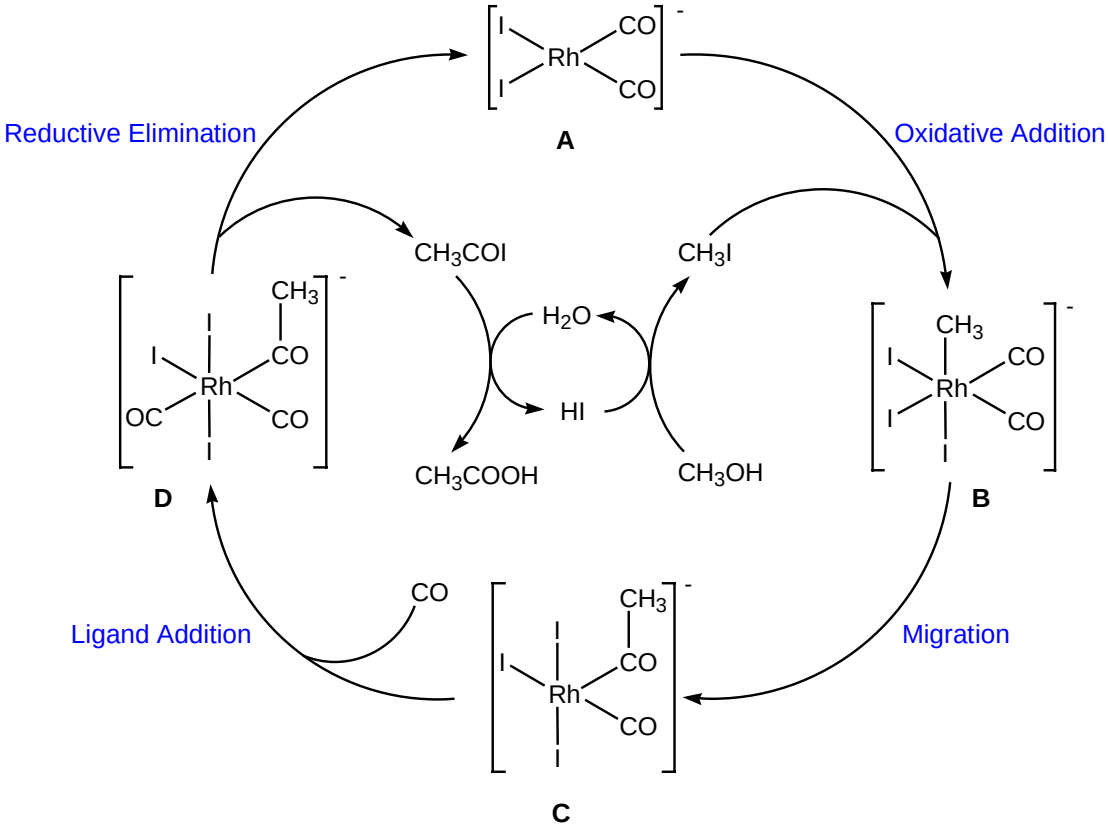

Scheme 4: Catalytic cycle of the rhodium-catalyzed methanol carbonylation (Monsanto process)

The anion *cis*-$[Rh(CO)_2I_2]^-$ (**A**) was found to be the initial catalytically active species.[43] Its interaction with the substrate CH_3I results in the formation of the hexacoordinated complex $[(CH_3)Rh(CO)_2I_3]^-$ (**B**),[52] which is kinetically unstable; it

transforms into the isomeric pentacoordinated acetyl complex $[(CH_3CO)Rh(CO)I_3]^-$ (**C**) as a result of the migration of the methyl group to the CO ligand.[53] The rhodium acetyl complex **C** is the only stable intermediate of the catalytic cycle;[25] it was isolated, and its structure was determined by X-ray crystallography.[54,55] The rhodium acetyl anion **C** was found to form dimers through a very weak Rh-I-Rh bridge [with a rhodium-iodine distance of 3.0 Å, as compared to 2.7 Å commonly found for Rh-I bonds[55]]. Complex **C** reacts rapidly with CO to form the six-coordinated dicarbonyl complex **D** with terminal CO.[55] This species has been characterized by IR and NMR spectroscopy as a *mer* isomer.[56] An isomerization to a *fac* isomer was proposed to facilitate the subsequent elimination of CH_3COI.[56] The *fac* isomer decomposes at room temperature to yield acetyl iodide CH_3COI and $[Rh(CO)_2I_2]^-$; the latter species starts the next catalytic cycle. Finally, acetic acid is formed by acetyl iodide hydrolysis.

2.2.4 Mechanistic Studies of the Rhodium-Catalyzed Process

Kinetic investigations have confirmed the catalytic cycle depicted in Scheme 4. The rate of methanol carbonylation depends on the concentrations of both the rhodium complex and methyl iodide.[57] The reaction rate is independent of the methanol concentration and the carbon monoxide pressure. The rate-determining step is probably the oxidative addition of methyl iodide to the metal center of the rhodium complex **A**, because the reaction rate is essentially of first order in both catalyst and methyl iodide concentrations under normal reaction conditions.

A substantial amount of water (14 - 15 wt.%) is required to achieve high catalyst activity and also to maintain good catalyst stability.[49-52] In fact, if the water content is less than 14-15 wt.%, the rate-determining step becomes the reductive elimination of the acetyl species, from catalyst species **D**. However, as rhodium also catalyzes the water-gas shift reaction (Scheme 5), the side reaction leading to CO_2 and H_2 is significantly affected by water and hydrogen iodide concentration in the reaction liquid.[58,59]

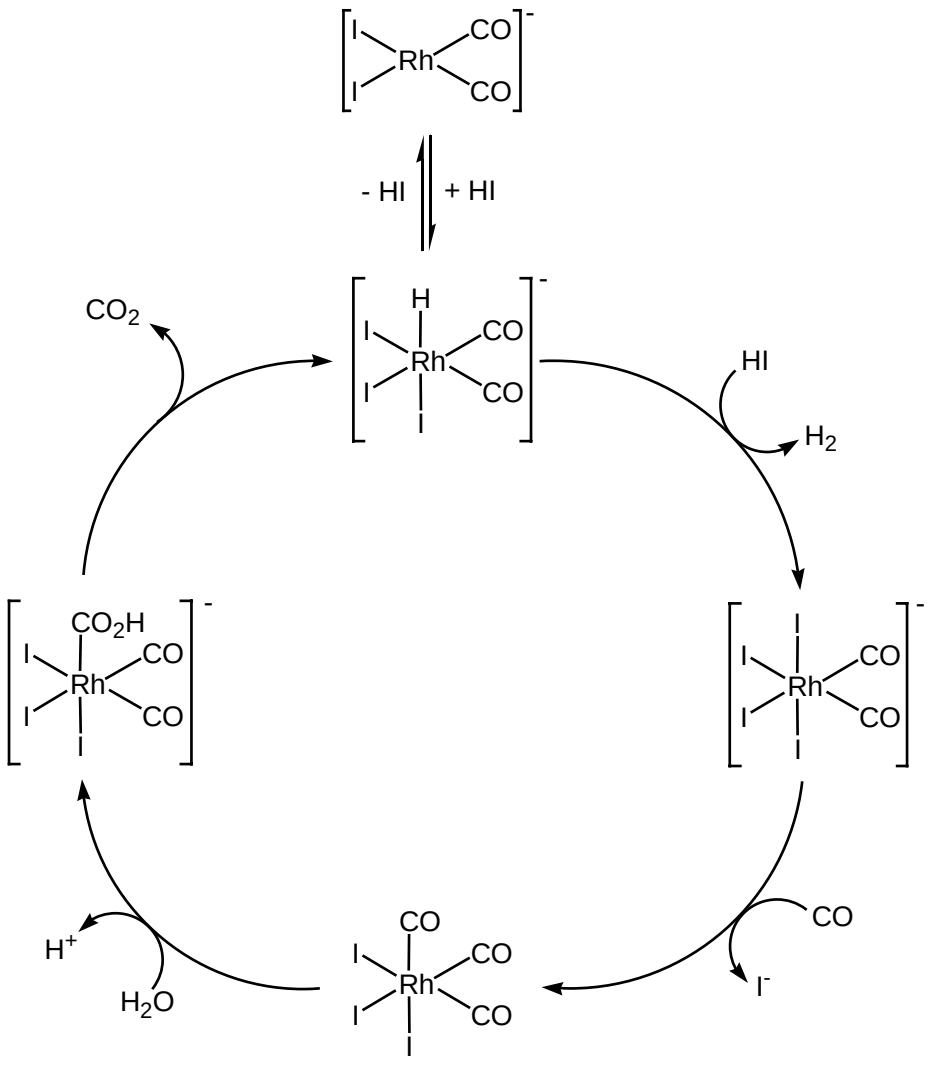

Scheme 5: Catalytic cycle of the water-gas shift reaction as side-reaction in the rhodium-catalyzed methanol carbonylation

Propionic acid is observed as the major liquid by-product in this process. This is produced by the carbonylation of ethanol which is often present as a minor impurity in the methanol feed. However, alternative routes to propionic acid must also be operating, since more propionic acid is observed than what can be accounted for by ethanol contamination of the feedstock. The rhodium catalyst can also generate acetaldehyde, which is supposed to undergo reduction by hydrogen to give ethanol, which subsequently yields propionic acid. One possible precursor for the generation of acetaldehyde is the rhodium-acetyl species, **D**, shown in Scheme 4.[59] Reaction of **D** with hydrogen iodide would yield acetaldehyde and $[Rh(CO)I_4]^-$. The latter species is well known in this system and is postulated as the principal cause of catalyst loss by precipitation of inactive rhodium triiodide.[59] However, under the commercial operating conditions of the original Monsanto process, these trace compounds do not present a problem to either product yield or product purity.

2.2.5 Heterogenized rhodium catalysts

In order to overcome the limitations of the homogeneous catalyst system (e.g. catalyst separation), the immobilization of rhodium complex on a support has been the subject of considerable research. Active carbon was investigated as a possible support and proposed for vapor-phase operation.[17,60] However, reaction rate and selectivity were poorer than with homogeneous catalysts. Inorganic oxides and zeolites were also studied as catalyst supports for use in vapor-phase operation.[61,62]

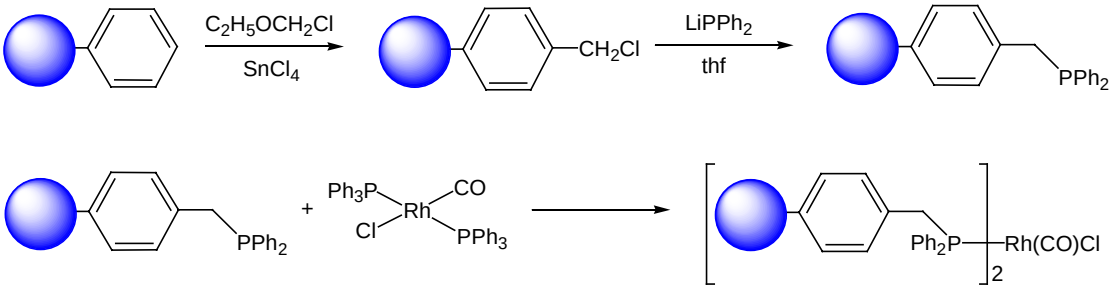

Scheme 6: Supporting the rhodium catalyst on a divinylbenzene-derived polymer

For example, attaching the Rh-phosphine ligand complex to alumina by silylation was attempted.[63,64] The resultant reaction rates for these catalysts were also found to be lower than those observed for the homogeneous system. To increase catalyst activity for operation in the liquid phase, ion exchange resins based on cross-linked polystyrene and incorporating pendant phosphines, or vinyl pyridine co-polymers have been evaluated (Scheme 6).[65-67]

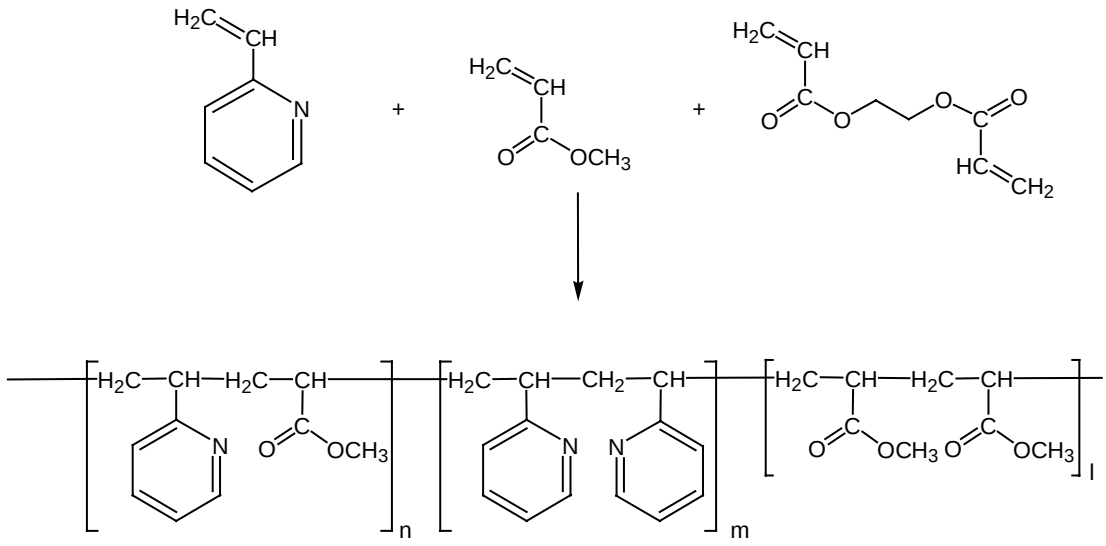

Scheme 7: Synthesis of a copolymer derived from vinyl pyridine and vinyl acetate

Although the activity of these catalysts in the liquid phase was comparable to Monsanto's homogeneous catalyst, there were problems with rhodium metal leaching from the resins and the decomposition of the resins during operation at

elevated temperature. Vinyl pyridine resin was known to be more robust and more thermostable than polystyrene resins (Schemes 7 and 8).[68]

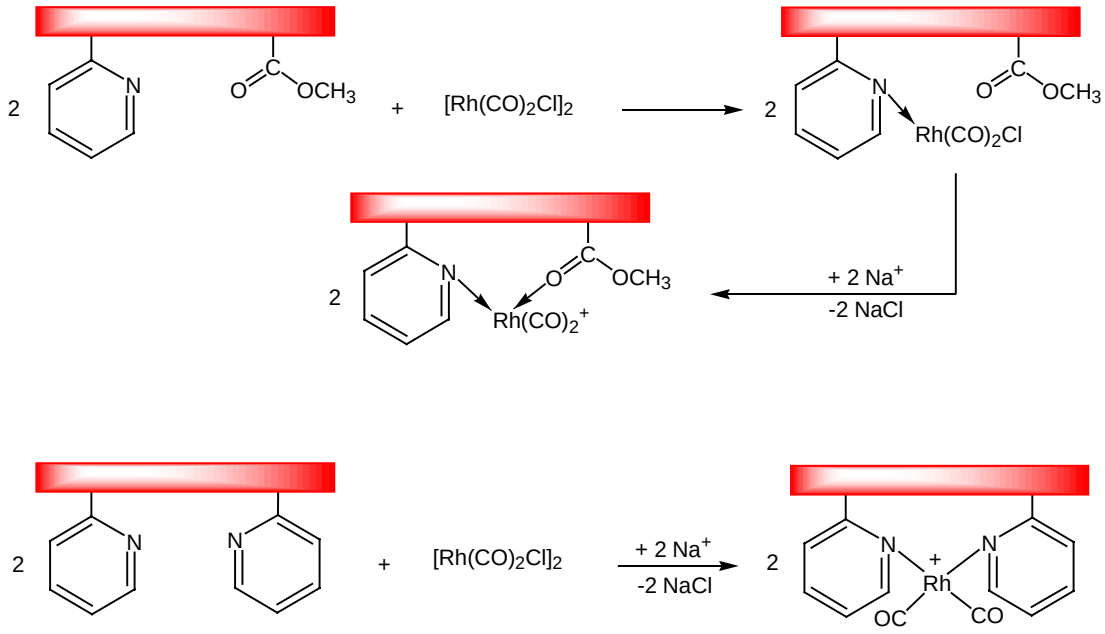

Scheme 8: Supporting the rhodium catalyst on copolymer derived from vinyl pyridine and vinyl acetate

Furthermore, Chiyoda introduced novel pyridine resins and catalysts that exhibited high activity, long catalyst life, and no significant rhodium loss.[69-71] Based on this heterogeneous rhodium catalyst, Chiyoda and UOP (Universal Oil Products) have jointly developed an improved methanol carbonylation process, called "Acetica process", for the production of acetic acid. Until the recent development of a commercial heterogeneous rhodium catalyst system by Chiyoda, no successful demonstration of such a catalyst had been known.[17] The heterogeneous catalyst commercialized for the Acetica process consists of rhodium complexed on a novel polyvinyl pyridine resin[72] which is tolerant of elevated temperatures and pressures. Under these reaction conditions, the

rhodium system is converted to its catalytically active anion form $[Rh(CO)_2I_2]^-$. Furthermore, the nitrogen atoms of the resin pyridine groups become positively charged after quaternization with methyl iodide. Thus, after counterion exchange, the active anionic rhodium complex $[Rh(CO)_2I_2]^-$ is blocked in the positive polymeric matrix by strong electrostatic interactions, as shown in Scheme 9.

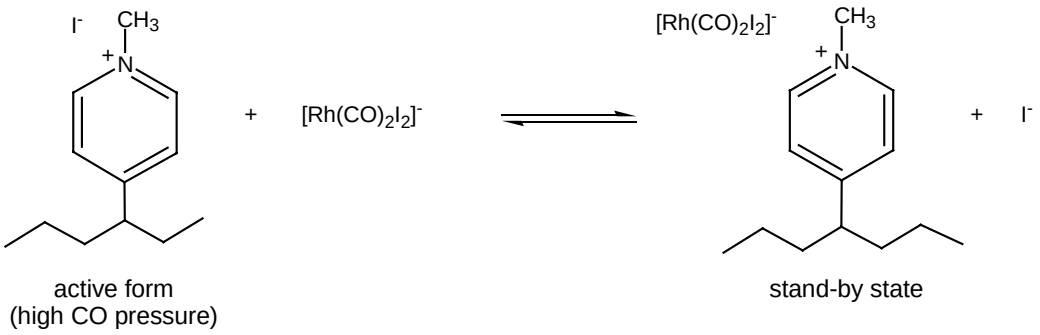

Scheme 9: Equilibrium between the active form and the stand-by state of the supported catalyst in the Acetica process

The concentration of rhodium on the solid phase is determined by the ion exchange equilibrium. Because equilibrium strongly favors the solid phase, virtually all the rhodium in the reaction mixture is immobilized. In the Acetica process, the methanol carbonylation reaction is conducted at moderate temperature (160-200°C) and pressure (30-60 bar) and at low water concentration without any additives. The catalyst exhibited no deactivation after continuous operation for more than 7000 h.[72]

With homogeneous methanol carbonylation routes, acetic acid productivity is directly proportional to the catalyst concentration in the reaction liquid, and as a consequence, the acetic acid production is restricted by the solubility of the active metal. Only limited success has been achieved in improving the catalyst solubility

by increasing the water concentration or by adding iodide salt stabilizers,[73-76] because both additives give rise to increased recycling costs, higher corrosion rates and separation problems. Immobilization of the catalyst significantly reduces the loss of expensive rhodium metal, because the catalyst is confined to the reactor rather than circulating downstream, where reduced pressures may cause losses of the catalyst by precipitation of rhodium or evaporation of volatile rhodium carbonyl compounds. The lower water content of 3-7 wt.%, typical of the Acetica process, results in reduced production of CO_2 and of hydrogenated by-products *via* the water-gas shift reaction. The lower water content also reduces the concentration of HI and thus the corrosion risk.

2.2.6 The Cativa™ Iridium Catalyst for Methanol Carbonylation

The potential use of iridium instead of rhodium was identified as part of the early work done by Monsanto.[25,26,40] However, the reaction rate exhibited by the rhodium catalyst system was superior to that of iridium. Recently, it was disclosed that an improved iridium catalyst, in combination with a promoter metal such as ruthenium, has higher activity and selectivity than reported in previous iridium systems.[77] The production of acetic acid using the iridium catalyst system has been commercialized in 1996 by BP-Amoco in two large-scale plants to date, and has received wide publicity as the "Cativa" process. Although much more iridium is required to achieve an activity comparable to the rhodium catalyst-based processes, the catalyst system is able to operate at reduced water levels (less than 8 wt.% for the Cativa process versus 14-15 wt.% for the conventional Monsanto process). Thus, lower by-product formation and improved carbon monoxide

efficiency are achieved, and steam consumption is decreased. Until the early 1990s, the difference in the prices of rhodium (17 $/g) and iridium (2 $/g) was the driving force for replacing rhodium by iridium. However, current price increases for iridium (16 $/g) negate the advantage in catalyst price.

One of the major advantages of the iridium-based process was the high stability of the iridium catalyst species.[78] Its robustness at low water concentrations (0.5 wt.%) is particularly significant and ideal for optimisation of the methanol carbonylation process. The iridium catalyst was also found to remain stable under a wide range of conditions that would cause the rhodium analogues to decompose completely to inactive and largely unrecoverable rhodium salts. Besides this stability, iridium is also much more soluble than rhodium in the reaction medium, and thus higher catalyst concentrations can be obtained, making much higher reaction rates achievable.

The unique differences between the rhodium and iridium catalytic cycles in methanol carbonylation have been investigated.[79] The anionic iridium cycle, shown in Scheme 10, is similar to the rhodium cycle, but contains several differences, responsible for the advantages of the Cativa™ over the Monsanto process. Model studies have shown that the oxidative addition of methyl iodide to the iridium center is about 150 times faster than the analogous reaction with rhodium.[79] This represents a dramatic improvement in the available reaction rates, as this step is now no longer rate-determining (as in the case of rhodium).

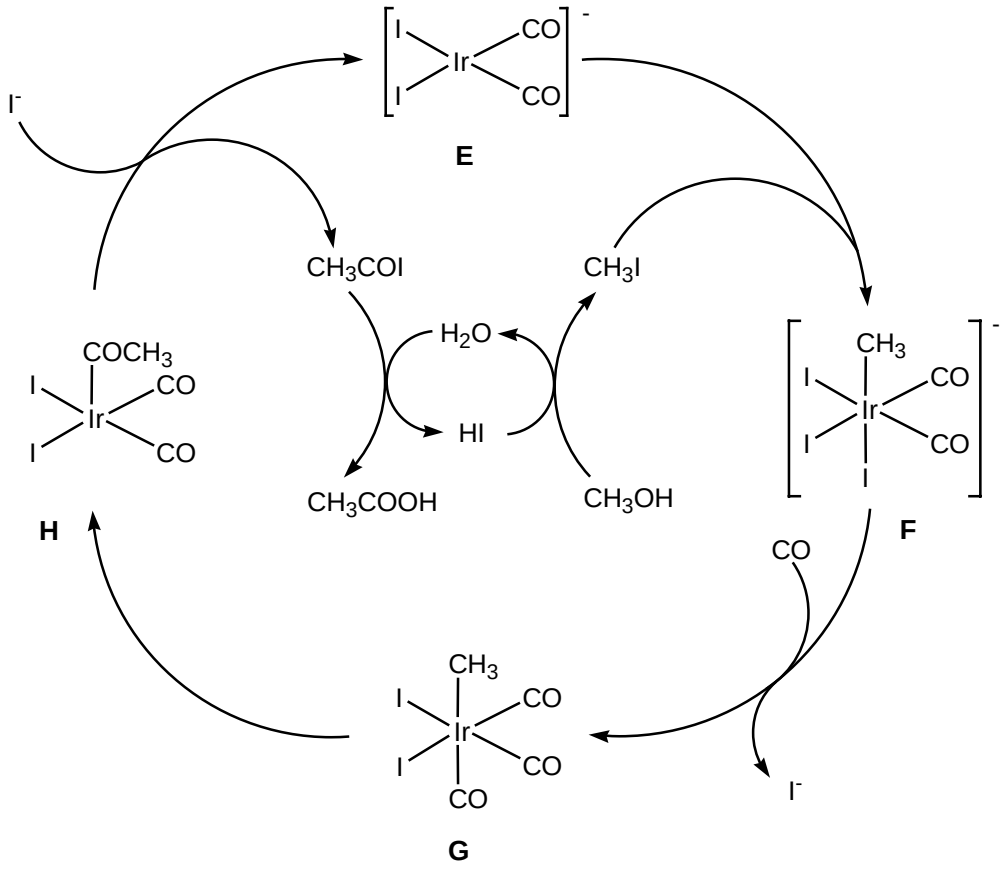

Scheme 10: Catalytic cycle of the iridium-catalyzed methanol carbonylation (Cativa process)

The slowest step in the iridium cycle is the subsequent migratory insertion of CO to form the iridium-acyl species, **G**, which involves the elimination of ionic iodide and the coordination of an additional CO ligand. The inverse rate dependence upon the concentration of ionic iodide suggests that very high reaction rates should be achievable by operating at low iodide concentrations. It also suggests that the inclusion of species capable of assisting in removing iodide should promote the rate-limiting step. Promoters for this system fall within two distinct groups: simple iodide complexes of zinc, cadmium, mercury, gallium and indium,[80] and carbonyl-iodo complexes of tungsten, rhenium, ruthenium and osmium.[81,82]

2.2.7 Mechanistic Studies of the Iridium-Catalyzed Process

The kinetics of the Cativa™ process are in accordance with the mechanism shown in Scheme 10. The effect on the reaction rate of adding five molar equivalents of promoter to one equivalent of the iridium catalyst is shown in Table 3.

Table 3: Effect of various additives on the rate for the iridium-catalysed carbonylation of methanol from batch autoclave data

Runs	Additive	Molar ratio[a]	Rate [mol/l/h]
1	None	-	8.2
2	LiI	1:1	4.3
3	$Ru(CO)_4I_2$	5:1	21.6
4	$Os(CO)_4I_2$	5:1	18.6
5	CdI_2	5:1	14.7
6	InI_3	5:1	14.8
7	$InI_3/Ru(CO)_4I_2$	5:1:1	19.4
8	$Ru(CO)_4I_2$	1:0	0

[a] molar ratio of additive to $[Ir(CO)_2I_2]^-$

A combination of promoters may also be used. None of these metals are effective as carbonylation catalysts in their own right, but all are effective when used in conjunction with an iridium complex. The presence of a promoter leads to a substantial increase in the proportion of "active anionic" species

$[(CH_3)Ir(CO)_2I_3]^-$, **F**, and a substantial decrease in the loss of iridium, by the formation of inactive $[Ir(CO)_3I_3]$ and $[Ir(CO)_2I_4]^-$ species, which are intermediates in the water-gas shift reaction (Eq. 7 and 8). A proposed mechanism for the promotion of iridium catalysis by a metal promoter $M(CO)_xI_y$, is given in Scheme 11.

$$[Ir(CO)_2I_2]^- + 2\,HI \longrightarrow [Ir(CO)_2I_4]^- + H_2 \qquad (7)$$

$$[Ir(CO)_2I_4]^- + CO \longrightarrow Ir(CO)_3I_3 + I^- \qquad (8)$$

The promotion is thought to occur *via* direct interaction of promoter and iridium species as shown. The rate of reaction is dependent upon the loss of iodide from $[(CH_3)Ir(CO)_2I_3]^-$. These metal promoters are believed to reduce the standing concentration of I^-, thus facilitating the loss of iodide from the catalytic species. It is also postulated that carbonyl-based promoters may then go on to donate CO in further steps of the catalytic cycle.

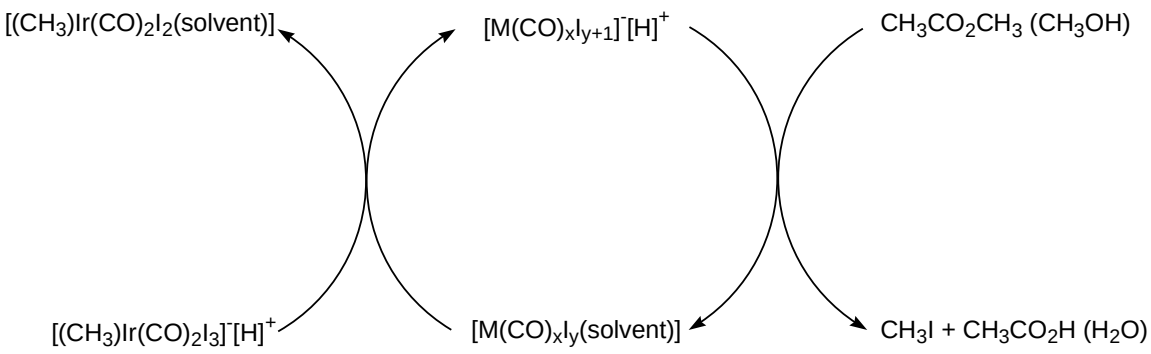

Scheme 11: Implication of metal promoters [such as $Ru(CO)_4I_2$] in the iridium-catalyzed methanol carbonylation (Cativa process)

2.2.8 Comparison between Monsanto and Cativa™ Systems

For the rhodium system the rate of the carbonylation reaction is dependent only upon the concentrations of rhodium and methyl iodide. However, the situation is more complex for the promoted iridium system.

(a) Water concentration. For the rhodium-catalyzed system, a decline in carbonylation rate is observed, as the water content is reduced below 8 wt.%. There are several possible explanations for this observation, one of which being the build-up of the "inactive" $[Rh(CO)_2I_4]^-$ species formed in the water-gas shift cycle at lower water concentrations, which is a precursor for the formation of insoluble RhI_3. Another explanation for the decline in the carbonylation rate is the change of the rate-determining step in the catalytic cycle from the oxidative addition to the reductive elimination (attack by water). This is consistent with the increased amount of acetaldehyde-derived by-products in a low-water concentration rhodium system, as the rhodium-acyl species, **D**, is longer lived. At lower water concentrations, the addition of ionic iodides (especially of alkali metal iodides) to the process has been found to stabilize the rhodium catalysts and to sustain the reaction rate by inhibiting the water-gas shift cycle, inhibiting the formation of $[Rh(CO)_2I_4]^-$ and its degradation to RhI_3, and by promoting the oxidative addition step of the catalytic cycle.[83-86] However, there is also a drawback in the lithium-promoted rhodium system: the acetaldehyde is not scavenged sufficiently by the catalyst system to form propionic acid and therefore the concentration of acetaldehyde increases, condensation reactions occur and higher

non-acidic compounds and iodide derivatives are formed, for example hexyl iodide. Further purification steps are then required.[87]

For the Cativa™ system, in contrast to the Monsanto system, the reaction rate increases with decreasing water content. A maximum value is reached at around 5 wt.%, and the iridium species observed are $[Ir(CO)_2I_4]^-$ (the "inactive" species which is formed in the water-gas shift cycle) and $[(CH_3)Ir(CO)_2I_3]^-$ (the "active" species in the anionic cycle). When the water concentration falls below 5 wt.%, the carbonylation rate declines, and the neutral "active" species $Ir(CO)_3I$ and the corresponding "inactive" water-gas shift species $Ir(CO)_3I_3$ are observed.

(b) Methyl acetate concentration. In the rhodium system, the carbonylation rate is independent of the methyl acetate concentration over a whole range of reactor compositions and process conditions.[88] By contrast, the Cativa™ system displays a strong rate dependence on the methyl acetate concentration, and the methyl acetate concentrations can be increased to far higher levels than in the rhodium system, leading to high reaction rates.

(c) Methyl iodide concentration. The reaction rate for Cativa™ has a reduced dependency on the methyl iodide concentration, as compared to the rhodium system. This is consistent with the fast rate of oxidative addition of methyl iodide to $[Ir(CO)_2I_2]^-$ giving $[(CH_3)Ir(CO)_2I_3]^-$.[89]

(d) CO partial pressure. The effect of CO partial pressure in the Cativa™ process is more pronounced than for the Monsanto process, the conversion being suppressed at pressure below 8 bars when operating in the ionic cycle.[90]

(e) Poisoning effects. In contrast to the Monsanto process, the Cativa™ process is easily poisoned by metals like iron and nickel, which inhibit the iodide loss step in the carbonylation cycle (Scheme 9).

2.3 Ligand-Accelerated Catalysis

The migratory insertion reaction of CO into metal-alkyl bonds is a fundamental step in the metal iodide-catalyzed carbonylation of methanol to acetic acid (and also in hydroformylation reactions).[91] The original $[Rh(CO)_2I_2]^-$ catalyst, developed at the Monsanto laboratories[92,25] and studied in detail by Forster and co-workers,[25,29,43] is largely used for the industrial production of acetic acid and anhydride. However, the conditions used industrially (30-60 bar pressure and 150-200°C)[57] have spurred the search for new catalysts, which could work in milder conditions.[52,79,93-100] The rate-determining step of the rhodium-based catalytic cycle is the oxidative addition of CH_3I, so that catalyst design focused on the improvement of this reaction.

The basic idea was that ligands which increase the electron density at the metal should promote oxidative addition, and consequently increase the overall rate of the reaction. For this purpose, other rhodium compounds have been synthesized in the last years, and they have been shown to be active catalysts of comparable or better performance as compared to the Monsanto catalyst.[93,97,101,102] The most important class of these rhodium complexes are those containing simple phosphine ligands such as PEt_3,[98] or diphosphine ligands of the type PPh_2-CH_2-CH_2-PPh_2.[96]

Cole-Hamilton *et al.* have been investigated the use of trialkylphosphines as promoters for rhodium-based carbonylation catalysts, because they are strongly electron-donating. Complexes of the type $Rh(PEt_3)_2(CO)X$ (X = Cl, Br or I) have a ν(CO) absorption centered around 1960 cm^{-1}, as compared to 1988 and 2059 cm^{-1} for $[Rh(CO)_2I_2]^-$, suggesting that the rhodium center is more electron-rich in the triethylphosphine complexes. $Rh(PEt_3)_2(CO)Cl$ turned out to be a very active catalyst precursor for acetic acid production: In the presence of 17.1 wt.% H_2O at 120 to 150 °C and 27 bar pressure, $Rh(PEt_3)_2(CO)I$ catalyses the carbonylation of methanol at a rate nearly twice as high as that of $[Rh(CO)_2I_2]^-$. Water acts to maintain the catalyst in its active form [as a rhodium(I) complex] and decreases the formation of inactive rhodium(III) complexes such as $[Rh(CO)_2I_4]^-$ or $Rh(PEt_3)_2(CO)I_3$. Thus, the rate of carbonylation is dramatically enhanced by a high water concentration. With low water concentrations, no appreciable benefit is obtained by using $Rh(PEt_3)_2(CO)Cl$ instead of $[Rh(CO)_2Cl]_2$ as catalyst precursor.

Addition of methyl iodide to $Rh(PEt_3)_2(CO)I$ in CH_2Cl_2 was shown to result in the formation of $(CH_3)Rh(PEt_3)_2(CO)I_2$ (Scheme 12).[98] The methyl group is *cis* with respect to the carbonyl ligand, as required for migratory insertion. There is no X-ray crystal structure analysis for complexes of the type $(CH_3)Rh(PR_3)_2(CO)X_2$. However, there are other six-coordinate rhodium(III) complexes resulting from oxidative addition of CH_3I, most of them have iodide and methyl ligands in mutually *trans* positions.[103-105] The isolation of the methyl complex from a catalytically active system is rather unlikely, since the insertion of carbon monoxide into the Rh-C bond is extremely rapid. For $[Rh(CO)_2I_2]^-$, the

methyl complex has a very short lifetime and was only detected as a transient by IR spectroscopy in neat methyl iodide,[52] while for the related $Rh(PPh_3)_2(CO)Cl$ the oxidative addition of methyl iodide gives the six-coordinate complex $(CH_3)Rh(PPh_3)_2(CO)(Cl)I$ in equilibrium with the five-coordinate insertion product, $(CH_3CO)Rh(PPh_3)_2(Cl)I$.[106] In the case of the triethylphosphine analogue, the higher electron density on the metal is responsible for the less facile methyl migration in $(CH_3)Rh(PEt_3)_2(CO)I_2$. Despite the stability of the methylrhodium(III) complex, preliminary kinetic studies suggest that oxidative addition of CH_3I is still rate-determining.

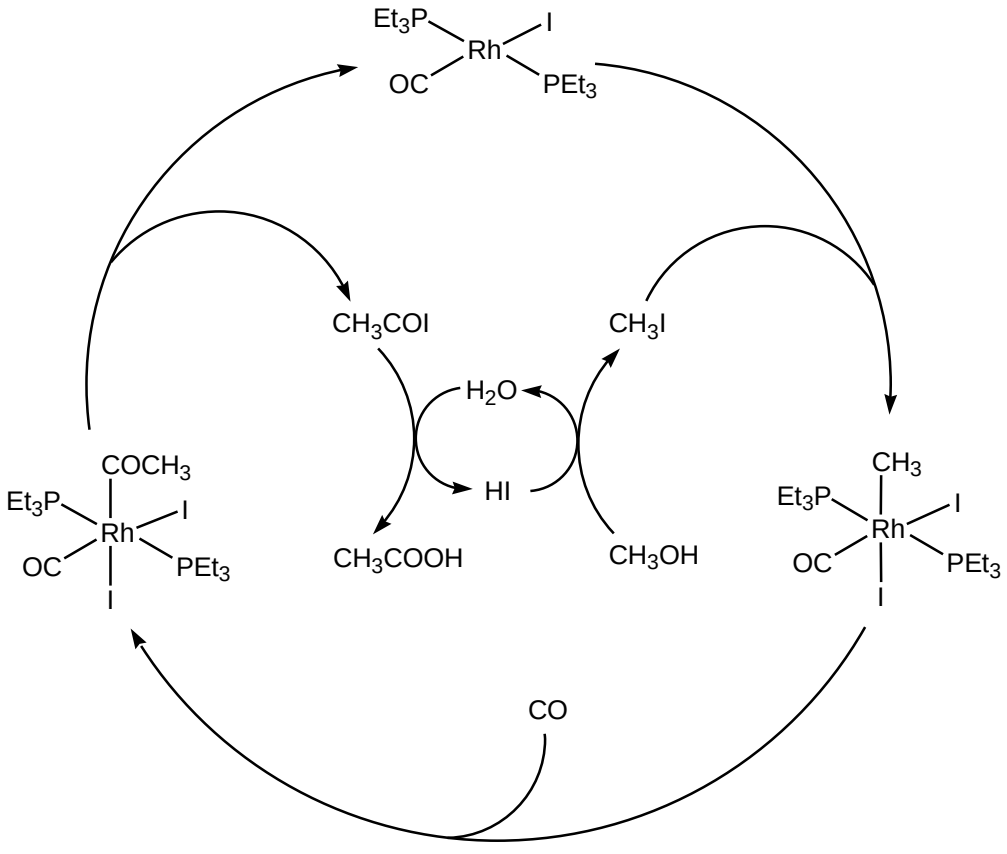

Scheme 12: Catalytic cycle of the methanol carbonylation catalyzed by the neutral complex $Rh(PEt_3)_2(CO)I$

Mixed bidentate ligands such as PPh_2-CH_2-$P(O)Ph_2$,[95] PPh_2-CH_2-$P(NPh)Ph_2$[101] and PPh_2-CH_2-$P(S)Ph_2$[102] have been shown to be effective in rhodium-catalyzed carbonylation of methanol. Wegman *et al.* have found that *cis*-$Rh[Ph_2P(CH_2)_2P(O)Ph_2](CO)Cl$ is a precursor to a very active catalyst for the carbonylation of methanol under mild reaction conditions.[95] Reaction of *cis*-$Rh[Ph_2P(CH_2)_2P(O)Ph_2](CO)Cl$ with CO results in the displacement of the rhodium-oxygen bond and the formation of a new species (υ(CO) 2096 and 2012 cm^{-1}) according to the equilibrium shown in Scheme 13.

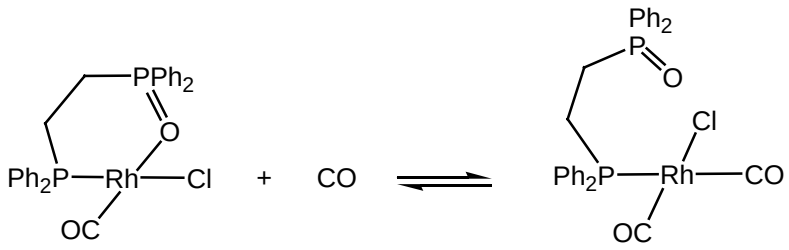

Scheme 13: Equilibrium between $Rh[\eta^2\text{-}Ph_2P(CH_2)_2P(O)Ph_2](CO)Cl$ and $Rh[\eta^1\text{-}Ph_2P(CH_2)_2P(O)Ph_2](CO)_2Cl$

The ratio of the η^2- and the η^1-complexes was determined to be approximatively 1 : 1 (at 22°C and 1 bar CO) by infrared spectroscopy. Infrared spectroscopic studies carried out under catalytic conditions at 80 °C and 3.5 bar CO (turnover frequency 400 h^{-1}) reveal only the η^1-coordinated phosphine oxide species. There is no indication of $[Rh(CO)_2I_2]^-$ which is the principal rhodium species present during catalysis with the Rh-I catalyst.[43] In addition there is no induction period as might be expected if dissociation of $Ph_2P(CH_2)_2P(O)Ph_2$ and subsequent formation of $[Rh(CO)_2I_2]^-$ is important.[25]

Baker *et al.* have found that the use of the diphosphinesulfide $Ph_2PCH_2P(S)Ph_2$ as a promoter for rhodium catalysed carbonylation of methanol

allows a substantial rate increase under industrially feasible conditions (180°C, 70 bar CO).[102] The initial experiments were carried out using a ligand/rhodium ratio of 4 : 1, but the optimum rate enhancement was observed when the discrete complex *cis*-Rh[η^2-$Ph_2PCH_2P(S)Ph_2$](CO)Cl was used as pre-catalyst. These authors showed that any additional phosphine quaternizes with CH_3I, and the addition of iodide inhibits the catalytic reaction (Scheme 14). Addition of three equivalents of $[(CH_3)PPh_3]I$ causes a similar retardation in rate. Rh[$Ph_2PCH_2P(S)Ph_2$](CO)Cl is readily formed upon mixing $[Rh(CO)_2Cl]_2$ with two equivalents of $Ph_2PCH_2P(S)Ph_2$ in CH_3OH, and there is no evidence for the formation of dinuclear complexes in this reaction.[107]

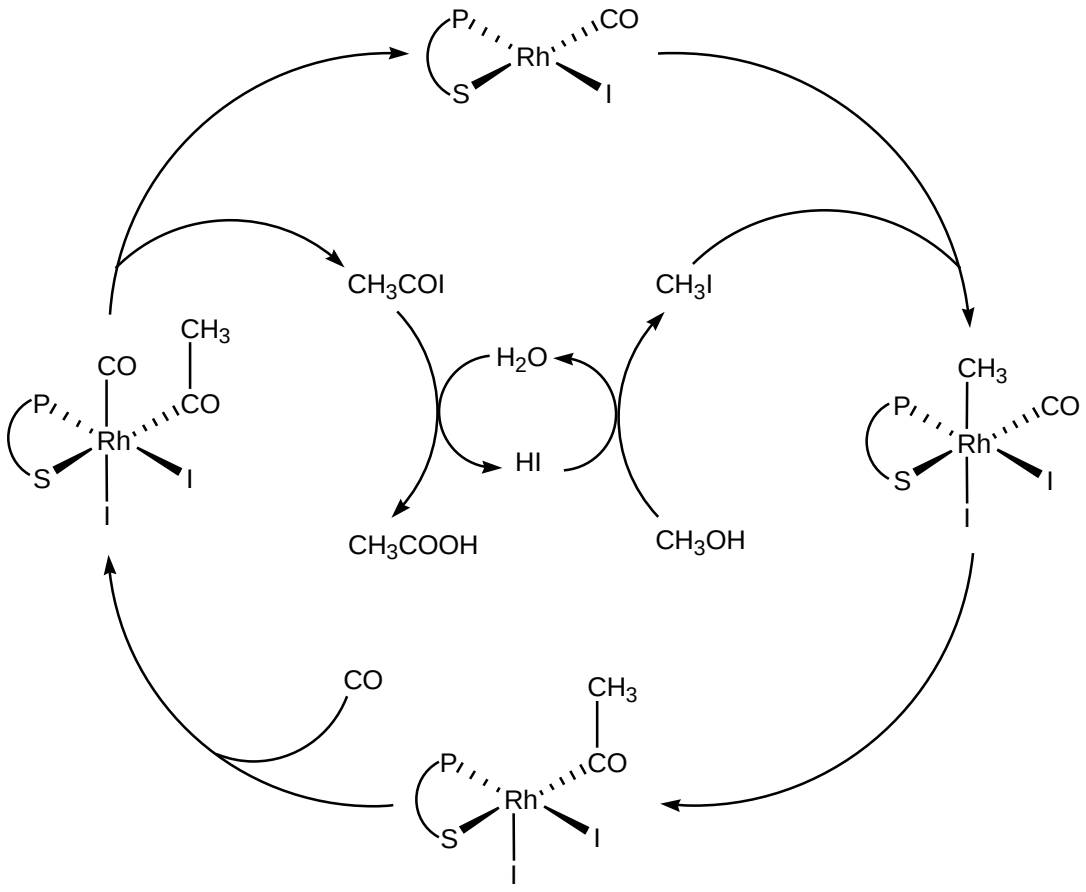

Scheme 14: Catalytic cycle of the methanol carbonylation catalyzed by the neutral complex Rh[$Ph_2PCH_2P(S)Ph_2$](CO)I

The X-ray crystal structure analysis of $Rh[Ph_2PCH_2P(S)Ph_2](CO)Cl$ confirms the stereochemistry at rhodium in which the phosphorus atom is *trans* with respect to the chloro ligand, while the sulfur atom is *trans* with respect to the carbonyl ligand; but the structure shows no unusual features to explain the unexpected stability of the catalyst at high temperatures. Unlike in the case of the oxygen analogue, in the case of $Rh[Ph_2PCH_2P(S)Ph_2](CO)Cl$, there is no evidence for a hemilabile behavior of the P-S ligand, while it has been assumed to be important for catalysis employing mixed-donor ligands.[108] These results showed for the first time that a discrete rhodium-phosphine complex can give a significant improvement in carbonylation activity over $[Rh(CO)_2I_2]^-$ under industrial conditions.

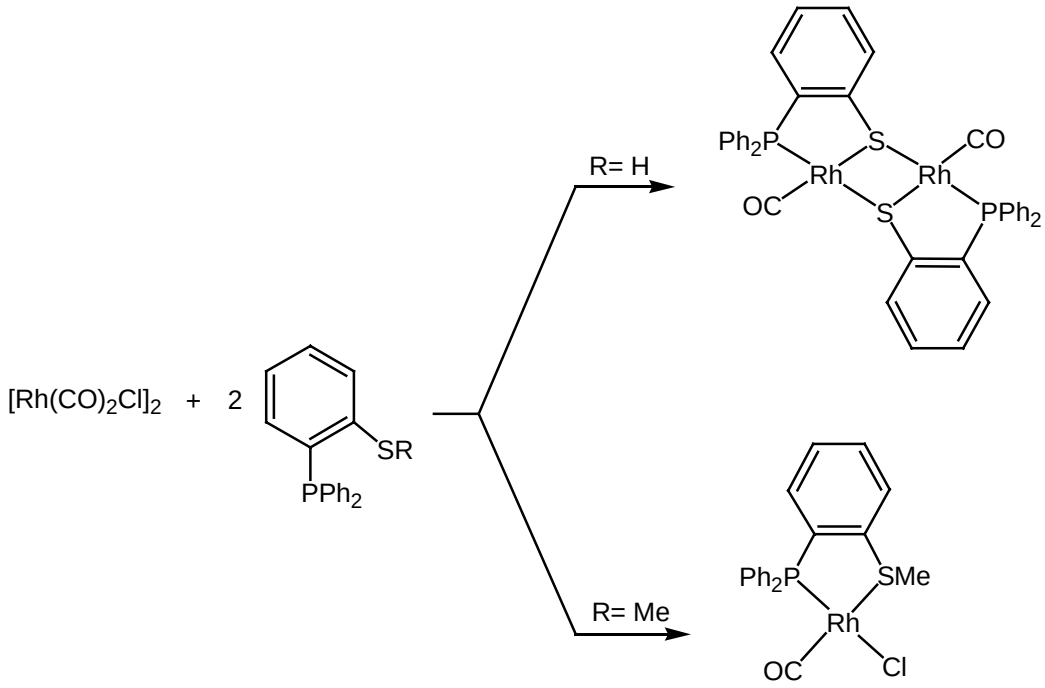

Scheme 15: Synthesis of rhodium phosphinothiolate and phosphinothioether complexes

Dilworth *et al.* described other methanol carbonylation catalysts which show significant improvements in absolute rates over those obtained with

$[Rh(CO)_2I_2]^-$.[93] Both, the dinuclear phosphinothiolate complex and the mononuclear phosphinothioether complex synthesized according to Scheme 15 efficiently catalyze the carbonylation of methanol with comparable rate. The authors proposed a mechanism similar to the cycle proposed for $Rh[Ph_2PCH_2P(S)Ph_2](CO)I$ (Scheme 14).[102]

Pringle *et al.* reported that rhodium complexes of unsymmetrical ethylene diphosphine ligands are more efficient catalysts than the symmetrical dppe analogues for methanol carbonylation and longer-lived than any other reported ligand-modified catalysts under industrial conditions.[110-113] The catalysts were prepared by addition of diphosphines to $[Rh(CO)_2Cl]_2$ in methanol (Scheme 16).

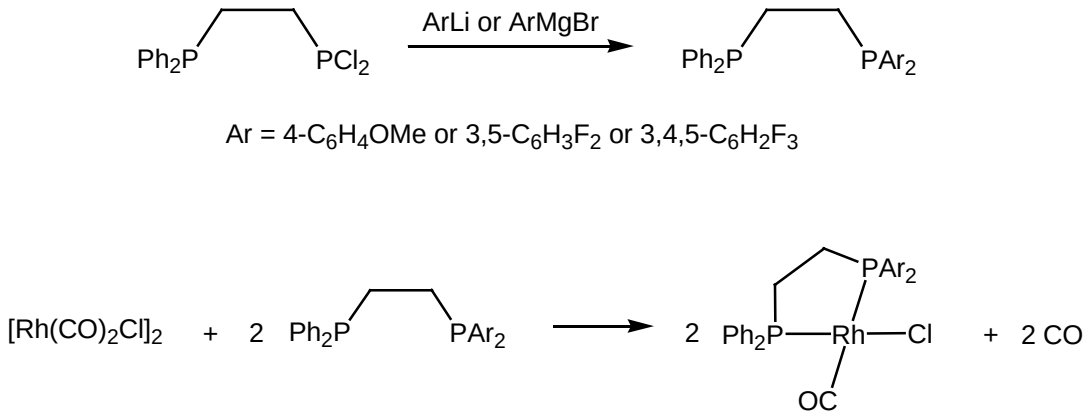

Scheme 16: Synthesis of rhodium complexes with unsymmetrical diphosphine ligands

In each case the conversion of methanol was greater than 98%, and the selectivity for acetic acid was greater than 99%; however, the carbonylation rates are lower for these diphosphine complexes than for the $[Rh(CO)_2I_2]^-$ catalyst. The following observations suggest that the catalyst is indeed a diphosphine-rhodium complex throughout the catalytic reaction and not $[Rh(CO)_2I_2]^-$. Infrared spectra

obtained *in situ* during catalysis with $Ph_2PCH_2CH_2P(3,4,5\text{-}C_6H_2F_3)_2$ showed the absence of the intense ν(CO) bands of $[Rh(CO)_2I_2]^-$ at 2059 and 1988 cm^{-1}. At the end of the catalytic reaction, ^{31}P NMR and IR spectra showed the presence of a mixture of diphosphine rhodium(III) carbonyl complexes. The product *fac*-$Rh[Ph_2PCH_2CH_2P(3,4,5\text{-}C_6H_2F_3)_2](CO)I_3$ was isolated from the reaction mixture, using the catalyst $Rh[Ph_2PCH_2CH_2P(3,4,5\text{-}C_6H_2F_3)_2](CO)Cl$.[110] The rate of catalysis is constant throughout a catalytic run and, after consumption of the entire methanol, a second aliquot of methanol was injected, the rate observed was the same as in the first run. This final observation not only confirms the integrity of the catalyst, but also shows its longevity to be greater than any previous rhodium-phosphine catalyst under these conditions, since every diphosphine complex executes over 500 turnovers without noticeable diminution of activity. The rhodium-diphosphine catalysts also resemble the iridium *Cativa* catalyst. The amount of propionic acid reported (formed during the water-gas shift reaction) for these diphosphine catalysts is significantly less than that with $[Rh(CO)_2I_2]^-$ as catalyst under the same conditions.

The greater nucleophilicity of Rh(diphosphine)(CO)I complexes,[100] as compared to $[Rh(CO)_2I_2]^-$, may partly explain the similarities between the rhodium-diphosphine and the iridium catalysts. Since the iridium catalysts are promoted by iodide-abstracting ruthenium complexes,[95,99,114] Pringle et *al.* checked whether or not $Ru(CO)_4I_2$ also promotes the rhodium catalyst containing the $Ph_2PCH_2CH_2P(3,4,5\text{-}C_6H_2F_3)_2$ ligand. Indeed, addition of $Ru(CO)_4I_2$ more than doubles the carbonylation rate.[110] The *asymmetry* of the diphosphine is also

crucial. Casey *et al.*[111] showed that unsymmetrical diphosphines are superior to the symmetrical analogues for hydroformylation catalysis and associated this with a preference of the better σ-donor for the axial site in the trigonal bipyramidal intermediates. It is noteworthy that P,O-,[95] P,N-[101] and P,S-donor[102] ligands used for methanol carbonylation are all unsymmetrical with one strong and one medium or weak donor atom.

Indeed, all these new ligands enhance the oxidative addition step but as a consequence they usually retard the subsequent CO insertion step, because the increased electron density at the metal also leads to a stronger Rh-CO bond. Optimal parameters are required to achieve the delicate balance between these two factors which will afford highly efficient catalysts. In fact, while the octahedral intermediate obtained from the square-planar precursor complex by CH_3I addition undergoes migratory insertion only under CO pressure with PEt_3 as ligands, it is relatively long-lived with the PPh_2-CH_2-CH_2-PPh_2 ligand. However, it is so reactive with the PPh_2-CH_2-P(S)Ph_2 ligand that its detection was rather difficult.[100] The fact that both, oxidative addition and CO insertion steps are accelerated with the latter ligand was quite unexpected. Therefore, it was assumed that the steric requirements of the PPh_2-CH_2-P(S)Ph_2 ligand destabilize the octahedral intermediate which would undergo migratory insertion to release such steric pressure.[100]

To summarize, we have shown that square-planar rhodium complexes containing two monophosphine ligands in *trans* positions such as *trans*-$Rh(PEt_3)_2(CO)Cl$ are highly active for methanol carbonylation, but less stable than

unsymmetrical diphosphine complexes such as *cis*-Rh($Ph_2PCH_2CH_2PAr_2$)(CO)Cl which are, however, less active catalysts.

For all these reasons, we decided to develop three different classes of new multifunctional ligands: nitrogen-donor ligands which are known to be electron-rich ligands (as PEt_3), sulfur ligands which are also known as good donors, and unsymmetrical diphosphine ligands containing suitable spacer groups between the two phosphorus atoms, in order to allow *trans* coordination in square-planar rhodium complexes. Complexes of this type can be expected to show high catalytic activity and good stability under the harsh conditions of methanol carbonylation.

Chapter 3

New Benzotriazole Ester Ligands: Synthesis, Coordination, Catalytic Properties

Benzotriazole (Hbta) is a nitrogen-containing heterocyle consisting of a five-membered ring containing three nitrogen atoms fused to a benzene ring. The molecule represents an aromatic system and reacts with a base to give the corresponding benzotriazolate anion (bta^-).[115]

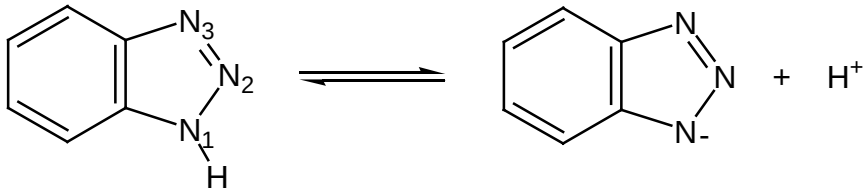

Hbta bta^-

For reasons which will be presented in the following section, this heterocycle appeared to be an interesting system for the design of multifunctional ligands that can be used to improve the activity of late transition metal catalysts in the carbonylation of methanol.

3.1 Nitrogen-Containing Ligands in Catalysis

For a long time, the coordination chemistry of late transition metals in low oxidation states has been dominated by phosphorus-containing ligands, while nitrogen-containing ligands, being much harder, were considered to be less suitable for binding to soft metal atoms.[116-118] Today it is obvious that many nitrogen-containing molecules, in particular bi-, ter- and tetradentate systems can

bind strongly to transition metal atoms, stabilizing both high and low oxidation states.[119-122]

The vast variety of nitrogen donor-ligands is impressive: No other element presents such a diversity of organic compounds. Most of these compounds are potential donor ligands, if a lone electron-pair is available at nitrogen. An appropriate classification of nitrogen-containing ligands can be based on the hybridization of nitrogen: sp^3, sp^2, and sp. Examples of nitrogen-containing ligands with sp^3-N and sp^2-N are given in Schemes 17 and 18, respectively.

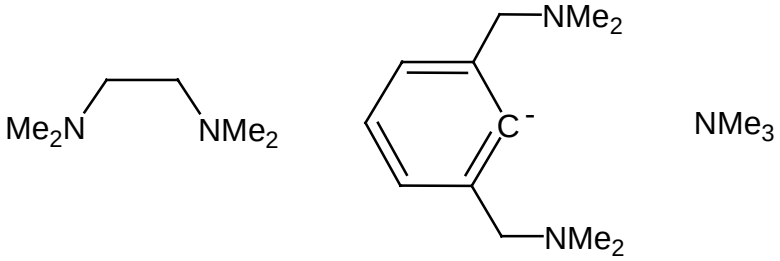

Scheme 17: Some nitrogen-donors with tertiary sp^3-hybridized N atoms

Ligands containing sp^2-hybridized nitrogen atoms, especially when the N atom is part of an aromatic system, have an extensive coordination chemistry, in particular when they are multidentate ligands. In contrast to the phosphorus atom, the nitrogen atom has no low-lying d orbitals available, so that nitrogen containing-ligands have only σ-donor (and no π-acceptor) properties. Therefore, the metal-nitrogen bond has a more pronounced ionic character than the metal-phosphorus bond. Furthermore, as M-N bonds are more affected by steric effects than M-P bonds, stable complexes with nitrogen-containing ligands can be expected for multidentate ligands making use of the chelating effect.

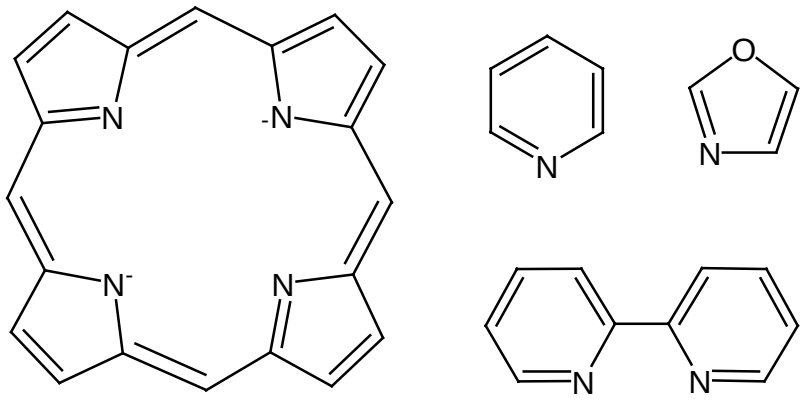

Scheme 18: Some nitrogen ligands with sp^2-hybridized N atoms

Nitrogen donors are frequently used as part of chelating systems with carbon-donors. The C,N-donors have played a significant role in rich chemistry because of their ready formation through a cyclometalation reaction.[123,124] Noteworthy is also the rich chemistry based on complexes of the N,C,N-terdentate ligand (Scheme 19).

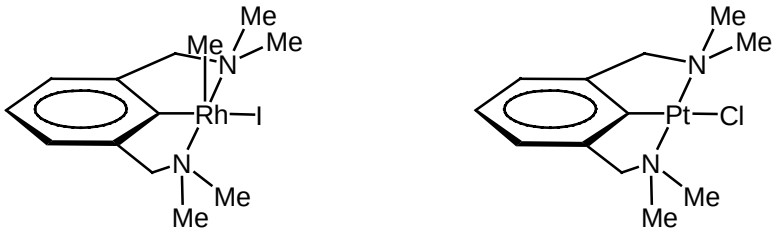

Scheme 19: Complexes with N,C,N-terdentate ligand

Other examples involve diimine ligands which, in the case of oxazolines and their derivatives, have been intensively studied in asymmetric catalysis.[125,126] Recently Gibson and Brookhart reported the discovery of highly active iron and cobalt polymerization catalysts containing bulky tridentate pyridine diimine ligands (Scheme 20).[127]

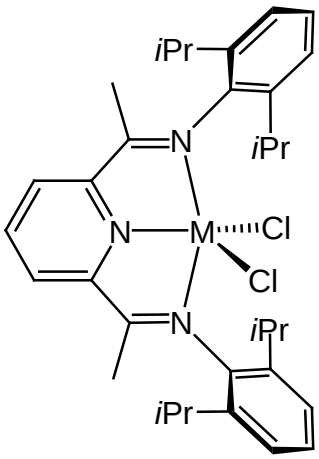

Scheme 20: Iron-and cobalt polymerization catalysts

In the chemistry of rhodium(I) and iridium(I), multidentate N-donor ligands have found only limited use in catalysis: Catalytic applications of Rh(I) and Ir(I) complexes have been reported for trispyrazolylborate,[128,132] triazacyclononane[129-134] and pyridine-2,6-diimine[135] ligands. These ligands act as multidentate ligands. By virtue of their strong σ-donor properties, they stabilize square-planar complexes, while enhancing the nucleophilicity of the rhodium(I) or iridium(I) center.

Chelating ligands containing nitrogen donors as well as phosphorus donor/acceptors are also known. The π-acceptor character of phosphorous can stabilize a metal center in a low oxidation state, while the σ-donor character of nitrogen makes the metal more susceptible to oxidative addition reactions. This can help to stabilize intermediates in catalytic reactions. Moreover the combination of *soft* (phosphorus) and *hard* (nitrogen) coordinating atoms in the same ligand framework may offer the advantage of providing free coordination sites along the catalytic pathway by the decoordination of either the phosphorus

or nitrogen ligator, depending on the nature of the reagent and of the formal oxidation state of the metal.[136]

We have seen that the most common nitrogen-containing ligand systems are heterocycles such as pyridine, imidazole, pyrazole, bipyridine, oxazoline and derivatives thereof.[137-141] Complexes of these ligands are known with almost all transition metals.[142-146] Benzotriazole and its derivatives are not frequently encountered in coordination chemistry, whereas Katritzky has published many papers concerning benzotriazole as a synthetic organic intermediate since 1985.[147-151] A few complexes of benzotriazole are known so far,[152] benzotriazole being coordinated as η^1-ligand through N(1) but also as η^2-ligand through N(2) and N(3).[153,154] With the catalytic perspective in mind, we decided to synthesize new ester ligands based on the benzotriazole unit. One important property of these potentially multidentate ligands is that they can stabilize metal ions in a variety of oxidation states and geometries. Moreover, the oxygen atom of the ester group can be weakly coordinated to soft metal centers and can be easily dissociated in solution, providing a vacant coordination site on demand, whereas their chelating effect confers stability to the catalyst precursor in the absence of substrate. This possible versatility is of particular interest for catalysis.

3.2 Ligand Syntheses

Recent advances in carbodiimide esterification led us to explore the possible use of these reagents for direct synthesis of our ligands.[155-158] Condensation occurs between equimolar mixtures of acids and alcohols driven by

the addition of water across the carbodiimide groups and producing the stable urea by-product.

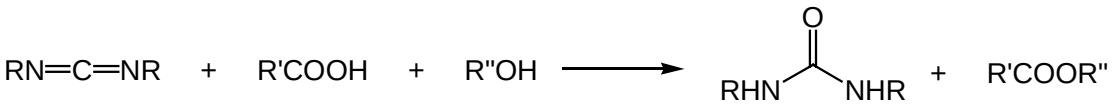

Since carbodiimides such as *N*,*N'*-dicyclohexylcarbodiimide (DCC) do not react with aliphatic alcohols or phenols except under drastic conditions,[155] one expects selective activation of the carboxylic acid, thus permitting direct esterification. This one occurs by *in situ* formation of activated acids, avoiding the need to prepare and handle preactivated acid derivatives such as acid chlorides. Since these derivatives are susceptible to hydrolysis by adventitious moisture present during the reaction, high conversion levels are only possible under rigorously anhydrous conditions.[156-158]

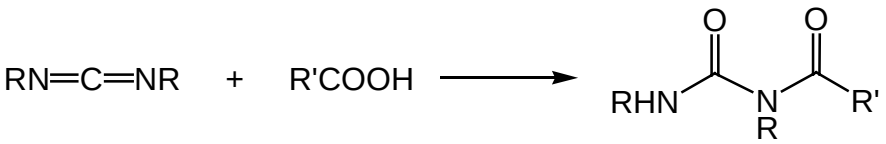

Although carbodiimide chemistry has been extensively used in peptide synthesis,[159] its use in esterification chemistry has been hampered by a side reaction that converts carboxylic acids to unreactive N-acylureas. It has recently been observed that this reaction can be suppressed by using hyperacylation agents such as 4-(dimethylamino)pyridine (DMAP) or 4-pyrrolidinopyridine (4-PPY).[156,160]

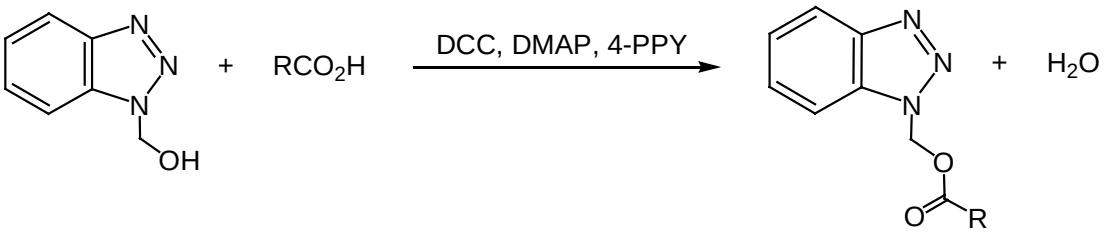

We decided to use N-hydroxymethylbenzotriazole as a starting compound, because recent works published by Katritzky has shown the versatility of this compound as a synthetic intermediate.[161,162] For the esterification reaction we used DCC in combination with an equimolar mixture of DMAP and 4-PPY as condensation reagents.

3.2.1 Preparation and Characterization

The new benzotriazole ligands **1** - **5** are directly accessible by condensation methods from hydroxymethylbenzotriazole and the corresponding mono- or diacids. They can be isolated in good yields as micro-crystalline powders by column chromatography (Scheme 21).

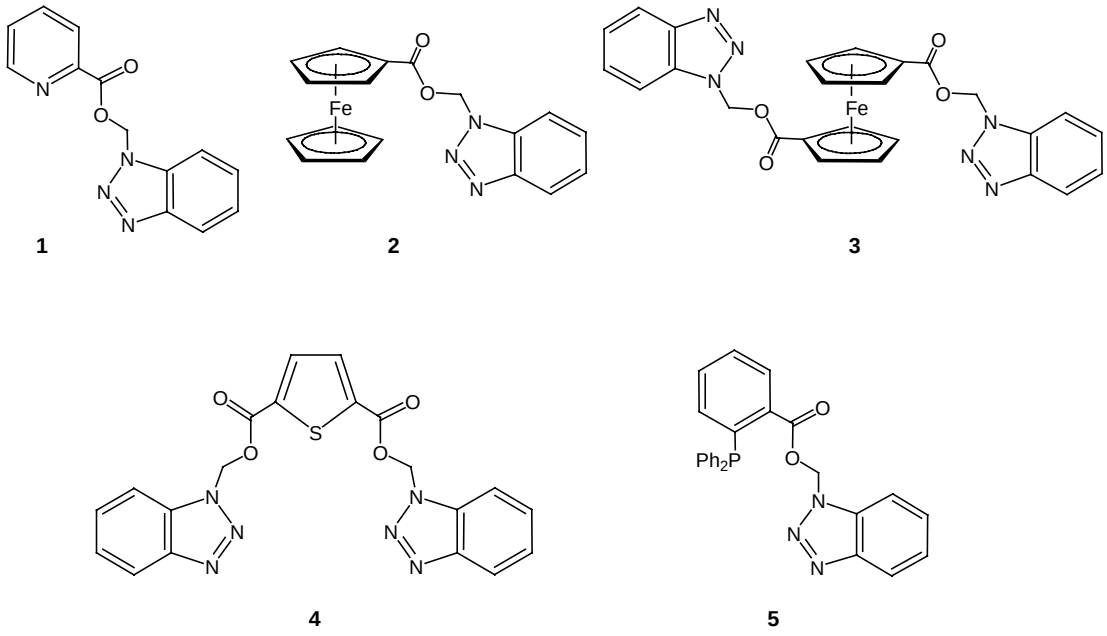

Scheme 21: Synthesis of **1** - **5**

Micro-analytical and NMR data are consistent with the structures shown. The successful coupling reaction is clearly evidenced by the ^{13}C NMR spectrum of **1** (Figure 3), in which we can easily distinguish the C(8) ester atom at 164.4 ppm and C(7) benzotriazole atom at 69.1 ppm from the other aromatic carbon atoms (11 signals).

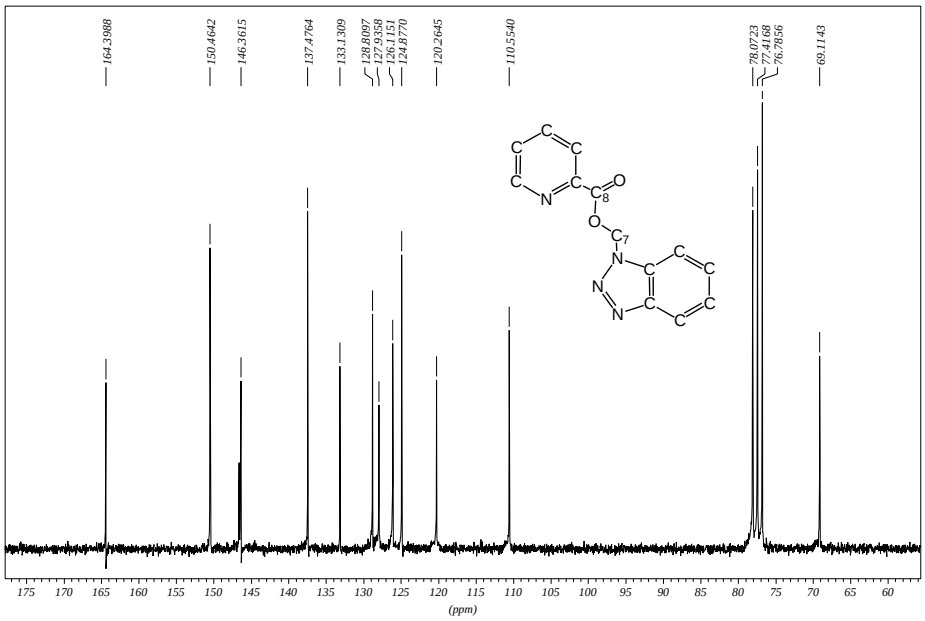

Figure 3: ^{13}C NMR spectrum of **1**

In the ^{1}H NMR spectrum of **2** (Figure 4), the successful coupling reaction of the hydroxymethylbenzotriazole and the ferrocene carboxylic acid moieties can be deduced from the chemical shift differences of Hb-Hc, compared to the Ha atoms of the unsubstituted Cp ring. Since the two Hc are close to the ester function, the difference with the two Hb atoms is apparent from the low field shift of 0.4 ppm for Hc. The characteristic signal of the methylene group (hydrogen atoms Hd) appears as a singlet at 6.77 ppm. In the aromatic region, two doublets and two triplets, each integrating as one proton, are observed. Hh is the

most deshielded (8.10 ppm), because it is close to the more electron-rich nitrogen atom of benzotriazole and He is the most shielded (7.43 ppm).

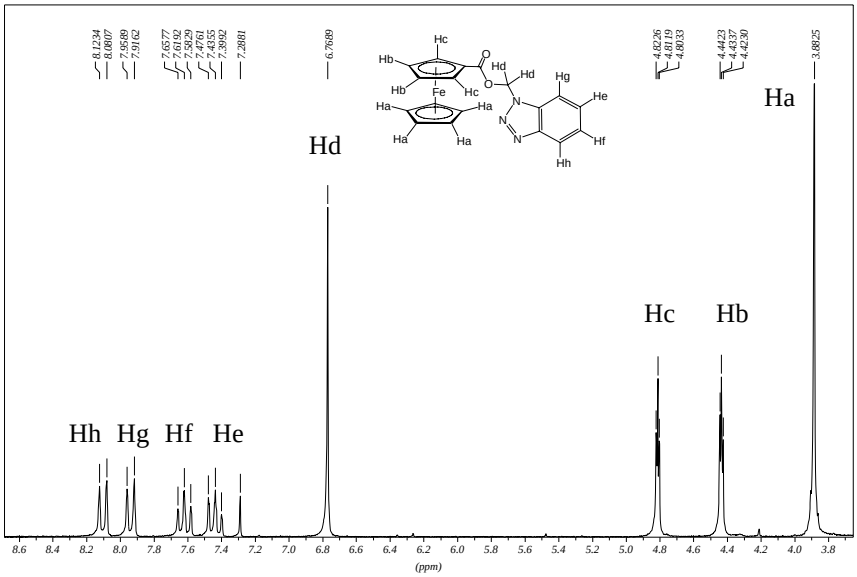

Figure 4: ^{1}H NMR spectrum of **2**

The IR, ^{1}H, ^{13}C NMR and MS spectra of **3**-**5** are as expected, the spectroscopic data are given in the experimental section.

3.2.2 X-ray Crystal Structure Analyses

The molecular structures for **1** and **2** have been confirmed by X-ray crystallography. Suitable single-crystals of **1** (colorless) have been obtained from ethyle acetate/hexane, and of **2** (orange-red) from acetone/hexane. The molecular structure of the ligand **1** is depicted in Figure 5. The pyridine ring is almost planar, the ring atoms being formally sp^2 hybridized. In accordance with the aromaticity, the C-C and C-N distances in the pyridine ring are shorter [C(9)-C(10) 1.381(3) Å, C(10)-C(11) 1.383(4) Å, C(9)-N(4) 1.338(3) Å] than those in the benzotriazole ring [C(1)-C(2) 1.391(3) Å, C(1)-C(6) 1.396(3) Å, C(4)-C(5) 1.408(3) Å, C(1)-N(1) 1.369(3) Å]. The two nitrogen-nitrogen bonds of the benzotriazole unit are in

accordance with the lengths of a single and a double bond [N(2)-N(3) 1.301(2) Å, N(1)-N(2) 1.367(3) Å]. The C(8)-O(1) bond distance [1.203(2) Å] and the C(8)-O(2) bond distance [1.346(2) Å] are similar than those reported for other pyridine esters (Table 4).[163,164]

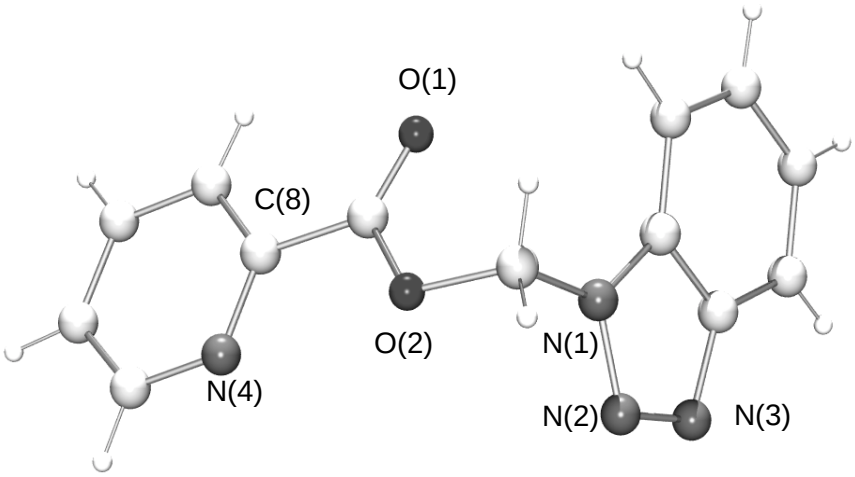

Figure 5: Molecular structure of **1**

Table 4: Selected bond lengths [Å] for **1**

C(9)-C(10)	1.381(3)	N(2)-N(3)	1.301(2)
C(10)-C(11)	1.383(4)	N(1)-N(2)	1.367(3)
C(9)-N(4)	1.338(3)	C(8)-O(1)	1.203(2)
C(1)-C(2)	1.391(3)	C(8)-O(2)	1.346(2)
C(1)-C(6)	1.396(3)		
C(1)-N(1)	1.369(3)		

The molecular structure of ligand **2** is given in Figure 6. Selected bond distances for **2** are given in Table 5. The ferrocene moiety is in the eclipsed conformation. In each molecule, the Cp rings are virtually parallel to each other (Cp-Fe-Cp angles: 5.30°). The distances of Fe to the C atoms of the Cp rings are normal and compare well with those of other ferrocene structures.[165] Interestingly,

the Cp internal C-C bond distances in the substituted Cp rings [C(9)-C(13) 1.430(3) Å, C(9)-C(10) 1.433(2) Å] are longer than in the unsubstituted Cp ring [C(14)-C(18) 1.409(4) Å, C(14)-C(15) 1.403(3) Å]. This has been documented before.[165] The distance of the carbonyl carbon to the Cp ring [C(8)-C(9) 1.456(2) Å] is normal C-C single bond distance. The methylenebenzotriazole substituent is rotated out of the ester plane by 79.45°, allowing no efficient interaction between the π-system of the Cp ring and the benzotriazole. A similar behavior has been observed for benzoylferrocene,[166] where the solid state structure shows the phenyl ring rotated out of the Cp plane by 40.4°. Steric interference does not allow coplanarity of the Cp and Ph groups.[166]

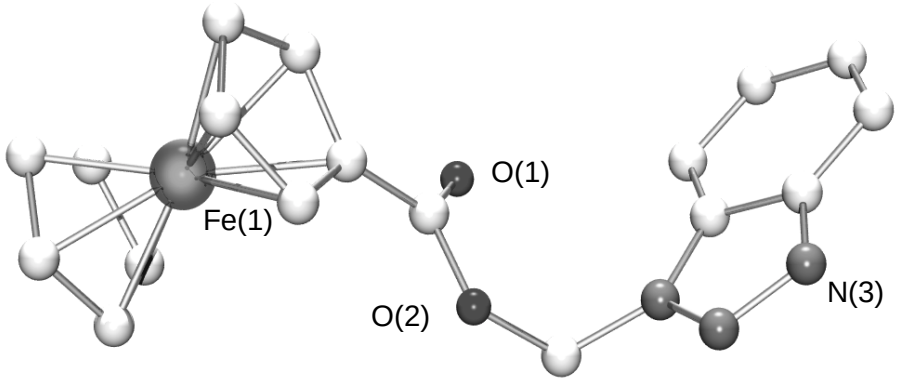

Figure 6: Molecular structure of **2**

Table 5: Selected bond lengths [Å] for **2**

C(9)-C(13)	1.430(3)	C(8)-O(2)	1.363(2)
C(9)-C(10)	1.433(2)	C(8)-C(9)	1.456(2)
C(14)-C(18)	1.409(4)	C(8)-O(1)	1.211(2)
C(14)-C(15)	1.403(3)		

Similar steric problems are most likely responsible for the arrangement of the benzotriazole substituent. The C(8)-O(1) bond distance of 1.211(2) Å is

shorter than those observed for ferrocenecarboxylic acid[167] (1.261(15) Å) and ferrocene dicarboxylic acid (1.228(3) Å).[168] However it is also longer than those of other ferrocenecarboxylic esters, such as 2-(1-hydroxyethyl)-1-ferrocenecarboxylic acid methyl ester[169] [C=O 1.205(4) Å] and 3-(diphenylphosphino)-1-ferrocene carboxylic acid methyl ester [C=O 1.204(3) Å].[170] The C(8)-O(2) bond distance [1.363(2) Å] is about 0.06 Å shorter than that of ferrocenecarboxylic acid benzotriazole ester [1.427(2) Å] which is known to have a weak and reactive ester bond, facilitating the amidation in the peptide-coupling reactions.[171] These crystallographic informations fit well with the good stability of our ester bond.

3.3 Coordination Chemistry

As a part of our preliminary studies on the coordination behavior of these new ligands, we examined their reactivity towards cobalt(II), rhodium(I) and iridium(I) compounds, since these metals are active in methanol carbonylation.

3.3.1 Cobalt(II) Complexes

The benzotriazole ligand **2** was found to coordinate easily to cobalt through the 3-N atom of the triazole unit. The reaction of **2** with CoI_2 in dichloromethane at room temperature gives quantitatively the cobalt(II) complex [Co(**2**)$_2$I$_2$] (**6**) as an air-stable solid (Scheme 22). This compound is moderately soluble in acetone and toluene, but only sparingly soluble in alcohols and insoluble in alkanes; **6** can be recrystallized from dichloromethane/hexane to give green crystals.

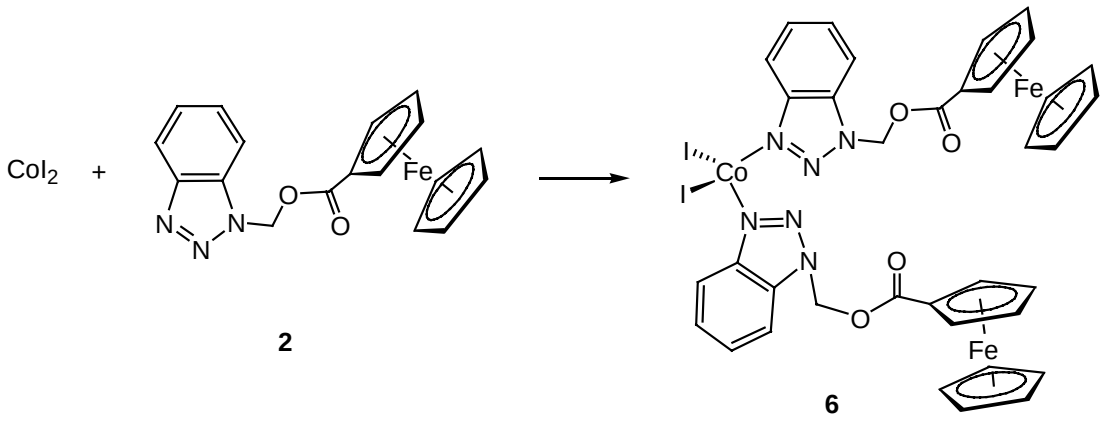

Scheme 22: Synthesis of **6**

The single-crystal X-ray structure analysis reveals that the cobalt(II) center is tetrahedrally coordinated to two iodine atoms and to the 3-N nitrogen atoms of two triazole ligands (Figure 7). The angles N(23)-Co(1)-N(3), N(23)-Co(1)-I(1), N(23)-Co(1)-I(2), N(3)-Co(1)-I(1), N(3)-Co(1)-I(2), I(1)-Co(1)-I(2) (103.5(2), 106.99(17), 113.42(17), 104.65(15), 110.97(15), 116.20(4)°, respectively) are not far from the ideal tetrahedral angle. The two cobalt-nitrogen bonds [Co(1)-N(3) 2.033(5), Co(1)-N(23) 2.044(5) Å] and the two cobalt-iodine bonds [Co(1)-I(1) 2.5510(11), Co(1)-I(2) 2.5692(11) Å] are almost equal in length and are normal for this kind of complexes.[172,173] Some deviation from regular tetrahedral geometry is indicated by the relatively large I(1)-Co(1)-I(2) and corresponding small N(23)-Co(1)-N(3) angles. Interligand repulsions between the iodine presumably are responsible for the observed distortion.[174] The two C=O bond distances (C(8)-O(1) 1.197(8) Å, C(28)-O(21) 1.195(8) Å) are shorter than this in the free ligand (1.211(2) Å). This is in line with the ν(CO) absorption at 1723 cm^{-1} observed for **6** in the infrared spectrum, while the free ligand absorbs at 1708 cm^{-1}.

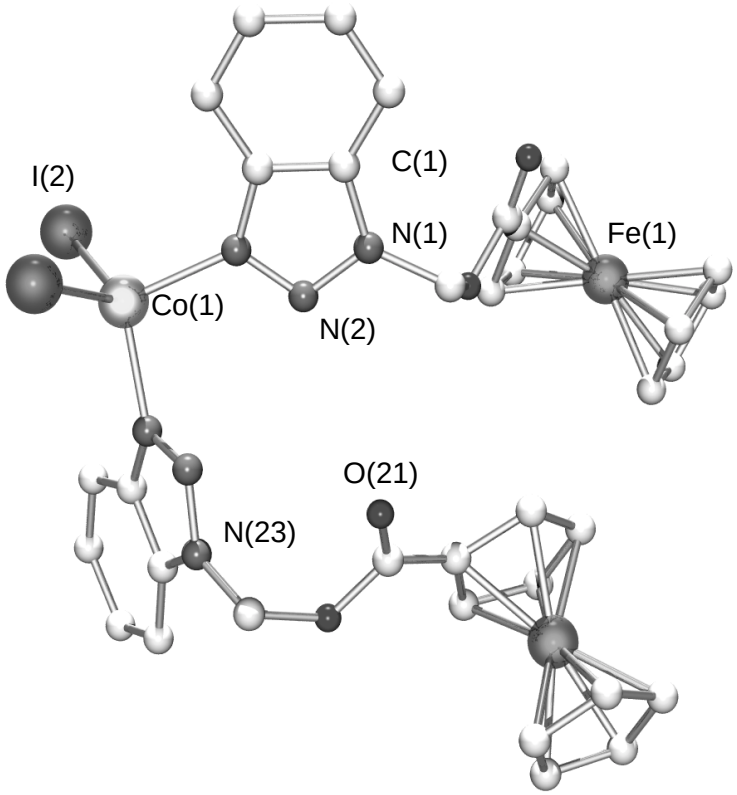

Figure 7: Molecular structure of **6**

Table 6: Selected bond lengths and angles [Å] for complex **6**

Co(1)-N(3)	2.033(5)	N(23)-Co(1)-N(3)	103.5(2)
Co(1)-N(23)	2.044(5)	N(23)-Co(1)-I(1)	106.99(17)
Co(1)-I(1)	2.5510(11)	N(23)-Co(1)-I(2)	113.42(17)
Co(1)-I(2)	2.5692(11)	N(3)-Co(1)-I(1)	104.65(15)
C(8)-O(1)	1.197(8)	N(3)-Co(1)-I(2)	110.97(15)
C(8)-O(2)	1.367(8)	I(1)-Co(1)-I(2)	116.20(4)

Thus, in **6** the ligand **2** is coordinated in a monodentate fashion through the 3-N atom of the benzotriazole unit. Since benzotriazole can also act as a N-N bridging ligand,[153,154] we can envisage complex **6** to coordinate to other metal centers. However, our repeated attempts to synthesize a bimetallic Co-Rh complex from $[Rh(CO)_2Cl]_2$ and **6** were unsuccessful.

The reaction of CoI_2 with ligand **4** in dichloromethane at room temperature yields the polymeric complex $[Co(C_6H_4N_3CH_2CO_2C_4H_2SCO_2CH_2C_6H_4N_3)I_2]_n$ (**7**) almost quantitatively (Scheme 23). Polymer **7** can be recrystallized from acetone/hexane over a period of several months to give green, air-stable crystals. The infrared spectrum of complex **7** exhibits one strong ν(CO) absorption at 1727 cm^{-1}, whereas the free ligand **4** exhibits two strong ν(CO) absorptions at 1749 and 1709 cm^{-1}.

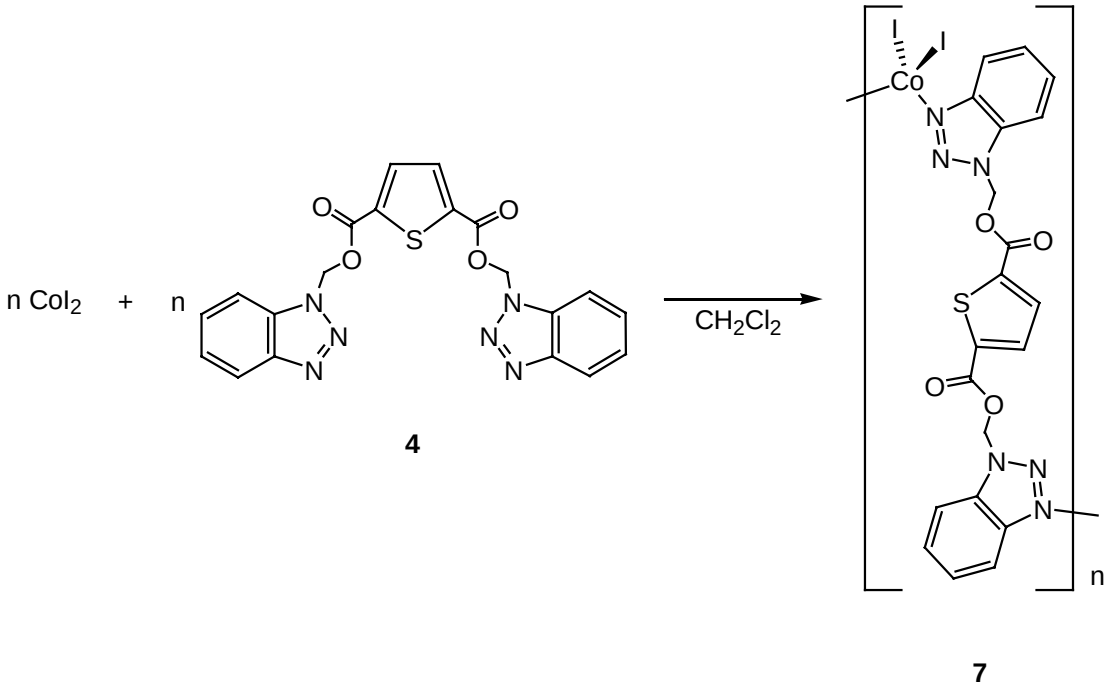

4 **7**

Scheme 23: Synthesis of **7**

As it is shown in Figure 8, ligand **4** acts in complex **7** as a bridging ligand rather than a bidentate ligand. Thus, the single-crystal X-ray structure analysis reveals **7** to be a coordination polymer, each cobalt(II) center being tetrahedrally coordinated to two iodine atoms and to the 3-N nitrogen atoms of two triazole ligands (Figure 9).

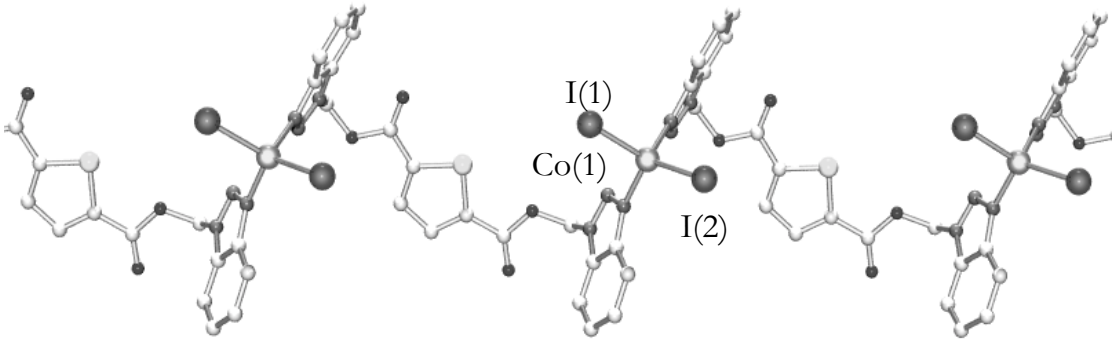

Figure 8: Molecular structure of **7**

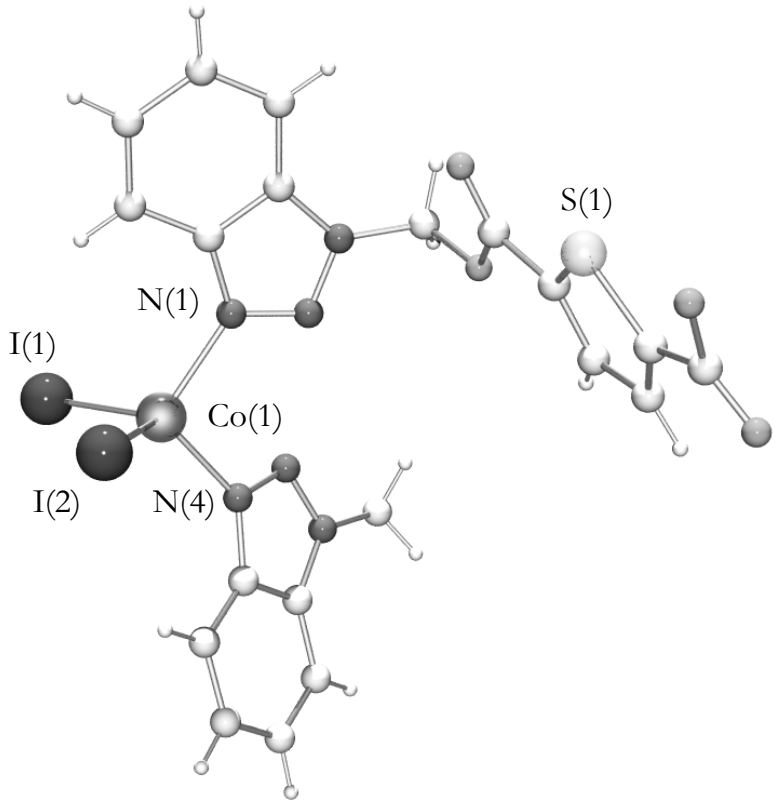

Figure 9: Molecular structure of the asymmetric unit of **7**

The angles N(6)-Co(1)-N(2), N(6)-Co(1)-I(1), N(6)-Co(1)-I(2), N(1)-Co(1)-I(1), N(1)-Co(1)-I(2), I(1)-Co(1)-I(2) (103.55(14), 106.20(10), 116.79(10), 112.04(10), 106.51(10), 111.57(2)°, respectively) are not far from the ideal

tetrahedral angles. The two cobalt-nitrogen bonds [Co(1)-N(1) 2.035(4), Co(1)-N(2) 2.020(3) Å] and the two cobalt-iodine bonds [Co(1)-I(1) 2.5563(7), Co(1)-I(2) 2.5714(7) Å] are almost equal in length and are comparable to those found for complex **6**.

3.3.2 Rhodium(I) and Iridium(I) Complexes

Ligand **4** was also found to coordinate easily to rhodium through the 3-N atom of the benzotriazole unit. The rhodium(I) complex is directly obtained from $[Rh(CO)_2Cl]_2$ and **4** using a 1 : 2 ratio in diluted solution of toluene at room temperature, in order to avoid the formation of polynuclear species, as in the case of complex **7**. Complex $[Rh(\mathbf{4})(CO)Cl]_2$ (**8**) is obtained as an air-stable yellow solid (Scheme 24).

Micro-analytical and NMR data are consistent with the composition proposed, the dimeric nature of the molecule clearly follows from the ESI mass spectrum which shows the molecular peak at m/z 1220. The highest mass ion corresponds to $[Rh(\mathbf{4})(CO)Cl]_2$ and related dinuclear and mononuclar fragments are observed. By preparative TLC, complex **8** separates into two isomers, the major isomer (**8a**) eluting as a brown band and the minor isomer (**8b**) eluting as a yellow band. On the basis of the infrared spectra, **8a** can be identified as *cisoid*-$[Rh(\mathbf{4})(CO)Cl]_2$, giving rise to two ν(CO) absorptions at 2086 cm^{-1} and 2013 cm^{-1}, while **8b** shows only one ν(CO) absorption at 1992 cm^{-1} characteristic for *transoid*-$[Rh(\mathbf{4})(CO)Cl]_2$.

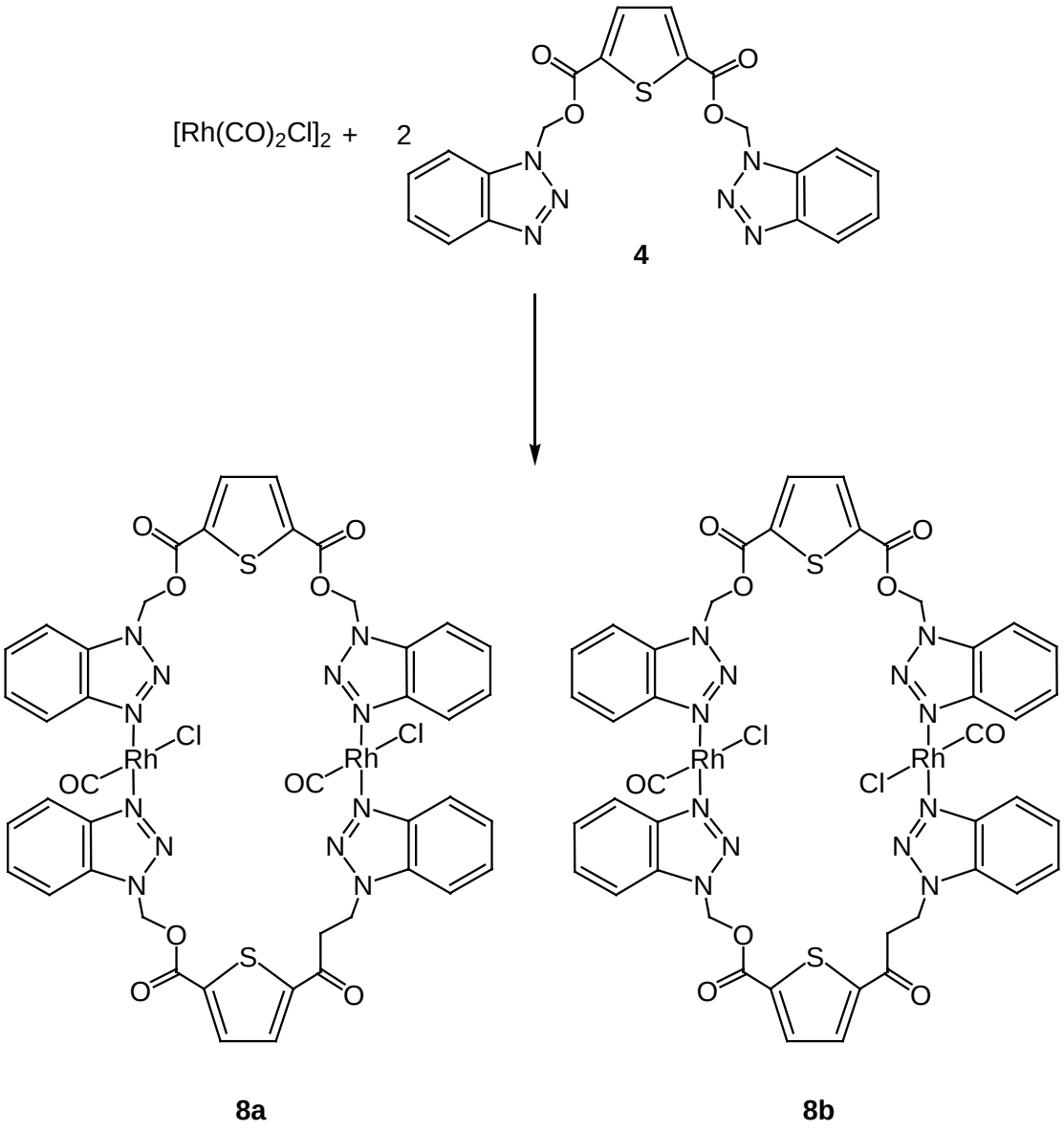

Scheme 24: Synthesis of **8a** and **8b**

The yellow color is indicative of square-planar, noninteracting rhodium centers.[175] Macrocycles of similar types have been reported for rhodium, $Rh_2[Ph_2P(CH_2)P(S)Ph_2]_2(CO)_2Cl_2$,[176] $Rh_2[(Ph_2P)_2py]_2(CO)_2Cl_2$,[177] but never used as catalysts. The coordination of ligand **4** in complex **8** can be deduced from the chemical shift differences of the methylene protons of the benzotriazole unit (δ = 7.09 ppm) by comparison to the free ligand (δ = 6.99 ppm). The symmetric

square-planar geometry is clear from the equivalency of the hydrogen atoms (Figure 10).

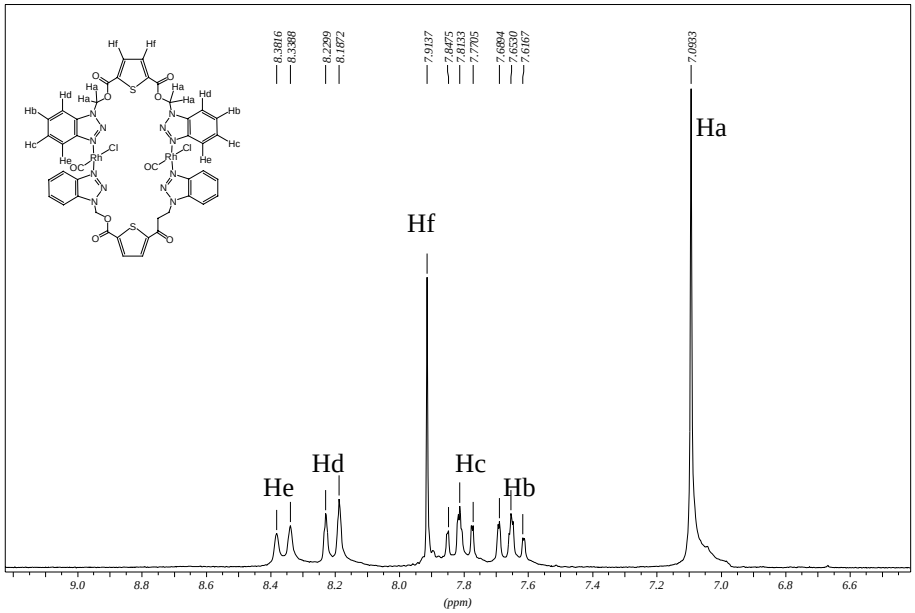

Figure 10: ^{1}H NMR spectrum of **8a**

The iridium complex $[Ir(cod)Cl]_2$ reacts analogously with two equivalents of **4** in refluxing toluene under carbon monoxide to give $[Ir(\mathbf{4})(CO)Cl]_2$ (**9**) as orange solid (Eq. 9). The infrared spectrum of **9** reveals also two strong ν(CO) absorptions at 2074 cm^{-1} and 1994 cm^{-1}, suggesting a *cisoid* arrangement of the carbonyl ligands. The ^{1}H, ^{13}C NMR and MS spectra are in accordance with **9** being *cisoid*-$[Ir(\mathbf{4})(CO)Cl]_2$.

$$\tfrac{1}{2}\,[Ir(cod)Cl]_2 \;+\; \mathbf{4} \xrightarrow{+\,CO} \tfrac{1}{2}\,[Ir(\mathbf{4})(CO)Cl]_2 \qquad (9)$$

The phosphine-containing ligand **5** (4 equivalents) reacts with $[Rh(CO)_2Cl]_2$ in dichloromethane to give the mononuclear complex *trans*-$Rh(C_6H_4N_3CH_2CO_2C_6H_4PPh_2)_2(CO)Cl$ **10** in high yield (Scheme 25).

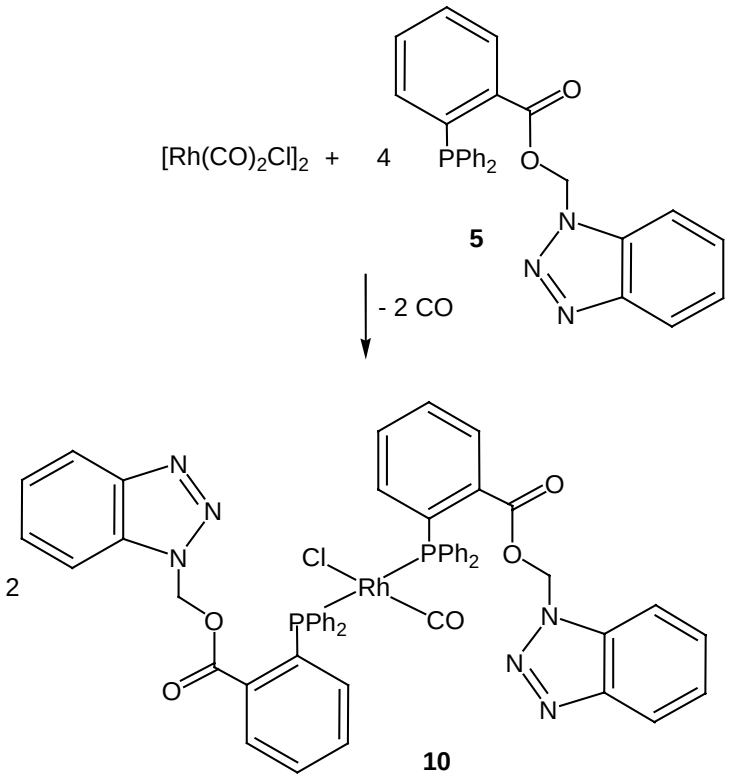

Scheme 25: Synthesis of **10**

The product is easily isolated by evaporation of the solvent and by washing of the residues with ether. The η^1-coordination, as well as the symmetric nature of the complex **10**, is reflected in the ^{31}P NMR spectra. As shown in Figure 11, the phosphorus atom displays a resonance at δ=33.7 as a doublet with a $^1J_{P\text{-}Rh}$ coupling constant near the expected value of 136 Hz.[178,179] Compared with the free ligand, the ^{31}P NMR signal is shifted about 40 ppm to lower field, which is typical for a η^1-coordinated phosphine.[178] The presence of the carbonyl ligand can be seen by ^{13}C NMR spectroscopy. Thus, in a typical chemical shift range of 188 ppm, the carbonyl carbon appears as a doublet of triplets with characteristic coupling constants of 65 Hz [$^1J_{C\text{-}Rh}$] and 22 Hz [$^2J_{P\text{-}C}$].[180] Furthermore, the triplet splitting indicates the presence of two magnetically equivalent phosphorus nuclei.

Final structural proof was obtained by an X-ray crystal-structure analysis of complex **10**. Its structure in the solid state is depicted in Figure 12.

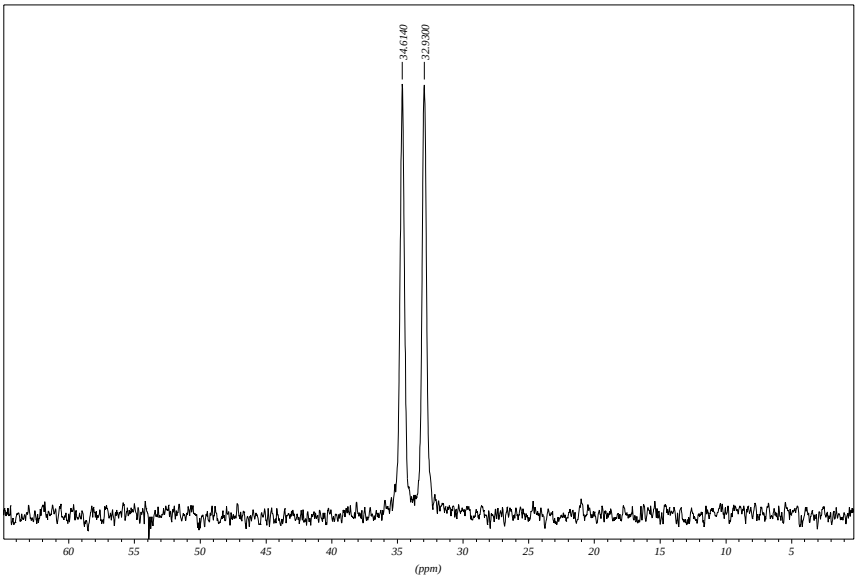

Figure 11: ^{31}P NMR spectrum of **10**

The single-crystal X-ray structure analysis of **10** shows the rhodium atom carrying two monophosphine ligands in *trans* position, one carbonyl ligand and one chloride. The metal atom is in a square-planar environment and the two Rh-P lengths of 2.32 Å (Table 7) compare well with the analogous triphenylphosphine complex.[181-183] The least square planes of the benzotriazole rings are tilted towards the Rh-P-CO-P-Cl least square plane by 71.2°.

Table 7: Selected bond lengths [Å] for complex **10**

P(1)-Rh(1)	2.3223(6)	C(27)-Rh(1)-Cl(1)	178.2(2)
C(8)-O(1)	1.205(3)	P(1a)-Rh(1)-C(27)	91.1(3)
C(27)-O(3)	1.190(7)	C(27)-Rh(1)-P(1)	88.9(3)
		P(1)-Rh(1)-Cl(1)	88.62(7)
		Cl(1)-Rh(1)-P(1a)	91.38(7)

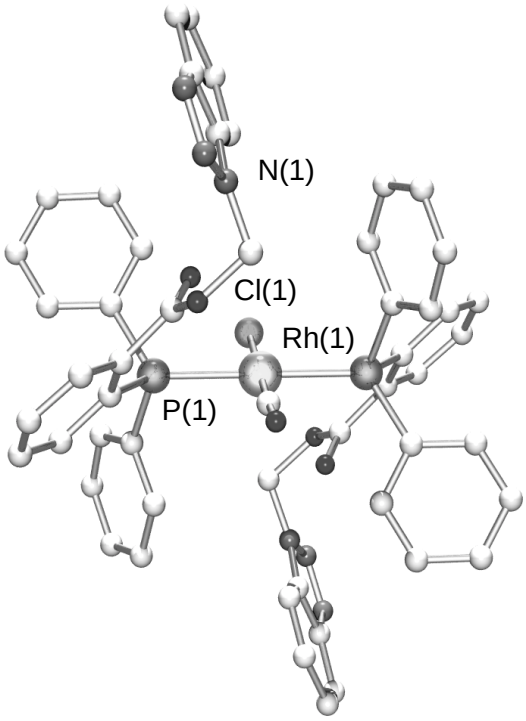

Figure 12: Molecular structure of **10**

The infrared stretching frequency of the CO ligand in *trans*-[$RhL_2(CO)Cl$] complexes is an ideal probe for determining the electronic properties of such a ligand. In analogy to the [$NiL(CO)_3$] complexes of Tolman,[184] a lower CO stretching frequency for a *trans*-[$RhL_2(CO)Cl$] complex corresponds to a enhanced electron density at the rhodium center and, hence, to a stronger σ-bonding of the ligand L.[185] Since monocarbonyl complexes provide easy-to-interpret infrared spectra with a single carbonyl band, complexes of this type have found wide application as probes for the electronic properties of donor ligands.[185]

The extensive literature available[186,187] allows a rapid evaluation of the electronic properties of a new ligand. Thus, for **10** the CO band is detected at 1949 cm^{-1}, which is about 16 cm^{-1} lower in energy than that of the triphenylphosphine complex $Rh(PPh_3)_2(CO)Cl$,[188] but 7 cm^{-1} higher in energy

than that of $Rh(PR_2R')_2(CO)Cl$ (R = N-pyrrolidinyl, R' = *tert*-butyl),[188] containing a very electron-rich phosphine ligand (Table 8). The ν(CO) value for **10** is significantly lower than those of most electron-rich alkylphosphine complexes $Rh(PR_3)_2(CO)Cl$ (R = Me: ν(CO) 1960, R = Et: ν(CO) 1956), which are often applied in catalysis. Tri-*tert*-butylphosphine, which is generally thought of as one of the most electron donating phosphines, actually forms a tetrahedral complex $Rh(P^tBu_3)_2(CO)Cl$ and can not be directly compared.[189]

Table 8: Comparison of IR data of *trans*-$[RhL_2(CO)Cl]$ complexes

Entry	Ligand	ν(CO) (cm^{-1})	Reference
1	P(*N*-pyrrolyl)$_3$	2023	188
2	$(PhO)_3P$	2016	190
3	Ph_3P	1965	191
4	$PhMe_2P$	1965	192
5	Me_3P	1960	191
6	Et_3P	1956	193
7	Cy_3P	1943	194
8	P(*N*-pyrrolidinyl)$_3$	1951	195
9	**5**	1949	This work
10	Bu^tP(*N*-pyrrolidinyl)$_2$	1942	195

Given this comparison, the phosphine **5** can be considered as a strong donor ligand. Moreover, the overall structural features of **10** being as expected (square planar coordination, *trans* diphosphine configuration), the bond lengths involving the rhodium atom are of particular interest. A comparison of bond lengths in **10** to those of other *trans*-$Rh(PR_3)_2(CO)Cl$ structures[194] shows that **10** has the shortest Rh-C carbonyl bond [1.722(7) Å] observed for this type of

complexes. Although the differences in bond lengths are small, these trends are consistent for all of $Rh(PR_3)_2(CO)Cl$ complexes structurally characterized.

The short Rh-C bond in **10** is consistent with the low-energy ν(CO) absorption in the infrared spectrum. Since the phosphine ligand **5** is electron-rich and therefore a good σ-donor ligand, the structure of **10** suggests that the long Rh-P distance may result from a reduced π-back-bonding from rhodium to phosphorus. The good σ-donor and poor π-acceptor character of ligand **5** is also reflected in the length of the rhodium-chlorine bond. As the rhodium atom has a 16 electron configuration, the reduced electron density at the metal is compensated in such complexes by enhanced donation of electrons from the chlorine lone pairs,[196] which causes in general a shortening of the Rh-Cl bond. However, since **5** is a good σ-donor ligand, the Rh-Cl bond [2.391(2) Å] in **10** is longer than in $Rh[P(N\text{-pyrrolyl})_3]_2(CO)Cl$ [2.350(4) Å] and comparable to that of $Rh(P^tBu_3)_2(CO)Cl$ [2.389(2) Å]. The Rh-C distance [1.722(7) Å] in **10** is shortened due to enhanced π-back-bonding to the carbonyl, as demonstrated by the carbonyl stretching frequency at 1949 cm^{-1}. Hence, ligand **5** compares to tri-*tert*-butylphosphine and not to triphenylphosphine as far as its donor/acceptor properties are concerned.

3.4 Catalytic Potential

3.4.1 Carbonylation of Methanol

The first methanol carbonylation process used cobalt catalysts, but required high temperatures and pressures, while rhodium or iridium catalysts are

more selective and operate under much milder conditions. However, because of the significantly lower cobalt prices, cobalt-based catalysts could be interesting, if activity and selectivity can be increased by suitable ligands.

For this reason, we tested ligands **2** and **4** in combination with CoI_2 for the catalytic carbonylation of methanol to give acetic acid and methyl acetate in the presence of methyl iodide and water. The reaction was carried out at 170°C under a CO pressure of 22 bar, the catalyst/substrate ratio being 1 : 2000. After 20 minutes, the reaction was interrupted, and the products were analyzed by GC. The results are presented in Table 6. The complexes **6** and **7** are formed *in situ* on mixing $[Rh(CO)_2Cl]_2$ with two equivalents of **2** and **4** in methanol. As control experiments, the catalytic reaction was carried out with cobalt(II) iodide and with the Monsanto catalyst $[Rh(CO)_2I_2]^-$, also formed *in situ* from $[Rh(CO)_2Cl]_2$ under the reaction conditions.[102] For entries 3 and 4 the conversion of methanol was greater than 98% and the selectivity for acetic acid was greater than 90%.

GC analysis of the liquid phase at the end of the reactions shows that the major product is methyl acetate, although acetic acid is also formed, the catalytic system containing water. As evidenced by Table 9, the catalytic activity increases in the presence of the nitrogen-containing ligands, **4** being the more active one (entry 4). We observed no induction period for the initial phase of the reaction, which explains the higher TOF obtained with N-donors cobalt systems after 20 minutes. If the catalytic reaction is prolonged for 1h, the two cobalt systems become slower than the rhodium system ($[Rh(CO)_2Cl]_2$: TOF 1211 h^{-1}; CoI_2/**2**:

TOF 914h^{-1}; CoI_2/**4**: TOF 1077 h^{-1}). In conclusion, the cobalt-based catalysts give activities comparable to those of the rhodium analogue only during a short period.

Table 9: Methanol carbonylation data[a]

Entry	Precursor	Ligand	TON[b]
1	CoI_2	-	312
2	$[Rh(CO)_2Cl]_2$	-	405
3	CoI_2	**2**	433
4	CoI_2	**4**	512

[a] Catalytic conditions: $[Rh(CO)_2Cl]_2$ or CoI_2 (57 µmol), ligand (0.24 mmol, 2 eq), CH_3OH (110.2 mmol), CH_3I (11.4 mmol), H_2O (81.9 mmol), 170 °C, 22 bar, 900 rpm, 20 min
[b] mol CH_3OH converted into CH_3COOH and CH_3COOCH_3 per mol catalyst precursor

GC analysis of the liquid phase at the end of the reactions shows that the major product is methyl acetate, although acetic acid is also formed, the catalytic system containing water. As evidenced by Table 9, the catalytic activity increases in the presence of the nitrogen-containing ligands, **4** being the most active one (entry 4). We observed no induction period for the initial phase of the reaction, which explains the higher TOF obtained with N-donors cobalt systems after 20 minutes. If the catalytic reaction is prolonged for 1h, the two cobalt systems become slower than the rhodium system ($[Rh(CO)_2Cl]_2$: TOF 1211 h^{-1}; CoI_2/**2**: TOF 914 h^{-1}; CoI_2/**4**: TOF 1077 h^{-1}). In conclusion, those cobalt-based catalysts give activities comparable to those of the rhodium analogue only during a short period.

The nitrogen-containing ligands **2**, **4** and **5** have also been tested in combination with $[Rh(CO)_2Cl]_2$ and $[Ir(cod)Cl]_2$. As for the cobalt systems, the

reactions were carried out at 170°C under a CO pressure of 22 bar, the catalyst/substrate ratio being 1 : 2000. After 20 minutes, the catalytic turnover number is found to be higher for all nitrogen-containing ligands system than for the Monsanto catalyst. Surprisingly, the most active combination is $[Rh(CO)_2Cl]_2$/ **4**, even though the difference with $[Rh(CO)_2Cl]_2$/**5** is not significant (Table 10).

Table 10: Methanol carbonylation data[a]

Entry	Precursor	Ligand	TON[b]
1	$[Rh(CO)_2Cl]_2$	-	405
2	$[Rh(CO)_2Cl]_2$	**2**	430
3	$[Rh(CO)_2Cl]_2$	**4**	780
4	$[Rh(CO)_2Cl]_2$	**5**	770
5	$[Ir(cod)Cl]_2$	**-**	250
6	$[Ir(cod)Cl]_2$	**2**	307
7	$[Ir(cod)Cl]_2$	**4**	323
8	$[Ir(cod)Cl]_2$	**5**	318

[a] Catalytic conditions: $[Rh(CO)_2Cl]_2$ or $[Ir(cod)Cl]_2$ (57 µmol), ligand (0.24 mmol, 4 eq), CH_3OH (110.2 mmol), CH_3I (11.4 mmol), H_2O (81.9 mmol), 170 °C, 22 bar, 900 rpm, 20 min
[b] mol CH_3OH converted into CH_3COOH and CH_3COOCH_3 per mol catalyst precursor

3.4.2 Complex Isolation from Catalytic Mixtures

From the reaction mixture of the catalytic reaction, we isolated the red-brown complex **11** by crystallisation of the organometallic residue from acetone. **11** is directly accessible in high yield from the reaction of **8** with methyliodide and carbon monoxide (1 bar) in acetone solution. **11** contains iodo ligands and *transoid* dicarbonyl motives, giving rise to a single ν(CO) absorption in the infrared spectrum. It was suggested for complexes containing phosphine ligands that the

dissociation of the phosphine may have occured during the catalytic process. In our case there is clearly a Rh-N bond cleavage. The facile conversion of **8** into **11** under ambient conditions demonstrates that fragmentation, ligand dissociation and rearrangement are readily occuring.

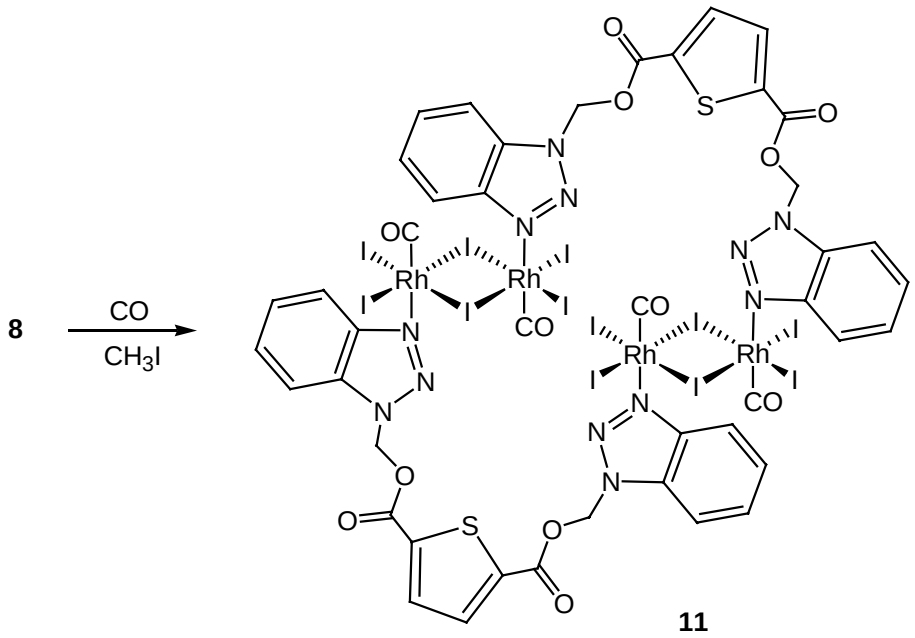

Scheme 26: Synthesis of **11**

In the single-crystal X-ray structure analysis, complex **11** turns out to be a macrocycle containing two dinuclear iodo-bridged Rh(III) units (Scheme 26). In **11**, the four rhodium atoms have a distorted octahedral coordination geometry, they are coordinated by the 3-N atoms of the benzotriazole units of **4** (Figure 13). The four rhodium-nitrogen bonds are almost equal in length. The two planar $Rh_2(\mu_2\text{-}I)_2$ rings are arranged perpendicular with respect to the cycle formed by the four rhodium atoms and the two ligands, Rh(1)-**4**-Rh(2)-Rh(3)-**4**-Rh(4). The bond distances and angles for each Rh_2I_6 unit are similar to those reported by Forster[197] for $[(MeCO)_2Rh_2(CO)_2I_6]^{2-}$ and by Dilworth[198] for $Rh_2(Ph_2PC_6H_4SMe)_2I_6$.

In contrast to the rhodium(I) macrocycle **8**, the rhodium(III) macrocycle **11** does not catalyse itself the carbonylation of methanol: the low catalytic activity observed (TON 100 after 20 min, TOF 5 min^{-1}) when **11** is used as the catalyst precursor is due to a partial decomposition of **11** to give $[Rh(CO)_2I_2]^-$. This is in line with what has been observed for other iodo-bridged dirhodium(III) complexes.[199] Nevertheless, it has also been shown that iodo-bridged dinuclear complexes can be formed and isolated in solid state. These evolve to mononuclear $[Rh(CO)_2I_3]^{2-}$ under CO or $[(COCH_3)Rh(CO)I_3]^-$ under catalytic conditions.

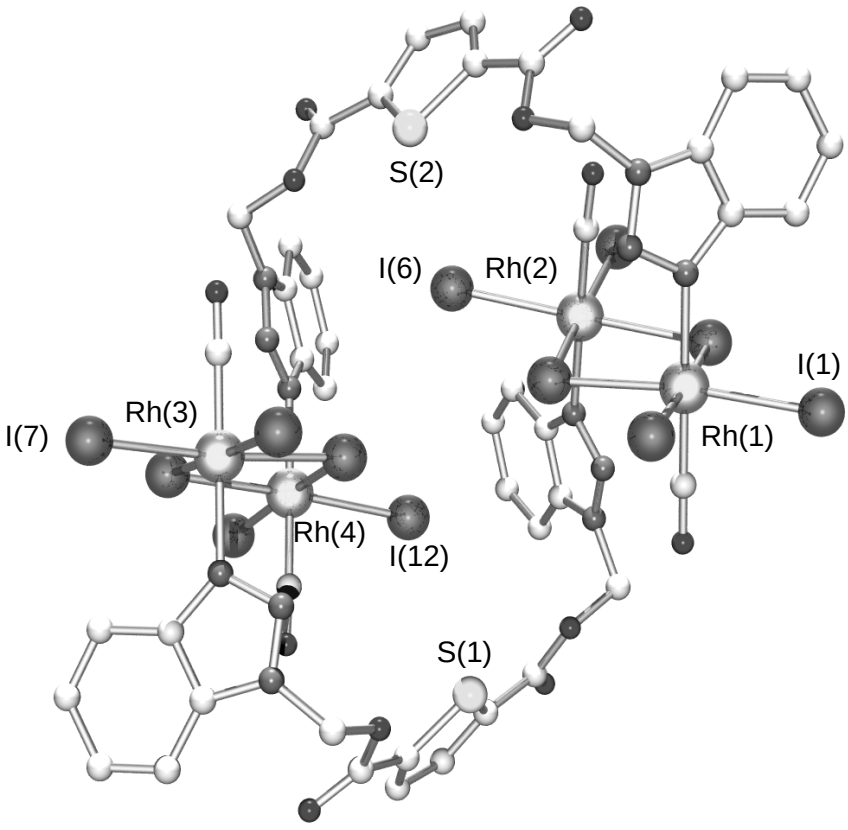

Figure 13: Molecular structure of **11**

3.5 Conclusion

The aim of this work was the synthesis of new nitrogen-donor ligands and

to study their ability to coordinate as ligand to transition metals. A high-yield route was developed to synthesize different ester derivatives of benzotriazole. The coordination chemistry of these multifunctional ligands studied with Rh(I) and Co(II) centers shows that all the ligands are modentate using the 3-N atom of the benzotriazole unit for coordination, except for **5** which is bound by the phosphorus atom. Nevertheless, there is no interaction between the oxygen atom of the ester function and the metal center.

To the best of our knowledge, **8** is the first macrocyclic dirhodium complex involved in the carbonylation of methanol. It is possible that the better catalytic performance of **8** with respect to that of the classical species $[Rh(CO)_2I_2]^-$ is due to its macrocyclic nature. Moreover, the macrocycle **8** has a relatively open cavity and should be able of binding a second, different metal in this cavity, which should act as a promoter (simple iodide complexes or carbonyl-iodide complexes). Since **5** contains nitrogen atoms in the benzotriazol unit, it may be possible to use **5** for the build-up of multinuclear complexes and to investigate its behavior towards different known promoters in methanol carbonylation.

Chapter 4

New Phosphinodithioic Ester Ligand: Synthesis, Coordination, Catalytic Properties

The organic chemistry of phosphinodithioate (**A**) and phosphorodithioate (**C**) derivatives is well developed,[200,201] complexes with platinum-group metals are also known.[202] In most of these complexes, phosphinodithioates and phosphorodithioates act as chelating ligands.[203] However, synthetic routes to phosphonodithioates (**B**) are scarce,[204] consequently the coordination chemistry of phosphonodithioates is hardly explored, although molecules of type **B** are the most interesting ones for coordination, since it is much easier to introduce different substituents than in molecules of type **A** and **C** (Scheme 27).

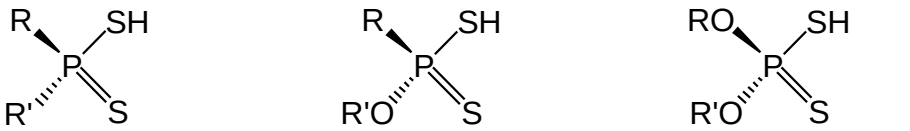

A
Phosphinodithioic acid

B
Phosphonodithioic acid
(O-esters)

C
Phosphorodithioic acid
(O,O'-diesters)

Scheme 27: Dithiophosphorus derivatives used as ligand

To date, no rhodium(I) complex containing phosphonodithioate ligands (derived from **B**) is known. It would be interesting to study complexes of this type, in particular with respect to their catalytic potential for the carbonylation of methanol.

4.1 Sulfur-Containing Ligands in Catalysis

As in other metal-catalyzed processes, the catalytically active complexes involved in the carbonylation of methanol are 16-electron species, which exhibit more reactive properties but also need to be stabilized. Lone-pair electrons on a ligator atom may by π-donation compensate the electron deficiency of the metal center in a 16-electron species. Sulfur-containing ligands possess, apart from σ-donor orbital, also lone-pair electrons in orbitals of correct symmetry for π-interaction with a metal d orbital. In fact, sulfur ligands have been shown to stabilize coordinatively unsaturated complexes (Scheme 28). Thus, Kalck *et al.*[205] reported the use of rhodium thiolates as hydroformylation catalysts. Also fluorothiolate and aminothiolate rhodium complexes are reported to catalyse the hydroformylation of olefins under mild conditions of pressure and temperature.[206]

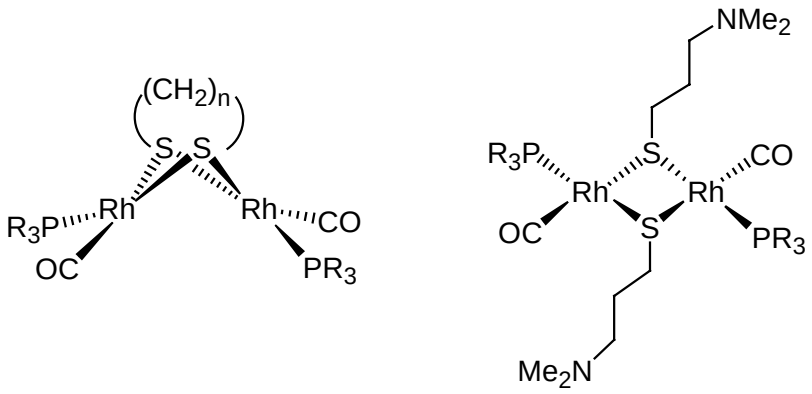

Scheme 28: Examples of dirhodium μ-thiolato used as catalyst precursor in the hydroformylation of olefins

Although thiolate complexes of Rh(I) and Ir(I) with tertiary phosphine co-ligands are well documented, most of them are di- or multinuclear containing bridging thiolates, but mononuclear Rh(I) or Ir(I) complexes are scarcely

known.[207] On the other hand, it has been shown by Eisenberg *et al.*,[208] that dinuclear rhodium(I) carbonyl complexes bearing dithiolate ligands are reactive towards primary alkyl iodides to give stable dinuclear rhodium(III) acetyl complexes, which ressemble monuclear intermediates in the carbonylation of methanol.

The chemistry of rhodium and iridium complexes with mixed phosphorus-sulfur chelating ligands is less well explored.[209] Complexes of the type M(η^2-$SCH_2CH_2PPh_2$)(PPh_3)(CO) (M = Rh, Ir) are accessible from the corresponding fluoro derivative and the phosphinothiol (Scheme 29). Very recently, Kang *et al.* described new phosphinothiolato ligands which coordinate to rhodium(I) to give active catalysts for the carbonylation of methanol.[210]

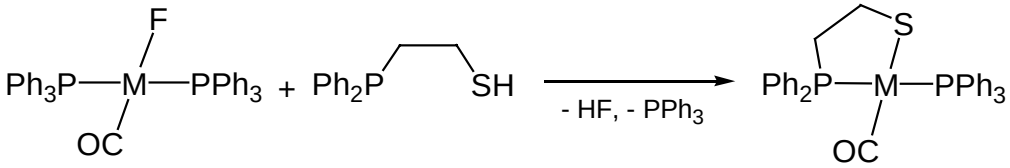

Scheme 29: Example of phosphinothiolato rhodium and iridium complexes

Prompted by the increasing success of sulfur-containing complexes in catalysis, we thought it would be interesting to study the coordination behavior of phosphinodithioates and the catalytic properties of the complexes obtained.

4.2 Ligand Synthesis

Phosphonodithioate syntheses from organophosphanyl chlorides or from P_4S_{10} involve several laborious reaction steps.[211] A new multi-steps synthesis of phosphonodithioic acid derivatives has been developed by Martin *et al.*, involving

the use of the appropriate Grignard reagent and 2-chloro-1,3,2-dithiaphospholane (Scheme 30).[212]

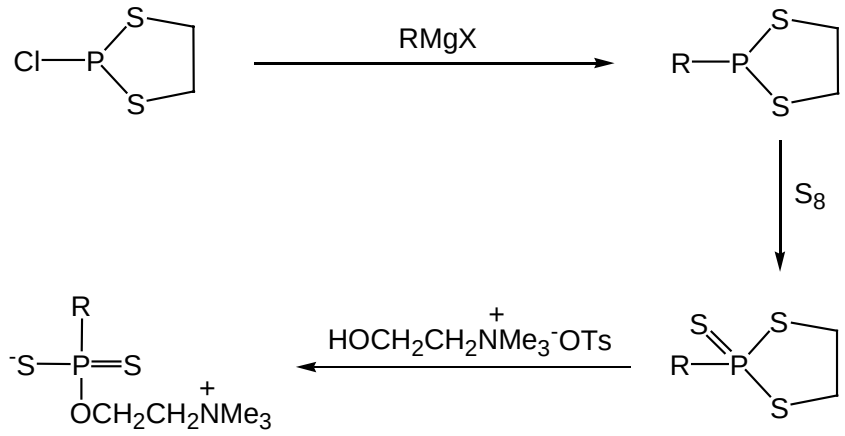

Scheme 30: General route to phosphonodithioic acid derivatives developed by Martin

Under the appropriate conditions, 1,3-dithia-2,4-diphosphetane 2,4-disulfide derivatives can give a ring opening, as shown for the well-known Lawesson's reagent.[213] For this reason, we decided to use the ferrocene derivative of Lawesson's reagent recently reported by Woollins *et al.*[214] for the synthesis of phosphonodithioates by ring opening with NEt_3.

4.2.1 Preparation and Characterization

The reaction of the ferrocene derivative of Lawesson's reagent $[(C_5H_5)Fe(C_5H_4)]_2P_2S_4$ with hydroxymethylbenzotriazole leads, in the presence of triethylamine, to the formation of the anion $[(C_5H_5)Fe(C_5H_4PS_2OCH_2C_6H_4N_3]^-$ (**12**) which is obtained as the yellow triethylammonium salt (Scheme 31).

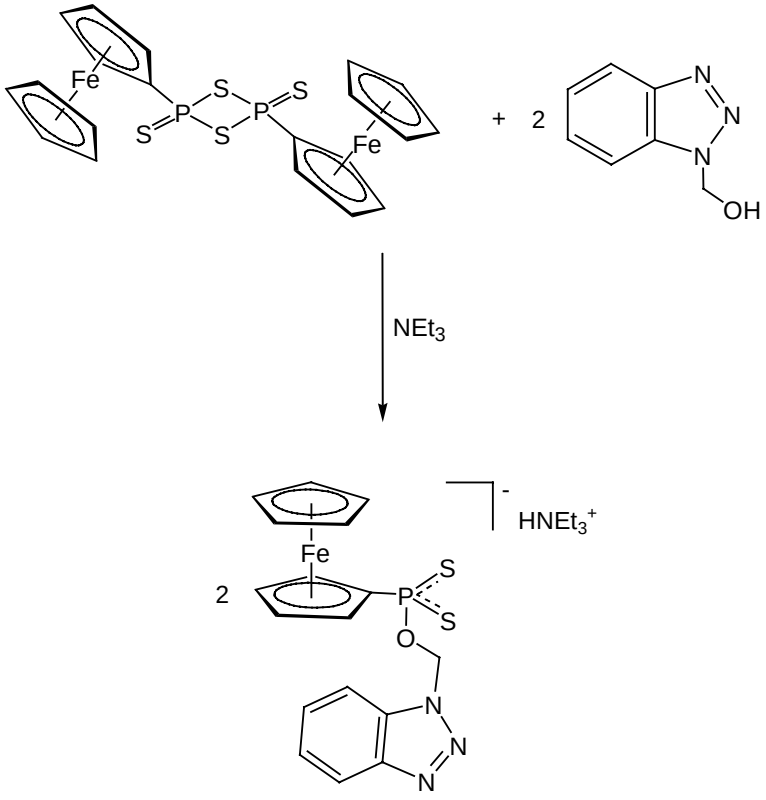

12

Scheme 31: Synthesis of **12**

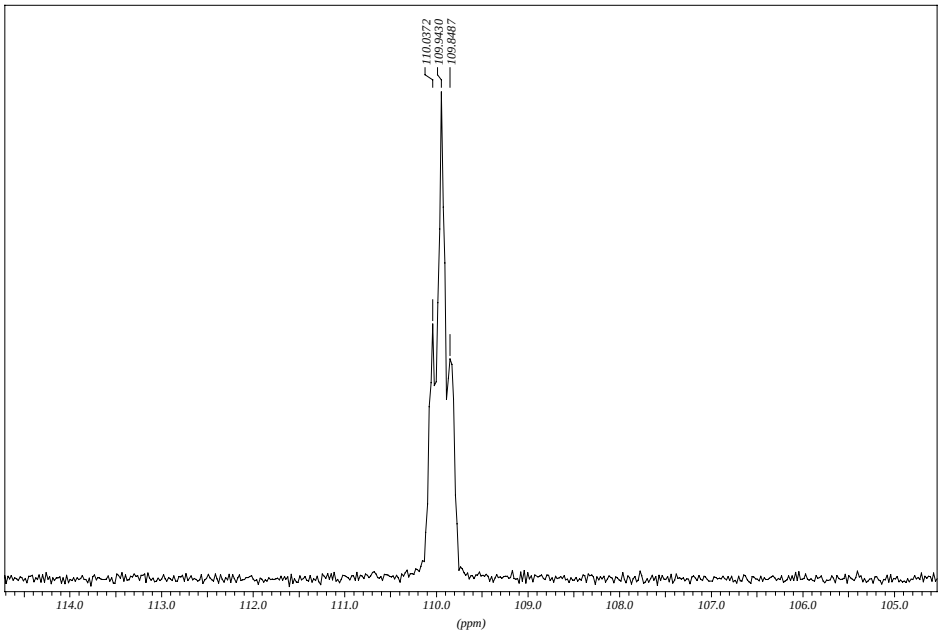

Figure 14: ^{31}P NMR spectrum of **12**

The phosphorus atom of the OPS_2 moiety in **12** gives rise to a signal at 110.2 ppm in the ^{31}P NMR spectrum (Figure 14), which is a triplet due to the coupling with the methylene hydrogen atoms of the benzotriazole unit. The ^{1}H NMR spectrum (Figure 15) of the triethylammonium salt of **12** shows the expected signals for the ferrocenyl and the benzotriazol groups, the signal of the methylene protons (δ = 6.5 ppm) shows up as a doublet because of the coupling with the phosphorus atom ($^{3}J_{H\text{-}P}$ = 8.5 Hz).

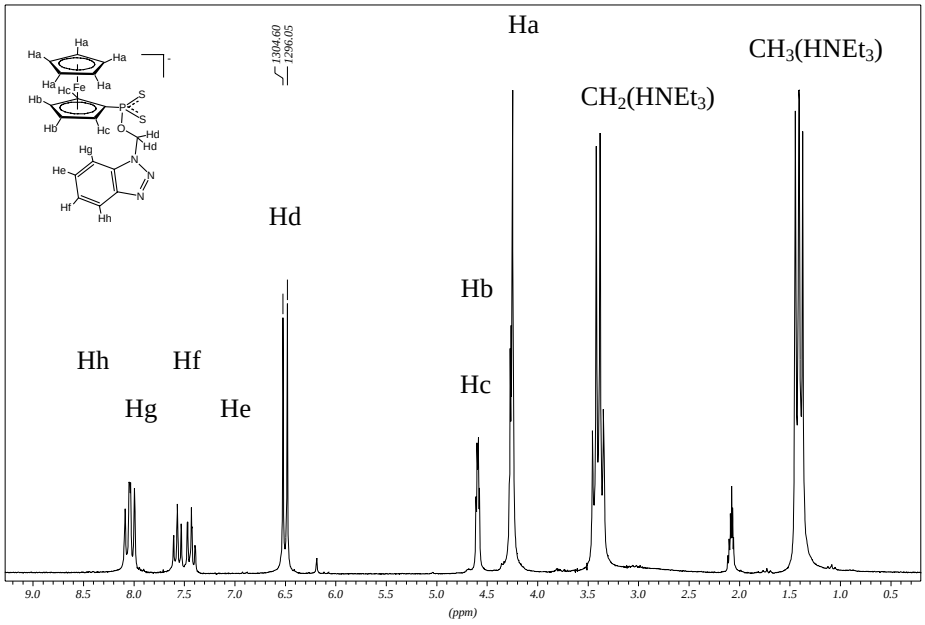

Figure 15: ^{1}H NMR spectrum of **12**

The IR, ^{13}C and MS spectra of **12** are as expected, the spectroscopic data are given in the experimental section.

4.2.2 X-Ray Crystal Structure Analysis

The single-crystal X-ray structure analysis of the triethylammonium salt of **12** reveals a distorted tetrahedral geometry of the phosphorus atom. The two PS bonds are equal in length [P(1)-S(1) 1.9739(10), P(1)-S(2) 1.9811(10) Å] and have a

partial π character, in agreement with those found [1.989(1) and 2.000(1) Å] for the amido derivative [^{i}PrNH$_3$][(MeOC$_6$H$_4$)P(^{i}PrNH)S$_2$].[215] The molecular structure of **12** is shown in Fig. 16, important bond lengths and angles are given in Table 11.

Table 11: Selected bond lengths [Å] and angles [°] for [NEt$_3$H]**12**

C(1)-P(1)	1.784(3)	S(1)-P(1)-S(2)	117.29(5)
O(1)-P(1)	1.645(2)	C(1)-P(1)-S(2)	111.90(10)
P(1)-S(1)	1.9739(10)	C(11)-O(1)-P(1)	118.77(18)
P(1)-S(2)	1.9811(10)	O(1)-P(1)-C(1)	96.78(12)
		O(1)-P(1)-S(1)	108.64(9)
		C(1)-P(1)-S(1)	112.06(10)
		O(1)-P(1)-S(2)	108.07(9)

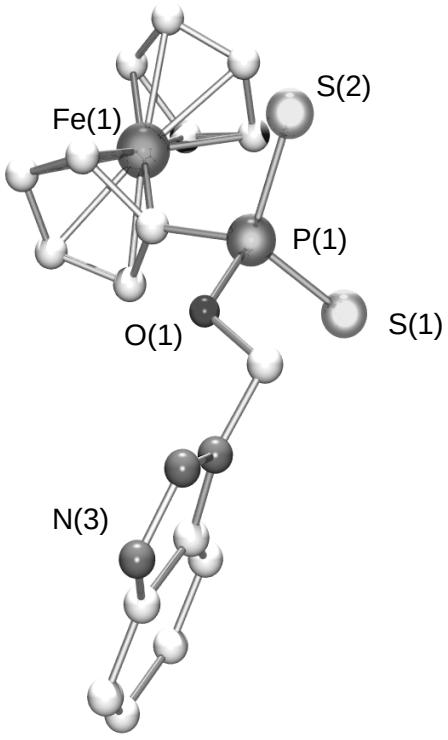

Figure 16: Molecular structure of **12**

4.3 Coordination Chemistry

Since a variety of nickel compounds are catalytically active for the carbonylation of methanol in the presence of iodine, we decided to investigate the coordination behavior of this new ligand not only with rhodium(I) but also with nickel(II) compounds.

4.3.1 Nickel(II) Complexes

Ligand **12** was found to coordinate easily to nickel(II). The nickel complex $Ni[(C_5H_5)Fe(C_5H_4PS_2OCH_2C_6H_4N_3)]_2$ (**13**) is obtained from the room-temperature reaction of **12** with anhydrous nickel(II) chloride in acetonitrile, from which it precipitates quantitatively (Scheme 32). It is soluble in dimethylsulfoxide and is characterized by correct NMR and micro-analytical data. The mass spectrum (electrospray) shows the expected molecular peak at m/z 915.

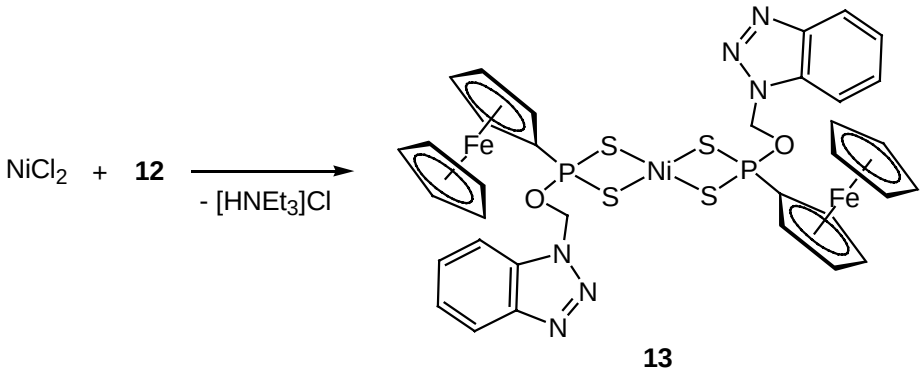

Scheme 32: Synthesis of **13**

Thus, in complex **13** the ligand **12** is coordinated in a bidentate fashion through the two sulfur atoms of the PS_2 moiety and the benzotriazole unit is not bound to the metal. Ligand **12** also reacts with other Ni(II) complexes: The reaction of the tetramethylcyclobutadiene complex $[Ni(C_4Me_4)Cl_2]_2$ with two

equivalents of **12** in dichloromethane gives the nickel complex Ni[(C_5H_5)Fe($C_5H_4PS_2OCH_2C_6H_4N_3$)](C_4Me_4)Cl (**14**) in good yield (Scheme 33). The product is isolated by evaporation of the solvent and washed with ether.

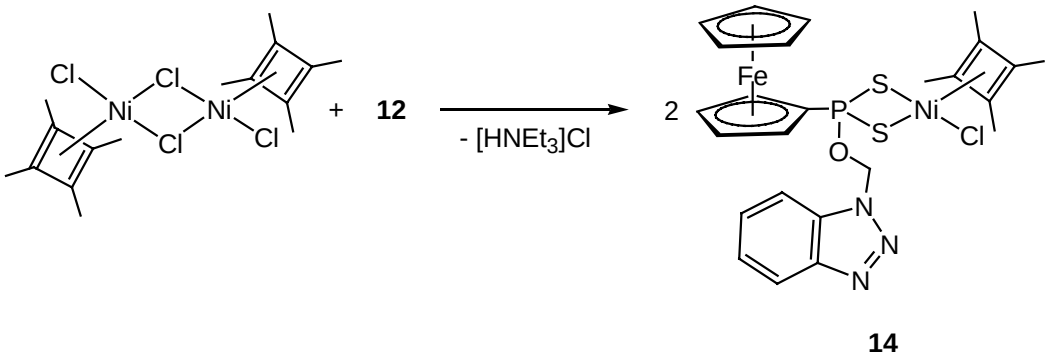

14

Scheme 33: Synthesis of **14**

The coordination of ligand **12** in complex **14** is clear from the chemical shift differences of the phosphorus atom in complex **14** (δ = 104.1 ppm) by comparison to the free ligand (δ = 110.1 ppm). The other analytical data (^{1}H NMR, ^{13}C NMR and MS spectra, microanalysis) are in accordance with the structure proposed.

4.3.2 Rhodium(I) Complexes

Ligand **12** is also found to coordinate to rhodium(I). The phosphonodithioate ligand **12** (2 equivalents) reacts with [Rh(cod)Cl]$_2$ in dichloromethane to give the mononuclear complex Rh[(C_5H_5)Fe($C_5H_4PS_2O$-$CH_2C_6H_4N_3$)](cod) (**15**) in high yield (Scheme 34). Complex **15** shows characteristic doublet resonances in the ^{31}P NMR spectrum (see experimental section) due to coupling of the phosphorus atoms to ^{103}Rh, indicating that **15** is mononuclear in solution.[216] This is in line with the findings for the analogous

dithiocarbamate derivative $Rh(S_2CNMe_2)(CO)_2$.[217] The ^1H NMR, ^{13}C NMR and MS spectra also reflect the structure proposed.

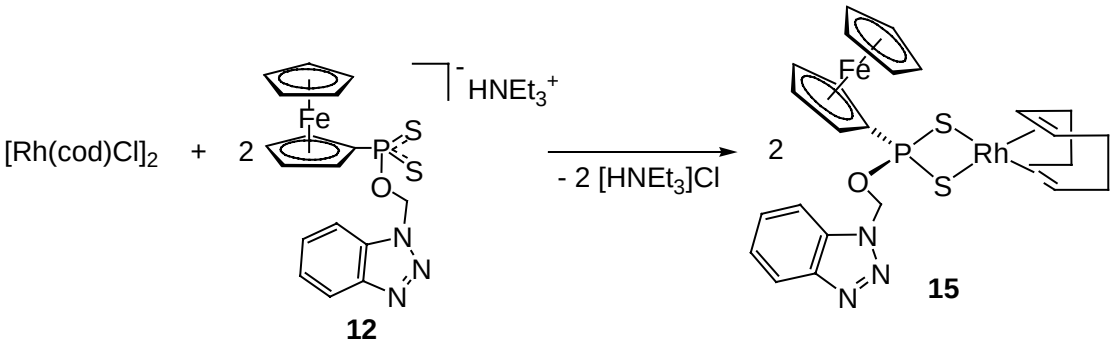

Scheme 34: Synthesis of the neutral complex **15**

The molecular structure of **15** is depicted in Fig. 17, important bond lengths and angles are given in Table 12.

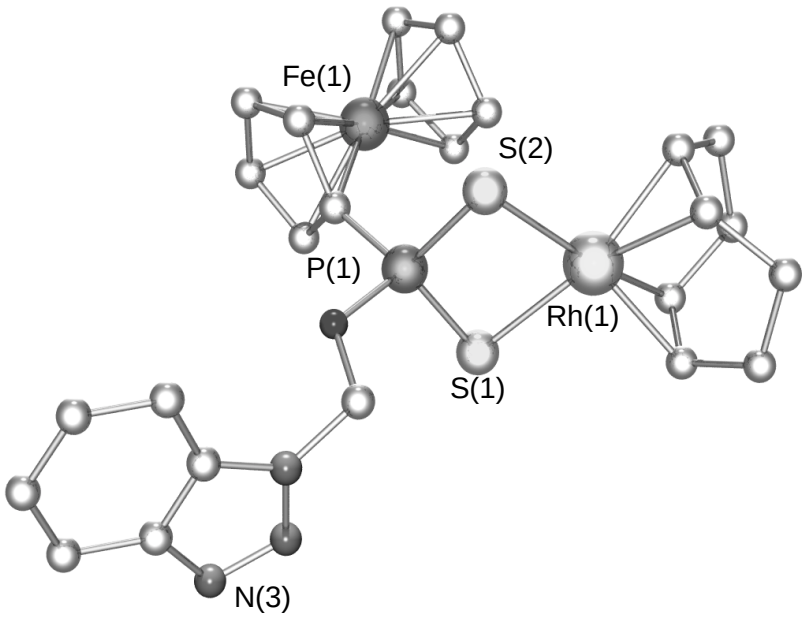

Figure 17: Molecular structure of **15**

The single-crystal X-ray structure analysis of **15** shows that the complex is indeed mononuclear. The metal atom is in a square-planar environment and is

coordinated by the two S atoms of one S,S-bidentate ligand. The two PS bonds are equal in length [P(1)-S(1) 1.991(2), P(1)-S(2) 2.003(2) Å] and have a partial π character; they are, however, longer than in the free ligand **12**.

Table 12: Selected bond lengths [Å] and angles [°] for compound **15**

C(11)-Rh(1)	2.157(6)	P(1)-S(1)-Rh(1)	84.98(7)
C(12)-Rh(1)	2.141(6)	P(1)-S(2)-Rh(1)	83.68(7)
C(15)-Rh(1)	2.159(6)	C(12)-Rh(1)-C(16)	98.6(2)
C(16)-Rh(1)	2.149(5)	C(16)-Rh(1)-C(11)	82.4(2)
O(1)-P(1)	1.609(3)	C(12)-Rh(1)-C(15)	82.4(3)
P(1)-S(1)	1.991(2)	C(11)-Rh(1)-C(15)	90.2(2)
P(1)-S(2)	2.003(2)	C(16)-Rh(1)-S(1)	91.56(18)
S(1)-Rh(1)	2.3817(16)	C(15)-Rh(1)-S(1)	94.8(2)
S(2)-Rh(1)	2.4219(13)	C(12)-Rh(1)-S(2)	93.50(17)
		S(1)-Rh(1)-S(2)	83.47(5)

Carbon monoxide reacts in dichloromethane with **15** to give quantitatively **16**. Similarly, the reaction of $[Rh(CO)_2Cl]_2$ with two equivalents of **12** affords $Rh[(C_5H_5)Fe(C_5H_4PS_2OCH_2C_6H_4N_3)](CO)_2$ (**16**) (Scheme 35). Complex **16** exhibits two strong ν(CO) absorptions in the infrared spectrum, as expected for a *cis*-dicarbonyl arrangement.[218] In the ^1H NMR spectrum (Figure 18) of complex **16**, the coordination of the ligand **12** is clear from the chemical shift differences of the methylene protons of the benzotriazole unit (δ = 6.88 ppm; $^3J_{H\text{-}P}$ = 11.9 Hz) when compared to the same protons of the free ligand (δ = 6.42 ppm; $^3J_{H\text{-}P}$ = 8.5 Hz).

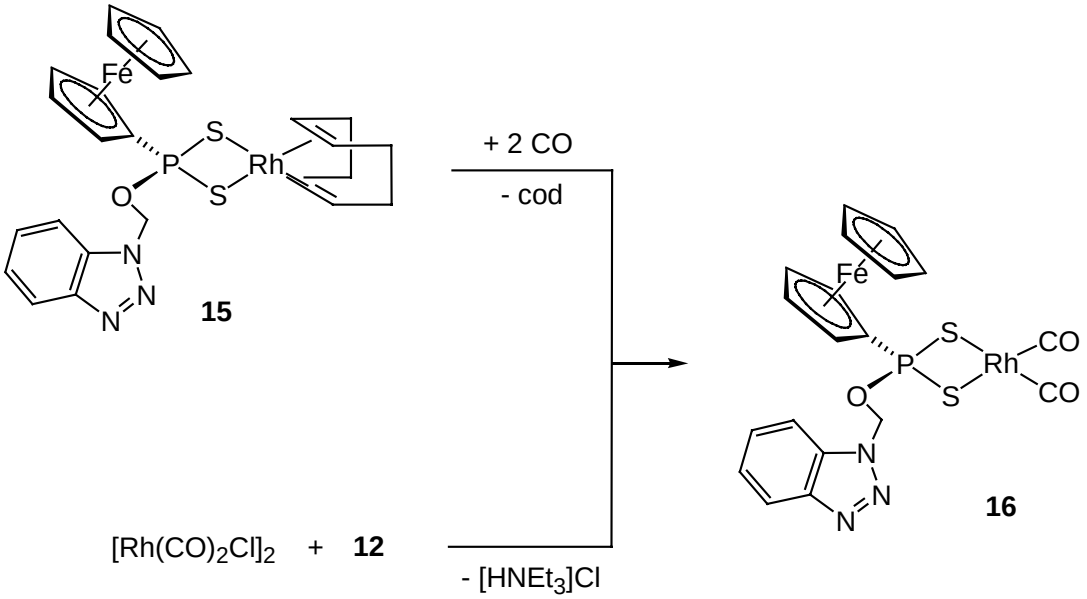

Scheme 35: Synthesis of **16**

The coordination of ligand **12** to the rhodium center is also reflected in the $^{31}P\{^{1}H\}$ NMR spectrum by the presence of a characteristic doublet.[218] The ^{13}C NMR, MS and microanalytical data are also in accordance with the structure proposed.

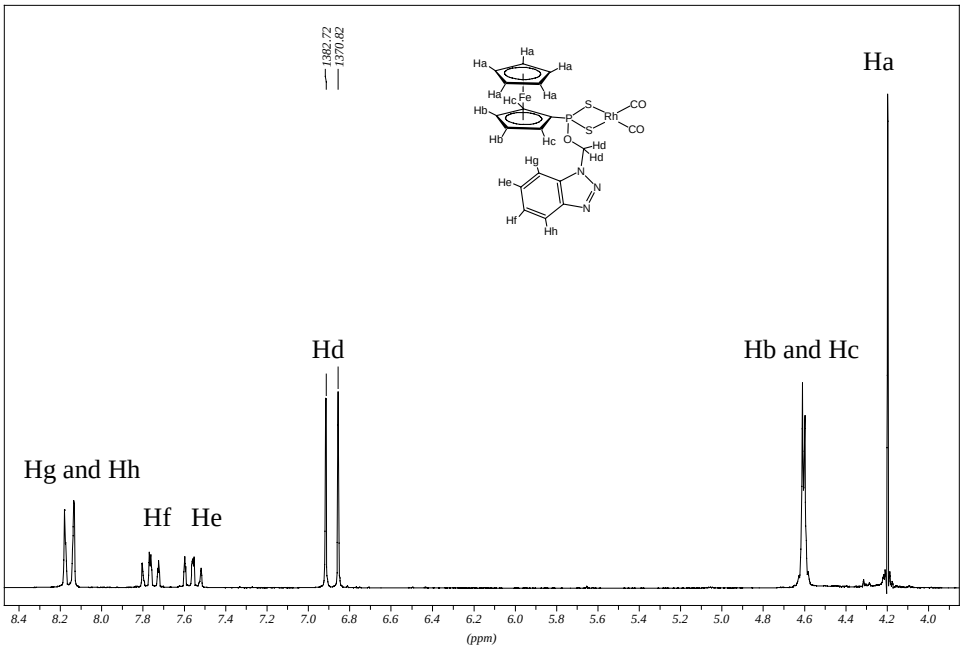

Figure 18: ^{1}H NMR spectrum of **16**

4.4 Catalytic Potential

4.4.1 Carbonylation of Methanol

The anion **12** was used as auxiliary ligand in the rhodium-catalyzed carbonylation of methanol. The catalytic reaction takes place in a mixture of methanol, iodomethane and water under a CO pressure of 22 bar at 170°C. The complex **16** is formed *in situ* on mixing $[Rh(CO)_2Cl]_2$ with two equivalents of **12** in methanol. In each case the conversion of methanol was greater than 98% and the selectivity for acetic acid was greater than 95%.

$$CH_3OH + CO \longrightarrow CH_3COOH$$

$$CH_3COOH + CH_3OH \longrightarrow CH_3COOCH_3 + H_2O$$

The results (Table 13) clearly demonstrate that the combination of rhodium and **12** improves the catalytic performance for the carbonylation of methanol. With respect to the classical Monsanto catalyst (entry 1), the catalytic turnover frequency increases from 16 to 25 min^{-1} by using the combination $[Rh(CO)_2Cl]_2$ / **12** (entry 2). Surprisingly, the combination $[Rh(CO)_2Cl]_2$ / **12** / PPh_3, also catalyzes the carbonylation of methanol under these conditions but it is less active, giving a TOF of only 20 min^{-1} (entry 3).

For a recycling experiment, the orange-red solution obtained after carbonylation reaction was evaporated to dryness under reduced pressure, giving a dark brown solid. With this solid as the catalyst, the catalytic reaction was repeated by maintaining the same experimental conditions as described above. Upon

recycling the catalyst for a second time, almost the same amount of conversion was found, being suggestive of higher catalyst stability.

Table 13: Methanol carbonylation data[a]

Entry	Precursor	Ligand	TON[b]
1	$[Rh(CO)_2Cl]_2$	-	323
2	$[Rh(CO)_2Cl]_2$	**12**	455
3	$[Rh(CO)_2Cl]_2$	**12**, PPh_3	403

[a] Catalytic conditions: $[Rh(CO)_2Cl]_2$ (57 µmol), ligand (0.24 mmol, 4 eq), CH_3OH (110.2 mmol), CH_3I (11.4 mmol), H_2O (81.9 mmol), 170 °C, 22 bar CO, 900 rpm, 20 min
[b] mol CH_3OH converted into CH_3COOH and CH_3COOCH_3 per mol catalyst precursor

In the nickel-catalyzed carbonylation of methanol the activity of nickel catalysts can be increased, and the volatility of nickel carbonyl derivatives can be lowered by the introduction of stabilizing ligands such as phosphines.[38-42] For this reason, we tested ligand **12** in combination with NiI_2 for the catalytic carbonylation of methanol to give acetic acid and methyl acetate in the presence of methyl iodide and water. The results of catalytic carbonylation of methanol are presented in Table 14. For comparison, the catalytic reactions were also carried out with nickel(II) iodide alone and with the Monsanto catalyst $[Rh(CO)_2I_2]^-$, which was formed *in situ* under the reaction conditions.[102]

GC analysis of the liquid phase at the end of the reactions shows that the major product is methyl acetate, although acetic acid is also formed, the catalytic system containing water. As evidenced by Table 14, the catalytic activity of the nickel systems increases in the presence of the sulfur ligand **12**, but $[Rh(CO)_2I_2]^-$ still remains the most active species.

Table 14: Methanol carbonylation data[a]

Entry	Precursor	Ligand	TON[b]
1	NiI_2	-	150
2	NiI_2	**12**	281
3	$[Rh(CO)_2Cl]_2$	-	323

[a] Catalytic conditions: $[Rh(CO)_2Cl]_2$ or NiI_2 (57 μmol), ligand (0.24 mmol, 4 eq), CH_3OH (110.2 mmol), CH_3I (11.4 mmol), H_2O (81.9 mmol), 170 °C, 22 bar, 900 rpm, 20 min
[b] mol CH_3OH converted into CH_3COOH and CH_3COOCH_3 per mol catalyst precursor

4.4.2 Complex Isolation from Catalytic Mixture

After completion of the carbonylation reaction, the nickel catalyst was recovered (as described on previous page). From this reaction mixture we isolated the brown complex $Ni[(C_5H_5)Fe(C_5H_4PS_2O)]_2$ (**17**) by crystallization of the organometallic residue from acetonitrile (Scheme 36). In **17**, the methylenebenzotriazole unit of the ligand has been lost, presumably due to the oxophilicity of phosphorus. This is in line with the findings that the complexes *cis*-$M[S_2P(S)(C_6H_4OMe)](PPh_3)_2$ [M = Ni(II), Pd(II) and Pt(II)] are readily oxidized in solution to give $M[S_2P(O)(C_6H_4OMe)](PPh_3)_2$.[219] Complex **17** is also directly accessible from the hydrolysis of **13** in refluxing aqueous acetonitrile solution. If the thermal reaction of **13** with water is stopped after 12h, both complexes **13** and **17** are present in the solution, **13** being the major one. The formation of **17** is evidenced by the ^{31}P NMR spectrum of the reaction mixture, which shows the signal for **13** at 110 ppm as well as a signal at 75.8 ppm attributed to **17** (by comparison with the isolated crystals).

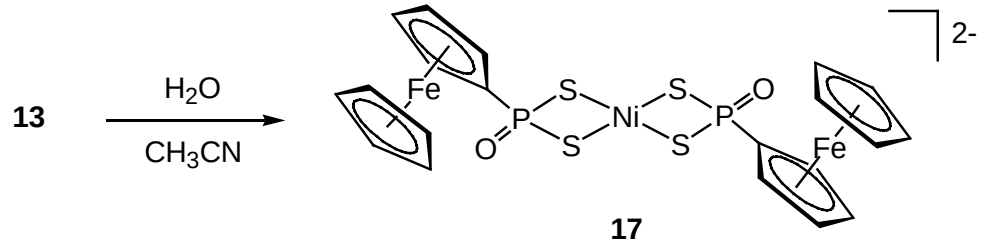

Scheme 36: Isolation of **17**

The single-crystal X-ray structure analysis of **17** reveals a square-planar complex, the metal being coordinated by the four S atoms of the two ligands. The four nickel-sulfur bonds are not equivalent, each ligand is coordinated by a shorter and a longer Ni-S bond [Ni-S(1) = Ni-S(1a) 2.2203(9), Ni-S(2) = Ni-S(2a) 2.2387(8) Å]. The two phosphorus atoms have a pseudo-tetrahedral geometry, the four P-S bonds being very similar [P(1)-S(1) = P(1)-S(1a) 2.2203(9), Ni-S(2) = Ni-S(2a) 2.2387(8) Å].

Thus the ligand **12** is coordinated in a bidentate fashion through the two sulfur atoms of the PS_2 moiety. The molecular structure of **17** is depicted in Fig. 19, important bond lengths and angles are given in Table 15.

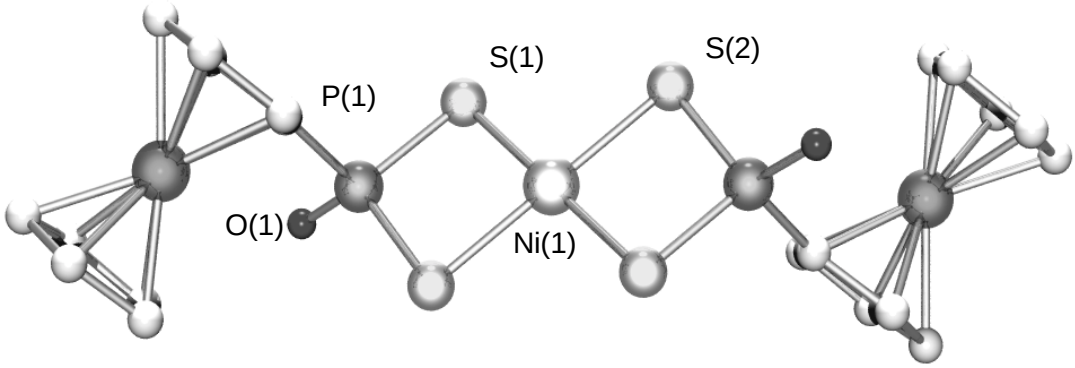

Figure 19: Molecular structure of **17**

Table 15: Selected bond lengths [Å] and angles [°] for compound **17**

P(1)-S(2)	2.0300(13)	C(5)-C(1)-P(1)	124.8(3)
P(1)-S(1)	2.0420(12)	C(2)-C(1)-P(1)	127.8(3)
S(1)-Ni(1)	2.2203(9)	O(1)-P(1)-C(1)	107.63(13)
S(2)-Ni(1)	2.2387(8)	O(1)-P(1)-S(2)	117.90(10)
Ni(1)-S(1a)	2.2203(9)	C(1)-P(1)-S(2)	108.64(12)
Ni(1)-S(2a)	2.2387(8)	O(1)-P(1)-S(1)	114.65(10)
		C(1)-P(1)-S(1)	109.15(11)
		S(2)-P(1)-S(1)	98.40(5)
		P(1)-S(1)-Ni(1)	86.53(4)
		P(1)-S(2)-Ni(1)	86.33(4)
		S(1a)-Ni(1)-S(2a)	87.47(3)
		S(1)-Ni(1)-S(2a)	92.53(3)
		S(1a)-Ni(1)-S(2)	92.53(3)
		S(1)-Ni(1)-S(2)	87.47(3)

4.5 Conclusion

In this chapter, it was our aim to synthesize a new phosphonodithioate ligand and to study its coordination chemistry. A high-yield route to the anion $[(C_5H_5)Fe(C_5H_4PS_2OCH_2C_6H_4N_3]^-$ (**12**) was developed; **12** crystallises as a triethylammonium salt. With rhodium(I) and nickel(II) complexes, **12** was found to react to give the complexes $Ni[(C_5H_5)Fe(C_5H_4PS_2OCH_2C_6H_4N_3]_2$ (**13**), $Ni[(C_5H_5)Fe(C_5H_4PS_2OCH_2C_6H_4N_3](C_4Me_4)Cl$ (**14**), $Rh[(C_5H_5)Fe(C_5H_4PS_2OCH_2C_6H_4N_3](cod)$ (**15**) and $Rh[(C_5H_5)Fe(C_5H_4PS_2OCH_2C_6H_4N_3](CO)_2$ (**16**). In these complexes, **12** behaves as a typical η^2-chelating ligand using the two sulfur atoms of the PS_2 unit for coordination. The new phosphodithioate ligand **12** gives, in combination with nickel(II) and rhodium(I) precursors, active catalysts for the

carbonylation of methanol and thus seems to stabilize the unsaturated species involved in the catalytic process. As **12** contains also nitrogen atoms in the benzotriazole unit, it may also be possible to coordinate a second metal atom.

Chapter 5

New Diphosphine Ester Ligands: Synthesis, Coordination, Catalytic Properties

As we have seen in *Chapter 2*, square-planar rhodium complexes containing two monophosphine ligands in *trans*-positions such as *trans*-[$Rh(PEt_3)_2(CO)Cl$] are known to be highly active for methanol carbonylation,[97] but less stable than unsymmetrical diphosphine complexes such as *cis*-[$Rh(Ph_2PCH_2CH_2PAr_2)(CO)Cl$] which are, however, less active catalysts.[110]

For this reason, we decided to develop diphosphine ligands containing suitable spacer groups between the two phosphorus atoms, in order to allow *trans*-coordination in square-planar rhodium and iridium complexes. Complexes of this type can be expected to combine high catalytic activity with thermal stability under the harsh conditions of methanol carbonylation, so that they can be recovered intact after the catalytic process.

5.1 *trans*-Spanning Diphosphine Complexes

Diphosphine ligands are predisposed for *cis* coordination. Therefore, it was not until 1961, when Issleib and Hohlfeld prepared a square planar nickel complex containing the bidentate diphosphine ligand $Cy_2P(CH_2)_5PCy_2$ in *trans*-coordination (Scheme 37), that the possibility of preparing transition metal complexes containing *trans*-spanning bidentate ligands was generally accepted.[220]

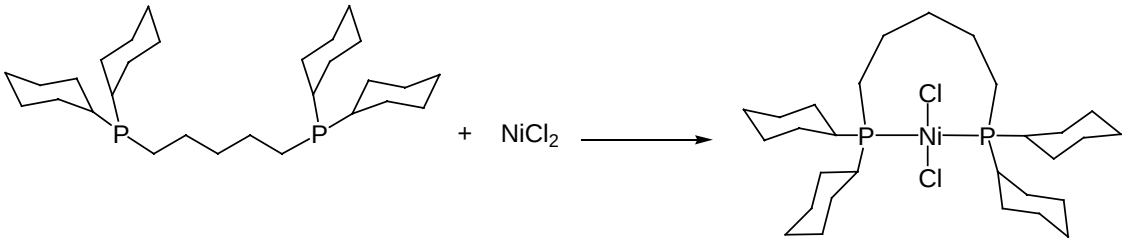

Scheme 37: Preparation of *trans*-Ni($Cy_2P(CH_2)_5PCy_2$)Cl_2, the first example of a *trans*-spanning diphosphine complex

Venanzi and coworkers extensively studied the ligand 2,11-bis(diphenylphosphinomethyl)benzo[c]phenanthrene which, because of its size and rigidity, was initially believed to be able to form *cis*-chelate rings.[221-224] This ligand has been used as a *trans*-spanning "spacer" to bridge distorted trigonal, pseudo-tetrahedral, square planar, square pyramidal, and octahedral metal centers (Scheme 38).

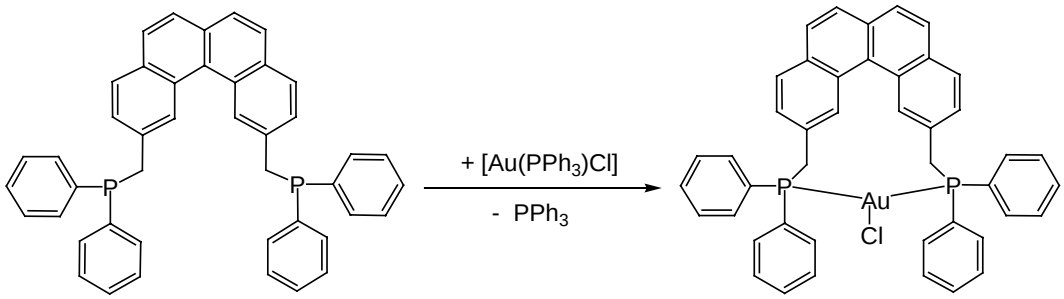

Scheme 38: Preparation of a *trans*-coordinated gold(I) complex

Kapoor *et al.* used a more easily accessible bidentate ligand, 3,3'-oxybis[(diphenylphosphino)methylbenzene], in order to investigate the effect of the restricted backbone flexibility on the *trans*-coordination of diphosphine ligands.[225] Notably, comparison of 2,11-bis(diphenylphosphinomethyl)benzo[c]-phenanthrene and 3,3'-oxybis[(diphenylphosphino)methylbenzene] ligands shows

that the addition of two freely rotating bonds in the latter ligand relative to the first is not detrimental to *trans*-chelation (Scheme 39).

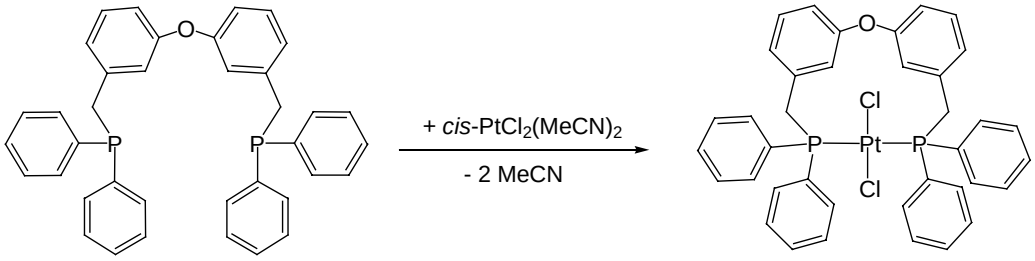

Scheme 39: Formation of a *trans*-platinum(II) complex

Further efforts with preformed *trans*-spanning ligands focused on strapping a transition metal center across the mouth of a calix[4]arene backbone. This approach requires a suitable coordinating moiety on the distal sites, and toward this end, terminal phosphine moieties were used by Matt and coworkers.[226-228] These ligands have short pendent arms in order to maximize localization of the metal center and are attached at the phenolic oxygen atoms, leaving two further sites where secondary coordination moieties may be appended (Scheme 40).

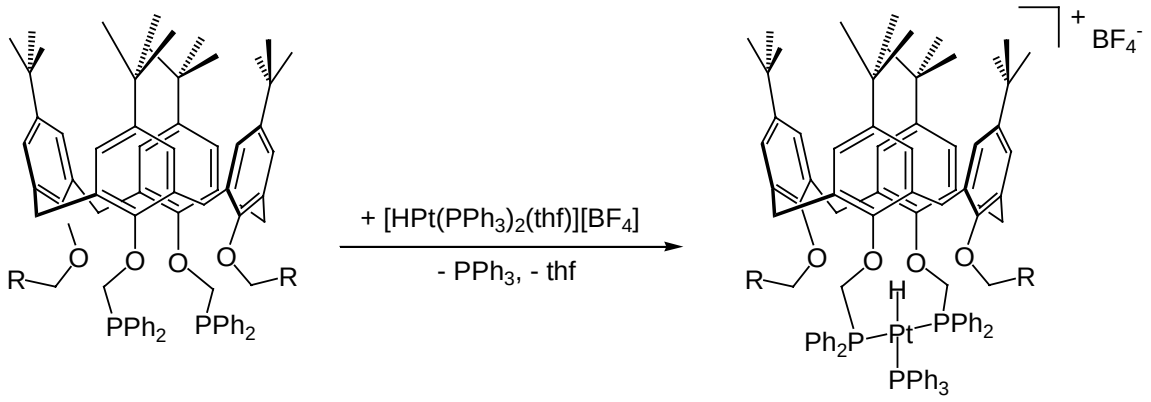

Scheme 40: Formation of a *trans*-(*p-tert*-butylcalix[4]arene)platinum(II) complex

Some authors suggested that mononuclear complexes with large rings (12 or 13 atoms) might be more stable than those with an intermediate-sized ring

(nine-membered rings) due to the increased flexibility of the larger ring size.[229] There are few instances in which larger rings are formed preferentially. As shown in Scheme 41, Shaw and coworkers showed the use of long-chain diphosphine ligands, $(^tBu)_2P(CH_2)_nP(^tBu)_2$ (n = 9, 10, or 12), to produce 12-45 membered metal chelate rings with platinum and palladium metal centers (in preference to open-chain polymeric species).[230] In addition to platinum and palladium complexes, Shaw and coworkers also synthesized complexes of the type $Ir[(^tBu)_2P(CH_2)_nP(^tBu)_2](CO)Cl$ (where n = 9, 10, or 12) to form *trans*-spanning monomers and dimers.[229,231] The molecular structures of $Ir[^tBu_2P(CH_2)_{10}P^tBu_2](CO)Cl$, $Pt[^tBu_2P(CH_2)_{12}P^tBu_2]Cl_2$, and $[Rh\{^tBu_2P(CH_2)_{10}P^tBu_2\}(CO)Cl]_2$ are similar inasmuch as either a chlorine or a carbonyl is gauche with respect to the sets of four *tert*-butyl groups on the *trans*-positioned phosphorus atoms.[231]

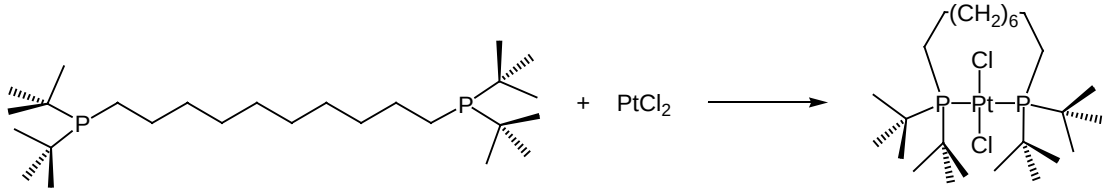

Scheme 41: Preparation of *trans*-$Pt[^tBu_2P(CH_2)_{12}P^tBu_2]Cl_2$

While diphosphines of the type $(^tBu)_2P(CH_2)_nP(^tBu)_2$ (n = 9, 10, 12) give mono-, bi-, and trinuclear complexes $M[(^tBu)_2P(CH_2)_nP(^tBu_2)]Cl_2$, the ligand $(^tBu)_2P(CH_2)_8P(^tBu)_2$ does not form any mononuclear complexes, therefore it was thought to be too small to span *trans*-positions.[232] This study shows that larger chelating ligands form *trans*-spanning diphosphine complexes more effectively than small or intermediate chelating ligands.

Thus, the relative amount of the mononuclear *trans*-complex formed increased with increasing chain length and reached a maximum with a metallacyclic ring size of 15 members.[233] Larger flexible rings (19 members or more) appear to be unstable in the *trans*-configuration. For complexes in which the square-planar coordination geometry of the metal is not doubtful [e.g. palladium(II) and platinum(II)], the chain length of the diphosphine ligand determines the nuclearity of the complexes formed: Polymeric *trans*-complexes are favored by relatively short chains (ca. six linkage atoms), cyclic *trans*-dimers are found with 10-12 linkage atoms, and *trans*-spanning monomers result from long chains (ca. 16 links).[234]

We have seen that the synthesis of transition metal complexes that contain *trans*-spanning bidentate tertiary phosphine ligands remains a challenge. The advantages of *trans*-spanning phosphine ligands are obvious: Unusual metal geometries can be enforced, certain ligand positions can be sterically crowded or shielded, and the *trans*-spanning linkages can be modified to include a variety of structures. Furthermore, there are already examples of transition metal complexes that contain two monodendate phosphine ligands with interesting reactivity.[235] However, to fully realize the reactive potential of transition-metal complexes that contain *trans*-spanning tertiary phosphine ligands, it may be necessary to develop *trans*-spanning ligands which coordinate strongly, so that isomerization or loss of the *trans*-spanning ligand is suppressed during a catalytic process.

5. 2 Ligand Syntheses

In general, easy synthetic accessibility is a major criterion for the design of new ligands. The ready availability of 2-diphenylphosphinobenzoic acid from the Wurtz coupling of sodium 2-chlorobenzoate and sodium diphenylphosphide[236] makes it an attractive building block for the synthesis of diphosphine ligands, *via* condensation of the acid function with diols, diamines or aminoalcohols.[237] Trost *et al.* have shown that two of the 2-diphenylphosphinobenzoic acid molecules can be coupled with a variety of chiral, bidentate backbones providing a system with enhanced enantioselectivities in the asymmetric allylic alkylation with palladium complexes with respect to other monodentate and bidentate phosphine systems (Scheme 42).

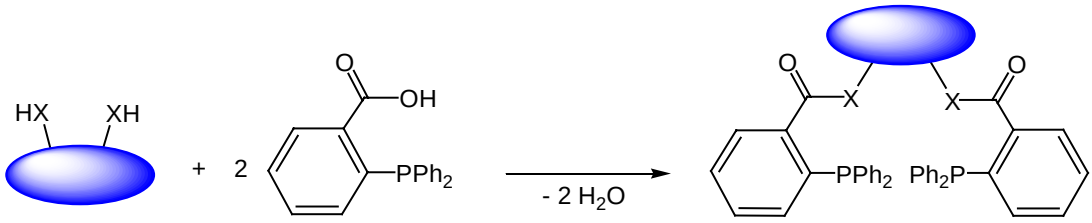

Scheme 42: Simple strategy for preparing phosphine ligands from chiral alcohols and amines

We decided to apply this strategy for preparing new *trans*-spanning achiral diphosphine ligands where the two Ph_2P-(C_6H_4)-CO moieties are connected *via* a bridge of tunable lengths.

5.2.1 Preparation

As in *Chapter 2*, we used DCC in combination with an equimolar mixture of DMAP and 4-PPY as condensation reagents. The new phosphine ligands **18** - **22** have been synthesized by condensation from 2-diphenyl-phosphinobenzoic acid with the corresponding aminoalcohols or diols (Scheme 43).

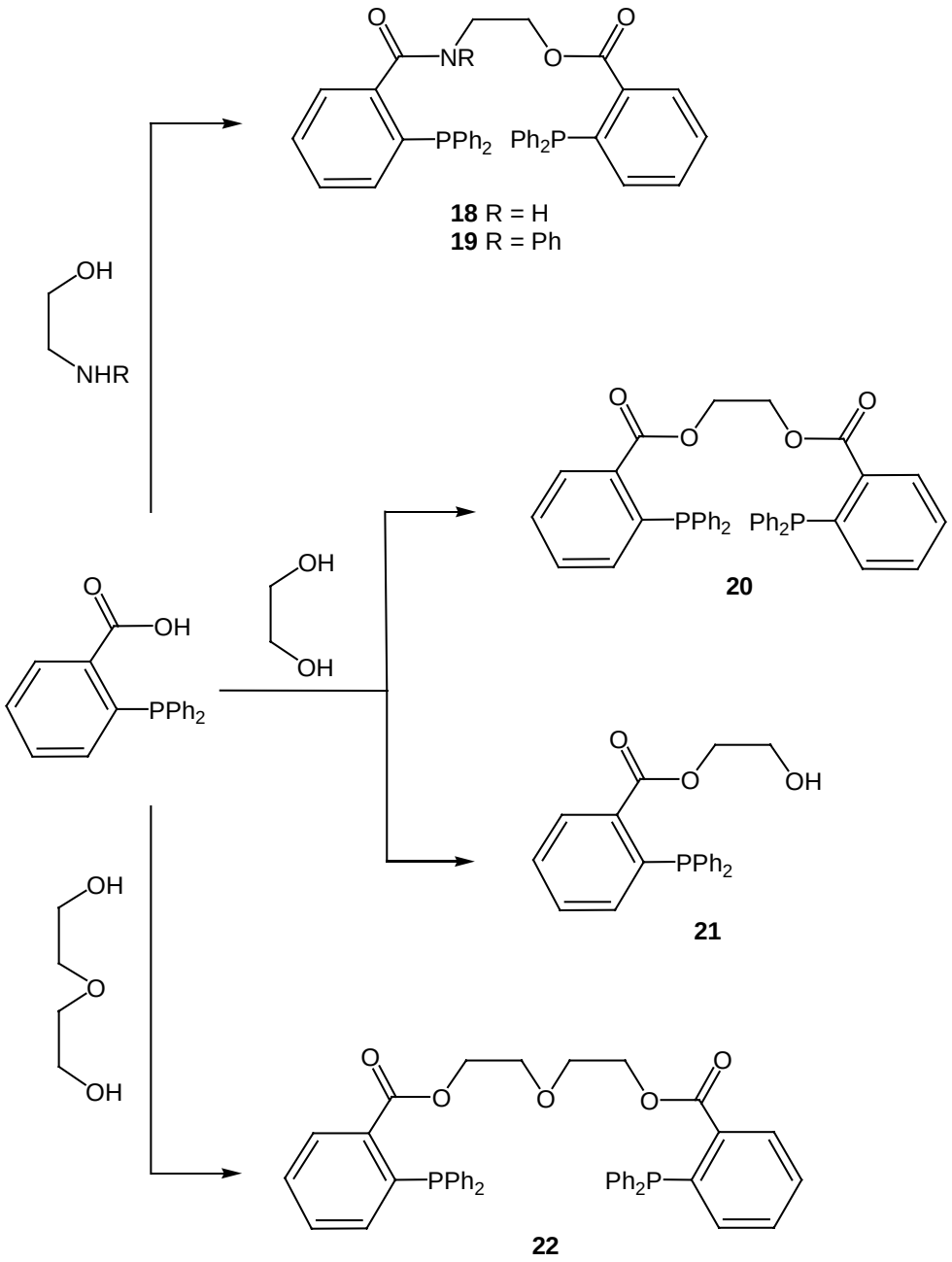

Scheme 43: Synthesis of ligands **18** - **22**

They can be isolated in good yields by column chromatography as white micro-crystalline powders. Noteworthy, the reaction with ethyleneglycol gives two compounds, **20** and **21**, which can be separated on silica gel.

5.2.2 Characterization

Whereas the diphosphine ligands **20** and **22** are symmetrical and give only one resonance in the $^{31}P\{^{1}H\}$ NMR spectrum, the unsymmetrical diphosphine ligands **18** and **19** should give rise to two ^{31}P signals. However, this is only observed for **19** (Figure 20), while in the case of **18** the two expected ^{31}P signals fortuitously coincide.

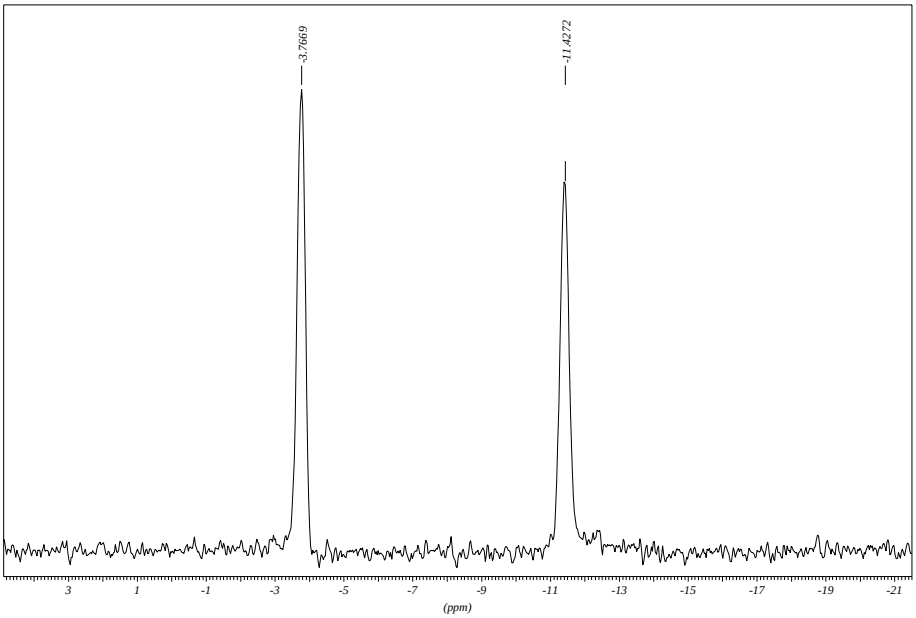

Figure 20: ^{31}P NMR spectrum of ligand **19**

All spectroscopic data of **18** - **22** are given in the Experimental Section. The ^{1}H NMR, ^{13}C NMR, MS spectra and microanalytical data are consistent with the structures proposed.

5.3 Coordination Chemistry

As a part of our studies on the coordination behavior of these new phosphine ligands, we studied their reactivity towards rhodium(I), iridium(I) and platinum(II) precursors and we compared the catalytic potential of the rhodium and iridium complexes obtained in the carbonylation of methanol.

5.3.1 Rhodium(I) Complexes

The diphosphine ligands **18** - **20** (2 equivalents) react with $[Rh(CO)_2Cl]_2$ to give the diphosphine complexes Rh(P-P)(CO)Cl (**23**: P-P = **18**; **24**: P-P = **19**; **25**: P-P = **20**) in high yields (Scheme 44). The products are easily isolated by evaporation of the solvent and washed with ether. Compounds **23** - **25** exhibit, as expected, one strong ν(CO) absorption in the infrared spectrum, the monomeric nature of these complexes can be deduced from the mass spectra. The CO stretching frequencies observed for complexes **23** - **25** are comparable to those reported for *trans*-$[Rh(PR_3)_2(CO)X]$[97,98] but lower than for the *cis* chelate Rh(dppe)(CO)I, providing evidence of the *trans* coordination. All complexes show only one resonance for the two equivalent phosphorus atoms in the $^{31}P\{^1H\}$ NMR spectrum (see Experimental Section), which appears as a doublet due to coupling of the phosphorus atoms to the rhodium metal center, in agreement with the *trans*-P,P stereochemistry. This is in line with the findings for the α-cyclodextrin-diphosphine complexes developed by Matt.[228] In the case of **24,** which contains the unsymmetrical diphosphine **19**, the ^{31}P signal at δ = 47.8 ppm [$^1J_{Rh-P}$ = 162 Hz] observed at room temperature is a doublet. However, upon cooling to -60°C (CD_2Cl_2), this signal splits up, the ABX pattern confirming the

trans arrangement [$^2J_{P\text{-}P}$ = 274 Hz]. This behavior is not due to a dynamic process operating in **24** but to the temperature dependence of these phosphorus chemical shifts.

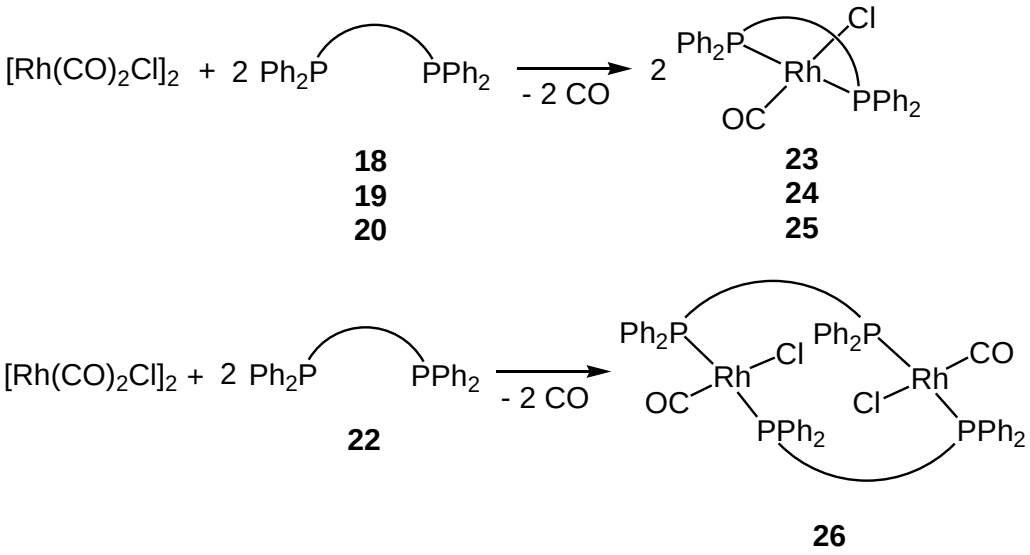

Scheme 44: Synthesis of the neutral rhodium complexes **23** - **26**

As we have seen in the introduction, the stability of the *trans*-monomer increases generally with increasing chain length and reaches a maximum with a metallacycle of 15 members.[238] In agreement with this statement, the complex $[Rh(CO)_2Cl]_2$ reacts with two equivalents of **22** to give the dinuclear complex $[Rh(P\text{-}P)(CO)Cl]_2$ **26** instead of the expected mononuclear metallacycle containing 16 ring members. Complex **26** also exhibits only one resonance for the four equivalent phosphorus atoms in the $^{31}P\{^1H\}$ NMR spectrum which appears as a doublet. The molecular structure of **26** is depicted in Fig. 21, important bond lengths and angles are given in Table 16.

The single-crystal X-ray structure analysis of **26** shows that the metal atoms are coordinated by the two P atoms of the two P,P-bidentate ligands. The two

metal atoms are in a square-planar environment, the angles P(2)-Rh(1)-P(1), C(21)-Rh(1)-Cl(1), P(2)-Rh(1)-C(21), C(21)-Rh(1)-P(1), P(1)-Rh(1)-Cl(1), Cl(1)-Rh(1)-P(2) being 175.24(5), 174.74(10), 90.33(9), 90.78(10), 91.74(9), 86.78(12)°, respectively. The two rhodium atoms are bridged by two diphosphine ligands, maintaining the *trans*-P,P-coordination geometry of each rhodium atom.

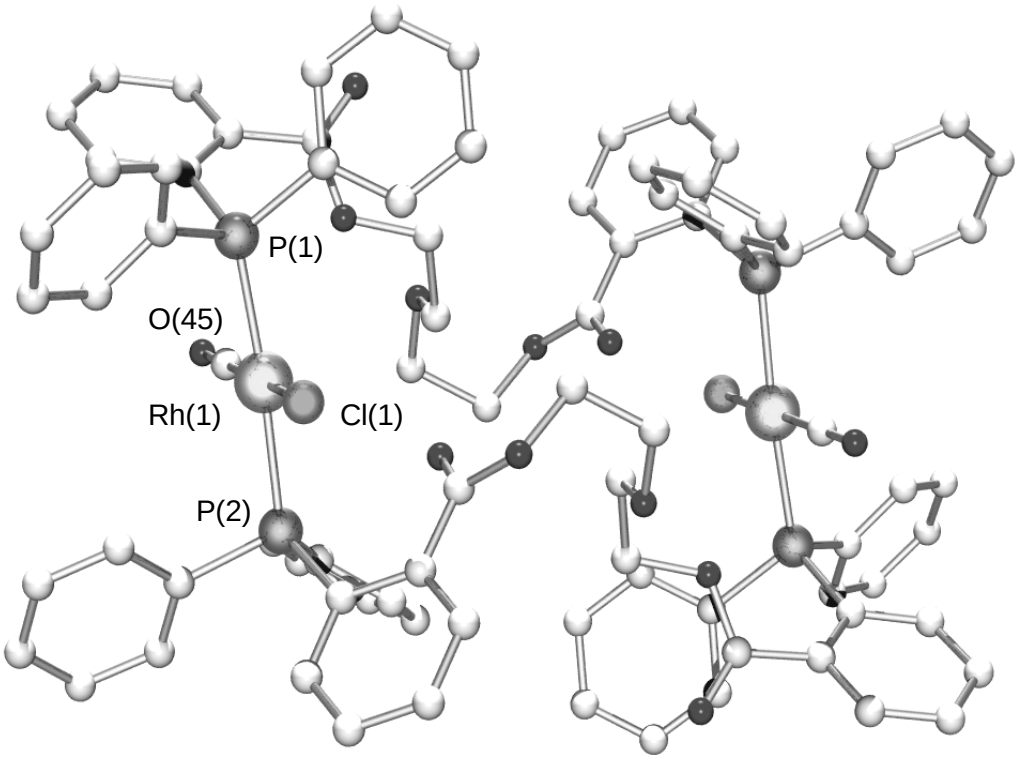

Figure 21: Molecular structure of the dinuclear complex **26**

Table 16: Selected bond lengths [Å] and angles [°] for complex **26**

Rh(1)-P(1a)	2.345(2)	P(2)-Rh(1)-P(1)	175.24(5)
Rh(1)-P(2a)	2.318(2)	C(21)-Rh(1)-Cl(1)	174.74(10)
Rh(2)-P(1b)	2.345(2)	P(2)-Rh(1)-C(21)	90.33(9)
Rh(2)-P(2b)	2.318(2)	C(21)-Rh(1)-P(1)	90.78(10)
		P(1)-Rh(1)-Cl(1)	91.74(9)
		Cl(1)-Rh(1)-P(2)	86.78(12)

The four P-Rh bonds are almost equal in length [P(1a)-Rh(1) = P(1b)-Rh(2) = 2.345(2), P(2a)-Rh(1) = P(2b)-Rh(2) = 2.318(2) Å]. These bond distances and angles are similar to those reported by Shaw[239] for *trans*-{Rh[(^{t}Bu)$_2$P(CH$_2$)$_{10}$P(^{t}Bu)$_2$](CO)Cl}$_2$ and *trans*-{Pd[(^{t}Bu)$_2$P(CH$_2$)$_{10}$P(^{t}Bu)$_2$]Cl$_2$}$_2$.

5.3.2 Iridium(I) Complexes

The diphosphines **18** - **20** were found to coordinate to iridium(I) through the two phosphorus atoms (Scheme 45). The chloro complexes Ir(P-P)(cod)Cl (**27**: P-P = **18**; **28**: P-P = **19**; **29**: P-P = **20**) are directly obtained from [Ir(cod)Cl]$_2$ and the corresponding diphosphine ligands, using a 1 : 2 ratio in dilute solution, in order to avoid the formation of [Ir(P-P)$_2$]Cl or polynuclear species, as observed with other diphosphines.[240] The phosphorus atoms of the P-Ir-P moieties give rise to a signal at about 20.5 ppm in the ^{31}P{^{1}H} NMR spectrum. On the basis of the spectroscopic data (see Experimental Section), we can formally represent complexes Ir(P-P)(cod)Cl (**27** - **29**) to contain a monodentate cyclooctadiene ligand in a square-planar coordination geometry: In the ^{1}H NMR spectrum the olefinic protons are clearly different, the signal at δ = 4.89 ppm can be assigned to the non-coordinated HC=CH group, while the signal at δ = 4.09 ppm can be assigned to the coordinated HC=CH group. This is in line with the values for the corresponding group in free cyclooctadiene (δ = 5.56 ppm) and in [Ir(cod)Cl]$_2$ (δ = 4.20 ppm). However, a trigonal bipyramidal coordination geometry with cod, behaving as a *cis*-bidentate ligand cannot be ruled out completely, as it was observed in Ir(diop)(cod)Cl or in Ir(pnp)(cod)H.[241,242] In the later cases, however, the diphosphine ligands isopropylidene-2,3-dihydroxy-1,4bis(diphenylphosphino)-

butane (diop) and (α-methylbenzyl)bis(2-(diphenylphos-phino)ethyl)amine (pnp) are *cis*-coordinated to iridium, while in **27** - **29** the diphosphine ligands **18** - **20** are *trans*-coordinated.

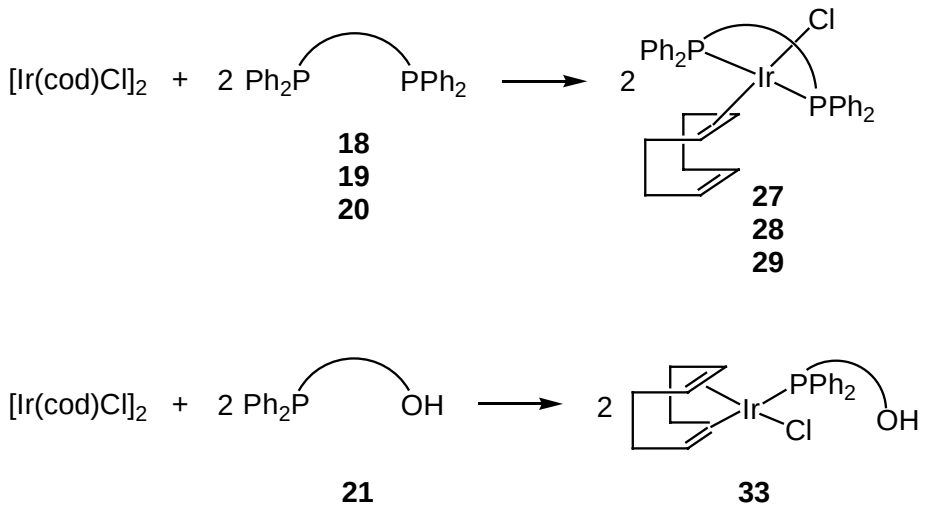

Scheme 45: Synthesis of the neutral iridium complexes **27** - **29** and **33**

Carbon monoxide reacts in dichloromethane with **27** - **29** to give almost quantitatively the carbonyl complexes **30** - **32**, which show only one $^{31}P\{^{1}H\}$ NMR resonance for the two equivalent phosphorus atoms, too, but it is shifted downfield to about 27.0 ppm (Scheme 46).

The analogous reaction of the cyclooctadienechloro complex $[Ir(cod)Cl]_2$ with two equivalents of **21** in dichloromethane gives the iridium complex Ir(**21**)(cod)Cl **33** in good yield. Complex **33** shows a broad signal at δ 20.3 ppm in the $^{31}P\{^{1}H\}$ NMR spectrum. The molecular structure of **33** is shown in Fig. 22, important bond lengths and angles are given in Table 17.

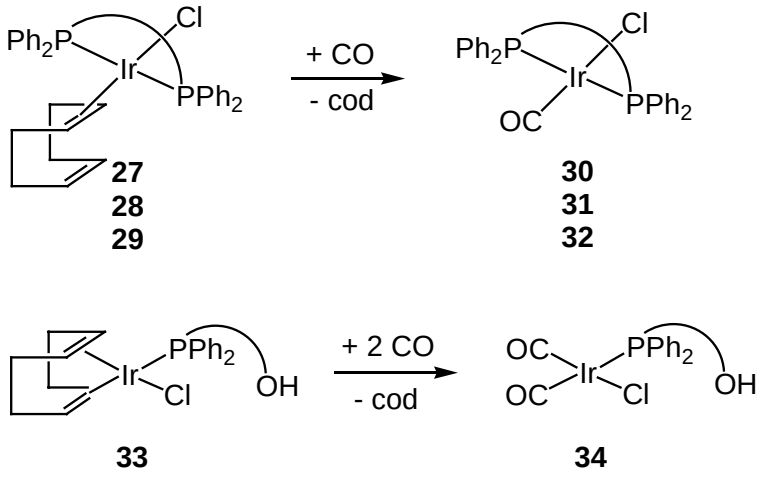

Scheme 46: Synthesis of the neutral iridium complexes **30** - **32** and **34**

The single-crystal X-ray structure analysis of **33** reveals a distorted square-planar coordination geometry of the iridium atom, the angles P(1)-Ir(1)-C(8), P(1)-Ir(1)-C(1), C(4)-Ir(1)-Cl(1), C(5)-Ir(1)-Cl(1), P(1)-Ir(1)-Cl(1) being 164.8(2), 158.2(2), 155.8(2), 164.4(2), 90.7(6), respectively. Complex **33** contains an Ir-Cl···HO hydrogen bonding interaction [Ir(1)-H(30) = 2.3209 Å, Cl(1)-H(30)-O(3) = 162.43°].

Table 17: Selected bond lengths [Å] and angles [°] for complex **33**

Ir(1)-P(1)	2.342(18)	P(1)-Ir(1)-C(8)	164.8(2)
Ir(1)-C(1)	2.182(7)	P(1)-Ir(2)-C(1)	158.2(2)
Ir(1)-C(4)	2.108(7)	C(4)-Ir(1)-Cl(1)	155.8(2)
Ir(1)-C(8)	2.154(7)	C(5)-Ir(1)-Cl(1)	164.4(2)
Ir(1)-Cl(1)	2.379(16)	P(1)-Ir(1)-Cl(1)	90.7(6)

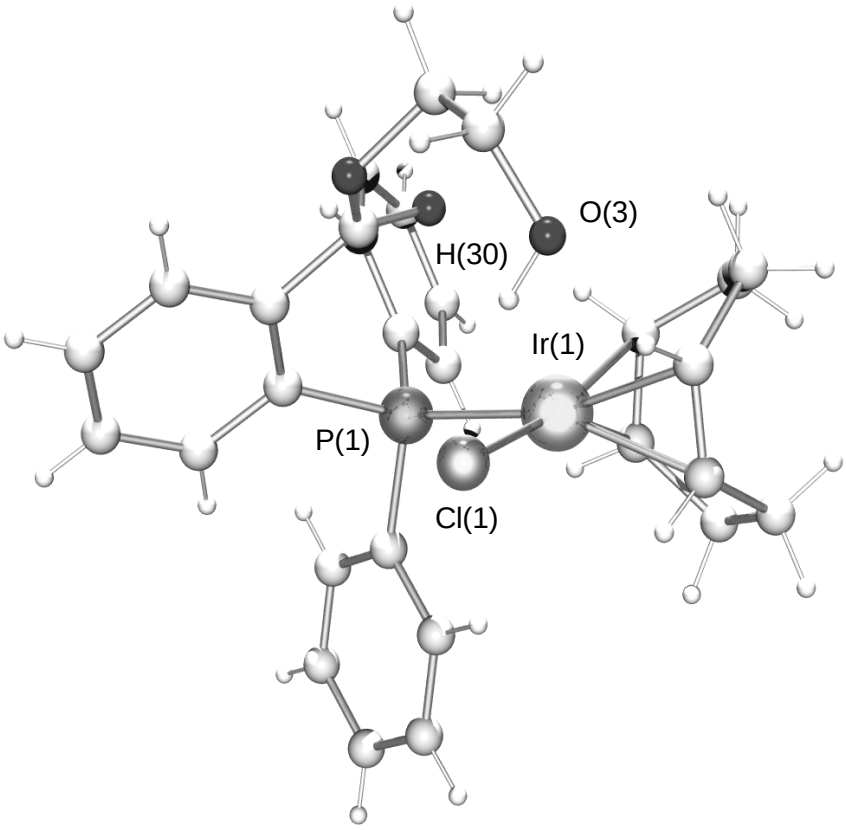

Figure 22: Molecular structure of the mononuclear complex **33**

5.3.3 Platinum(II) Complexes

The *trans* coordination of the diphosphine ligands in the mononuclear complexes, assumed for **23** - **25**, **27** - **29** and **30** - **32** on the basis of their spectroscopic data, was finally confirmed by a single-crystal X-ray structure analysis of the platinum complex Pt(**19**)I_2 (**35**). Complex **35** is obtained almost quantitatively from the reaction of Pt(cod)I_2 with the diphosphine ligand (**19**) in dichloromethane (Scheme 47). In the $^{31}P\{^1H\}$ NMR spectrum, the two phosphorus atoms gives rise to two very close signals at δ = 12.1 ppm and δ = 11.6 ppm, showing the characteristic satellites due to ^{31}P-^{195}Pt coupling. In the ^1H NMR spectrum, **35** gives rise to the expected signals of ligand **19**.

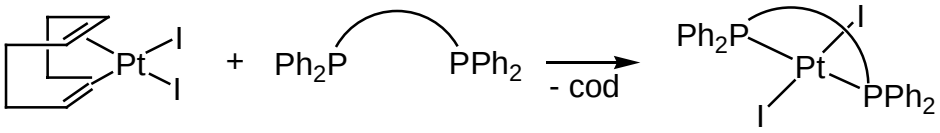

19 **35**

Scheme 47: Synthesis of the neutral platinum complex **35**

The *trans* coordination of **19** in **35** is unambiguously revealed by a single-crystal X-ray structure analysis which shows a square-planar coordination geometry around the platinum metal center. The Pt atom is coordinated to two I atoms and to the two P atoms of the diphosphine ligand. The two platinum-phosphorus bonds [Pt(1)-P(1) 2.31(9), Pt(1)-P(2) 2.33(9) Å] and the two platinum-iodine bonds [Pt(1)-I(1) 2.61(5), Pt(1)-I(2) 2.62(5) Å] are almost equal in length. The molecular structure of **35** is depicted in Fig. 23, important bond lengths and angles are given in Table 18.

Table 18: Selected bond lengths [Å] and angles [°] for complex **35**

Pt(1)-P(1)	2.0300(13)	P(1)-Pt(1)-P(2)	178.40(4)
Pt(1)-P(2)	2.0420(12)	P(1)-Pt(1)-I(1)	93.52(3)
Pt(1)-I(1)	2.2203(9)	P(1)-Pt(1)-I(2)	89.29(3)
Pt(1)-I(2)	2.2387(8)	P(2)-Pt(1)-I(2)	86.05(3)
		P(2)-Pt(1)-I(2)	91.30(3)
		I(1)-Pt(1)-I(2)	173.22(10)

These bond distances are similar to those reported by Feringa *et al.* for *trans*-dichloro{bis[*N*-(2-diphenylphosphino)phenyl]-2,6-pyridinedicarboxamide}-platinum.[243] The angles P(1)-Pt(1)-P(2), P(1)-Pt(1)-I(1), P(1)-Pt(1)-I(2), P(2)-Pt(1)-I(1), P(2)-Pt(1)-I(2), I(1)-Pt(1)-I(2) [178.40(4), 93.52(3), 89.29(3), 86.05(3),

91.30(3), 173.22(10)°, respectively] are not far from those of the ideal square-planar geometry.

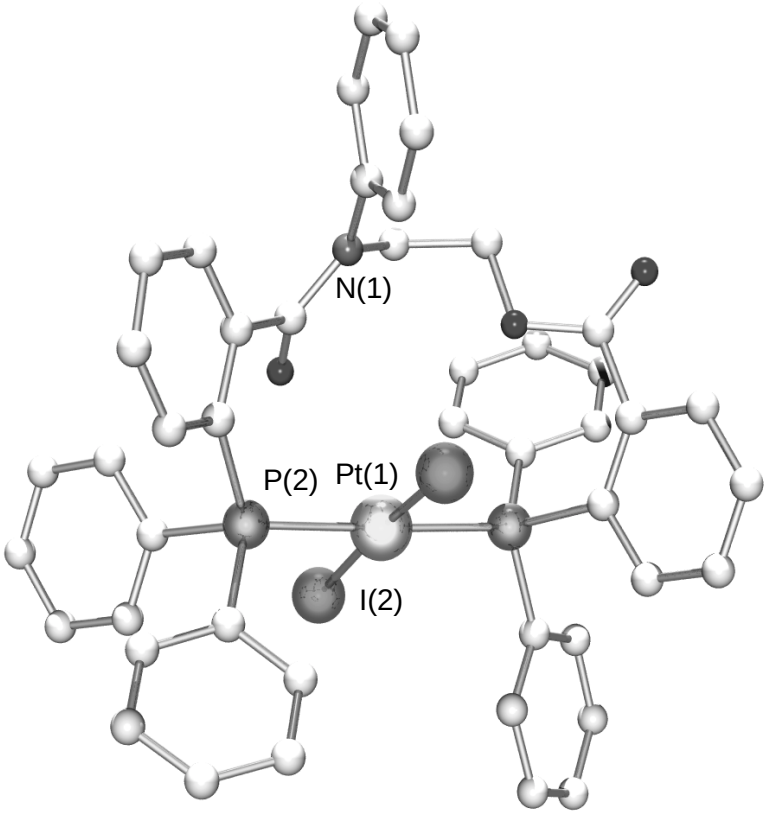

Figure 23: Molecular structure of the mononuclear complex **35**

5.4 Carbonylation Potential

5.4.1 Catalytic Carbonylation of Methanol

The diphosphine ligands **18**, **19**, **20** and **22** have been tested in combination with $[Rh(CO)_2Cl]_2$ or $[Ir(cod)Cl]_2$ for the catalytic carbonylation of methanol to give acetic acid and methylacetate in the presence of iodomethane and water.

$$CH_3OH + CO \longrightarrow CH_3COOH$$

$$CH_3COOH + CH_3OH \longrightarrow CH_3COOCH_3 + H_2O$$

The reaction was carried out at 170°C under a CO pressure of 22 bar, the catalyst / substrate ratio being 1 : 2000. After 15 minutes the reaction was stopped, and the products were analyzed by GC for the determination of the quantities formed. The results of the catalytic carbonylation of methanol are presented in Table 19.

Table 19: Methanol carbonylation data[a]

Entry	Precursor	Ligand	TON[b]
1	$[Rh(CO)_2Cl]_2$	**-**	381
2	$[Rh(CO)_2Cl]_2$	**18**	732
3	$[Rh(CO)_2Cl]_2$	**19**	803
4	$[Rh(CO)_2Cl]_2$	**20**	672
5	$[Rh(CO)_2Cl]_2$	**22**	650
6	$[Ir(cod)Cl]_2$	**-**	227
7	$[Ir(cod)Cl]_2$	**18**	312
8	$[Ir(cod)Cl]_2$	**19**	350
9	$[Ir(cod)Cl]_2$	**20**	321

[a] Catalytic conditions: $[Rh(CO)_2Cl]_2$ or $[Ir(cod)Cl]_2$ (57 μmol), ligand (0.24 mmol, 4 eq), 15 min, CH_3OH (110.2 mmol), CH_3I (11.4 mmol), H_2O (81.9 mmol), 170 °C, 22 bar CO, 900 rpm
[b] mol CH_3OH converted into CH_3COOH and CH_3COOCH_3 per mol catalyst precursor

In each case the conversion of methanol was greater than 98% and the selectivity for acetic acid was greater than 99%. The complexes **23** - **26** are formed *in situ* on mixing $[Rh(CO)_2Cl]_2$ with two equivalents of **18** - **20** or **22** in methanol. As a control experiment, the catalytic reaction was carried out with the Monsanto catalyst $[Rh(CO)_2I_2]^-$, which was also formed *in situ* from $[Rh(CO)_2Cl]_2$ under the reaction conditions (entry 1).[102]

As evidenced by Table 19, the catalytic activity increases considerably in the presence of a rhodium precursor with the diphosphine ligands **18**, **19**, **20** or **22**, ligand **19** being the most active one (entry 3). The combination $[Rh(CO)_2Cl]_2$ / **19** catalyzes the carbonylation of methanol at a rate nearly double that of $[Rh(CO)_2I_2]^-$. By comparison of the system $[Rh(CO)_2Cl]_2$ / **20** with the system $[Rh(CO)_2Cl]_2$ / **22**, we can note that changing the distance between the two esters by modifying the length of the tether showed little variation in catalytic activity. Noteworthy the rates for the iridium systems (entries 6-9) were all lower than the commercial $[Rh(CO)_2I_2]^-$ catalyst. Moreover, rhodium and iridium complexes of unsymmetrical diphosphine ligands are more efficient catalysts than their symmetrical analogues for methanol carbonylation. In the ester ligands, a source of rotational freedom may result from rotation about the acyl-oxygen bond. We rigidified this linkage by going to the analogous amide linkage as in ligands **18** and **19** (Figure 24).

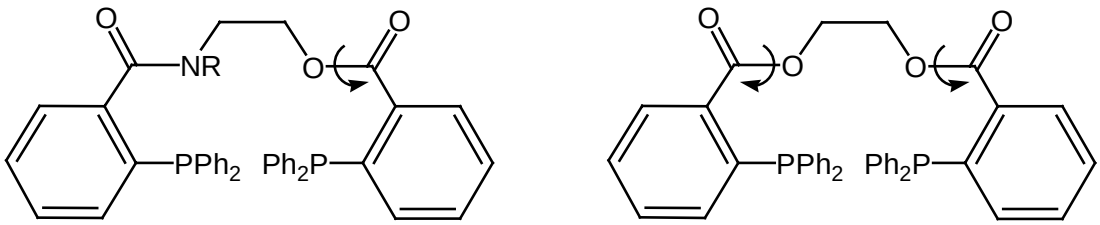

Figure 24: Restricted rotation of amides with respect to esters

By comparison with **18**, the better activity obtained with **19** can be explained by the increased steric hindrance of the nitrogen atom and we can postulate that an interaction between the -NH group of **18** and the metal center decreases the catalytic potential of the complex formed.

5.4.2 Complex Isolation from the Reaction Mixture

In the case of the most active combination, $[Rh(CO)_2Cl]_2$ / ligand **19**, the catalyst stays active throughout several catalytic runs: An homogeneous orange-red solution is obtained after the catalytic reaction, containing two rhodium diphosphine complexes. By IR and ^{31}P NMR analysis, one of them is identified to be the iodo analogue of the rhodium(I) complex **24** [δ = 47.8 ppm, $^1J_{Rh\text{-}P}$ = 164 Hz, ν(CO) = 1970 cm^{-1}], the other one is the rhodium(III) complex **36** [δ = 30.8 ppm, $^1J_{Rh\text{-}P}$ = 100 Hz]. This mixture is still active for further catalytic runs, showing almost the same catalytic activity.

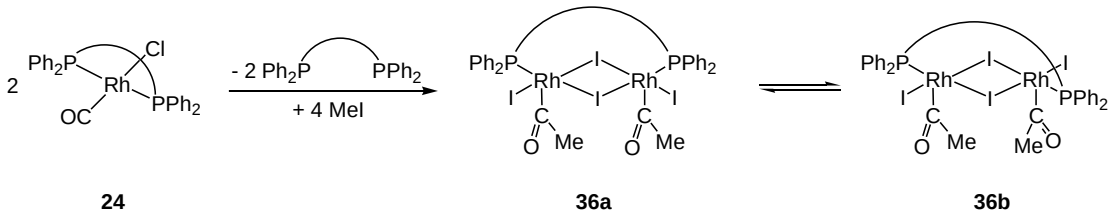

24 **36a** **36b**

Scheme 48: Formation of the neutral rhodium complexes **36a** and **36b**

The red complex **36** can be isolated from the organometallic residue of the catalytic reaction by cristallisation from acetone; it is also directly accessible from the reaction of **24** with methyliodide in acetone solution (Scheme 48). **36** is a dinuclear Rh(III) complex in which the rhodium atoms are bridged by one diphosphine and two iodo ligands, both rhodium atoms carrying an acetyl ligand and a terminal iodo ligand. Complex **36** exists in two isomers **36a** and **36b**, depending on the *cis* or *trans* arrangement of the two terminal iodo ligands at the two rhodium atoms. The two isomers present in solution are separated by fractional crystallization from acetone: **36a** crystallizes rapidly, while **36b** takes several hours to crystallize after elimination of **36a**.

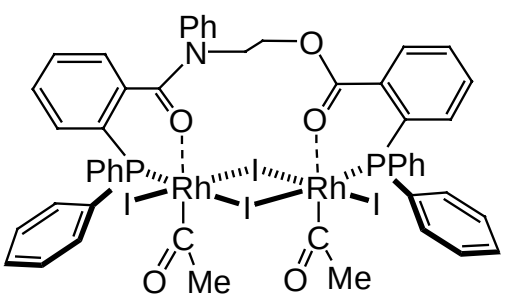

36a

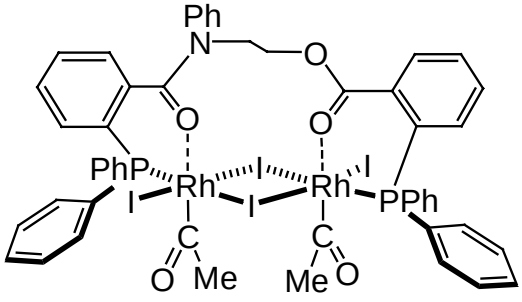

36b

The Rh-COMe bond lengths of **36a** are relatively long, 2.11 and 2.15 Å, as compared with most other rhodium acetyl complexes, which generally have bond lengths around 2.00 Å, which is also the case of **36b** (1.99 and 2.02 Å). The long Rh-COMe bond must reflect a large *trans* influence of the carbonyl groups of the ligand. As a consequence, the Rh-O bonds in **36a** (2.33 and 2.29 Å) are shorter than those observed for **36b** (2.33 and 2.38 Å). The geometry of the six-membered chelation ring formed by these Rh-O interactions can explain the relative stability of the two complexes and more generally of the catalytic system. In the case of **36a**, the acetyl ligands have the same orientation, the acetyl oxygen atoms pointing towards the H atom of a phenyl group, because there is an intramolecular contact between these two atoms (2.59 and 2.61 Å). In **36b**, the acetyl groups form also hydrogen bonds (2.46 and 2.65 Å) and show for this reason an opposite orientation. It is noteworthy that in both isomers **36a** and **36b**, the rhodium atoms do not have a square pyramidal but an octahedral coordination geometry (Figure 25 and 26), thanks to the carbonyl oxygen atoms of the ligand chain (Rh-O 2.33 and 2.29 Å in **36a**, 2.33 and 2.38 Å in **36b**). The six-membered chelating ring is approximately planar, the two Rh-P bonds (2.28 and 2.27 Å) are equal in length for **36a** and **36b**.

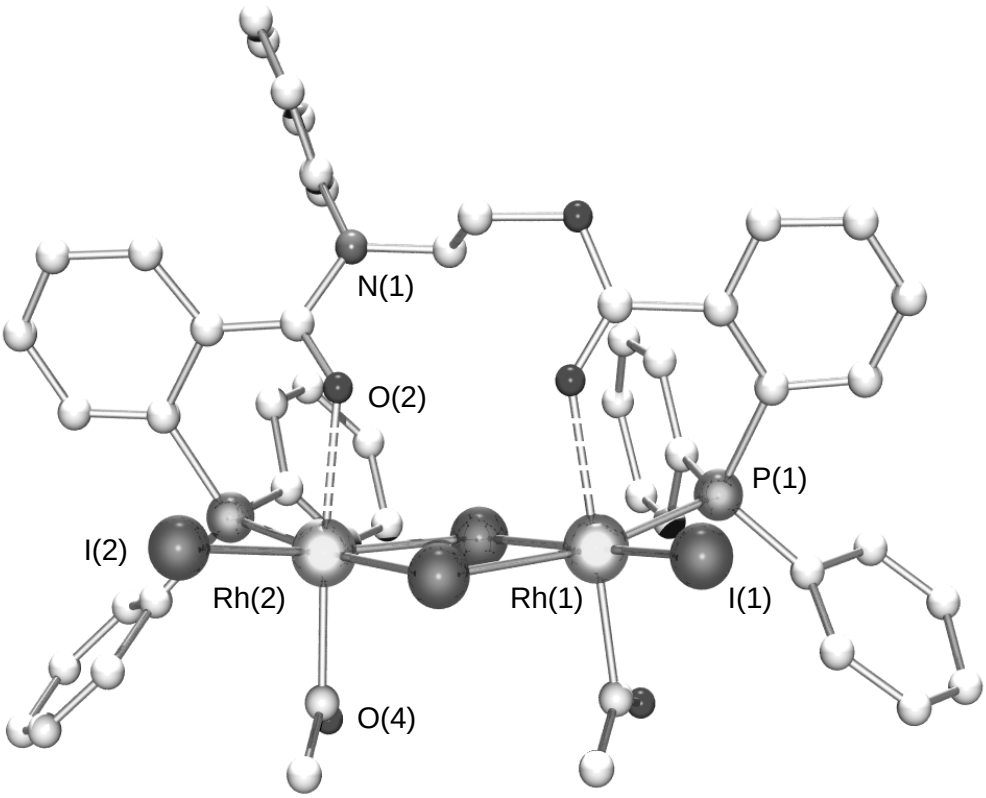

Figure 25: Molecular structure of complex **36a**

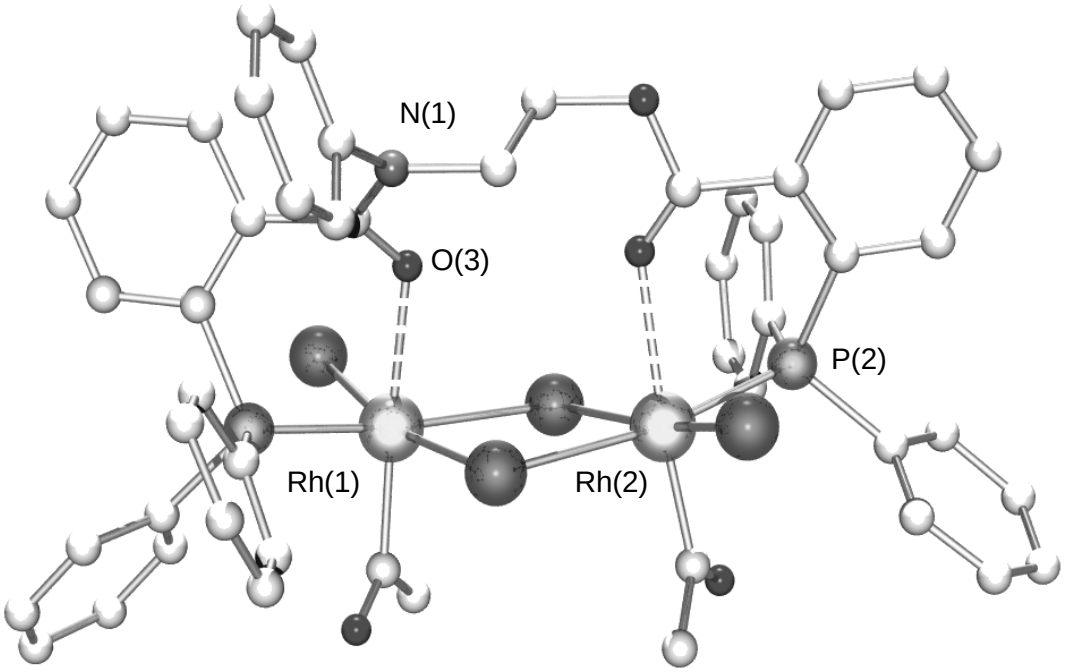

Figure 26: Molecular structure of complex **36b**

It is dangerous to assume that in a labile system, the species isolated from a solution fully characterizes the species present in the solution. Furthermore, it has been shown that iodo-bridged dinuclear complexes can be formed and isolated in solid state but evolved to mononuclear $[Rh(CO)_2I_3]^{2-}$ under CO or $[(COCH_3)Rh(CO)I_3]^-$ under catalytic conditions.[199] It is also known that this type of rhodium acetyl dimers are very easily cleaved with a phosphine.[55] Hence the bridge opening reaction of **36** should be facile. In our case, the highest mass ion observed in the ESI mass spectrum of the mixture obtained after a catalytic run corresponds to the mononuclear fragment (COMe)Rh(**19**)I_2. The ^{13}C NMR spectrum shows two poorly resolved acetyl carbonyl signals at δ = 211.38 ppm and δ = 207.49 ppm. The complex (COMe)Rh(**19**)I_2 is certainly one of the complexes involved in the catalytic process but unfortunately our experiments do not give sufficient information to characterize all the species.

5.5 Conclusion

We developed a new route to synthesize *trans*-spanning ligands **18** - **22**, which coordinate to rhodium(I), iridium(I) and platinum(II), in order to find active and stable catalysts for the carbonylation of methanol. Pringle *et al.* have supposed that the dissymmetry of the diphosphine ligand is very important for the catalytic activity and the stability of rhodium complexes in the carbonylation of methanol,[110] as it has been shown for the rhodium-phosphine-catalyzed hydroformylation of olefins by Casey *et al.*[244] Indeed, the rhodium complex Rh(**19**)(CO)Cl (**24**), containing an unsymmetrical diphosphine ligand, turned out

to be more active and more stable under catalytic conditions than the classical Monsanto system.

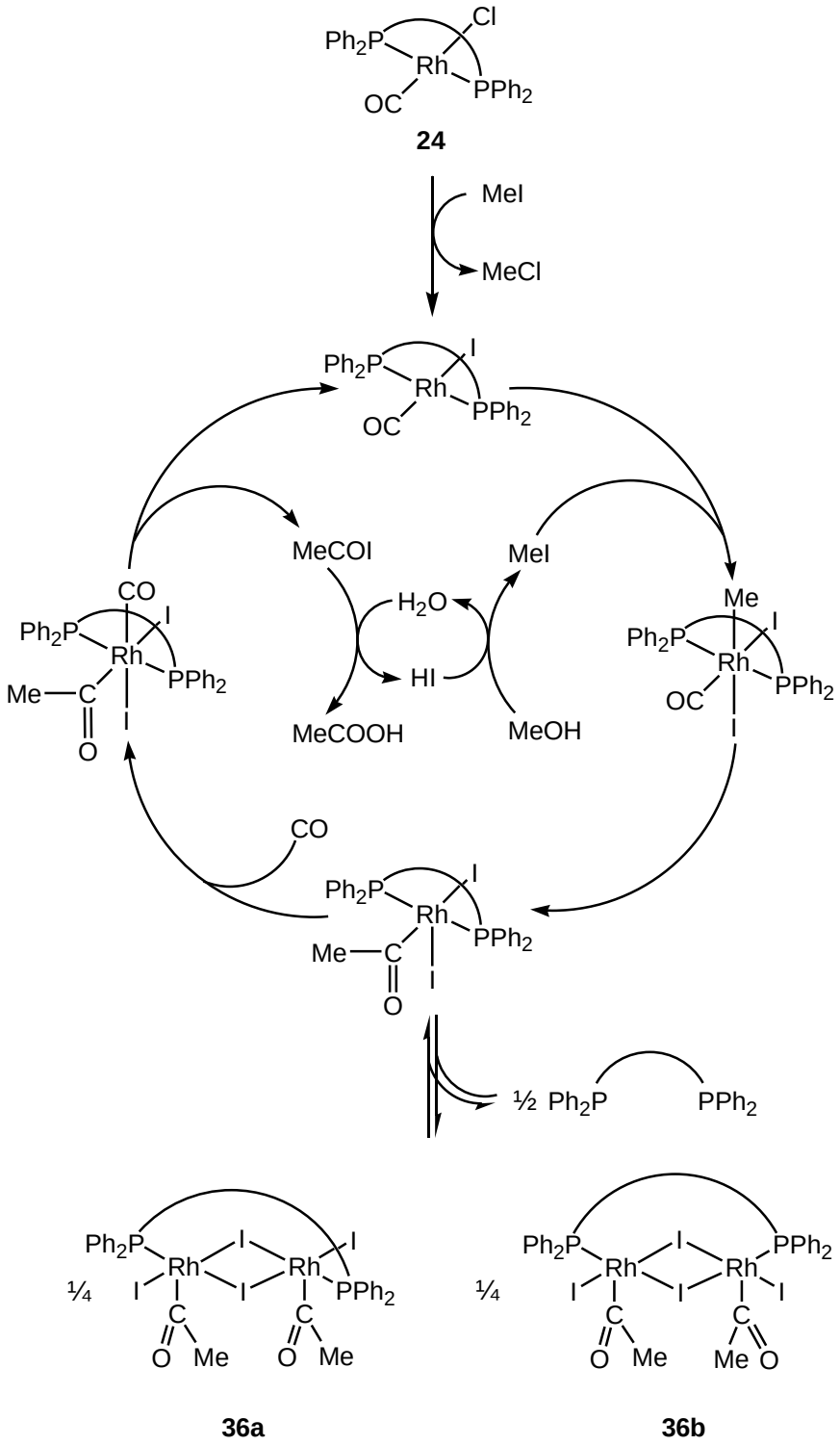

Scheme 49: Proposed mechanism for the catalytic cycle of the methanol carbonylation catalyzed by the neutral Rh(**19**)(CO)Cl (**24**)

During the formation of the dinuclear complex $(COMe)_2Rh_2$(**19**)I_4 (**36**) from two mononuclear complexes **24**, one of the two diphosphine ligands is liberated. Phosphine loss during the catalytic process has already been proposed by Cole-Hamilton *et al.* in the case of $Rh(PEt_3)_2(CO)I$, without the supposed monophosphine species $Rh(PEt_3)(CO)I$ being isolated.[97] Oxidative addition of iodomethane to **24** yields the rhodium(III) acetyl complex **36**, presumably through the intermediacy of the corresponding mononuclear methylrhodium(III) complex. The facile migratory insertion of carbon monoxide during oxidative addition of iodomethane to carbonyl rhodium(I) complexes is well known.[245,246]

On the basis of these observations, we propose the catalytic cycle shown in Scheme 49 for the mechanism of the carbonylation of methanol catalyzed by **24**. A similar cycle has been proposed for the same reaction catalyzed by $Rh(Ph_2PCH_2PSPh_2)(CO)I$, in which several intermediates have been detected spectroscopically.[102] The dinuclear complex isomers **36a** and **36b** formed by elimination of a diphosphine ligand may be considered as a reservoir for the active mononuclear species. The formation of the dinuclear complexes **36a** and **36b** can be suppressed by using an excess of the diphosphine ligand.

Since unsymmetrical diphosphine ligands seem to be efficient, it would be interesting to synthesize new diphosphine ester ligands, especially with *tert*-butyl groups on the *trans*-disposed phosphorus atoms. In fact, these substituents should be able to form *trans*-spanning diphosphine complexes with increased steric hindrance. It would also be interesting to change the substituents on the nitrogen atom of the ligand.

Conclusion and Perspectives

In this thesis, we developed three different classes of new multifunctional ligands, studied their coordination chemistry with group VIII metals and their catalytic potential for the carbonylation of methanol. It appears that the ester diphosphine ligands we developed have the most interesting perspectives for catalysis. These ligands allow *trans* coordination in square-planar rhodium(I), iridium(I) and platinum(II) complexes. By virtue of their good σ-donor properties and their π-capability, they form Rh(I) and Ir(I) complexes, which are highly active catalysts. New ligands of this type can be designed very easily in the lines which we developed.

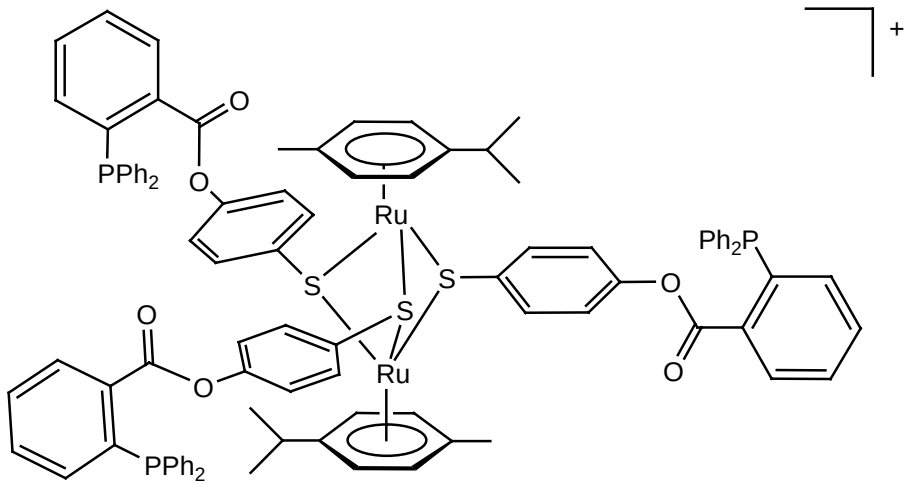

Figure 27

Thus, we have obtained very recently the new ruthenium-phosphine dendritic molecule shown in Figure 27 from 2-diphenylphosphinobenzoic acid and $Ru_2(p\text{-}CH_3\text{-}C_6H_4\text{-}^iPr)_2(S\text{-}C_6H_4\text{-}p\text{-}OH)_3Cl$ by using our condensation method.

This compound used as a ligand in combination with $[Rh(CO)_2Cl]_2$ for the catalytic carbonylation of methanol show a very high catalytic activity.

This preliminary result demonstrates the high potential of multifunctional phosphine ligands developed by our condensation method for coordination and catalysis. The versatility of this concept is almost without limit.

Chapter 7

Experimental Section

7.1 Apparatus

All reactions were carried out under nitrogen, using standard Schlenk techniques. Catalytic reactions were performed in a high pressure Schlenk tube able to withstand 8 bars of internal pressure or were carried out in 100 ml autoclaves equipped with glass-lined steel vessels.

In appropriate cases thin layer chromatography (TLC) was used to purify compounds.[247] TLC plates were prepared by placing a uniform 0.5 mm layer of the appropriate support (Al_2O_3 or SiO_2; G or G/UV_{254}, Macherey-Nagel) on 20x20 cm glass plates.[248] After charging the plates with the support they were allowed to air dry for 1h and then dried in an oven at 125°C for 12h. When strictly anhydrous conditions were necessary, freshly activated plates were used.

7.2 Solvents and Gases

Solvents were purified and dried according to standard laboratory practices.[249] Distillation of solvents was carried out under an N_2 atmosphere. Laboratory gases were purchased from Carbagas and used directly from the cylinders without further purification.

7.3 Starting material

The compounds $[Ir(cod)Cl]_2$,[250] $[Rh(CO)_2Cl]_2$,[251] $[Rh(cod)Cl]_2$,[252] $[Ni(C_4Me_4)Cl_2]_2$,[253] and $[(C_5H_5)_2Fe(C_5H_4)]_2P_2S_4$[214] were prepared as described previously. All other reagents were purchased (Fluka) and used as received.

7.4 Instrumentation and Analyses

7.4.1 Infrared Spectroscopy

Infrared spectra were recorded with a Perkin-Elmer 1720X FT-IR spectrometer in transmission mode where the absorptions are given in reciprocal centimetres (cm^{-1}). A standard press was used to produce KBr pellets. Intensity data are described with the following abbreviations: vs = very strong, s = strong, m = medium, w = weak, vw = very weak, sh = shoulder.

7.4.2 NMR Spectroscopy

Nuclear magnetic resonance spectra were recorded using a Varian Gemini 200 BB instrument or a Bruker AMX 400 spectrometer and referenced by using the resonances of the residual non-deuterated solvents. ^1H NMR: internal standard solvent, external standard TMS; ^{13}C NMR: internal standard solvent, external standard TMS; ^{31}P NMR: external standard 85% H_3PO_4. Chemical shifts are given in ppm and coupling constants *J* in Hz (br = broad, s = singulet, d = doublet, t = triplet, dd = doublet of doublet, m = multiplet).

7.4.3 Gas Chromatography

Gas chromatography was performed on a Dani 86.10 gas chromatograph equipped with a split-mode capillary injection system and flame ionisation detector using a Cp-wax 52-CB capillary column (25m x 0.32mm).

7.4.4 Elemental Analyses

Microanalyses were carried out by the Laboratory of Pharmaceutical Chemistry, University of Geneva (Switzerland) or by the Mikroelementar-analytisches Laboratorium, ETH Zürich (Switzerland).

7.4.5 Mass Spectra

FAB and ESI mass spectra were measured by Professor T. A. Jenny of the University of Fribourg (Switzerland).

7.5 Compounds of Chapter 2

7.5.1 Synthesis of ($C_6H_4N_3CH_2CO_2C_5H_4N$) (1)

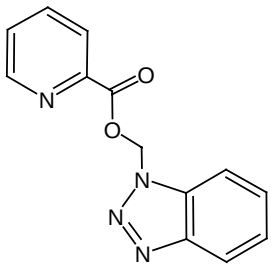

A solution of 2-pyridinecarboxylic acid (826 mg, 6.71 mmol), *N*,*N*-dicyclohexylcarbodiimide (2.7 g, 13.1 mmol), 4-(dimethylamino)pyridine (122 mg, 1 mmol), 4-pyrrolidinopyridine (148 mg, 1 mmol) and hydroxymethylbenzotriazole (1.1 g, 7.4 mmol) in CH_2Cl_2 (40 mL) was allowed to stand at room

temperature under nitrogen, until the esterification was complete. The resulting solution was filtered through Celite to remove *N*,*N*-dicyclohexyl urea, and the filtrate was concentrated under reduced pressure. The residue was chromatographed on a silica gel column (150 g), eluting with ethyl acetate/hexane (1/1). The product was isolated from the third fraction by evaporation of the solvent, giving 1.1 g (65 %) of **1** as a white solid.

Crystals suitable for X-ray diffraction analysis were grown by slow evaporation of a 1:1 ethyl acetate/hexane solution. Elemental analysis (%) calculated for $C_{13}H_{10}N_4O_2$ (254.2): C 61.4, H 4.0; found C 61.1, H 4.3; IR (KBr): 3283m, 3071vw, 3050vw, 3002vw, 2927s, 2852m, 2119vw, 1695vs (C=O ester), 1645s (C=O amide), 1584vw, 1519s, 1432m, 1349m, 1119m, 748m, 694m cm^1; ESI-MS: *m*/*z*: 254 $[M]^+$; ^{1}H NMR (200 MHz, [D$_6$]Acetone, 21°C): δ = 8.60 (d, 1H; ArH), δ = 8.10 (d, 1H; ArH), δ = 7.93 (d, 1H; ArH), δ = 7.65 (t, 1H; ArH), δ = 7.62 (t, 1H; ArH), δ = 7.44 (t, 1H, ArH), δ = 7.28 (t, 2H; ArH), δ = 6.82 (s, 2H, -CH_2); ^{13}C NMR (50 MHz, [D$_6$]Acetone, 21°C): δ = 164.40, 150.46, 146.63, 146.36, 137.48, 133.13, 128.81, 127.94, 126.11, 124.88, 120.26, 110.55, 69.11.

7.5.2 Synthesis of ($C_6H_4N_3CH_2CO_2C_5H_4FeC_5H_5$) (2)

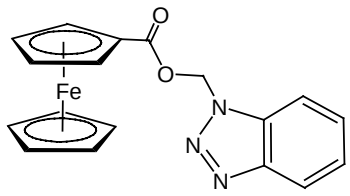

A solution of ferrocenecarboxylic acid (1.4 g, 6.54 mmol), *N*,*N*-dicyclohexylcarbodiimide (2.7 g, 13.1 mmol), 4-(dimethylamino)pyridine (122 mg, 1 mmol), 4-pyrrolidinopyridine (148 mg, 1 mmol) and

hydroxymethylbenzotriazole (1.04 g, 7.04 mmol) in CH_2Cl_2 (40 mL) was allowed to stand at room temperature under nitrogen, until the esterification was complete. The resulting solution was filtered through Celite to remove *N*,*N*-dicyclohexyl urea, and the filtrate was concentrated under reduced pressure. The residue was chromatographed on a silica gel column (150 g), eluting with acetone/hexane (1/4). The product was isolated from the third fraction by evaporation of the solvent, giving 1.3 g (58 %) of **2** as an orange solid.

Crystals suitable for X-ray diffraction analysis were grown by slow evaporation of a 1:1 acetone/hexane solution. Elemental analysis (%) calculated for $C_{18}H_{15}Fe_1N_3O_2$ (361.2): C 59.9, H 4.2; found C 60.1, H 4.3; IR (KBr): 3118vw, 3040vw, 2928m, 1708vs (C=O ester), 1459s, 1276m, 1108s, 967m, 746m cm^1; ESI-MS: *m*/*z*: 361 $[M]^+$; ^1H NMR (200 MHz, [D6]Acetone, 21°C): δ = 8.10 (d, 1H; ArH, $^3J_{H\text{-}H}$ = 8.54 Hz), δ = 7.93 (d, 1H; ArH, $^3J_{H\text{-}H}$ = 8.54 Hz), δ = 7.62 (t, 1H; ArH), δ = 7.44 (t, 1H, ArH), δ = 6.82 (s, 2H, $-CH_2$), δ = 4.82 (m, 2H, CpH), δ = 4.44 (m, 2H, CpH), δ = 3.90 (s, 5H; CpH); ^{13}C NMR (50 MHz, [D6]Acetone, 21°C): δ = 171.30, 147.30, 146.39, 133.06, 133.03, 128.67, 124.93, 120.34, 110.74, 72.46, 72.43, 70.76, 70.16, 70.03, 70.00, 69.95, 69.01, 68.98, 67.62.

7.5.3 Synthesis of $(C_6H_4N_3CH_2CO_2C_5H_4Fe)_2$ (3)

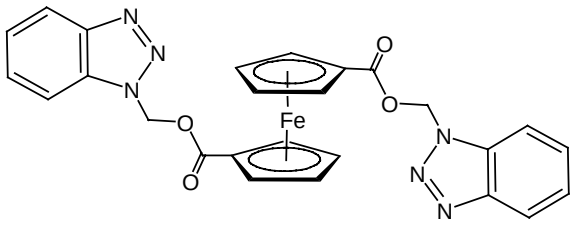

A solution of ferrocenedicarboxylic acid (1.7 g, 6.59 mmol), *N*,*N*-dicyclohexylcarbodiimide (5.5 g, 26.6 mmol), 4-(dimethylamino)pyridine (122 mg,

1 mmol), 4-pyrrolidinopyridine (148 mg, 1 mmol) and hydroxymethylbenzotriazole (1.94 g, 13.04 mmol) in CH_2Cl_2 (40 mL) was allowed to stand at room temperature under nitrogen, until the esterification was complete. The resulting solution was filtered through Celite to remove *N*,*N*-dicyclohexyl urea, and the filtrate was concentrated under reduced pressure. The residue was chromatographed on a silica gel column (150 g), eluting with acetone/hexane (1/1). The product was isolated from the fourth fraction by evaporation of the solvent, giving 1.3 g (51 %) of **3** as an orange solid.

Elemental analysis (%) calculated for $C_{26}H_{20}Fe_2N_6O_4$ (592.2): C 52.7, H 3.4; found C 52.9, H 3.5; IR (KBr): 3100vw, 3050vw, 2927s, 1723vs (C=O ester), 1452m, 1270s, 1155m, 1102s, 968m cm[1]; ESI-MS: *m*/*z*: 592 $[M]^+$; ^{1}H NMR (200 MHz, [D$_6$]Acetone, 21°C): δ = 8.10 (d, 4H; ArH, $^3J_{H\text{-}H}$ = 8.43 Hz), δ = 7.71 (t, 2H; ArH), δ = 7.51 (t, 2H, ArH), δ = 6.89 (s, 4H, -CH_2), δ = 4.66 (t, 4H, CpH), δ = 4.19 (t, 4H, CpH); ^{13}C NMR (50 MHz, [D$_6$]Acetone, 21°C): δ = 171.30, 147.30, 146.39, 133.06, 133.03, 128.67, 124.93, 120.34, 110.74, 72.46, 72.43, 70.76, 70.16, 70.03, 70.00, 69.95, 69.01, 68.98, 67.62.

7.5.4 Synthesis of $C_6H_4N_3CH_2CO_2C_4H_2S_1CO_2CH_2C_6H_4N_3$ (4)

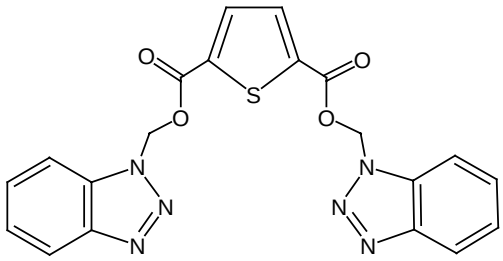

A solution of 2,5-thiophenedicarboxylic acid (1.72 g, 10 mmol), *N*,*N*-dicyclohexylcarbodiimide (2.3 g, 11 mmol), 4-(dimethylamino)pyridine (122 mg, 1

mmol), 4-pyrrolidinopyridine (148 mg, 1 mmol) and hydroxymethylbenzotriazole (3.3 g, 22 mmol) in CH_2Cl_2 (40 mL) was allowed to stand at room temperature under nitrogen, until the esterification was complete. The resulting solution was filtered to remove *N*,*N*-dicyclohexyl urea and the filtrate was concentrated under reduced pressure. The residue was chromatographed on silica gel (80g), eluting with hexane/ether (1/1) to afford 2.7 g (62%) of **1** as a white solid.

Elemental analysis (%) calculated for $C_{20}H_{14}S_1O_4N_6$ (434.4): C 55.29, H 3.25, N 19.35; found C 55.25, H 3.27, N 19.31; IR (KBr): 3029vw, 2979w, 1749s, 1709vs, 1532m, 1452m, 1280s, 1240s, 1159m, 1069s, 989m, 743s, 543m, 493m cm^{-1}; FAB-MS (positive ion): *m*/*z*: 435 [M^+]; ^{1}H NMR (200 MHZ, [D_6]Acetone, 21°C): δ = 8.07 (m, 4H), δ = 7.87 (s, 2H), δ = 7.68 (t, 2H), δ = 7.37 (t, 2H), δ = 6.99 (s, 4H); ^{13}C NMR (50 MHz, [D_6]Acetone, 21°C): δ = 160.46, 146.31, 138.28, 134.73, 132.95, 128.94, 124.97, 120.44, 110.17, 68.82.

7.5.5 Synthesis of $[C_6H_4N_3CH_2CO_2C_6H_4PPh_2]$ (5)

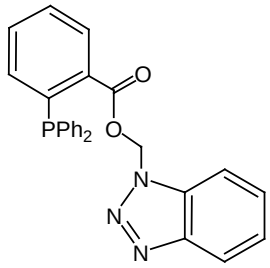

A solution of 2-diphenylphosphinobenzoic acid (1.4 g, 4.6 mmol), *N*,*N*-dicyclohexylcarbodiimide (1.3 g, 6.3 mmol), 4-(dimethylamino)pyridine (122 mg, 1 mmol), 4-pyrrolidinopyridine (148 mg, 1 mmol) and hydroxymethylbenzotriazole (750 mg, 5.0 mmol) in CH_2Cl_2 (40 mL) was allowed to stand at room temperature

under nitrogen, until the esterification was complete. The resulting solution was filtered through Celite to remove *N*,*N*-dicyclohexyl urea, and the filtrate was concentrated under reduced pressure. The residue was chromatographed on a silica gel column (150 g), eluting with diethyl ether/hexane (1/1). The product was isolated from the third fraction by evaporation of the solvent, giving 1.3 g (65 %) of **5** as a white solid.

Elemental analysis (%) calculated for $C_{26}H_{20}N_3O_2P_1$ (437.4): C 71.4, H 4.6; found C 71.1, H 4.3; IR (KBr): 3051vw, 2927s, 2852m, 1723vs (C=O ester), 1584vw, 1434m, 1244s, 1049m, 984m, 695s cm^{1}; ESI-MS: *m*/*z*: 437 $[M]^+$; ^{1}H NMR (200 MHz, [D$_6$]Acetone, 21°C): δ = 8.06-7.46 (m, 1H; ArH), δ = 6.94 (s, 2H, -CH$_2$); ^{13}C NMR (50 MHz, [D$_6$]Acetone, 21°C): δ = 165.76, 146.36, 142.38, 141.82, 137.69, 137.47, 134.68, 133.25, 132.96, 132.38, 132.01, 131.67, 131.62, 128.62, 124.73, 120.19, 110.48, 68.73; ^{31}P NMR (81 MHz, [D$_6$]Acetone, 21°C) : -2.7 (s).

7.5.6 Synthesis of $CoI_2(C_6H_4N_3CH_2CO_2C_5H_4FeC_5H_5)_2$ (6)

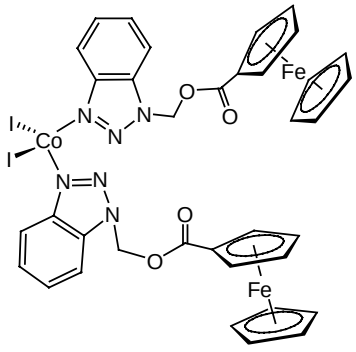

A solution of CoI_2 (200 mg, 0.62 mmol) in dichloromethane (10 ml) was added dropwise to a solution of ferrocene(carboxylato-methylenebenzotriazole) **2**

(431 mg, 1.25 mmol) in the same solvent (10 ml). The resulting solution was stirred at room temperature for 1h. The product precipitated as green solid, which was filtered off, washed with hexane (20 ml) and dried *in vacuo* (174 mg, 75%). Crystals suitable for X-ray diffraction analysis were grown by slow evaporation of a 1:3 acetone/hexane solution.

Elemental analysis (%) calculated for $C_{36}H_{30}Co_1Fe_2I_2N_6O_4$ (1035.1): C 41.8, H 2.9; found C 41.5, H 3.1; IR (KBr): 3092m, 3030vw, 1723vs (C=O ester), 1455m, 1269s, 1199m, 782m, 481m cm[1]; ESI-MS: *m/z*: 1035 $[M]^+$

7.5.7 Synthesis of $[CoI_2(C_6H_4N_3CH_2CO_2C_4H_2S_1CO_2CH_2C_6H_4N_3)]_n$ (7)

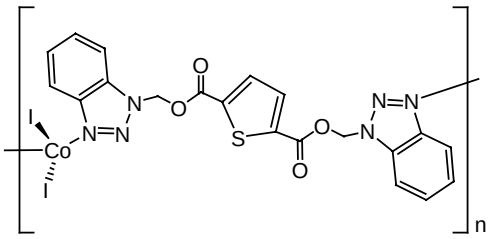

A solution of CoI_2 (100 mg, 0.31 mmol) in dichloromethane (10 ml) was added dropwise to a solution of thiophene-2,5-di(carboxylato-methylenebenzotriazole) (140 mg, 0.32 mmol) in the same solvent (10 ml). The resulting solution was stirred at room temperature for 1h. The product precipitated as green solid, which was filtered off, washed with hexane (20 ml) and dried *in vacuo* (174 mg, 75%).

Crystals suitable for X-ray diffraction analysis were grown by slow evaporation of a 1:3 acetone/hexane solution. Elemental analysis (%) calculated for $C_{20}H_{14}CoI_2N_6O_4S$ (747.17): C 32.2, H 1.9; N 11.25 found C 32.6, H 1.6, N

11.3. IR (KBr): 3029vw, 2979w, 1727vs, 1532m, 1452m, 1280s, 1240s, 1159m, 1069s, 989m, 743s, 543m, 493m cm^{-1}.

7.5.8 Synthesis of $[Rh(C_6H_4N_3CH_2CO_2C_4H_2S_1CO_2CH_2C_6H_4N_3)(CO)Cl]_2$ (8)

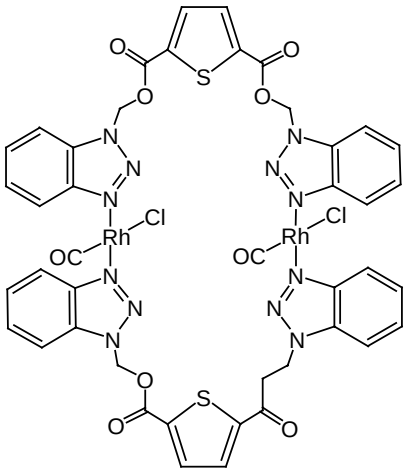

A solution of $[Rh(CO)_2Cl]_2$ (100 mg, 0.26 mmol) and **4** (248 mg, 0.57 mmol) in toluene (20 ml) was stirred at room temperature for 2h. The solution was filtered then evaporated to dryness. The resulting yellow solid was washed with ether (10 ml) and dried under vacuum (240 mg, 77%).

Elemental analysis (%) calculated for $C_{42}H_{28}Cl_2N_{12}O_{10}Rh_2S_2$ (1201.6): C 41.98, H 2.35, N 13.99; found C 42.25, H 2.27, N 13.81; IR (KBr): 3035vw, 2975w, 2086s, 2013vs, 1727vs, 1529m, 1455m, 1237s, 1159m, 1070s, 984m, 746s, 493m cm^{-1}; ESI-MS: *m/z*: 1220 [M + H_2O]; ^{1}H NMR (200 MHz, [D_6]Acetone, 21°C): δ = 8.35 (d, 4H), δ = 8.20 (d, 4H), δ = 7.91 (s, 4H), δ = 7.80 (m, 4H), δ = 7.67 (m, 4H), δ = 7.09 (s, 8H); ^{13}C NMR (50 MHz, [D_6]Acetone, 21°C): δ = 183.52, 160.35, 145.89, 138.18, 135.74, 133.42, 129.58, 125.98, 120.09, 111.66, 70.16.

7.5.9 Synthesis of $[Ir(C_6H_4N_3CH_2CO_2C_4H_2SCO_2CH_2C_6H_4N_3)(CO)Cl]_2$ (9)

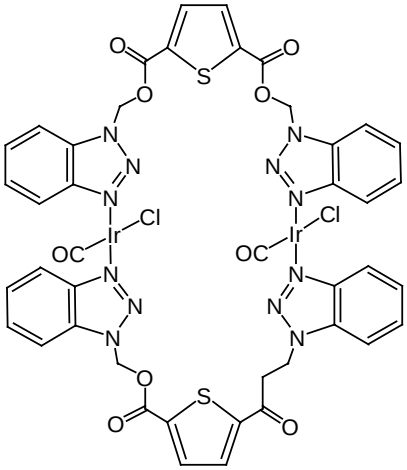

A solution of $[Ir(cod)Cl]_2$ (175 mg, 0.26 mmol) and thiophene-2,5-di(carboxylatomethylenebenzotriazole) **4** (248 mg, 0.57 mmol) in toluene (20 ml) was stirred at reflux for 12h under 1 bar of carbon monoxide. The solution was filtered and then evaporated to dryness. The resulting yellow-orange solid was washed with ether (10 ml) and dried under vacuum (240 mg, 67%).

Elemental analysis (%) calculated for $C_{42}H_{28}Cl_2Ir_2N_{12}O_{10}S_2$ (1380.2): C 36.6, H 2.0; found C 36.9, H 2.2; IR (KBr): 3324m, 3071vw, 2928s, 2852m, 2074s, 1990vs, 1727vs (C=O ester), 1584vw, 1527m, 1454m, 1234m, 1070m, 744m, 634m cm^1; ESI-MS: *m/z*: 1380 $[M]^+$; ^1H NMR (200 MHz, $[D_6]$Acetone, 21°C): δ = 8.17 (d, 4H), δ = 7.86 (s, 4H), δ = 7.81 (m, 4H), δ = 7.6 (m, 4H), δ = 7.05 (s, 8H); ^{13}C NMR (50 MHz, $[D_6]$Acetone, 21°C): δ = 160.37, 145.36, 138.23, 135.14, 132.82, 129.73, 125.52, 120.52, 111.23, 69.82.

7.5.10 Synthesis of $Rh[C_6H_4N_3CH_2CO_2C_6H_4PPh_2]_2(CO)Cl$ (10)

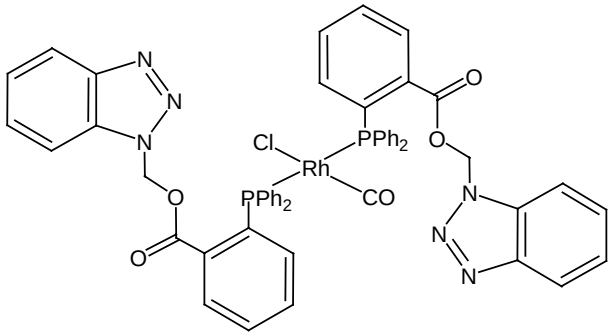

A solution of $[Rh(CO)_2Cl]_2$ (50 mg, 0.13 mmol) and **5** (246 mg, 0.56 mmol) in acetonitrile (20 ml) was stirred at room temperature for 2h. Then the solvent was removed under reduced pressure. The resulting yellow solid was washed with ether (10 ml) and dried under vacuum (210 mg, 0.20 mmol, 78 %).

Elemental analysis (%) calculated for $C_{53}H_{40}Cl_1N_6O_5P_2Rh_1$ (1041.2): C 61.1, H 3.9; found C 61.5, H 4.1; IR (KBr): 3058m, 2926m, 1949vs, 1730vs (C=O ester), 1480w, 1452vw, 1435s, 1275s, 1156m, 1096s, 1055m, 986m, 962m, 743s, 696s cm^{-1}; ESI-MS : *m/z*: 844 $[M\text{-}Cl]^+$; ^1H NMR (200 MHz, $[D_6]$Acetone, 21°C): δ = 8.04 (m, 4H; ArH), δ = 7.83 (m, 8H, ArH), δ = 7.45 (m, 22H; ArH), 7.17 (m, 2H; ArH), 6.74 (s, 4H; $-CH_2$); ^{13}C NMR (50 MHz, $[D_6]$Acetone, 21°C): δ = 171.25, 153.62, 144.80, 144.42, 138.54-125.20, 68.62, 49.92; ^{31}P NMR (81 MHz, $[D_6]$Acetone, 21°C) : 33.7 (d, $^1J(^{103}Rh\text{-}^{31}P)$ = 136 Hz).

7.5.11 Synthesis of $[Rh(C_6H_4N_3CH_2CO_2C_4H_2SCO_2CH_2C_6H_4N_3)(CO)I_3]_4$ (11)

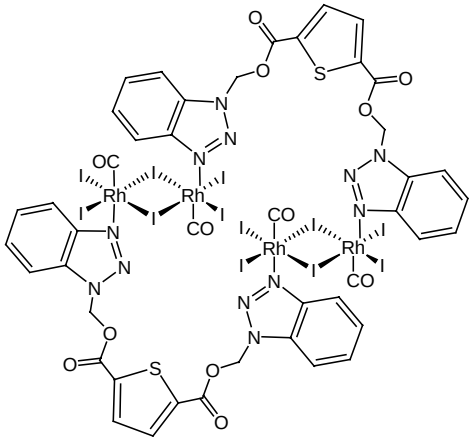

A solution of **4** (100 mg, 0.08 mmol), ethanoic acid (1 ml) and iodomethane (1 ml) were dissolved in acetone (20 ml) under an atmosphere of carbon monoxide. After heating at reflux for 1h, the resulting brownish solution was filtered and then the solvent was evaporated to dryness. The remaining red-brown solid was washed with ether and dried *in vacuo* (388 mg, 59%).

Crystals suitable for X-ray diffraction analysis were grown by slow evaporation of an acetone solution. IR (KBr): 3035vw, 2975w, 2059s, 1729vs, 1524m, 1455m, 1246s, 1076s, 746s, 519m cm^{-1}; ^{1}H NMR (200 MHz, $[D_6]$DMSO, 21°C): δ = 8.65 (d, 4H), δ = 8.53 (d, 4H), δ = 8.01-7.88 (m, 12H), δ = 7.15 (s, 8H); ^{13}C NMR (50 MHz, $[D_6]$DMSO, 21°C): δ = 192.53, 160.26, 147.04, 138.56, 134.93, 133.40, 129.21, 125.50, 120.11, 111.66, 70.28.

7.6 Compounds of Chapter 3

7.6.1 Synthesis of $[HNEt_3][(C_5H_5)Fe(C_5H_4PS_2OCH_2C_6H_4N_3)]$ (anion 12)

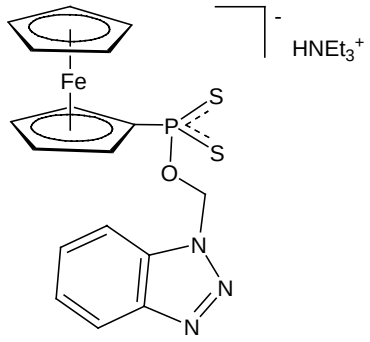

A solution of $[(C_5H_5)_2Fe(C_5H_4)]_2P_2S_4$ (2.6 g, 4.6 mmol), hydroxymethylbenzotriazole (1.4 g, 9.3 mmol) and triethylamine (1.3 ml, 9.3 mmol) in tetrahydrofuran (50 ml) was stirred at room temperature. After 3h the solvent was removed under reduced pressure. The resulting yellow-green solid was washed with acetone (2 × 25 ml), toluene (10 ml) and dried under vacuum (2.3 g, 94%).

Crystals suitable for X-ray diffraction analysis were grown by slow evaporation of a 1:1 CH_2Cl_2/pentane solution; Elemental analysis (%) calculated for $C_{23}Fe_1H_{31}N_4O_1P_1S_2$ (530.5): C 52.1, H 5.9; found C 52.3, H 5.9; IR (KBr): 3062vw, 2940w, 1609w, 1495m, 1469m, 1455m, 1382m, 1313m, 1269m, 1173m, 1162m, 1130w, 1106m, 1039vs, 1016s, 925w, 896vw, 808vs, 753s, 665vs, 636m, 588s, 502m, 483m, 452m, 433w cm^{-1}; ^{31}P NMR (81 MHz, $CDCl_3$, 21°C): δ = 110.16 (t; $^3J_{H-P}$ = 8.5 Hz); ^1H NMR (200 MHz, $CDCl_3$, 21°C): δ = 7.99 (d, 1H), δ = 7.77 (d, 1H), δ = 7.44 (t, 1H), δ = 7.34 (t, 1H), δ = 6.42 (d, 2H; $^3J_{H-P}$ = 8.5 Hz), δ = 4.65 (s, 2H), δ = 4.30 (s, 2H), δ = 4.26 (s, 5H), δ = 3.20 (q, 6H), δ = 1.33 (t,

9H); ^{13}C NMR (50 MHz, $CDCl_3$, 21°C): δ = 146.51, 133.38, 127.94, 124.59, 119.90, 111.38, 72.20, 72.05, 71.18, 71.15, 70.91, 70.80, 46.50, 9.05.

7.6.2 Synthesis of Ni[(C$_5$H$_5$)Fe(C$_5$H$_4$PS$_2$OCH$_2$C$_6$H$_4$N$_3$)]$_2$ (13)

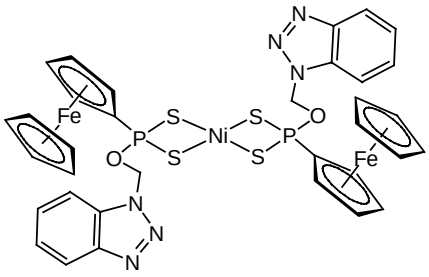

A solution of $NiCl_2$ (100 mg, 0.77 mmol) and [NEt_3H]**12** (1.02 g, 1.93 mmol) in acetonitrile/water (1 : 1, 30 ml) was stirred at room temperature for 2h. The red-brown precipitate was isolated by filtration, washed with acetonitrile (10 ml) and dried *in vacuo* (625 mg, 89%).

Elemental analysis (%) calculated for $C_{34}H_{30}Fe_2N_6Ni_1O_2P_2S_4$ (915.2): C 44.6, H 3.3; found C 44.2, H 3.5; ^{31}P NMR (81 MHz, [D_6]DMSO, 21°C): δ = 107.3 (s); ^{1}H NMR (200 MHz, [D_6]DMSO, 21°C): δ = 7.98 (dd, 2H), δ = 7.49 (t, 1H), δ = 7.37 (t, 1H), δ = 6.31 (d, 2H), δ = 4.37 (s, 2H), δ = 4.14 (s, 2H), δ = 4.12 (s, 5H); ^{13}C NMR (50 MHz, [D_6]DMSO, 21°C): δ = 146.38, 133.48, 128.24, 124.92, 119.83, 112.35, 72.26, 72.05, 70.70, 70.15, 70.05.

7.6.3 Synthesis of Ni(C$_4$Me$_4$)[(C$_5$H$_5$)Fe(C$_5$H$_4$PS$_2$OCH$_2$C$_6$H$_4$N$_3$)]Cl (14)

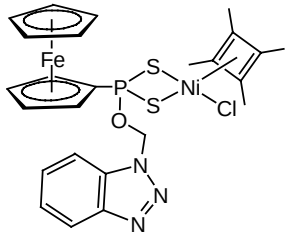

A solution of $[Ni(C_4Me_4)Cl_2]_2$ (100 mg, 0.21 mmol) in chloroform (10 ml) was added dropwise to a solution of the triethylammonium salt of **12** (300 mg, 0.47 mmol) in the same solvent (10 ml). The resulting solution was stirred at room temperature for 2h, then the solvent was removed under reduced pressure. The residue was extracted with acetone (10 ml), the solution was filtered and then the solvent was evaporated to dryness. The remaining purple solid was washed with hexane (20 ml) and dried *in vacuo* (94 mg, 75%).

Elemental analysis (%) calculated for $C_{25}Fe_1H_{27}N_3Ni_1O_1P_1S_2$ (595.1): C 50.4, H 4.5; found C 50.1, H 4.6; $^{31}P\{^1H\}$ NMR($CDCl_3$): δ = 104.1 (s); ^1H NMR (200 MHz, $CDCl_3$, 21°C): δ = 8.18 (d, 1H), δ = 8.04 (d, 1H), δ = 7.55 (t, 1H), δ = 7.38 (t, 1H), δ = 6.73 (d, 2H; $^3J_{H\text{-}P}$ = 8.5 Hz), δ = 4.44 (s, 2H), δ = 4.37 (s, 2H), δ = 4.01 (s, 5H); ^{13}C NMR (50 MHz, $CDCl_3$, 21°C): δ = 146.45, 133.25, 128.50, 124.87, 120.04, 111.60, 105.62, 72.07, 71.94, 71.23, 71.07, 70.44, 31.37, 11.18.

7.6.4 Synthesis of Rh(cod)[$(C_5H_5)Fe(C_5H_4PS_2OCH_2C_6H_4N_3)$] (15)

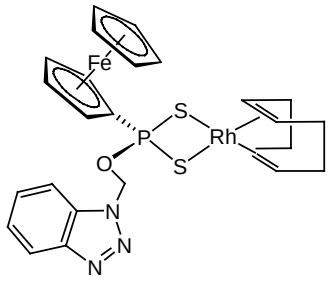

100 mg (0.2 mmol) of $[Rh(cod)Cl]_2$ and 320 mg (0.5 mmol) of $[NEt_3H]$**12** were dissolved in dichloromethane (20 ml). The resulting solution was stirred at room temperature for 2h, and then the solvent was removed under reduced pressure. The residue was extracted with diethyl ether (20 ml), the solution was

filtered and then the solvent was evaporated to dryness. The remaining orange solid was washed with hexane (10 ml) and dried *in vacuo* (105 mg, 82%).

Crystals suitable for X-ray diffraction analysis were grown by slow evaporation of a 1:3 CH_2Cl_2/pentane solution; Elemental analysis (%) calculated for $C_{25}Fe_1H_{27}N_3O_1P_1Rh_1S_2$ (639.4): C 46.9, H 4.2; found C 46.9, H 4.6; $^{31}P\{^1H\}$NMR([D$_6$]acetone): δ = 110.1 (d; $^2J_{Rh\text{-}P}$ = 12.8 Hz); ^{1}H NMR (200 MHz, [D$_6$]Acetone, 21°C): δ = 8.17 (d, 1H), δ = 8.13 (d, 1H), δ = 7.73 (t, 1H), δ = 7.52 (t, 1H), δ = 6.76 (d, 2H; $^3J_{H\text{-}P}$ = 11.0 Hz), δ = 4.30 - 4.59 (m, 9H); ^{13}C NMR (50 MHz, [D$_6$]Acetone, 21°C): δ = 146.55, 133.35, 128.65, 127.04, 124.78, 120.10, 111.08, 72.40, 72.15, 71.38, 71.17, 71.01, 70.83, 29.05.

7.6.5 Synthesis of $Rh(CO)_2[(C_5H_5)Fe(C_5H_4PS_2OCH_2C_6H_4N_3)]$ (16)

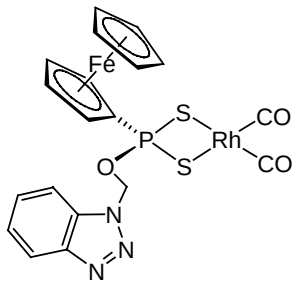

A solution of $[Rh(CO)_2Cl]_2$ (100 mg, 0.26 mmol) and $[NEt_3H]$**12** (410 mg, 0.65 mmol) in acetonitrile (20 ml) was stirred at room temperature for 2h. Then the solvent was removed under reduced pressure. The residue was dissolved in acetone (10 ml), the solution was filtered then evaporated to dryness. The resulting orange solid was washed with hexane (10 ml) and dried under vacuum (115 mg, 76%).

Elemental analysis (%) calculated for $C_{19}Fe_1H_{15}N_3O_3P_1Rh_1S_2$ (587.2): C 38.9, H 2.6; found C 38.6, H 2.8; IR (KBr): 3067vw, 2953w, 1614w, 1494m, 1454m, 1388m, 1289m, 1187m, 1151m, 1000vs, 970s, 858s, 753s, 601m, 583m, 503m, 481m, 452m, 432 w cm^{-1}.- $^{31}P\{^1H\}$ NMR([D_6]acetone): δ = 123.1 (d; $^2J_{Rh-P}$ = 12.8 Hz); ^1H NMR (200 MHz, [D_6]Acetone, 21°C): δ = 8.17 (d, 1H), δ = 8.13 (d, 1H), δ = 7.76 (t, 1H), δ = 7.59 (t, 1H), δ = 6.88 (d, 2H; $^3J_{H-P}$ = 11.9 Hz), δ = 4.59 (m, 4H), δ = 4.18 (s, 5H); ^{13}C NMR (50 MHz, [D_6]Acetone, 21°C): δ = 184.29 (d), 182.44 (d), 146.60, 133.33, 128.84, 125.19, 120.20, 111.05, 72.91, 72.78, 71.64, 71.46, 71.32, 71.29, 70.76.

7.6.6 Synthesis of $Ni[(C_5H_5)Fe(C_5H_4PS_2O)]_2$ (17)

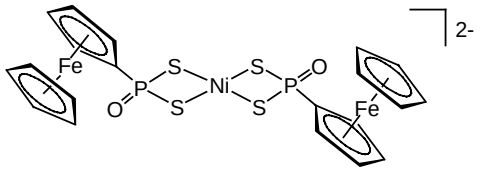

100 mg (0.77 mmol) of $NiCl_2$ and 1.02 g (1.93 mmol) of $[NEt_3H]$**12** were dissolved in acetonitrile/water (1 : 1, 20 ml). After heating at reflux for 1h, the resulting brownish solution was filtered and then the solvent was evaporated to dryness. The remaining brown-orange solid was washed with the same mixture of solvents and dried *in vacuo* (388 mg, 59%).

Crystals suitable for X-ray diffraction analysis were grown by slow evaporation of a 1:3 acetone/pentane solution. Elemental analysis (%) calculated for $C_{32}H_{50}Fe_2N_2Ni_1O_2P_2S_4$ (855.3): C 44.9, H 5.9; found C 44.6, H 5.6; ^{31}P NMR (81 MHz, $CDCl_3$, 21°C): δ = 75.8 (s); ^1H NMR (200 MHz, $CDCl_3$, 21°C): δ = 11.95 (s, 2H), δ = 4.74 (s, 4H), δ = 4.44 (s, 10H), δ = 4.33 (m, 4H), δ = 3.36 (m,

12H), δ = 1.50 (m, 15H); ^{13}C NMR (50 MHz, $CDCl_3$, 21°C): δ = 70.05, 45.99, 9.17.

7.7 Compound of Chapter 4

7.7.1 Synthesis of $Ph_2PC_6H_4C(O)NH(CH_2)_2C(O)OC_6H_4PPh_2$ (18)

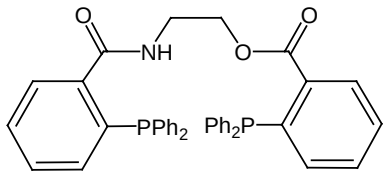

A solution of 2-diphenylphosphinobenzoic acid (1 g, 3.26 mmol), *N*,*N*-dicyclohexylcarbodiimide (2.7 g, 13.05 mmol), 4-(dimethylamino)pyridine (100 mg, 0.82 mmol), 4-pyrrolidinopyridine (100 mg, 0.68 mmol) and ethanolamine (0.1 mL, 1.62 mmol) in CH_2Cl_2 (40 mL) was allowed to stand at room temperature under nitrogen, until the esterification was complete. The resulting solution was filtered through Celite to remove *N*,*N*-dicyclohexyl urea, and the filtrate was concentrated under reduced pressure. The residue was chromatographed on a silica gel column (150 g), eluting with hexane/acetone (2/1). The product was isolated from the third fraction by evaporation of the solvent, giving 220 mg (0.33 mmol, 20 %) of **18** as a white solid.

Elemental analysis (%) calculated for $C_{40}H_{33}N_1O_3P_2$ (637.6): C 75.3, H 5.2; found C 75.1, H 5.3; IR (KBr): 3283m, 3071vw, 3050vw, 3002vw, 2927s, 2852m, 2119vw, 1695vs (C=O ester), 1645s (C=O amide), 1584vw, 1519s, 1432m, 1349m, 1119m, 748m, 694m cm^1; ESI-MS: *m*/*z*: 637 $[M]^+$; ^{1}H NMR (200 MHz, $[D_6]$Acetone, 21°C): δ = 8.41 (s, 1H; -NH), δ = 7.50-7.19 (m, 28H, ArH), δ =

3.87-3.75 (m, 2H; -OCH_2-), δ = 3.47-3.41 (m, 2H, N-CH_2-); ^{13}C NMR (50 MHz, [D_6]Acetone, 21°C): δ = 170.73, 153.77, 144.90, 144.55, 137.74-126.10, 68.71, 49.81; ^{31}P NMR (81 MHz, [D_6]Acetone, 21°C) : -12.47 (br s).

7.7.2 Synthesis of $Ph_2PC_6H_4C(O)N(Ph)(CH_2)_2C(O)OC_6H_4PPh_2$ (19)

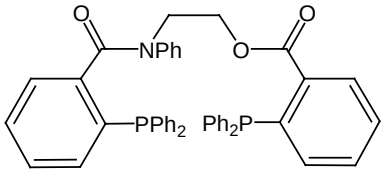

A solution of 2-diphenylphosphinobenzoic acid (1.12 g, 3.65 mmol), *N*,*N*-dicyclohexyl-carbodiimide (900 mg, 4.36 mmol), 4-(dimethylamino)pyridine (100 mg, 0.82 mmol), la 4-pyrrolidinopyridine (100 mg, 0.68 mmol) and N-(2-hydroxyethyl)-aniline (0.18 mL, 1.47 mmol) in CH_2Cl_2 (50 mL) was allowed to stand at room temperature under nitrogen, until the esterification was complete. The resulting solution was filtered through Celite to remove *N*,*N*-dicyclohexyl urea, and the filtrate was concentrated under reduced pressure. The residue was chromatographed on a silica gel column (150 g), eluting with hexane/diethyl ether (1/1). The product was isolated from the third fraction by evaporation of the solvent, giving 483 mg, (0.68 mmol, 46%) of **19**as a white solid.

Elemental analysis (%) calculated for $C_{46}H_{37}N_1O_3P_2$ (713.7): C 77.4, H 5.2; found C 76.9, H 5.4; IR (KBr): 3441vw, 3053vw, 2927vw, 2852vw, 1717s (C=O ester), 1650s (C=O amide), 1586vw, 1494w, 1434m, 1268m, 1253s, 1141vw, 1111w, 745s, 697vs cm^{-1}; ESI-MS: *m*/*z*: 736 $[M + Na]^+$; ^1H NMR (200 MHz, [D_6]DMSO, 21°C): δ = 7.88-6.81 (m, 33H, ArH), δ = 4.34 (br, 2H; -OCH_2-), δ = 4.16 (br, 2H; -NCH_2-); ^{13}C NMR (50 MHz, [D_6]DMSO, 21°C): δ = 170.42,

166.54, 144.31-140.45, 138.40-137.66, 134.85-127.97, 63.04, 48.59; ^{31}P NMR (81 MHz, [D$_6$]DMSO, 21°C) : -4.84 ppm, (s, phosphorus ester), -12.22 ppm (s, phosphorus amide).

7.7.3 Syntheses of $Ph_2PC_6H_4CO_2(CH_2)_2CO_2C_6H_4PPh_2$ (20) and $Ph_2PC_6H_4CO_2(CH_2)_2OH$ (21)

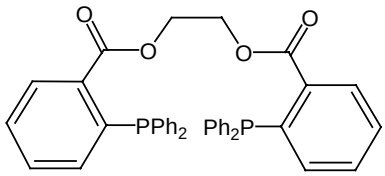

20

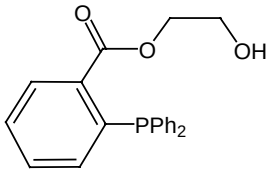

21

A solution of 2-diphenylphosphinobenzoic acid (1 g, 3.26 mmol), *N*,*N*-dicyclohexyl-carbodiimide (2.7 g, 13.05 mmol), 4-(dimethylamino)pyridine (100 mg, 0.82 mmol), la 4-pyrrolidinopyridine (100 mg, 0.68 mmol) and ethylene glycol (0.09 ml, 1.61 mmol) in CH_2Cl_2 (50 mL) was allowed to stand at room temperature under nitrogen, until the esterification was complete. The resulting solution was filtered through Celite to remove *N*,*N*-dicyclohexyl urea, and the filtrate was concentrated under reduced pressure. The residue was chromatographed on a silica gel column (150 g), eluting with hexane/diethyl ether (1/1). The products were isolated from the second (**21**) and the third (**20**) fractions, giving 772 mg (1.21 mmol, 75 %) of **20** and 100 mg (0.31 mmol, 19 %) of **21** as white solids.

Analytical data for **20**: Elemental analysis (%) calculated for $C_{40}H_{32}O_4P_2$ (638.6): C 75.2, H 5.0; found C 75.4, H 5.4; IR (KBr): 3325w, 3052w, 2928m, 2850m, 1715vs (C=O ester), 1626m, 1584w, 1435s, 1270vs, 1254vs, 1117m,

1056s, 989w, 746vs, 696vs cm^{-1}; ESI-MS: *m/z*: 639 $[M]^+$; ^1H NMR (200 MHz, $CDCl_3$, 21°C): δ = 8.10-7.20 (m, 28H, ArH), δ = 4.31 (t, 2H; -OCH_2-; $^3J_{H-H}$ = 4.6 Hz), δ = 3.72 (t, 2H; -OCH_2-; $^3J_{H-H}$ = 4.6 Hz); ^{13}C NMR (50 MHz, $CDCl_3$, 21°C): δ = 167.59, 157.55, 139.06-125.04, 67.64, 61.16; ^{31}P NMR (81 MHz, $CDCl_3$, 21°C) : - 4.21 (br s).

Analytical data for **21**: Elemental analysis (%) calculated for $C_{21}H_{19}O_3P_1$ (350.3): C 72.0, H 5.5; found C 72.4, H 5.4; IR (KBr): 3328br, 2928w, 1708vs (C=O ester), 1627m, 1582w, 1462vw, 1437m, 1271vs, 1141m, 1109m, 1057s, 749s, 699vs cm^{-1}; ESI-MS: *m/z*: 350 $[M]^+$; ^1H NMR (200 MHz, $CDCl_3$, 21°C): δ = 8.10-6.92 (m, 14H, ArH), δ = 4.32 (s, 1H; -OH), δ = 3.95-3.87 (m, 2H; -OCH_2-), δ = 3.52-3.48 (m, 2H; -C(O)OCH_2-); ^{13}C NMR (50 MHz, $CDCl_3$, 21°C): δ = 166.80, 154.19, 140.91, 138.30, 135.22-128.67, 63.21, 50.21; ^{31}P NMR (81 MHz, $CDCl_3$, 21°C) : - 3.71 (br s).

7.7.4 Synthesis of $Ph_2PC_6H_4CO_2(CH_2)_2O(CH_2)_2CO_2C_6H_4PPh_2$ (22)

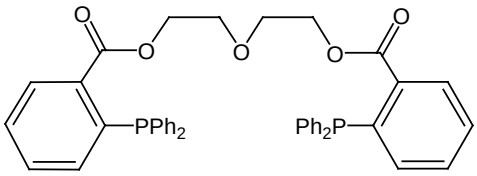

A solution of 2-diphenylphosphinobenzoic acid (1 g, 3.26 mmol), *N*,*N*-dicyclohexyl-carbodiimide (2.7 g, 13.05 mmol), 4-(dimethylamino)pyridine (100 mg, 0.82 mmol), la 4-pyrrolidinopyridine (100 mg, 0.68 mmol) and diethylene glycol (0.16 ml, 1.63 mmol) in CH_2Cl_2 (50 mL) was allowed to stand at room temperature under nitrogen, until the esterification was complete. The resulting solution was filtered through Celite to remove *N*,*N*-dicyclohexyl urea, and the

filtrate was concentrated under reduced pressure. The residue was chromatographed on a silica gel column (150 g), eluting with hexane/diethyl ether (1/1). The product was isolated from the third fraction by evaporation of the solvent, giving 567 mg, (0.82 mmol, 51%) of **22** as a white solid.

Elemental analysis (%) calculated for $C_{42}H_{36}O_5P_2$ (682.7): C 73.9, H 5.3; found C 73.6, H 5.6; IR (KBr): 3431m, 3054vw, 2928w, 2875w, 1718vs (C=O ester), 1650vw, 1584vw, 1479vw, 1434m, 1270s, 1254vs, 1117s, 1056m, 989vw, 746s, 696s cm^{-1}; ESI-MS: *m/z*: 705 $[M + Na]^+$; ^1H NMR (200 MHz, $CDCl_3$, 21°C): δ = 8.20-6.89 (m, 28H, ArH), δ = 4.31 (t, 4H; -OCH_2-; $^3J_{H-H}$ = 4.8 Hz), δ = 3.60 (t, 4H; -(CO)OCH_2-; $^3J_{H-H}$ = 4.8 Hz); ^{13}C NMR (50 MHz, $CDCl_3$, 21°C): δ = 167.92, 140.93, 140.43, 138.24, 138.03, 134.62-133.73, 132.27, 131.08, 131.03, 129.16-128.51, 69.08, 64.42; ^{31}P NMR (81 MHz, $CDCl_3$, 21°C) : - 3.91 ppm (s).

7.7.5 Synthesis of $Rh[Ph_2PC_6H_4C(O)NH(CH_2)_2CO_2C_6H_4PPh_2](CO)Cl$ (23)

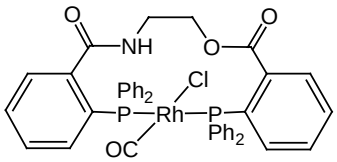

A solution of $[Rh(CO)_2Cl]_2$ (50 mg, 0.13 mmol) and **18** (89 mg, 0.14 mmol) in dichloromethane (20 ml) was stirred at room temperature for 2h. Then the solvent was removed under reduced pressure. The residue was dissolved in acetone (10 ml), the solution was filtered, then evaporated to dryness. The resulting yellow solid was washed with hexane (10 ml) and dried under vacuum (62 mg, 0.08 mmol, 62 %).

Elemental analysis (%) calculated for $C_{47}H_{37}Cl_1N_1O_4P_2Rh_1$ (804.0): C 61.2, H 4.1; found C 61.5, H 4.3; IR (KBr): 3441m, 2926m, 2852w, 1981vs, 1698vs (C=O ester), 1645vs (C=O amide), 1585w, 1494vw, 1435s, 1277s, 1092m, 748m, 697vs cm^{-1}; ESI-MS : *m/z*: 844 [M]; ^1H NMR (200 MHz, [D_6]Acetone, 21°C): δ = 8.13 (s, 1H; -NH), δ = 7.72-7.19 (m, 28H, ArH), δ = 3.98-3.67 (m, 2H; -OCH_2-), δ = 3.52-3.41 (m, 2H, N-CH_2-); ^{13}C NMR (50 MHz, [D_6]Acetone, 21°C): δ = 171.25, 153.62, 144.80, 144.42, 138.54-125.20, 68.62, 49.92; ^{31}P NMR (81 MHz, [D_6]Acetone, 21°C) : 35.2 (d, $^1J_{Rh-P}$ = 159 Hz).

7.7.6 Synthesis of $Rh[Ph_2PC_6H_4C(O)NPh(CH_2)_2CO_2C_6H_4PPh_2](CO)Cl$ (24)

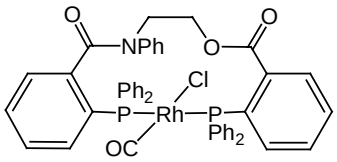

A solution of $[Rh(CO)_2Cl]_2$ (50 mg, 0.13 mmol) and **19** (100 mg, 0.14 mmol) in dichloromethane (20 ml) was stirred at room temperature for 2h. Then the solvent was removed under reduced pressure. The residue was dissolved in acetone (10 ml), the solution was filtered, then evaporated to dryness. The resulting yellow solid was washed with hexane (10 ml) and dried under vacuum (71 mg, 0.08 mmol, 62 %).

Elemental analysis (%) calculated for $C_{47}H_{37}Cl_1N_1O_4P_2Rh_1$ (880.1): C 64.1, H 4.2; found C 64.5, H 4.3; IR (KBr): 3441m, 2926m, 2852w, 1971vs, 1718s (C=O ester), 1627vs (C=O amide), 1585w, 1494vw, 1435s, 1277s, 1092m, 747m, 697vs cm^{-1}; ESI-MS : *m/z*: 844 [M-Cl]; ^1H NMR (200 MHz, $CDCl_3$, 21°C): δ = 8.03-6.25 (m, 33H, ArH), δ = 4.73-4.71 (br, 2H; -OCH_2-), δ = 4.24-3.51 ppm (br,

2H; -NCH_2-); ^{13}C NMR (50 MHz, $CDCl_3$, 21°C): δ = 170.42, 166.54, 144.31-140.45, 138.40-137.66, 134.85-127.97, 63.04, 48.59; ^{31}P NMR (81 MHz, $CDCl_3$, -60°C) : 45.1 (dd, $^1J_{Rh-P}$ = 164 Hz, $^2J_{P-P}$ = 274 Hz), 46.9 (m).

7.7.7 Synthesis of Rh[$Ph_2PC_6H_4CO_2(CH_2)_2CO_2C_6H_4PPh_2$](CO)Cl (25)

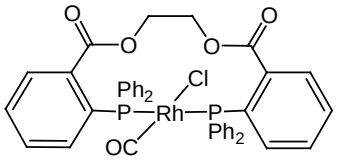

A solution of $[Rh(CO)_2Cl]_2$ (50 mg, 0.13 mmol) and **20** (240 mg, 0.38 mmol) in acetonitrile (20 ml) was stirred at room temperature for 2h. The solution was filtered then, evaporated to dryness. The resulting yellow solid was washed with ether (3 × 10 ml) and dried under vacuum (97mg, 0.12 mmol, 92%).

Elemental analysis (%) calculated for $C_{41}H_{32}Cl_1O_5P_2Rh_1$ (805.1): C 61.2, H 4.0; found C 60.9, H 4.2; IR (KBr): 3422w, 2927vw, 2850vw, 1965s, 1708vs (C=O ester), 1626m, 1572w, 1435m, 1275m, 1145vw, 1117vw, 1059vw, 747w, 694m cm^{-1}; ESI-MS: *m/z*: 805 $[M]^+$; ^1H NMR (200 MHz, CD_2Cl_2, 21°C): δ = 8.02-6.75 (m, 28H, ArH), δ = 4.32 (t, 2H; -OCH_2-; $^3J_{H-H}$ = 5.8 Hz), 3.98 (t, 2H; -OCH_2-; $^3J_{H-H}$ = 5.8 Hz); ^{13}C NMR (50 MHz, CD_2Cl_2, 21°C): δ = 165.46, 134.59-130.54, 129.55, 127.60, 66.40, 59.03; ^{31}P NMR (81 MHz, CD_2Cl_2, 21°C) : 37.2 (d, $^1J_{Rh-P}$ = 136.7 Hz).

7.7.8 Synthesis of $[Rh[Ph_2PC_6H_4CO_2(C_4H_8O)CO_2C_6H_4PPh_2](CO)Cl]_2$ (26)

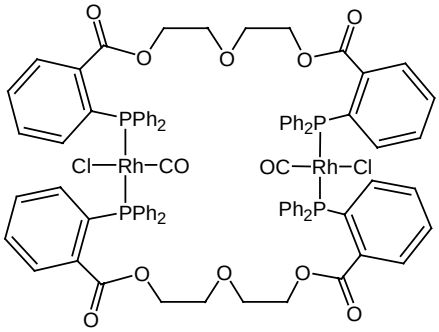

A solution of $[Rh(CO)_2Cl]_2$ (50 mg, 0.13 mmol) and **22** (178 mg, 0.26 mmol) in acetonitrile (20 ml) was stirred at room temperature for 2h. The solution was filtered then evaporated to dryness. The resulting yellow solid was washed with ether (3 × 10 ml) and dried under vacuum (84 mg, 0.10 mmol, 77%). Crystals suitable for X-ray diffraction analysis were grown by slow evaporation of a 1:3 acetone/hexane solution.

Elemental analysis (%) calculated for $C_{86}H_{72}O_{12}P_4Rh_2Cl_2$ (1698.1): C 60.8, H 4.3; found C 60.9, H 4.2; IR (KBr): 3423m, 2924w, 2875w, 1968vs, 1716vs (C=O ester), 1480vw, 1435m, 1275s, 1112m, 1063m, 748s, 696s cm^{-1}; ESI-MS : *m/z*: 1698 $[M]^+$; ^1H NMR (200 MHz, $CDCl_3$, 21°C): δ = 8.13-7.05 (m, 56H, ArH), δ = 4.25-4.04 (br, 8H; -OCH_2-), 3.58-3.22 ppm (br, 8H; -OCH_2-); ^{13}C NMR (50 MHz, $CDCl_3$, 21°C): δ = 207.79, 166.36, 135.51-128.21, 72.51; 68.89, 64.40, 61.86; ^{31}P NMR (81 MHz, $CDCl_3$, 21°C) : 34.89 (d, $^1J_{Rh-P}$ = 136.7 Hz).

7.7.9 Synthesis of $Ir[Ph_2PC_6H_4C(O)NH(CH_2)_2CO_2C_6H_4PPh_2](cod)Cl$ (27)

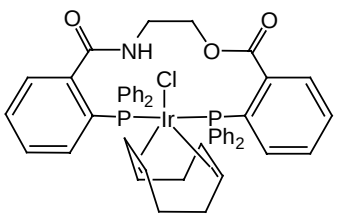

A solution of $[Ir(cod)Cl]_2$ (50 mg, 0.07 mmol) in dichloromethane (10 ml) was added to a solution of **18** (192 mg, 0.30 mmol) in the same solvent (10 ml). After refluxing for 12h, the resulting orange solution was filtered, and then the solvent was evaporated to dryness. The remaining yellow-orange solid was washed three times with ether and dried *in vacuo* (178 mg, 0.17 mmol, 60 %).

Elemental analysis (%) calculated for $C_{48}H_{45}Cl_1Ir_1N_1O_3P_2$ (973.5): C 59.2, H 4.7; found C 59.5, H 4.3; IR (KBr): 3438br, 3253m, 3053vw, 2928s, 2854m, 1695vs (C=O ester), 1630vs (C=O amide), 1533m, 1451vw, 1434vw, 1367w, 1346vw, 1093w, 747w, 697m cm^{-1}; ^1H NMR (200 MHz, $CDCl_3$, 21°C): δ = 8.02 (br s, 1H; -NH), δ = 8.06-7.02 (m, 40H, ArH), δ = 4.98-4.13 (br, 2H; -CH=CH- (cod)), δ = 3.66-3.32 (m, 4H; $-OCH_2-$ and $-NCH_2-$), δ = 2.39-1.73 (m, 8H; $-CH_2-$ (cod)); ^{13}C NMR (50 MHz, $CDCl_3$, 21°C): δ = 179.11, 176.57, 166.45, 163.67, 160.61, 154.85, 154.37, 139.88-124.58, 55.11, 50.64, 49.96, 49.55, 34.37, 32.25, 31.23, 30.11, 29.77, 28.43, 26.73; ^{31}P NMR (81 MHz, $CDCl_3$, 21°C) : 20.93 (br s).

7.7.10 Synthesis of $Ir[Ph_2PC_6H_4C(O)NPh(CH_2)_2CO_2C_6H_4PPh_2](cod)Cl$ (28)

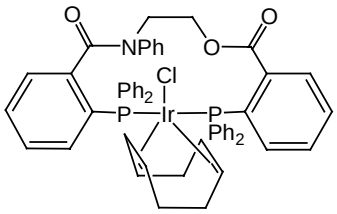

A solution of $[Ir(cod)Cl]_2$ (50 mg, 0.07 mmol) in toluene (10 ml) was added dropwise to a solution of **19** (214 mg, 0.30 mmol) in the same solvent (10 ml). After refluxing for 12h, the resulting orange solution was filtered, and then the

solvent was evaporated to dryness. The remaining yellow-orange solid was washed three times with ether and dried *in vacuo* (96 mg, 0.09 mmol, 65 %).

Elemental analysis (%) calculated for $C_{54}H_{49}O_3P_4Ir_1Cl_1N_1$ (1049.6): C 61.8, H 4.7; found C 61.9, H 4.3; IR (KBr): 3427vw, 2928m, 2851w, 1717s (C=O ester), 1651s (C=O amide), 1583w, 1234m, 1272s, 1142m, 1056m, 746s cm^{-1}; ESI-MS: *m/z*: 1049 $[M]^+$; ^1H NMR (200 MHz, $CDCl_3$, 21°C): δ = 8.01-6.89 (m, 33H, ArH), δ = 4.80 (br, 2H; -CH=CH- (cod)), δ = 4.25 (br, 2H; -OCH_2-), δ = 3.49 (br, 2H; -NCH_2-), δ = 3.35 m, 2H; -CH=CH- (cod)), δ = 2.20-1.80 (m, 8H; -CH_2- (cod)); ^{13}C NMR (50 MHz, $CDCl_3$, 21°C): δ = 170.21, 167.32, 136.53-128.64, 68.30, 60.24, 33.46, 32.17, 29.94, 29.63, 22.95; ^{31}P NMR (81 MHz, $CDCl_3$, 21°C) : 21.64 (br s).

7.7.11 Synthesis of Ir[$Ph_2PC_6H_4CO_2(CH_2)_2CO_2C_6H_4PPh_2$](cod)Cl (29)

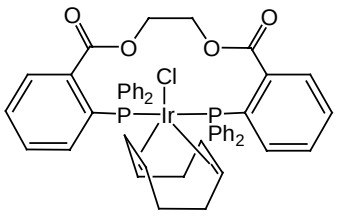

A solution of $[Ir(cod)Cl]_2$ (50 mg, 0.07 mmol) in toluene (10 ml) was added dropwise to a solution of **20** (192 mg, 0.30 mmol) in the same solvent (10 ml). After refluxing for 12h, the resulting orange solution was filtered, and then the solvent was evaporated to dryness. The remaining yellow-orange solid was washed three times with ether and dried *in vacuo* (96 mg, 0.10 mmol, 71 %).

Elemental analysis (%) calculated for $C_{48}H_{44}Cl_1Ir_1O_4P_2$ (974.5): C 59.2, H 4.5; found C 59.3, H 4.7; IR (KBr): 3427br, 2928m, 2851w, 1710s (C=O ester),

1626m, 1583w, 1234m, 1272s, 1142m, 1056m, 746s cm^{-1}; ESI-MS : *m/z*: 1059 [M + CH_2Cl_2]$^+$; ^{1}H NMR (200 MHz, $CDCl_3$, 21°C): δ = 8.20-6.89 (m, 28H, ArH), δ = 4.90 (br, 2H; -CH=CH- (cod)), δ = 4.44-4.40 (br, 2H; -OCH_2-), δ = 4.09 (br, 2H; -OCH_2-), δ = 3.49 (m, 2H; -CH=CH- (cod)), δ = 2.20 ppm (m, 8H; -CH_2- (cod)); ^{13}C NMR (50 MHz, $CDCl_3$, 21°C): δ = 167.64, 135.43-128.34, 68.30, 60.24, 33.46, 32.17, 29.94, 29.63, 22.95; ^{31}P NMR (81 MHz, $CDCl_3$, 21°C) : 20.43 (br s).

7.7.12 Synthesis of Ir[$Ph_2PC_6H_4C(O)NH(CH_2)_2CO_2C_6H_4PPh_2$](CO)Cl (30)

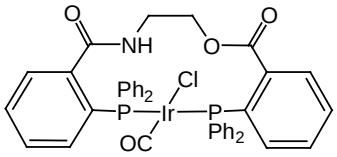

An orange solution of **27** (100 mg, 0.10 mmol) in dichloromethane (50 ml) was stirred at room temperature under CO. After 5min the resulting yellow solution was filtered, and then the solvent was evaporated to dryness. The remaining yellow solid was washed three times with ether/pentane (5 : 1, 10 ml), three times with pentane (10 ml) and dried *in vacuo* (45 mg, 0.05 mmol, 50 %).

Elemental analysis (%) calculated for $C_{43}H_{36}Cl_1Ir_1O_6P_2$ (893.3): C 55.1, H 3.7; found C 54.8, H 4.0; IR (KBr): 3283m, 3053vw, 2925vw, 1950 vs, 1695vs (C=O ester), 1645s (C=O amide), 1295m, 1275s, 1112m, 749w, 744s, 694s cm^{-1}; ^{1}H NMR (200 MHz, $CDCl_3$, 21°C): δ = 8.05 (br s, 1H; -NH), δ = 8.10-7.05 (m, 40H, ArH), δ = 3.68-3.30 (m, 4H; -OCH_2- and -NCH_2-); ^{13}C NMR (50 MHz, $CDCl_3$, 21°C): δ = 180.13, 176.57, 166.45, 163.67, 160.61, 154.85, 154.37, 139.88-124.58, 55.11, 50.64; ^{31}P NMR (81 MHz, $CDCl_3$, 21°C) : 27.10 (br s).

7.7.13 Synthesis of Ir[$Ph_2PC_6H_4C(O)NPh(CH_2)_2CO_2C_6H_4PPh_2$](CO)Cl (31)

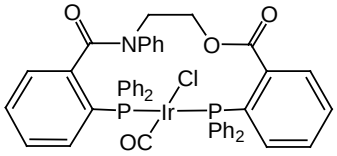

An orange solution of **28** (100 mg, 0.10 mmol) in dichloromethane (50 ml) was stirred at room temperature under CO. After 5min the resulting yellow solution was filtered, and then the solvent was evaporated to dryness. The remaining yellow solid was washed three times with ether/pentane (5 : 1, 10 ml), three times with pentane (10 ml) and dried *in vacuo* (40 mg, 0.041 mmol, 41 %).

Elemental analysis (%) calculated for $C_{43}H_{36}Cl_1Ir_1O_6P_2$ (969.4): C 58.2, H 3.8; found C 58.0, H 4.1; IR (KBr): 3422vw, 3053vw, 2925vw, 1951 vs, 1718vs (C=O ester), 1650s (C=O amide), 1295m, 1275s, 1112m, 749w, 744s, 694s cm^{-1}; ^1H NMR (200 MHz, $CDCl_3$, 21°C): δ = 8.01-6.89 (m, 33H, ArH), δ = 4.25 (br, 2H; -OCH_2-), δ = 3.49 (br, 2H; -NCH_2-); ^{13}C NMR (50 MHz, $CDCl_3$, 21°C): δ = 170.21, 167.32, 136.53-128.64, 68.30, 60.24; ^{31}P NMR (81 MHz, $CDCl_3$, 21°C) : 27.93 (br s).

7.7.14 Synthesis of Ir[$Ph_2PC_6H_4CO_2(CH_2)_2CO_2C_6H_4PPh_2$](CO)Cl (32)

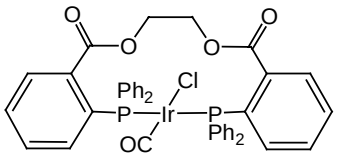

An orange solution of **29** (100 mg, 0.10 mmol) in dichloromethane (50 ml) was stirred at room temperature under CO. After 5min the resulting yellow solution was filtered, and then the solvent was evaporated to dryness. The

remaining yellow solid was washed three times with ether/pentane (5 : 1, 10 ml), three times with pentane (10 ml) and dried *in vacuo* (45 mg, 0.05 mmol, 50 %).

Elemental analysis (%) calculated for $C_{43}H_{36}Cl_1Ir_1O_6P_2$ (894.3): C 55.0, H 3.6; found C 54.6, H 4.2; IR (KBr): 3422vw, 3053vw, 2925vw, 1944 vs, 1720vs (C=O ester), 1434s, 1295m, 1275s, 1112m, 749w, 744s, 694s cm^{-1}; ESI-MS : *m/z*: 894 $[M]^+$; ^1H NMR (200 MHz, $CDCl_3$, 21°C): δ = 8.22-6.90 (m, 28H, ArH), δ = 4.40-4.29 (m, 2H; -OCH_2-), δ = 3.74-3.71 (m, 2H; -OCH_2-); ^{13}C NMR (50 MHz, $CDCl_3$, 21°C): δ = 167.64, 135.43-128.34, 68.30, 60.24; ^{31}P NMR (81 MHz, $CDCl_3$, 21°C) : 27.52 (br s).

7.7.15 Synthesis of Ir[$Ph_2PC_6H_4CO_2(CH_2)_2OH$](cod)Cl (33)

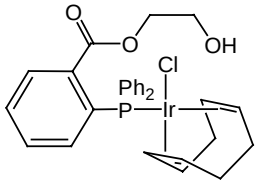

A solution of $[Ir(cod)Cl]_2$ (50 mg, 0.07 mmol) in dichloromethane (10 ml) was added dropwise to a solution of **21** (52 mg, 0.15 mmol) in the same solvent (10 ml). Then the solution was heated to reflux for 12h. After filtration of the cooled down solution, the solvent was evaporated to dryness. The remaining yellow-orange solid was washed three times with ether and dried *in vacuo* (96 mg, 0.10 mmol, 71 %).

Crystals suitable for X-ray diffraction analysis were grown by slow evaporation of a 1:3 acetone/hexane solution. Elemental analysis (%) calculated for $C_{29}H_{31}Cl_1Ir_1O_3P_1$ (686.2): C 50.8, H 4.5; found C 50.9, H 4.2; IR (KBr):

3340br, 2932w, 1705vs (C=O ester), 1627w, 1437vw, 1368vw, 1274vs, 1144m, 1095m, 105ws, 747m, 694s cm^{-1}; ^{1}H NMR (200 MHz, $CDCl_3$, 21°C): δ = 8.15-6.80 (m, 14H, ArH), δ = 4.91 (m, 2H; -CH=CH- (cod)), δ = 4.42 (m, 2H; -CH=CH- (cod)), δ = 4.10-4.06 (m, 2H; -(CO)OCH_2-), δ = 3.68-3.66 (m, 2H; -OCH_2-), δ = 2.42-2.20 ppm (m, 8H; -CH_2- (cod)); ^{13}C NMR (50 MHz, $CDCl_3$, 21°C): δ = 166.80, 154.19, 140.91, 138.30, 135.22-128.67, 63.21, 50.21; ^{31}P NMR (81 MHz, $CDCl_3$, 21°C) : 20.28 (br s).

7.7.16 Synthesis of $Ir[Ph_2PC_6H_4CO_2(CH_2)_2OH](CO)_2Cl$ (34)

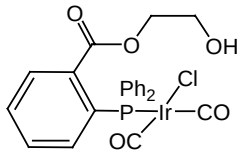

An orange solution of **33** (100 mg, 0.15 mmol) in dichloromethane (50 ml) was stirred at room temperature under CO. After 5min the resulting yellow solution was filtered, and then the solvent was evaporated to dryness. The remaining yellow solid was washed three times with ether/pentane (5 : 1, 10 ml), three times with pentane (10 ml) and dried *in vacuo* (57 mg, 0.09 mmol, 60 %).

Elemental analysis (%) calculated for $C_{23}H_{19}Cl_1Ir_1O_5P_1$ (634.0): C 43.6, H 3.0; found C 44.0, H 3.2; IR (KBr): 3440vw, 3054vw, 2067.2, 1985vs, 1707s (C=O ester), 1647m, 1579w, 1435s, 1277s, 746s $cm^{-1}.cm^{-1}$; ^{1}H NMR (200 MHz, $CDCl_3$, 21°C): δ = 8.22-6.90 (m, 28H, ArH), δ = 4.40-4.29 (m, 2H; -OCH_2-), δ = 3.74-3.71 (m, 2H; -OCH_2-); ^{13}C NMR (50 MHz, $CDCl_3$, 21°C): δ = 167.64, 135.43-128.34, 68.30, 60.24; ^{31}P NMR (81 MHz, $CDCl_3$, 21°C): 27.52 (br s).

7.7.17 Synthesis of $Pt[Ph_2PC_6H_4C(O)N(Ph)(CH_2)_2C(O)OC_6H_4PPh_2]I_2$ (35)

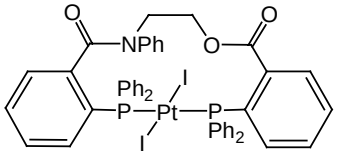

A solution of $Pt(cod)I_2$ (50 mg, 0.09 mmol) and **19** (70 mg, 0.10 mmol) in dichloromethane (20 ml) was stirred at room temperature for 12h. Then the solvent was removed under reduced pressure. The resulting yellow solid was washed with hexane (10 ml) and dried under vacuum (70 mg, 0.06 mmol, 67 %).

Crystals suitable for X-ray diffraction analysis were grown by slow evaporation of a 1:3 dichloromethane/hexane solution. Elemental analysis (%) calculated for $C_{46}H_{37}NO_3P_2Pt$ (1162.6): C 47.5, H 3.2; found C 47.7, H 3.3; IR (KBr): 3432vw, 3054m, 2922s, 2848m, 1707s (C=O ester), 1619s (C=O amide), 1593m, 1493m, 1480m, 1435s, 1252m, 1091m, 745m, 694vs, 520vs cm^{-1}; ESI-MS : *m/z*: 849 $[M]^+$; ^1H NMR (200 MHz, $CDCl_3$, 21°C): δ = 8.03-6.25 (m, 33H, ArH), δ = 4.73-4.71 (br, 2H; $-OCH_2-$), δ = 4.24-3.51 ppm (br, 2H; $-NCH_2-$); ^{13}C NMR (50 MHz, $CDCl_3$, 21°C): δ = 170.42, 166.54, 144.31-140.45, 138.40-137.66, 134.85-127.97, 63.04, 48.59; ^{31}P NMR (81 MHz, $CDCl_3$, 21°C) : 11.92 ($^1J(^{195}Pt-^{31}P)$ = 2702 Hz).

7.8 Catalytic runs

In a typical experiment, 24 mg (0.06 mmol) $[Rh(CO)_2Cl]_2$ and 0.12 mmol of ligand were dissolved in methanol (4.46 ml). To this solution, placed in a 100 ml stainless steel autoclave, 11 mmol of iodomethane and 200 mmol of water were added. After purging three times with CO, the autoclave was pressurised

with carbon monoxide (25 bar) and heated to 170°C under vigorous stirring of the reaction mixture (900 rpm). After 20 min, the autoclave was cooled to room temperature, and the pressure was released. The solution was filtered and analysed by GC.

Other catalytic runs were performed in the same way using the conditions specified in the corresponding tables.

Chapter 8

Crystallographic Data

Intensity data were collected on a Stoe Image Plate Diffraction system[254] using MoKα graphite monochromated radiation. The structure was solved by direct methods using the programme SHELXS-97.[255] The refinement and all further calculations were carried out using SHELXL-97.[256] The H-atoms were included in calculated positions and treated as riding atoms using SHELXL default parameters. The non-H atoms were refined anisotropically, using weighted full-matrix least-squares on F^2. Structure calculations, checking for higher symmetry and preparations of molecular plots were performed with the PLATON[257] package. Further experimental details are given in the following tables.

Lists of atomic coordinates, anisotropic displacement parameters and crystallographic data (excluding structure factors) have been deposited with the Cambridge Crystallographic Data Centre, CCDC no. 179635 (**1**), 179636 (**2**), 179637 (**6**), 173832 (**7**), 179638 (**10**), 160381 (**11**), 157385 (**12** triethylammonium salt), 157386 (**15**), 157387 (**17**), CCDC 178634 (**26**), 178812 (**33**), 178813 (**35**), 178933 (**36a**), and 178932 (**36b**). Copies of this information may be obtained free of charge from The Director, CCDC, 12 Union Road, Cambridge CB2 1EZ, UK (Fax: +44-1223-336033; e-mail: deposit@ccdc.cam.ac.uk or www: http://www.ccdc.cam.ac.uk).

Table 20: Summary of X-ray single-crystal data for **1**

Empirical formula	$C_{13}H_{10}N_4O_2$
Crystal color	Colorless
Molecular mass	254.25
Temperature [K]	223(2)
Crystal system	Monoclinic
Space group	C 2/c
a [Å]	11.3242(13)
b [Å]	10.6104(15)
c [Å]	19.8168(19)
α[°]	90
β[°]	97.432(8)
γ[°]	90
Volume [Å^3]	2361.1(5)
Z	8
D_c [g cm^{-3}]	1.431
μ [mm^{-1}]	0.101
F (000)	1056
θ range [°]	2.07-25.48
Unique refl. with $I > 2\sigma(I)$	2204
Final *R*1, *w*R2 (observed data)	0.0474, 0.0907
Parameters/restraints	213/0
GoF	1.129
Residual density (max/min) [eÅ^{-3}]	0.227/-0.164

$R1 = [\Sigma(||Fo|-|Fc||)/\Sigma|Fo|]$; $\omega R^2 = \{[\Sigma(\omega(Fo^2-Fc^2)^2)/\Sigma(\omega Fo^4)]^{1/2}\}$

Table 21: Summary of X-ray single-crystal data for **2**

Empirical formula	$C_{18}H_{15}Fe_1N_3O_2$
Crystal colour	Orange
Molecular mass	361.18
Temperature [K]	223(2)
Crystal system	Triclinic
Space group	*P -1*
a [Å]	5.732(5)
b [Å]	10.716(5)
c [Å]	13.740(5)
α[°]	109.809(5)
β[°]	97.364(5)
γ[°]	102.569(5)
Volume [Å^3]	756.0(8)
Z	2
D_c [g cm^{-3}]	1.587
μ [mm^{-1}]	1.013
F (000)	372
θ range [°]	2.10-25.49
Unique refl. with $I > 2\sigma(I)$	2802
Final *R*1, *w*R2 (observed data)	0.0226, 0.0532
Parameters/restraints	278/0
GoF	1.101
Residual density (max/min) [eÅ^{-3}]	0.242/-0.240

$R1 = [\Sigma(||Fo|-|Fc||)/\Sigma|Fo|]$; $\omega R^2 = \{[\Sigma(\omega(Fo^2-Fc^2)^2)/\Sigma(\omega Fo^4)]^{1/2}\}$

Table 22: Summary of X-ray single-crystal data for **6**

Empirical formula	$C_{36}H_{30}I_2N_6O_4Co_1 \cdot CH_2Cl_2$
Crystal colour	Green
Molecular mass	1120.02
Temperature [K]	223(2)
Crystal system	Triclinic
Space group	*P -1*
a [Å]	11.4520(13)
b [Å]	12.614(2)
c [Å]	15.5990(19)
α[°]	98.605(14)
β[°]	100.875(9)
γ[°]	110.255(12)
Volume [Å^3]	2018.7(5)
Z	2
D_c [g cm^{-3}]	1.843
μ [mm^{-1}]	2.823
F (000)	1094
θ range [°]	2.07-25.00
Unique refl. with $I > 2\sigma(I)$	7103
Final *R*1, *w*R2 (observed data)	0.0522, 0.1053
Parameters/restraints	487/0
GoF	1.067
Residual density (max/min) [eÅ^{-3}]	1.053/-1.316

$R1 = [\Sigma(||Fo|-|Fc||)/\Sigma|Fo|]$; $\omega R^2 = \{[\Sigma(\omega(Fo^2-Fc^2)^2)/\Sigma(\omega Fo^4)]^{1/2}\}$

Table 23: Summary of X-ray single-crystal data for **7**

Empirical formula	$C_{23}H_{21}I_2N_6O_4S_1Co_1$
Crystal colour	Green
Molecular mass	790.25
Temperature [K]	153(2)
Crystal system	Triclinic
Space group	*P -1*
a [Å]	8.7294(7)
b [Å]	12.8364(11)
c [Å]	14.2166(12)
α[°]	90.648(10)
β[°]	91.198(10)
γ[°]	95.957(10)
Volume [Å^3]	1583.9(2)
Z	2
D_c [g cm^{-3}]	1.657
μ [mm^{-1}]	2.592
F (000)	764
θ range [°]	2.13-25.84
Unique refl. with $I > 2\sigma(I)$	5713
Final *R*1, *w*R2 (observed data)	0.0305, 0.0971
Parameters/restraints	363/10
GoF	1.073
Residual density (max/min) [eÅ^{-3}]	0.833/-0.514

$R1 = [\Sigma(||Fo|-|Fc||)/\Sigma|Fo|]$; $\omega R^2 = \{[\Sigma(\omega(Fo^2-Fc^2)^2)/\Sigma(\omega Fo^4)]^{1/2}\}$

Table 24: Summary of X-ray single-crystal data for **10**

Empirical formula	$C_{53}H_{40}Cl_1N_6O_5P_2Rh_1$
Crystal colour	Yellow
Molecular mass	1041.21
Temperature [K]	153(2)
Crystal system	Monoclinic
Space group	*P* $2_1/n$
a [Å]	9.8950(9)
b [Å]	15.7363(10)
c [Å]	15.0518(15)
α[°]	90
β[°]	94.107(12)
γ[°]	90
Volume [Å^3]	2337.7(3)
Z	2
D_c [g cm^{-3}]	1.479
μ [mm^{-1}]	0.548
F (000)	1064
θ range [°]	1.87-25.95
Unique refl. with $I > 2\sigma(I)$	4434
Final *R*1, *w*R2 (observed data)	0.0289, 0.0659
Parameters/restraints	322/0
GoF	0.918
Residual density (max/min) [eÅ^{-3}]	0.428/-0.457

$R1 = [\Sigma(||Fo|-|Fc||)/\Sigma|Fo|]$; $\omega R^2 = \{[\Sigma(\omega(Fo^2-Fc^2)^2)/\Sigma(\omega Fo^4)]^{1/2}\}$

Table 25: Summary of X-ray single-crystal data for **11**

Empirical formula	$C_{66.5}H_{73}I_{12}N_{12}O_{19.5}Rh_4S_2$
Crystal color	Red-brown
Molecular mass	3350.93
Temperature [K]	153(2)
Crystal system	triclinic
Space group	*P-1*
a [Å]	27.693(2)
b [Å]	14.3087(13)
c [Å]	13.6096(11)
α[°]	103.300(10)
β[°]	80.091(10)
γ[°]	79.420(10)
Volume [Å^3]	5027.9(7)
Z	2
D_c [g cm^{-3}]	2.213
μ [min^{-1}]	4.434
F (000)	3120
θ range [°]	1.84-25.83
Unique refl. with $I > 2\sigma(I)$	11752
Final *R*1, *w*R2 (observed data)	0.0578, 0.1600
Parameters/restraints	740/0
GoF	1.009
Residual density (max/min) [eÅ^{-3}]	2.941/-2.508

$R1 = [\Sigma(||Fo|-|Fc||)/\Sigma|Fo|]$; $\omega R^2 = \{[\Sigma(\omega(Fo^2-Fc^2)^2)/\Sigma(\omega Fo^4)]^{1/2}\}$

Table 26: Summary of X-ray single-crystal data for **12**

Empirical formula	$C_{23}H_{31}Fe_1N_4OPS_2$
Crystal color	Yellow
Molecular mass	530.46
Temperature [K]	153(2)
Crystal system	monoclinic
Space group	*C2/c*
a [Å]	11.9317(7)
b [Å]	10.4665(9)
c [Å]	39.806(2)
α[°]	90
β[°]	95.054(7)
γ[°]	90
Volume [Å^3]	4951.7(6)
Z	8
D_c [g cm^{-3}]	1.423
μ [min^{-1}]	0.866
F (000)	2224
θ range [°]	2.15-22.50
Unique refl. with $I > 2\sigma(I)$	2944
Final *R*1, *w*R2 (observed data)	0.0330, 0.0856
Parameters/restraints	293/0
GoF	1.009
Residual density (max/min) [eÅ^{-3}]	0.343/-0.288

$R1 = [\Sigma(||Fo|-|Fc||)/\Sigma|Fo|]$; $\omega R^2 = \{[\Sigma(\omega(Fo^2-Fc^2)^2)/\Sigma(\omega Fo^4)]^{1/2}\}$

Table 27: Summary of X-ray single-crystal data for **15**

Empirical formula	$C_{26}H_{29}Cl_2Fe_1N_3O_1P_1RhS_2$
Crystal color	Orange
Molecular mass	724.27
Temperature [K]	153(2)
Crystal system	monoclinic
Space group	$P2_1/c$
a [Å]	6.3599(4)
b [Å]	20.1621(13)
c [Å]	22.3423(15)
α[°]	90
β[°]	97.011(8)
γ[°]	90
Volume [Å^3]	2843.5(3)
Z	4
D_c [g cm^{-3}]	1.692
μ [min^{-1}]	1.508
F (000)	1464
θ range [°]	2.15-25.08
Unique refl. with $I > 2\sigma(I)$	5346
Final *R*1, *w*R2 (observed data)	0.0445, 0.0995
Parameters/restraints	334/0
GoF	0.857
Residual density (max/min) [eÅ^{-3}]	0.731/-1.279

$R1 = [\Sigma(||Fo|-|Fc||)/\Sigma|Fo|]$; $\omega R^2 = \{[\Sigma(\omega(Fo^2-Fc^2)^2)/\Sigma(\omega Fo^4)]^{1/2}\}$

Table 28: Summary of X-ray single-crystal data for **17**

Empirical formula	$C_{32}H_{50}Fe_2N_2NiO_2P_2S_4$
Crystal color	Brown
Molecular mass	855.33
Temperature [K]	153(2)
Crystal system	monoclinic
Space group	$P2_1/c$
a [Å]	8.9648(8)
b [Å]	17.0764(13)
c [Å]	12.0475(10)
α[°]	90
β[°]	90.991(10)
γ[°]	90
Volume [Å^3]	1844.0(3)
Z	2
D_c [g cm^{-3}]	1.540
μ [min^{-1}]	1.627
F (000)	892
θ range [°]	2.07-25.85
Unique refl. with $I > 2\sigma(I)$	3348
Final *R*1, *w*R2 (observed data)	0.0309, 0.0569
Parameters/restraints	305/0
GoF	0.836
Residual density (max/min) [eÅ^{-3}]	0.319/-0.371

$R1 = [\Sigma(||Fo|-|Fc||)/\Sigma|Fo|]$; $\omega R^2 = \{[\Sigma(\omega(Fo^2-Fc^2)^2)/\Sigma(\omega Fo^4)]^{1/2}\}$

Table 29: Summary of X-ray single-crystal data for **26**

Empirical formula	$C_{92}H_{84}Cl_2O_{14}P_4Rh_2$
Crystal color	Yellow
Molecular mass	1814.2
Temperature [K]	153(2)
Crystal system	Triclinic
Space group	P -1
a [Å]	10.910(5)
b [Å]	13.533(5)
c [Å]	14.576(5)
α[°]	89.327(5)
β[°]	87.031(5)
γ[°]	78.907(5)
Volume [Å^3]	2109.0(14)
Z	2
D_c [g cm^{-3}]	1.428
μ [mm^{-1}]	0.595
F (000)	932
θ range [°]	0.931-25.87
Unique refl. with $I > 2\sigma(I)$	7621
Final *R*1, *w*R2 (observed data)	0.0327, 0.0430
Parameters/restraints	516/0
GoF	0.881
Residual density (max/min) [eÅ^{-3}]	0.985/-0.817

$R1 = [\Sigma(||Fo|-|Fc||)/\Sigma|Fo|]$; $\omega R^2 = \{[\Sigma(\omega(Fo^2-Fc^2)^2)/\Sigma(\omega Fo^4)]^{1/2}\}$

Table 30: Summary of X-ray single-crystal data for **33**

Empirical formula	$C_{29}H_{31}Cl_1Ir_1O_3P_1$
Crystal color	Yellow
Molecular mass	686.16
Temperature [K]	153(2)
Crystal system	Monoclinic
Space group	*P* $2_1/n$
a [Å]	10.2660(9)
b [Å]	19.4528(17)
c [Å]	13.2522(12)
α[°]	90
β[°]	105.411(10)
γ[°]	90
Volume [Å^3]	2551.3(4)
Z	4
D_c [g cm^{-3}]	1.786
μ [mm^{-1}]	5.431
F (000)	1352
θrange [°]	1.91-25.92
Unique refl. with $I > 2\sigma(I)$	4766
Final *R*1, *w*R2 (observed data)	0.0682, 0.0737
Parameters/restraints	314/0
GoF	0.970
Residual density (max/min) [eÅ^{-3}]	1.443/-0.806

$R1 = [\Sigma(||Fo|-|Fc||)/\Sigma|Fo|]$; $\omega R^2 = \{[\Sigma(\omega(Fo^2-Fc^2)^2)/\Sigma(\omega Fo^4)]^{1/2}\}$

Table 31: Summary of X-ray single-crystal data for **35**

Empirical formula	$C_{46}H_{37}I_2N_1O_3P_2Pt_1 \cdot CH_2Cl_2$
Crystal colour	Orange
Molecular mass	1247.52
Temperature [K]	153(2)
Crystal system	Triclinic
Space group	*P-1*
a [Å]	11.8425(12)
b [Å]	11.9247(11)
c [Å]	18.5076(18)
α[°]	93.712(12)
β[°]	102.166(12)
γ[°]	117.611(11)
Volume [Å^3]	2223.8(4)
Z	2
D_c [g cm^{-3}]	1.863
μ [mm^{-1}]	4.777
F (000)	1200
θrange [°]	1.96-25.98
Unique refl. with $I > 2\sigma(I)$	8067
Final *R*1, *w*R2 (observed data)	0.0241, 0.0536
Parameters/restraints	551/0
GoF	0.910
Residual density (max/min) [eÅ^{-3}]	0.907/-0.968

$R1 = [\Sigma(||Fo|-|Fc||)/\Sigma|Fo|]$; $\omega R^2 = \{[\Sigma(\omega(Fo^2-Fc^2)^2)/\Sigma(\omega Fo^4)]^{1/2}\}$

Table 32: Summary of X-ray single-crystal data for **36a**

Empirical formula	$C_{50}H_{43}I_4N_1O_5P_2Rh_2 \bullet 3CH_3COCH_3$
Crystal color	Red
Molecular mass	1687.45
Temperature [K]	153(2)
Crystal system	Triclinic
Space group	*P-1*
a [Å]	12.5407(12)
b [Å]	14.7810(14)
c [Å]	17.6206(17)
α[°]	105.625(11)
β[°]	98.237(11)
γ[°]	99.102(11)
Volume [Å^3]	3046.0(5)
Z	2
D_c [g cm^{-3}]	1.840
μ [mm^{-1}]	2.673
F (000)	1636
θ range [°]	1.98-25.98
Unique refl. with $I > 2\sigma(I)$	11121
Final *R*1, *w*R2 (observed data)	0.0749, 0.1382
Parameters/restraints	358/0
GoF	0.659
Residual density (max/min) [eÅ^{-3}]	1.495/-1.849

$R1 = [\Sigma(||Fo|-|Fc||)/\Sigma|Fo|]$; $\omega R^2 = \{[\Sigma(\omega(Fo^2-Fc^2)^2)/\Sigma(\omega Fo^4)]^{1/2}\}$

Table 33: Summary of X-ray single-crystal data for **36b**

Empirical formula	$C_{50}H_{43}I_4N_1O_5P_2Rh_2$
Crystal color	Red
Molecular mass	1513.21
Temperature [K]	153(2)
Crystal system	Triclinic
Space group	P-1
a [Å]	13.436(5)
b [Å]	14.749(5)
c [Å]	18.551(5)
α[°]	105.924(5)
β[°]	98.502(5)
γ[°]	107.114(5)
Volume [Å^3]	3272.4(19)
Z	2
D_c [g cm^{-3}]	1.536
μ [mm^{-1}]	2.475
F (000)	1444
θ range [°]	2.10-25.88
Unique refl. with $I > 2\sigma(I)$	11768
Final *R*1, *w*R2 (observed data)	0.0567, 0.1732
Parameters/restraints	504/0
GoF	0.958
Residual density (max/min) [eÅ^{-3}]	6.619/-1.322

$R1 = [\Sigma(||Fo|-|Fc||)/\Sigma|Fo|]$; $\omega R^2 = \{[\Sigma(\omega(Fo^2-Fc^2)^2)/\Sigma(\omega Fo^4)]^{1/2}\}$

Chapter 9

List of Schemes

Chapter 2

Chapter 3

Chapter 4

Chapter 5

Chapter 10

List of Figures

Chapter 2

Chapter 3

Chapter 4

Chapter 5

Summary

The aim of the present work was to synthesize new multifunctional ligands, to study their coordination properties and to exploit their catalytic potential for the carbonylation of methanol.

The first part of this thesis reports on the synthesis of new nitrogen-containing ligands, which are known to be electron-rich ligands, based on the benzotriazole unit. The new benzotriazole ligands **1** - **5** are directly accessible by condensation methods from hydroxymethylbenzotriazole and the corresponding mono- or diacids.

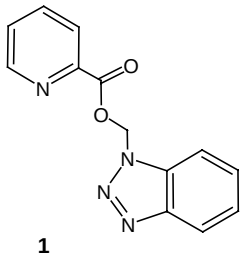

1

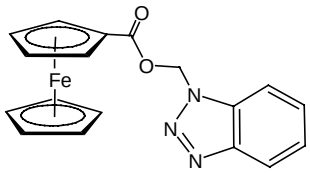

2

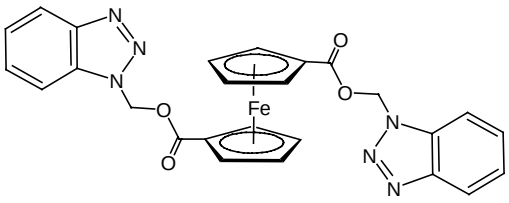

3

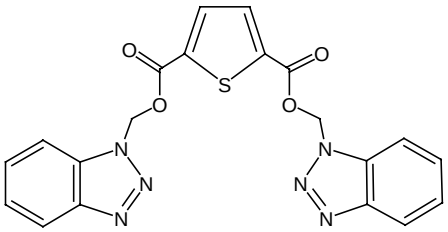

4

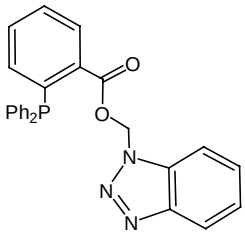

5

The benzotriazole ligand **2** was found to coordinate easily to cobalt through the 3-N atom of the triazole unit to give complex **6**. The single-crystal X-ray structure analysis reveals that the cobalt(II) center is tetrahedrally coordinated

to two iodine atoms and to the 3-N nitrogen atoms of two monodentate triazole ligands.

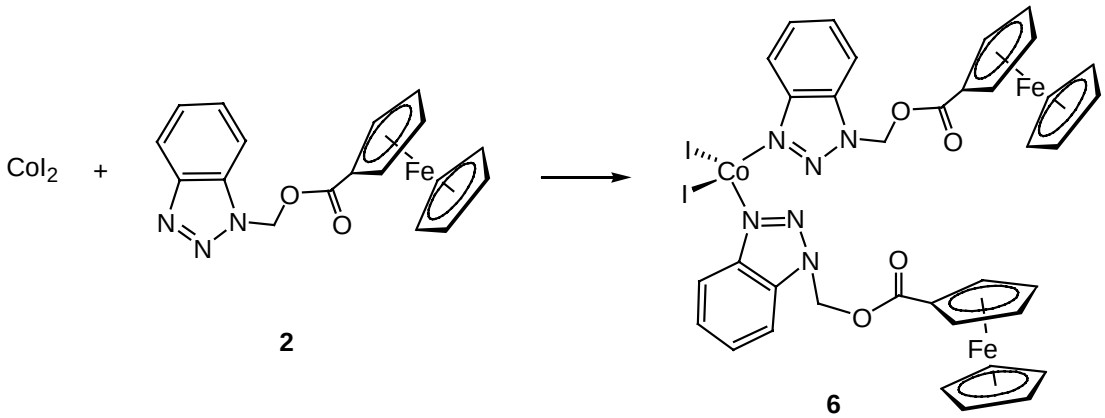

The reaction of CoI_2 with ligand **4** at room temperature yields the polymeric complex $[Co(C_6H_4N_3CH_2CO_2C_4H_2SCO_2CH_2C_6H_4N_3)I_2]_n$ (**7**) almost quantitatively. The single-crystal X-ray structure analysis reveals **7** to be a coordination polymer, each cobalt(II) center being tetrahedrally coordinated to two iodine atoms and to the 3-N nitrogen atoms of **4** which acts as bridging ligand.

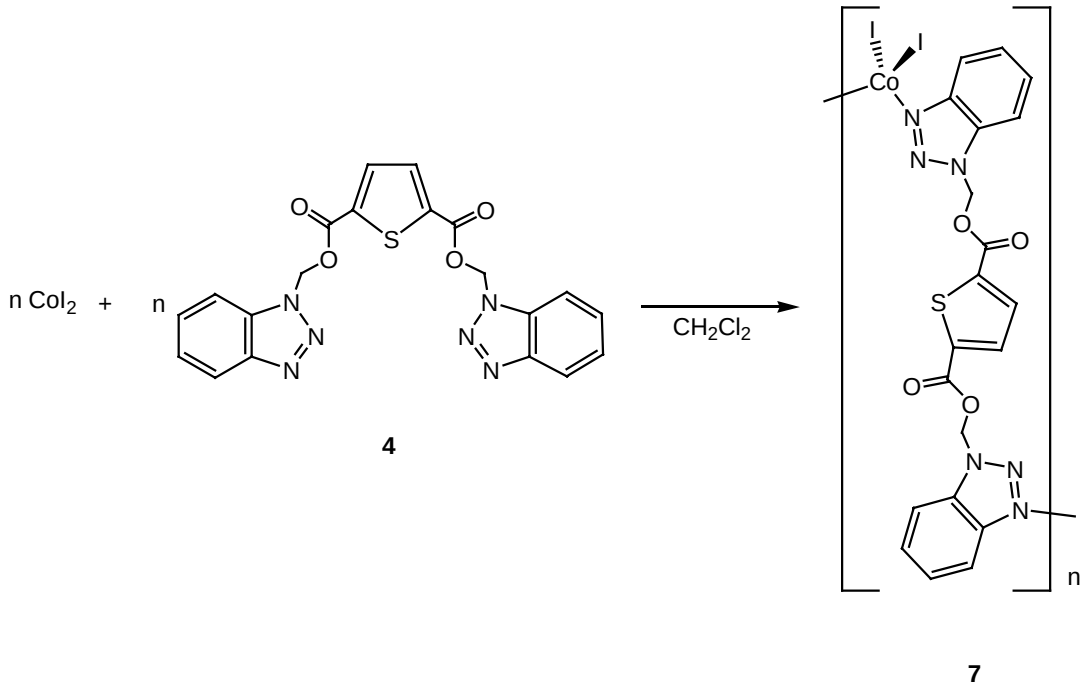

Ligand **4** was also found to coordinate easily to rhodium(I) or iridium(I) through the 3-N atom of the benzotriazole unit. Complex [Rh(**4**)(CO)Cl]$_2$ (**8**) is obtained from [Rh(CO)$_2$Cl]$_2$ and **4** using a 1 : 2 ratio in diluted solution of toluene at room temperature, in order to avoid the formation of polynuclear species, as in the case of complex **7**. Complex **8** separates into two isomers, the major isomer (**8a**) eluting as a brown band and the minor isomer (**8b**) eluting as a yellow band.

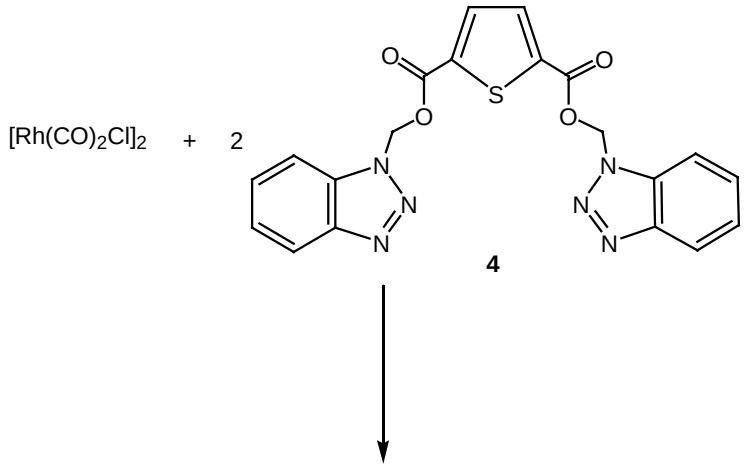

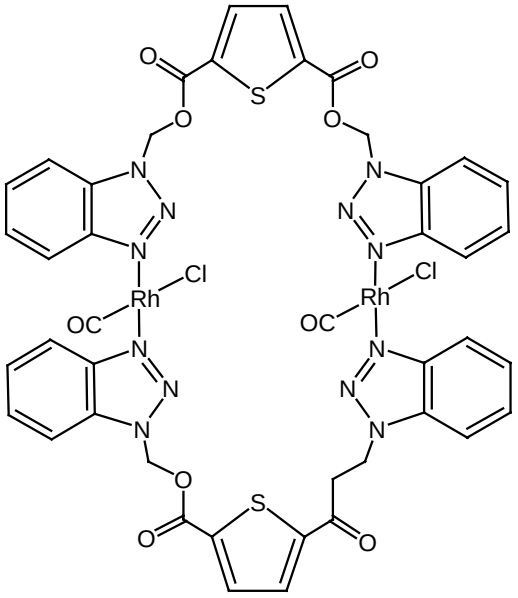

8a

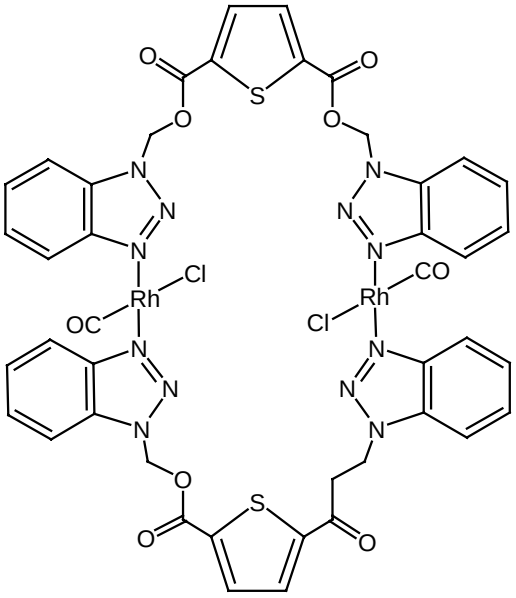

8b

The iridium complex $[Ir(cod)Cl]_2$ reacts analogously with two equivalents of **4** under carbon monoxide to give $[Ir(\mathbf{4})(CO)Cl]_2$ (**9**) as orange solid. The phosphine-containing ligand **5** reacts with $[Rh(CO)_2Cl]_2$ to give the mononuclear complex *trans*-$Rh[C_6H_4N_3CH_2CO_2C_6H_4P(C_6H_5)_2]_2(CO)Cl$ (**10**) in high yield.

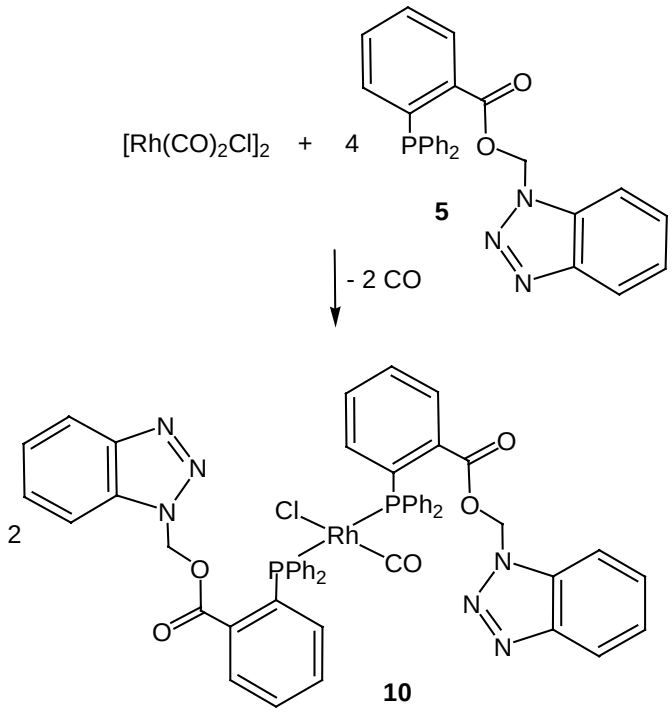

The single-crystal X-ray structure analysis of **10** shows the rhodium atom carrying two monophosphine ligands in *trans* position, one carbonyl ligand and one chloride, the metal atom being in a square-planar environment.

For the carbonylation of methanol, the catalytic activity increases in the presence of the nitrogen-containing ligands synthesized. The most active combination is $[Rh(CO)_2Cl]_2$/**4**, even though the difference with $[Rh(CO)_2Cl]_2$/**5** is not significant. From the reaction mixture of the catalytic reaction we isolated the red-brown complex **11** by crystallisation of the organometallic residue from

acetone. In accordance with the suggestion that dissociation of phosphine ligands from phosphine complexes may occur during the catalytic process, in **11** a Rh-N bond cleavage has taken place. The facile conversion of **8** into **11** under ambient conditions demonstrates that fragmentation, ligand dissociation and rearrangement occur easily.

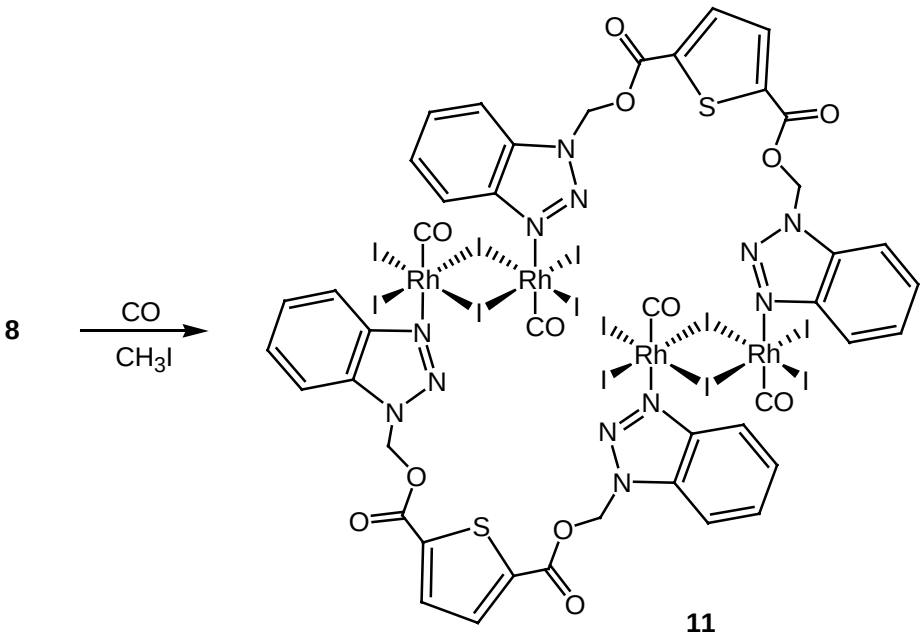

In the second part of this work, light is shed on the synthesis of a new phosphonodithioate ligand. The reaction of the ferrocene derivative of Lawesson's reagent $[(C_5H_5)_2Fe(C_5H_4)]_2P_2S_4$ with hydroxymethylbenzotriazole leads, in the presence of triethylamine, to the formation of the anion $[(C_5H_5)Fe(C_5H_4PS_2OCH_2C_6H_4N_3]^-$ (**12**) which is obtained as the yellow triethylammonium salt.

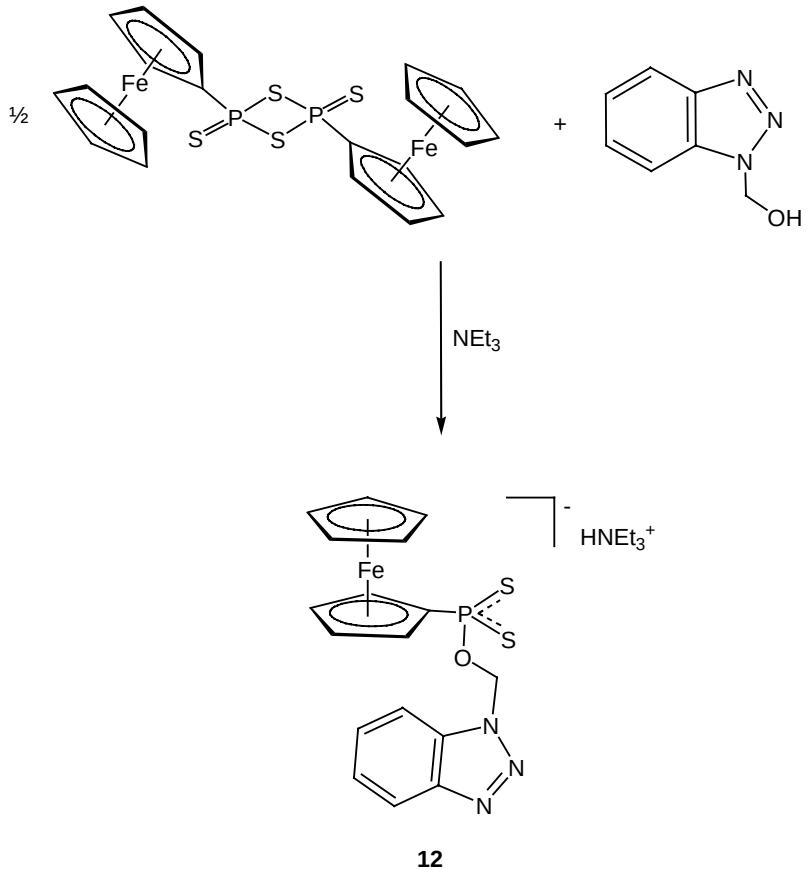

12

Ligand **12** was found to coordinate easily to nickel(II). The nickel complex $Ni[(C_5H_5)Fe(C_5H_4PS_2OCH_2C_6H_4N_3)]_2$ (**13**) is obtained from the room-temperature reaction of **12** with anhydrous nickel(II) chloride.

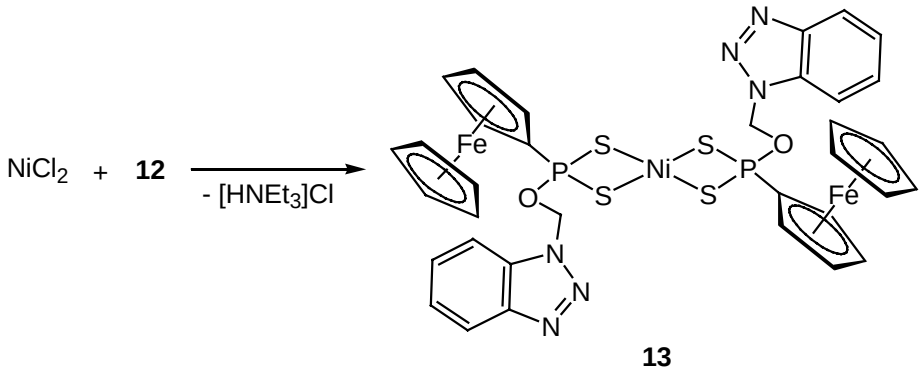

13

In complex **13** the ligand **12** is coordinated in a bidentate fashion through the two sulfur atoms of the PS_2 moiety and the benzotriazole unit is not bound to

the metal. Ligand **12** also reacts with other Ni(II) complexes: The reaction of the tetramethylcyclobutadiene complex $[Ni(C_4Me_4)Cl_2]_2$ with two equivalents of **12** gives the nickel complex $Ni(C_4Me_4)[(C_5H_5)Fe(C_5H_4PS_2OCH_2C_6H_4N_3)]Cl$ (**14**) in good yield.

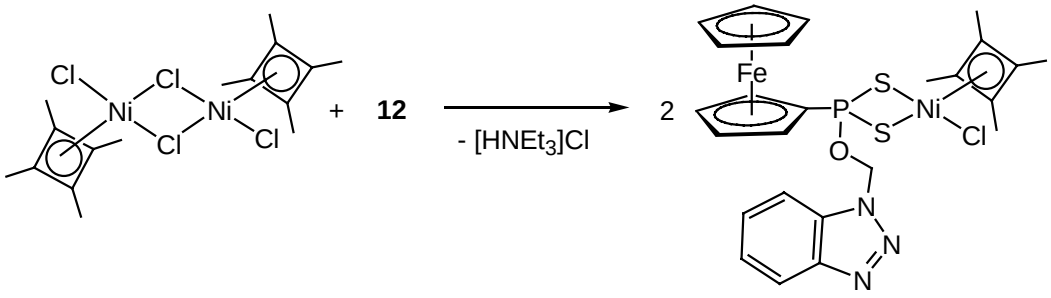

14

Ligand **12** is also found to coordinate to rhodium(I). The phosphonodithioate ligand **12** (2 equivalents) reacts with $[Rh(cod)Cl]_2$ to give the mononuclear complex $Rh(cod)[(C_5H_5)Fe(C_5H_4PS_2OCH_2C_6H_4N_3)]$ (**15**).

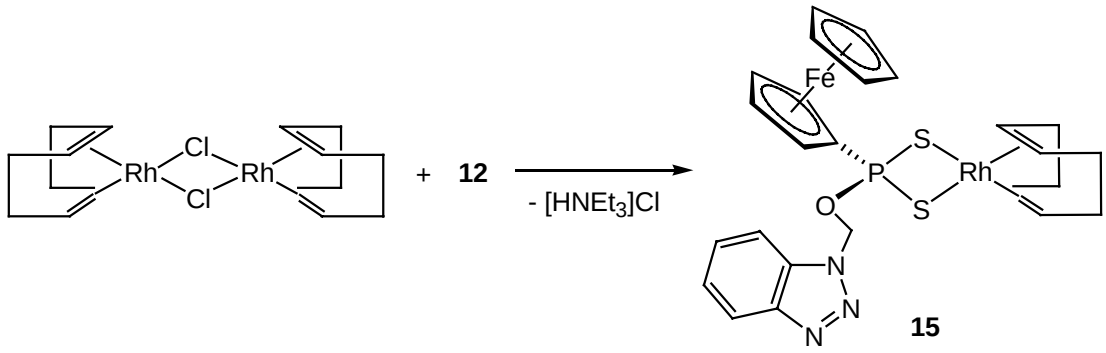

15

The single-crystal X-ray structure analysis of **15** shows that the complex is indeed mononuclear. The metal atom is in a square-planar environment and is coordinated by the two S atoms of one S,S-bidentate ligand. Carbon monoxide reacts in dichloromethane with **15** to give quantitatively (**16**). Similarly, the reaction

of $[Rh(CO)_2Cl]_2$ with two equivalents of **12** affords $Rh[(C_5H_5)Fe(C_5H_4PS_2OCH_2\text{-}C_6H_4N_3)](CO)_2$ **16**.

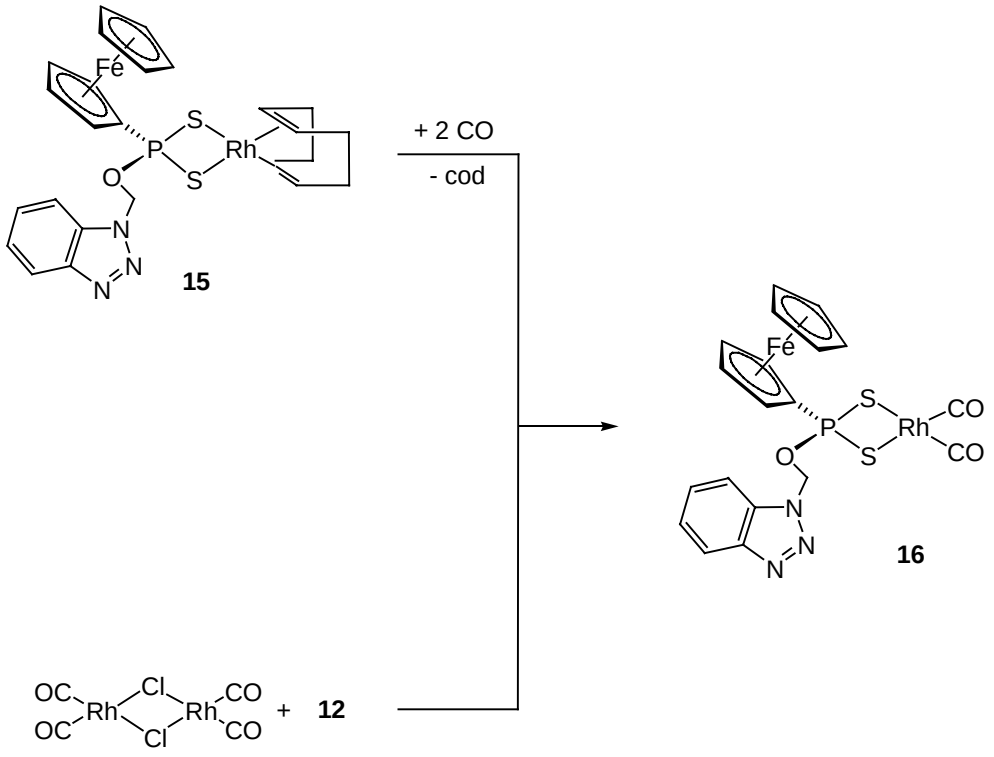

The new phosphodithioate ligand **12** gives in combination with nickel(II) and rhodium(I) complexes, active catalysts for the carbonylation of methanol and seems to stabilize the unsaturated species involved in the catalytic process. On the other hand, the catalytic activity of the nickel systems increases in the presence of the sulfur ligand **12**, but $[Rh(CO)_2I_2]^-$ still remains the most active species.

After completion of the carbonylation reaction, the catalyst was recovered and from this reaction mixture we isolated the brown complex $Ni[(C_5H_5)Fe(C_5H_4PS_2O)]_2$ (**17**) by crystallization of the organometallic residue from acetonitrile. The single-crystal X-ray structure analysis of **17** reveals a square-

planar complex, the metal being coordinated by the four S atoms of the two ligands.

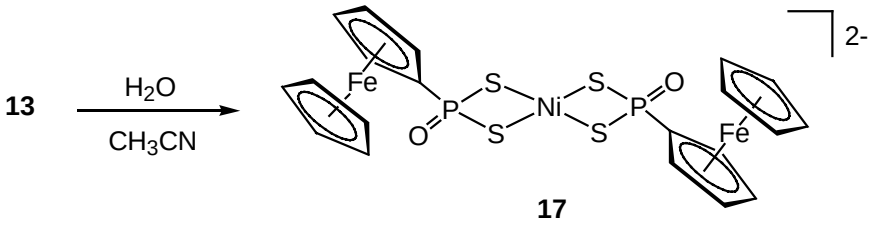

17

In the third part of this thesis, we describe new *trans*-diphosphine complexes that contain *trans*-spanning bidentate tertiary phosphine ligands by a condensation route. The new phosphine ligands **18** - **22** have been synthesized from 2-diphenyl-phosphinobenzoic acid and the corresponding aminoalcohols or diols.

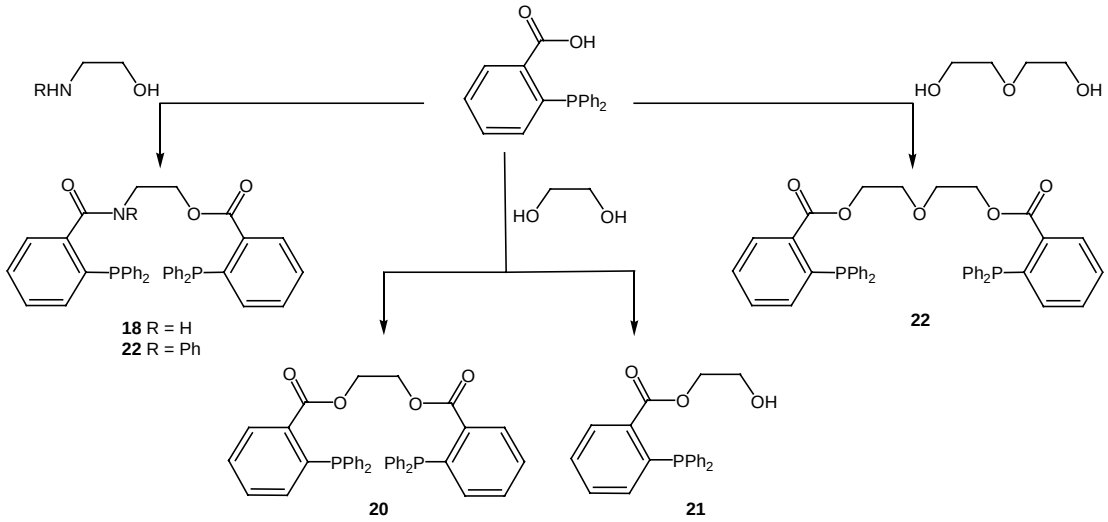

The diphosphine ligands **18** - **20** (2 equivalents) react with $[Rh(CO)_2Cl]_2$ to give the diphosphine complexes Rh(P-P)(CO)Cl (**23**: P-P = **18**; **24**: P-P = **19**; **25**: P-P = **20**) in high yields. By contrast, the complex $[Rh(CO)_2Cl]_2$ reacts with two equivalents of **22** to give the dinuclear complex $[Rh(P\text{-}P)(CO)Cl]_2$ (**26**) instead of the expected mononuclear metallacycle containing 16 ring members.

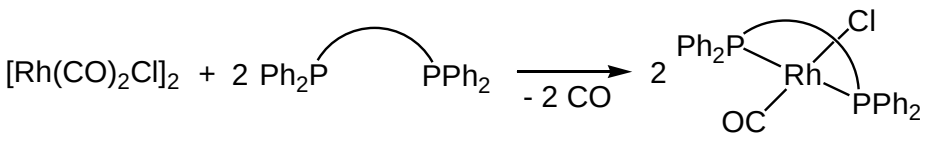

18
19
20

23
24
25

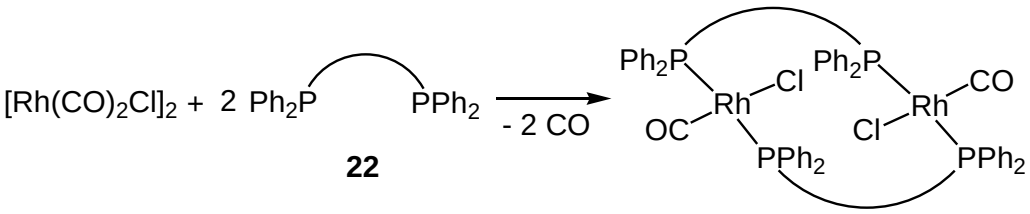

22

26

The single-crystal X-ray structure analysis of **26** shows the two rhodium atoms being bridged by two diphosphine ligands, maintaining the *trans*-P,P-coordination geometry of each rhodium atom.

The diphosphines **18** - **20** were also found to coordinate to iridium(I) through the two phosphorus atoms. The chloro complexes Ir(P-P)(cod)Cl (**27**: P-P = **18**; **28**: P-P = **18**; **29**: P-P = **20**) are directly obtained from $[Ir(cod)Cl]_2$ and the corresponding diphosphine ligands.

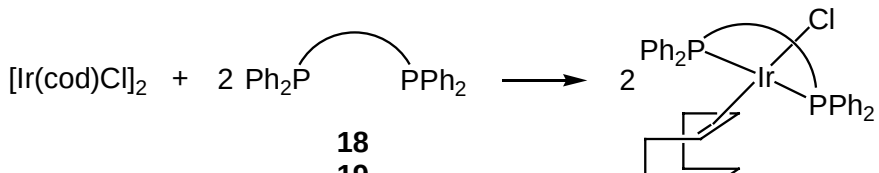

18
19
20

27
28
29

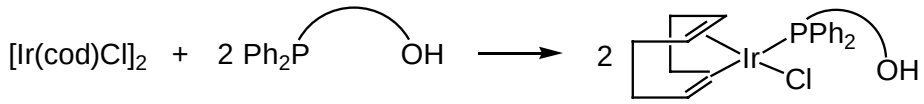

21

33

Carbon monoxide reacts in dichloromethane with **27** - **29** to give almost quantitatively the carbonyl complexes **30** - **32**. The analogous reaction of the

cyclooctadienechloro complex $[Ir(cod)Cl]_2$ with two equivalents of **21** in dichloromethane gives the iridium complex Ir(**21**)(cod)Cl (**33**). The single-crystal X-ray structure analysis of **33** reveals a distorted square-planar coordination geometry of the iridium atom.

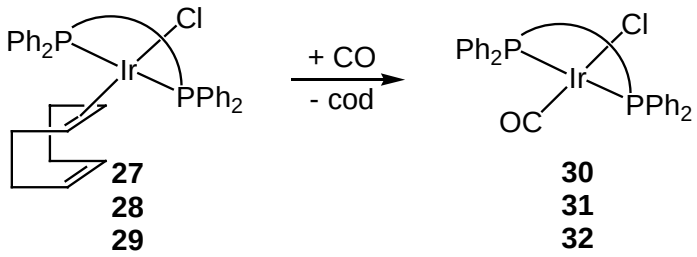

27 **28** **29** **30** **31** **32**

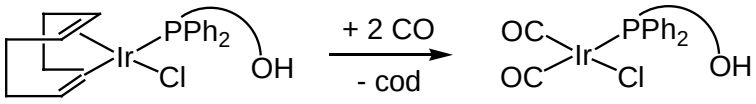

33 **34**

The *trans* coordination of the diphosphine ligands in the mononuclear complexes, assumed for **23** - **25**, **27** - **29** and **30** - **32** on the basis of their spectroscopic data, was finally confirmed by a single-crystal X-ray structure analysis of the platinum complex Pt(**19**)I_2 (**35**). Complex **35** is obtained almost quantitatively by the reaction of $Pt(cod)I_2$ with the diphosphine ligand (**19**). The single-crystal X-ray structure analysis shows a square-planar coordination geometry of **35**. The Pt atom is coordinated to two I atoms and to the two P atoms of the diphosphine ligand.

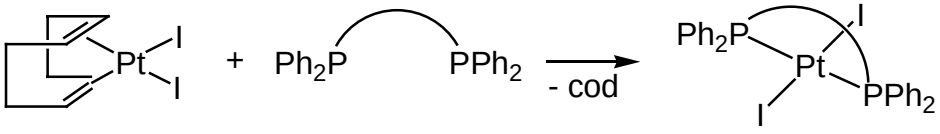

19 **35**

The results of the carbonylation of methanol show that the catalytic activity increases considerably in the presence of the diphosphine ligands **18**, **19**, **20** or **22**, ligand **19** being the most active one.

The red complex **36** can be isolated from the organometallic residue of the catalytic reaction by crystallisation from acetone; it is also directly accessible from the reaction of **7** with methyliodide in acetone solution. Complex **36** exists in two isomers **36a** and **36b**, depending on the *cis* or *trans* arrangement of the two terminal iodo ligands at the two rhodium atoms. The two isomers present in solution are separated by fractional crystallization from acetone: **36a** crystallizes rapidly, while **36b** takes several hours to crystallize after elimination of **36a**.

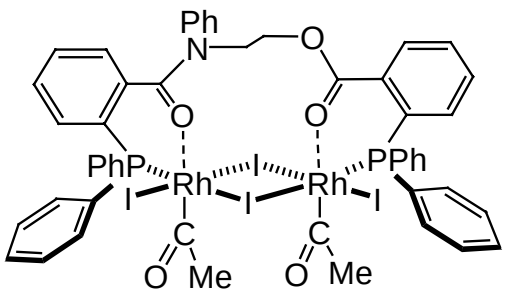

36a

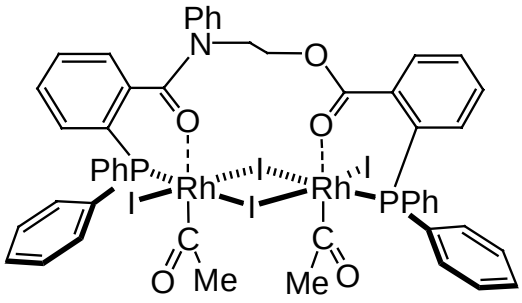

36b

It is noteworthy that in both isomers **36a** and **36b**, the rhodium atoms do not have a square pyramidal but an octahedral coordination geometry, thanks to the carbonyl oxygen atoms of the ligand chain, as revealed by the single-crystal X-ray structures analyses of **36a** and **36b**.

On the basis of these observations, we propose a catalytic cycle for the mechanism of the carbonylation of methanol catalyzed by **24**. Oxidative addition of iodomethane to **24** yields the rhodium(III) acetyl complex **36**, presumably

through the intermediacy of the corresponding mononuclear methylrhodium(III) complex. The dinuclear complex isomers **36a** and **36b** formed by elimination of a diphosphine ligand may be considered as a reservoir for the active mononuclear species.

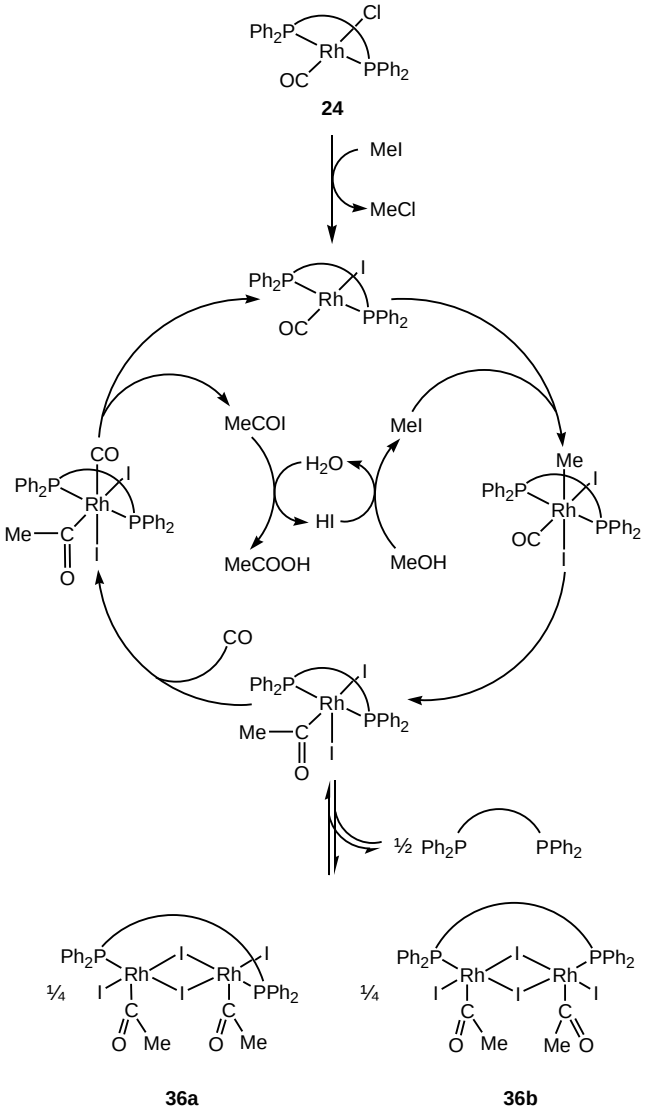

Of the three classes of multifunctional ligands synthesized, the ester diphosphine ligands seem to be the most promising one with respect to their coordination properties and to their catalytic potential. As the synthetic concept we developed for these ligands is very versatile, new ligands of this type can be designed without problems.

Résumé

Le but de ce travail de thèse a été de synthétiser de nouveaux ligands multifonctionnels, d'étudier leurs propriétés de coordination et d'exploiter leur potentiel catalytique pour la carbonylation du méthanol.

La première partie de cette thèse a pour but la synthèse de nouveaux ligands azotés à unité benzotriazole. Les ligands **1** - **5** ont été obtenus directement par condensation à partir d'hydroxymethylbenzotriazole et du monoacide ou du diacide correspondant.

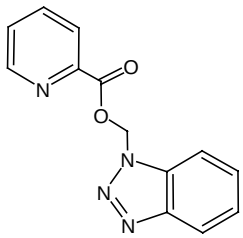

1

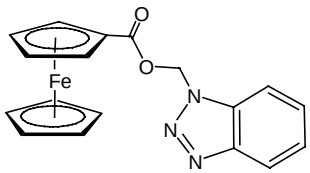

2

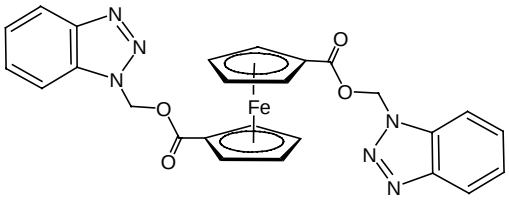

3

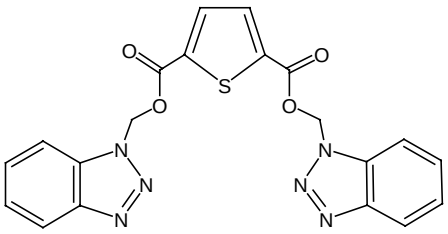

4

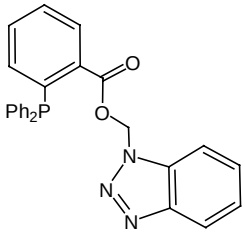

5

Le ligand **2** peut se coordonner au cobalt(II) par l'atome 3-N de l'unité benzotriazole. La structure aux rayons X révèle que le centre métallique est lié de façon tétraédrique à deux atomes d'iode et à deux atomes d'azote de deux ligands.

Le ligand **2** se coordonne donc de façon monodentée par les atomes 3-N de l'unité benzotriazole.

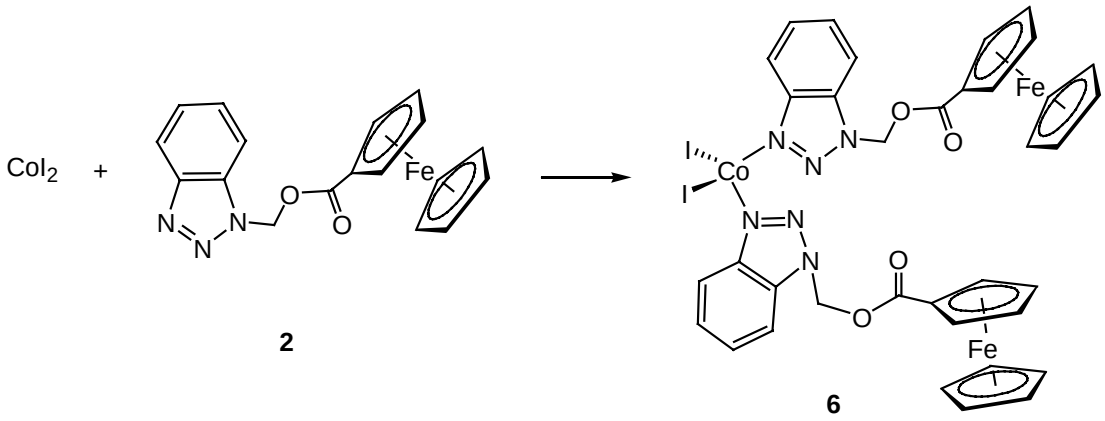

2 **6**

La réaction de CoI_2 avec le ligand **4** à température ambiante permet la formation de l'espèce polymérique $[Co(C_6H_4N_3CH_2CO_2C_4H_2SCO_2CH_2C_6H_4N_3)I_2]_n$ (**7**). Le ligand **4** agit comme ligand pontant et non comme ligand bidenté. La résolution de la structure aux rayons X nous permet de confirmer la nature polymérique de **7**, chaque atome de cobalt étant lié de façon tétraédrique à deux atomes d'iode et deux atomes d'azote.

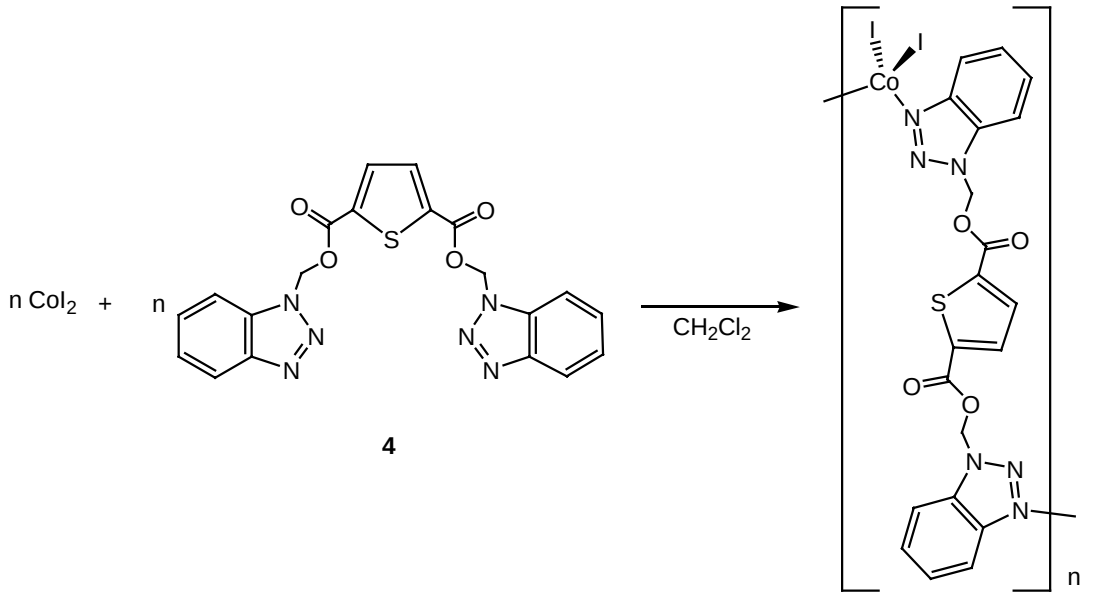

4 **7**

Le ligand **4** se coordonne également facilement au rhodium(I) et à l'iridium(I) par son atome d'azote 3-N. Le complexe [Rh(**4**)(CO)Cl]$_2$ (**8**) est obtenu à partir de [Rh(CO)$_2$Cl]$_2$ et du ligand **4** en utilisant un rapport 1 : 2 en solution diluée dans le toluène pour éviter la formation d'espèces polymériques, comme dans le cas de **7**. Par chromatographie sur silice, on peut séparer deux isomères, l'isomère majoritaire (**8a**) éluant sous forme d'une bande brune et le produit minoritaire (**8b**) éluant sous forme d'une bande jaune.

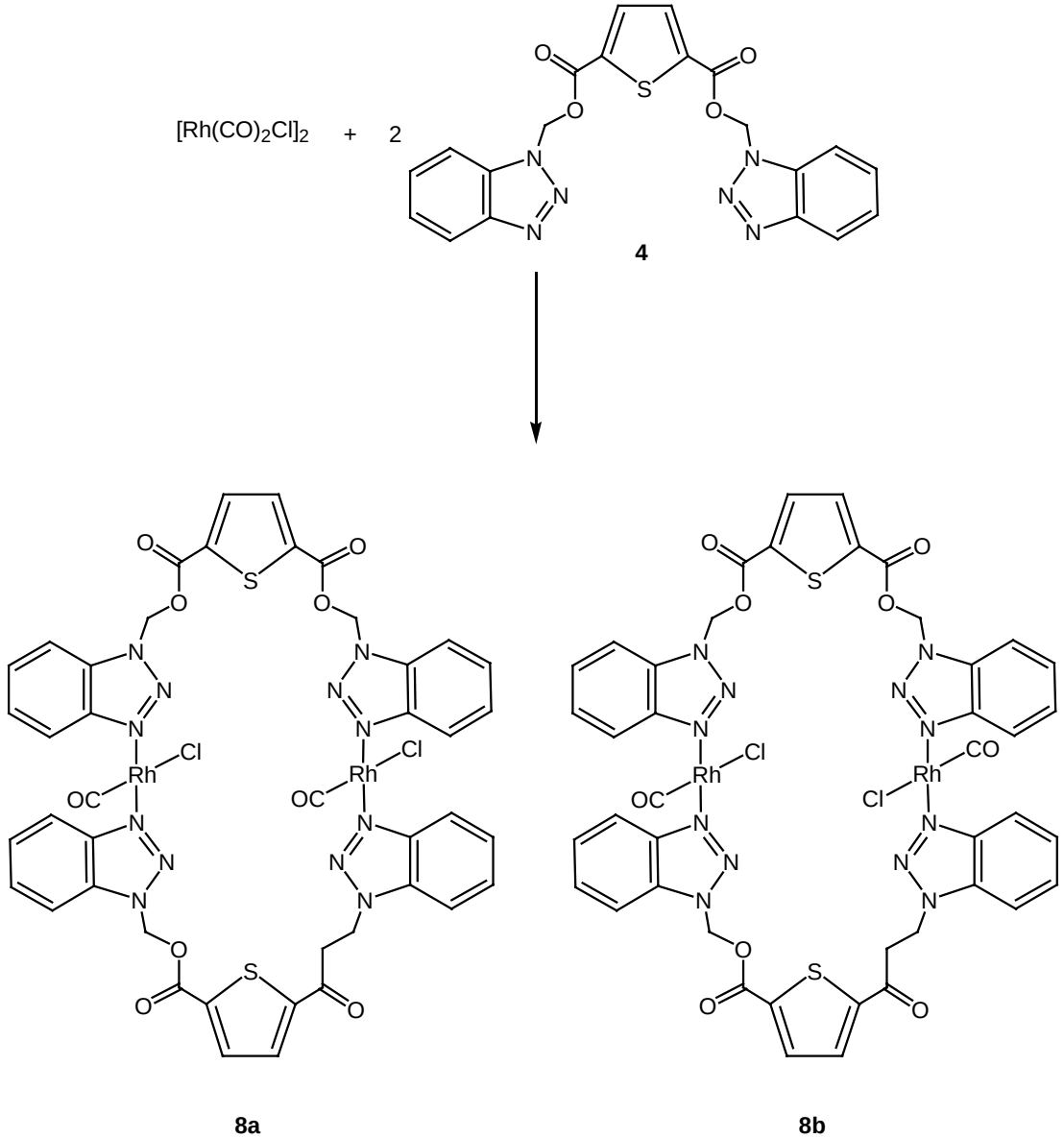

Le complexe d'iridium $[Ir(cod)Cl]_2$ réagit de façon analogue avec deux équivalents de **4** sous monoxide de carbone pour donner $[Ir(\mathbf{4})(CO)Cl]_2$ (**9**). Le ligand monophosphine **5** réagit avec le complexe $[Rh(CO)_2Cl]_2$ pour donner le complexe mononucléaire *trans*-$Rh[C_6H_4N_3CH_2CO_2C_6H_4P(C_6H_5)_2]_2(CO)Cl$ (**10**). La structure aux rayons X montre que le complexe **10** possède un atome de rhodium dans un environnement carré-plan qui est lié à deux ligands phosphine, un ligand carbonyle et un ligand chlore.

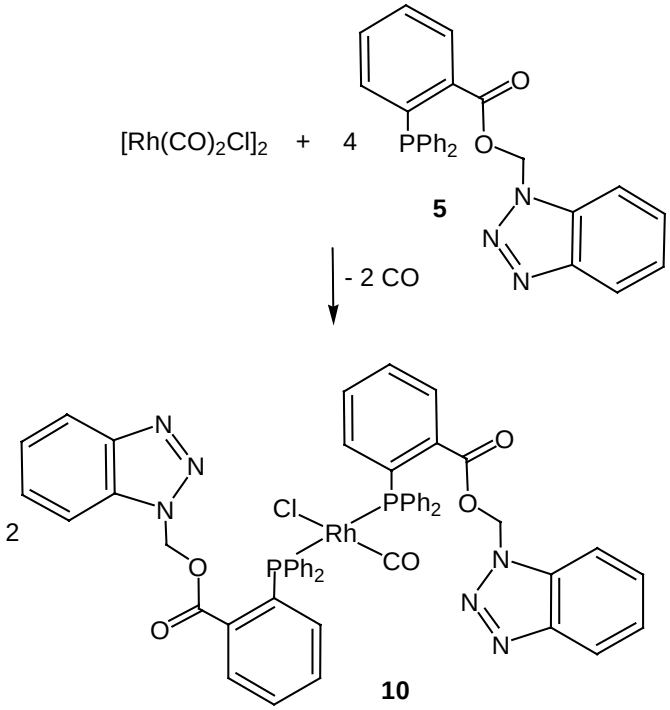

Puis nous avons testé l'activité catalytique du précurseur $[Rh(CO)_2Cl]_2$ associé à nos différents ligands azotés. La combinaison la plus active a été trouvée pour $[Rh(CO)_2Cl]_2$ / **4**, même si la différence avec le système $[Rh(CO)_2Cl]_2$ / **5** n'est pas vraiment significative.

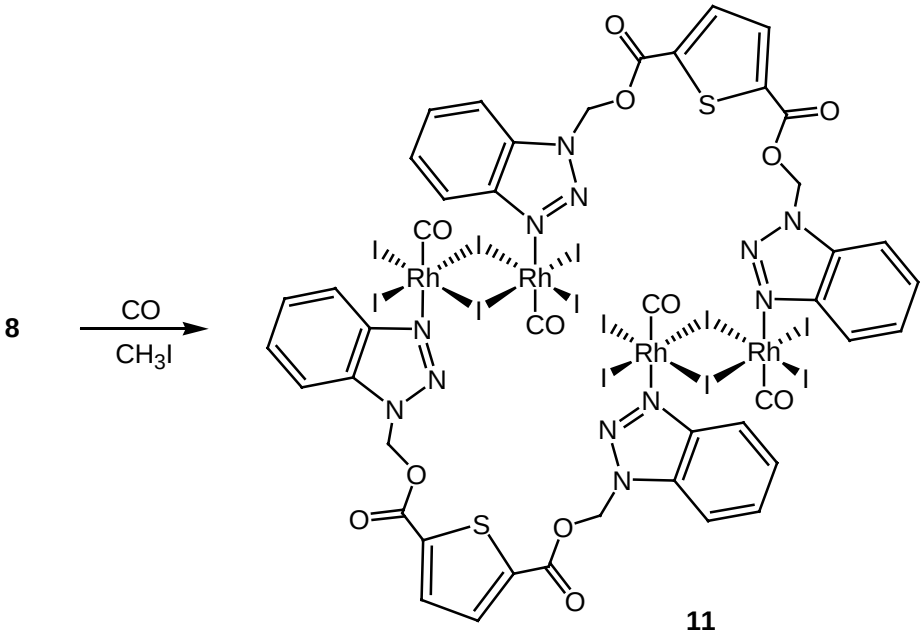

11

Le complexe rouge-brun (**11**) est isolé à partir de la solution catalytique par cristallisation dans l'acétone. Il a déjà été suggéré que, durant le cycle catalytique de la carbonylation du méthanol, un ligand monophosphine pouvait se dissocier du complexe. Dans notre cas il y a clairement rupture d'une liaison Rh-N. La conversion facile de **8** en **11** démontre qu'une fragmentation et un réarrangement peuvent facilement se produire pendant un cycle catalytique.

Dans la seconde partie de ce travail, nous verrons la synthèse d'un nouveau ligand phosphonodithioate. La réaction du dérivé ferrocénique du réactif de Lawesson $[(C_5H_5)_2Fe(C_5H_4)]_2P_2S_4$ avec l'hydroxymethylbenzotriazole donne, en présence de triéthylamine, l'anion $[(C_5H_5)Fe(C_5H_4PS_2OCH_2C_6H_4N_3]^-$ (**12**) qui est obtenu sous forme d'un sel jaune de triéthylammonium.

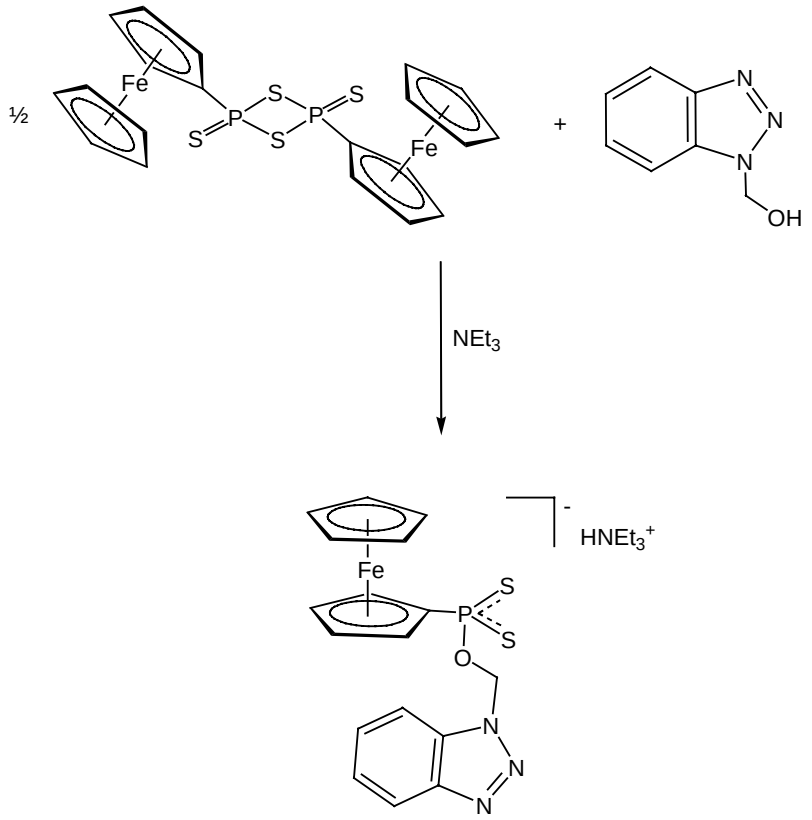

12

Le ligand **1** se coordonne facilement aux dérivés de nickel(II). En effet le complexe $Ni[(C_5H_5)Fe(C_5H_4PS_2OCH_2C_6H_4N_3)]_2$ (**13**) est obtenu aisément à température ambiante par réaction du chlorure de nickel(II) avec le ligand **12**. Le ligand **1** est coordonné de façon bidentée par ses deux atomes de soufre alors que l'unité benzotriazole n'est pas liante.

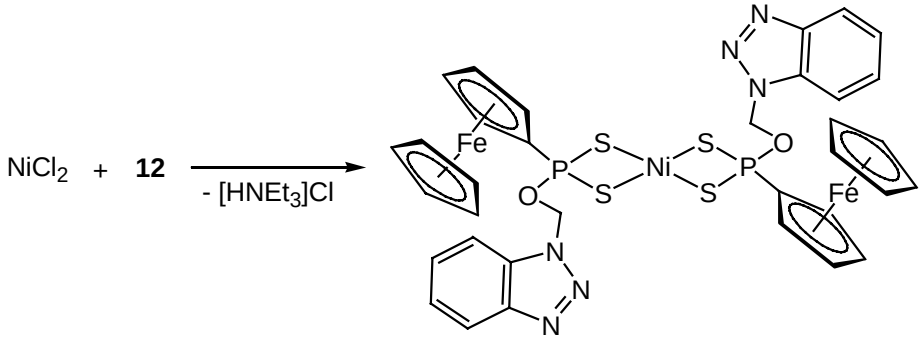

13

Le ligand **12** peut également réagir avec d'autres complexes de nickel: la réaction du complexe $[Ni(C_4Me_4)Cl_2]_2$ avec deux équivalents de **12** permet la formation du complexe $Ni(C_4Me_4)[(C_5H_5)Fe(C_5H_4PS_2OCH_2C_6H_4N_3)]Cl$ (**14**).

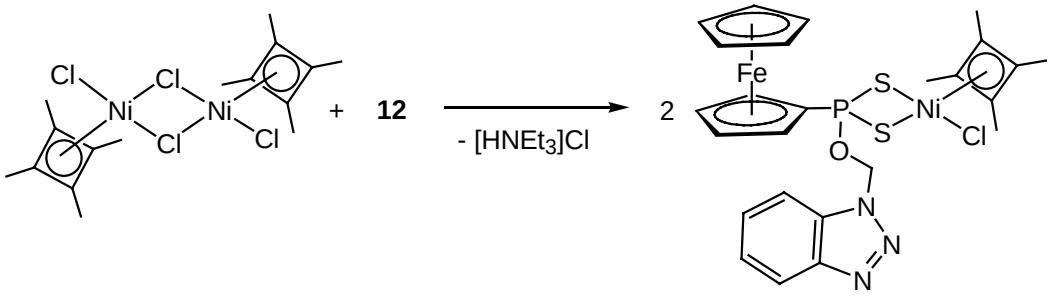

14

Le dérivé phosphonodithioate **12** peut également facilement se lier au rhodium(I). En effet la réaction du dérivé de cyclooctadiène $[Rh(cod)Cl]_2$ avec deux équivalents de ligand donne le complexe mononucléaire $Rh(cod)[(C_5H_5)Fe(C_5H_4PS_2OCH_2C_6H_4N_3)]$ (**15**). La résolution de la structure aux rayons X nous confirme que le complexe **15** est bien mononucléaire. L'atome métallique se situe dans un environnement carré-plan et est lié à deux atomes de soufre d'un même ligand.

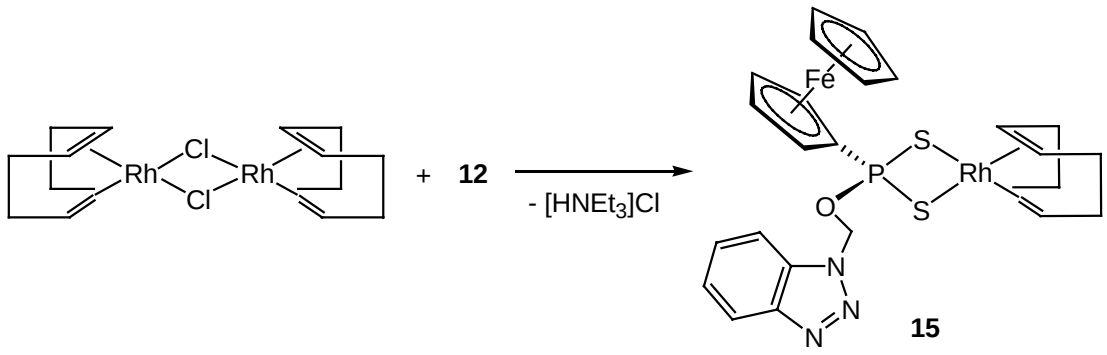

15

On peut faire réagir le complexe **15** avec du monoxyde de carbone, ce qui donne quantitativement le complexe carbonylé $Rh(CO)_2[(C_5H_5)Fe(C_5H_4PS_2O\ CH_2C_6H_4N_3)]$ (**16**). La réaction de $[Rh(CO)_2Cl]_2$ avec le ligand **12** conduit également au complexe **16**.

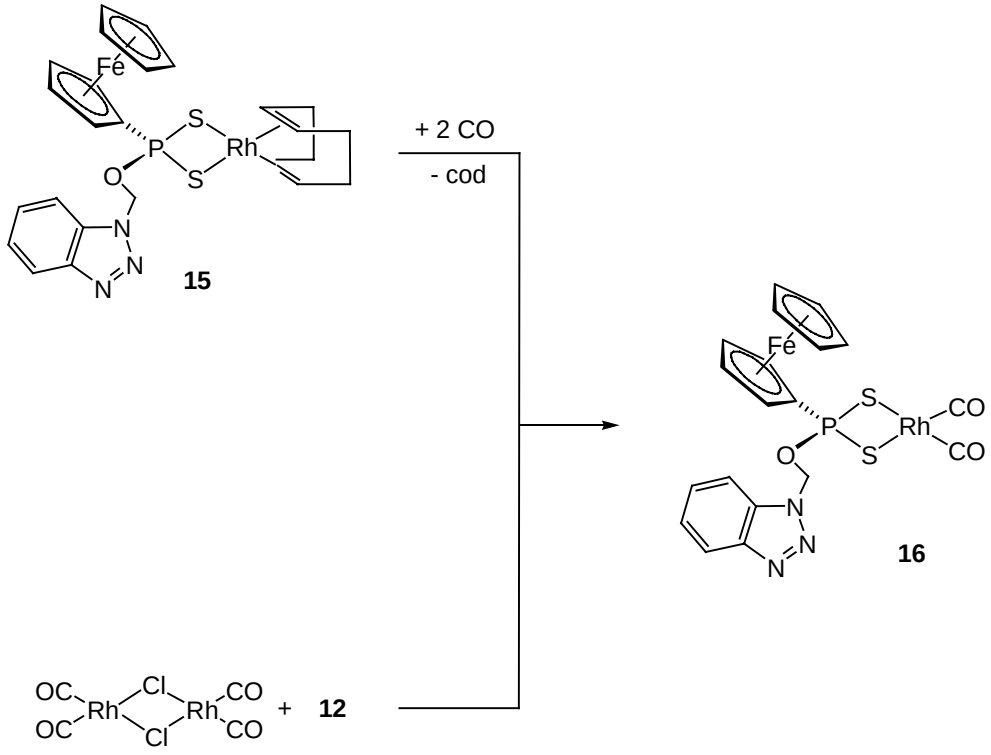

Associé à des dérivés métalliques de nickel(II) et de rhodium(I), le ligand **12** donne des catalyseurs actifs en carbonylation et semble ainsi stabiliser par coordination les complexes insaturés impliqués dans le procédé catalytique. Cependant, l'activité catalytique du système de nickel(II) reste inférieure à celle du système classique $[Rh(CO)_2I_2]^-$. On peut isoler du milieu catalytique le complexe $Ni[(C_5H_5)Fe(C_5H_4PS_2O)]_2$ (**17**) par cristallisation du résidu organométallique dans l'acétonitrile. La structure aux rayons X montre l'environnement carré-plan du métal qui est lié à quatre atomes de soufre de deux ligands différents.

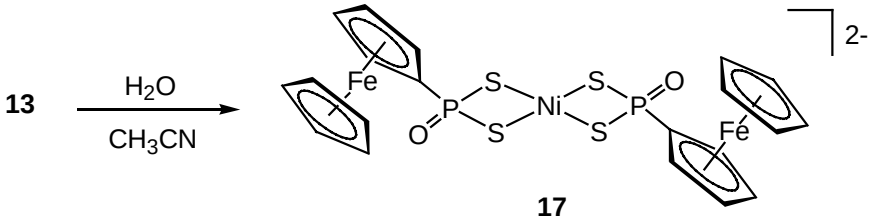

Dans la troisième partie, nous décrivons une nouvelle voie de synthèse de complexes portant des diphosphines *trans*. Les nouveaux ligands phosphine **18** - **22** ont été synthétisés par condensation à partir de l'acide 2-diphénylphosphinobenzoïque et de l'aminoalcool ou du diol correspondant.

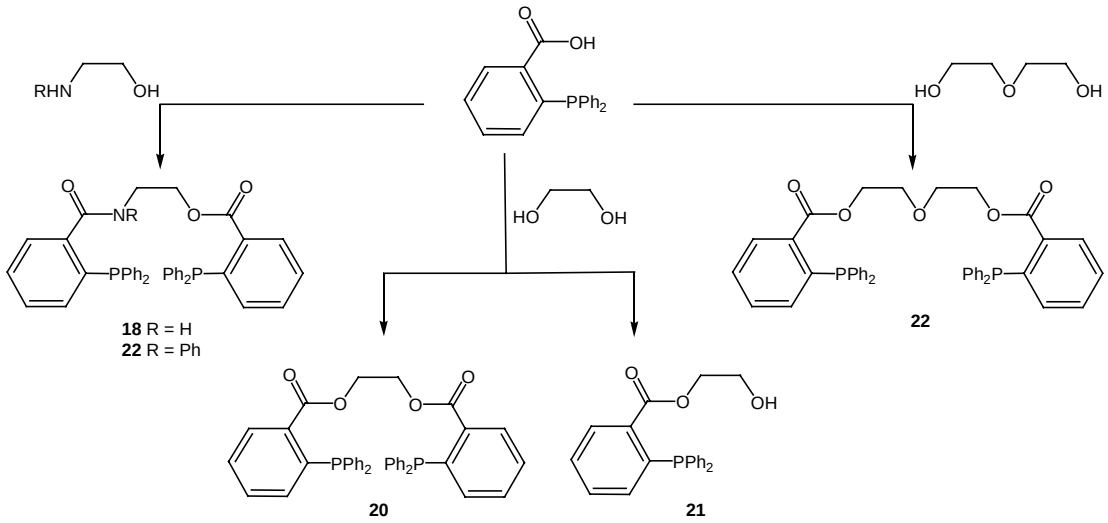

Les diphosphines **18** - **20** réagissent avec le précurseur $[Rh(CO)_2Cl]_2$ pour donner les complexes diphosphine Rh(P-P)(CO)Cl (**23**: P-P = **18**; **24**: P-P = **19**; **25**: P-P = **20**). Par contre, en faisant réagir $[Rh(CO)_2Cl]_2$ avec deux équivalents de diphosphine **22**, on obtient le complexe dinucléaire (**26**) au lieu du métallacycle mononucléaire à 16 chaînons prévu. La structure aux rayons X montre que les deux atomes de rhodium sont pontés par deux ligands diphosphine en maintenant la géométrie de coordination *trans* pour chaque atome de rhodium.

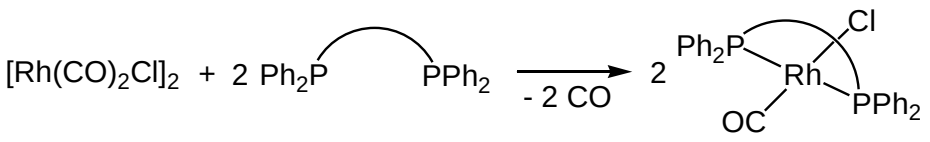

18
19
20

23
24
25

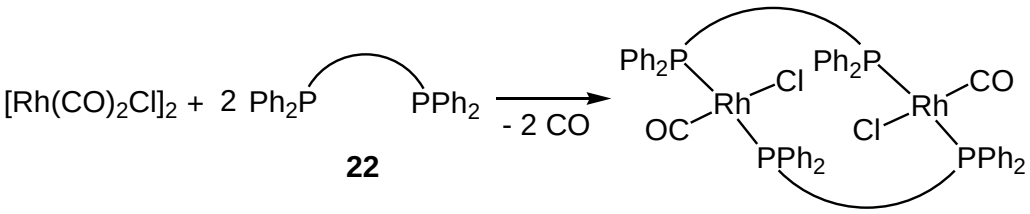

22

26

Les diphosphines **18** - **20** peuvent également se lier à l'iridium(I) par les deux atomes de phosphore. Les complexes Ir(P-P)(cod)Cl (**27**: P-P = **18**; **28**: P-P = **19**; **29**: P-P = **20**) sont obtenus à partir de $[Ir(cod)Cl]_2$ et de la diphosphine correspondante. La réaction des complexes **27** - **29** avec le monoxide de carbone permet la formation des complexes carbonylés (**30**) - (**32**).

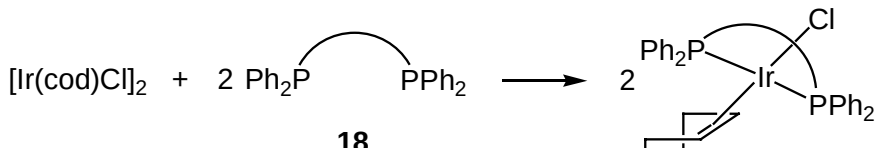

18
19
20

27
28
29

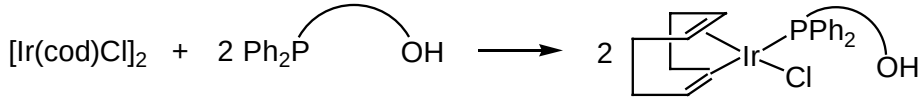

21

33

De la même façon, la réaction de $[Ir(cod)Cl]_2$ avec deux équivalents de **21** conduit au complexe d'iridium Ir(**21**)(cod)Cl (**33**). La résolution de la structure aux rayons X permet d'établir l'environnement carré-plan de l'atome d'iridium.

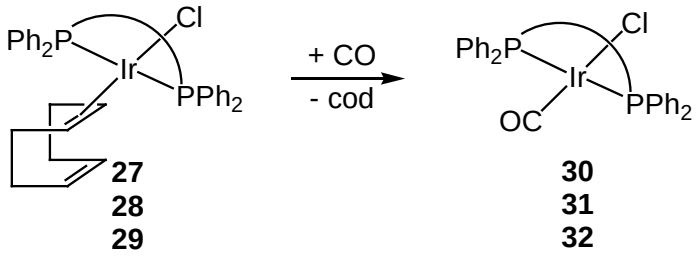

27 **28** **29** **30** **31** **32**

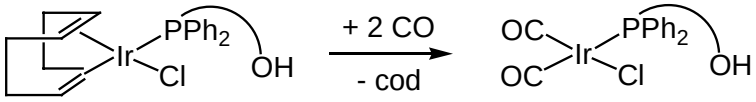

33 **34**

La coordination en *trans* de ces ligands diphosphine dans les complexes mononucléaires a été finalement confirmée par une structure aux rayons X du complexe de platine Pt(**19**)I_2 (**35**). Le complexe **35** est obtenu par réaction de Pt(cod)I_2 avec le ligand diphosphine **19**.

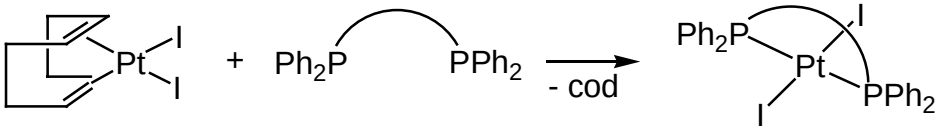

19 **35**

L'analyse structurale montre une géométrie de coordination carré-plan pour **35**. L'atome de platine est coordonné à deux atomes d'iode et deux atomes de phosphore du ligand diphosphine.

Les résultats des tests effectués en carbonylation du méthanol montrent que l'activité catalytique est considérablement augmentée en présence des ligands diphosphine **18**, **19**, **20** ou **22**, le ligand **19** étant le plus efficace. Le complexe rouge **36** peut être isolé à partir du résidu organométallique issu de la réaction catalytique par cristallisation dans l'acétone.

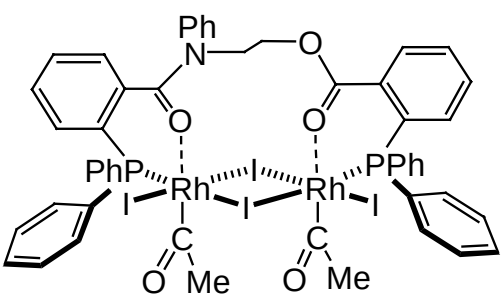

36a

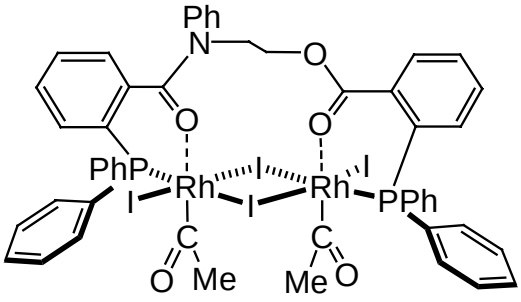

36b

On peut également l'obtenir directement par réaction de **24** avec l'iodure de méthyle dans l'acétone. Le complexe **36** existe sous la forme de deux isomères **36a** et **36b** suivant l'arrangement *cis* ou *trans* des ligands terminaux iodo des deux atomes de rhodium.

Les deux isomères présents en solution sont séparés par cristallisation fractionnée dans l'acétone: **36a** cristallise rapidement, alors que **36b** met plusieurs heures à cristalliser après élimination de **36a**. Il est à noter que, pour les deux isomères **36a** et **36b**, l'atome de rhodium présente comme prévu une géométrie de coordination octaédrique, grâce aux atomes d'oxygène des fonctions carbonyl du ligand.

D'après ces observations, nous pouvons proposer un cycle catalytique pour le mécanisme de carbonylation du méthanol catalysée par **24**. L'addition oxydante de l'iodométhane sur **24** permets de former le complexe de rhodium(III) **36**, vraisemblablement par l'intermédiaire du complexe mononucléaire méthylrhodium(III) correspondant. Les isomères dinucléaires **36a** et **36b**, formés par élimination d'un ligand diphosphine, peuvent être considérés comme réservoir à espèces actives mononucléaires.

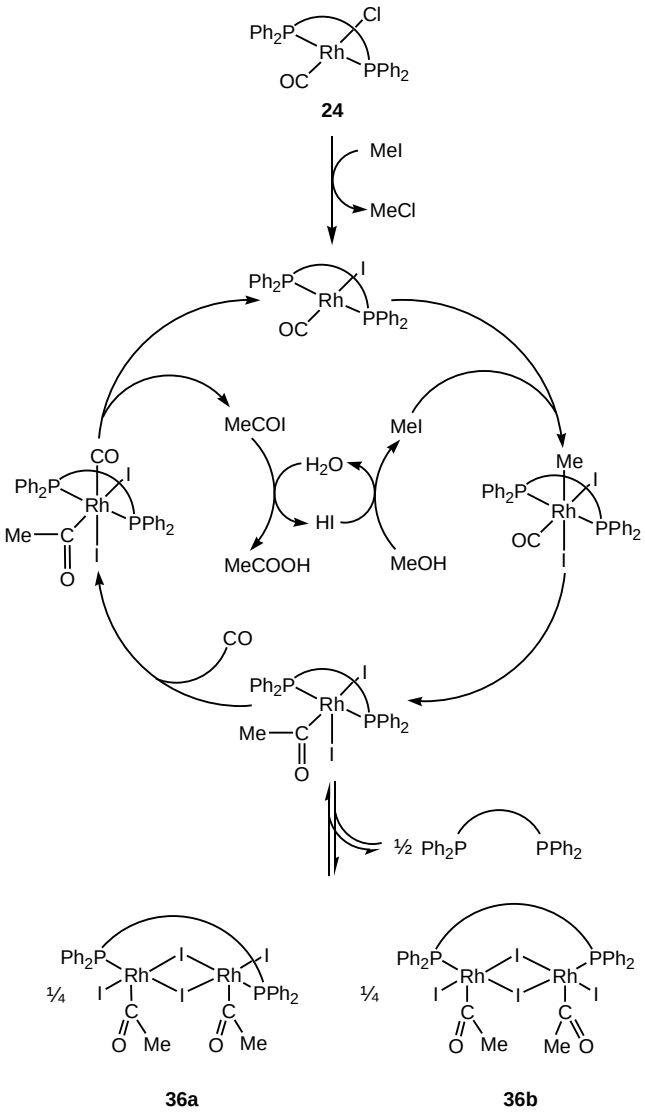

Des trois classes de ligands multifonctionnels synthétisés, les ligands diphosphine ester semblent être les plus prometteurs au regard de leurs propriétés de coordination et de leur potentiel catalytique. Etant donné que notre concept synthétique est très souple, de nouveaux ligands de ce type peuvent être élaborés très facilement.

References

1. van Leeuwen, P. W. N. M.; Morokuma, K; van Lenthe, J. H.; *Theoritical Aspects of Homogeneous Catalysis*; Kluwer Academic Publishers, **1995**.
2. Herrmann, W. A.; Cornils, B.; *Applied Homogeneous Catalysis with Organometallic Compounds*, VCH Weinheim, **1999**.
3. Young, J. F.; Osborn, J. A.; Jardine, F. H.; Wilkinson, G.; *Chem. Comm.*, **1965**, 131.
4. Osborn, J. A.; Jardine, F. H.; Young, J. F.; Wilkinson, G.; *J. Chem. Soc. A.*, **1966**, 1711.
5. Dickson, R. S.; *Organometallic Chemistry of Rhodium and Iridium*; Academic Press, London, **1983**, p. 277.
6. Kobayashi, K.; *Chem. Econ. Eng. Rev.*, **1984**, *16(6)*, 32.
7. Süss-Fink, G; Haak, S.; Ferrand, V.; Stoeckli-Evans, H.; *J. Chem. Soc., Dalton Trans.*, **1997**, 3861.
8. Süss-Fink, G; Haak, S.; Ferrand, V.; Stoeckli-Evans, H.; *J. Mol. Catal.* A, **1999**, *143*, 163.
9. Haak, S.; Neels, A.; Stoeckli-Evans, H.; Süss-Fink, G.; Thomas, C. M.; *Chem. Commun.*, **1999**, 1959.
10. Parshall, G. W.; Ittel, S. D.; *Homogeneous Catalysis*, 2nd Edition, Wiley-Interscience, New York, **1992**, p. 96.
11. Weissermel, K.; Arpe, H.-J.; *Industrial Organic Chemistry*, 3rd Edition, VCH, Weinheim, **1997**.

12. Dickson, R. S.; *Organometallic Chemistry of Rhodium and Iridium*; Academic Press, London, **1983**, p. 277.

13. Colquhoun, H. M.; Thompson, D. J.; Twigg, M. V.; *Carbonylation: Direct Synthesis of Carbonyl Compounds*, Plenum Press, New York, **1991**.

14. Itami, H.; *Chem. Econ. Eng. Rev.*, **1984**, *16(4)*, 21.

15. Kobayashi, K.; *Chem. Econ. Eng. Rev.*, **1982**, *14(4)*, 20.

16. Yoneda, N.; Kuzano, S.; Yasui, M.; Pujado, P.; Wilcher, S.; *Applied Catalysis A: General*, **2001**, *221*, 253.

17. Howard, M. J.; Jones, M. D.; Roberts, M. S.; Taylor, S. A.; *Catal. Today*, **1993**, *18*, 325.

18. Gauss, M.; Seidel, A.; Torrence, P.; Heymanns, P.; *Applied Homogeneous: Catalysis with Organometallic Compounds*, VHC, New York, **1996**, *vol. 1*, p. 104.

19. Agreda, V. H.; Zoeller, J. R.; *Acetic Acid and Its Derivatives*, Marcel Dekker, New York, **1993**, *Chapters 1-6*, p. 3.

20. Wagner, F. S.; *Kirk-Othmer Encyclopedia of Chemical Technology*, 4th Edition, **1991**, *vol. 1*, p. 121.

21. Mullen, A.; N*ew Syntheses with Carbon Monoxide*; Springer Verlag, Berlin, **1980**, p.243.

22. Falbe, J.; *Synthesen mit Kohlenmonoxid*; Springer Verlag, Berlin, **1977**.

23. Falbe, J.; *Methodicum Chimicum*, Georg Thieme Verlag, Stuttgart, **1975**, *vol. 5*.

24. Kutepow, N. V.; Himmele, W.; *Ullmanns Encyclopädie der technischen Chemie*, 4th edition, Verlag Chemie, Weinheim, **1975**, *vol. 9*, p. 155.

25. Forster, D.; *Adv. Organometal. Chem*, **1979**, *17*, 255.

26. Paulik, F.; Roth, J. E.; *J. Chem. Soc., Chem. Commun.*, **1968**, 1578.

27. von Kutepow, N.; Himmele, W.; Hohenschutz, H.; *Chem. Ing. Techn.*, **1965**, *37*, 297.

28. Gauthier-Lafaye, J.; Perron, R.; *Eur. Pat. Appl*, **1981**, 35458.

29. Forster, D.; Singleton, M.; *J. Mol. Catal.*, **1982**, *17*, 299.

30. Nozaki, K.; *Chem. Abstr.*, **1974**, *81*, 120023d.

31. von Kutepow, N.; Müller, F.-J.; *Chem. Abstr.*, **1974**, *81*, 135473z.

32. Imamoto, T.; Kusomoto, T.; Yokoyama, M.; *Bull. Chem. Soc. Jpn.*, **1982**, *55*, 643.

33. Paulik, F. E.; Hershman, A.; Knox, W. R.; Roth, J. F.; *Chem. Abstr.*, **1970**, *72*, 110807y.

34. Heck, R. F.; *J. Am. Chem. Soc.*, **1963**, *85*, 2013.

35. Hagemeyer, H. J.; *Chem. Abstr.*, **1956**, *50*, 16835d.

36. Naglieri, A. N.; Rizkalla, N.; *Chem. Abstr.*, **1978**, *89*, 42469c.

37. Fujimoto, K.; Shikada, T.; Omata, K.; Tominaga, H.; *Ind. Eng. Chem., Prod. Res. Dev.*, **1982**, *21*, 429.

38. Ritzkalla, N.; *Industrial chemicals via C1 processes*, Am. Chem. Soc., **1987**, 61.

39. *US Patent* to Eastman, **1979**, 4133963.

40. *European Chemical News*, 26 May-1 June **1997**.

41. Moser, W. R.; Marshik-Guerts, B. J.; Okrasinski, S. J.; *J. Mol. Catal. A: Chem.,* **1999**, *143*, 57.

42. Moser, W. R.; Marshik-Guerts, B. J.; Okrasinski, S. J.; *J. Mol. Catal. A: Chem.*, **1999**, *143*, 71.

43. Forster, D.; *J. Am. Chem. Soc.*, **1976**, *98*, 846.

44. Gates, B. C.; *Catalytic Chemistry*; Wiley: New York **1992**.

45. Koga, N.; Morokuma, K.; *J. Am. Chem. Soc.*, **1993**, *115*, 6883.

46. Sakaki, S.; Ujino, Y.; Sugimoto, M.; *Bull. Chem. Soc. Jpn.*, **1996**, *69*, 3047.

47. Sakaki, S.; Ieki, M.; *J. Am. Chem. Soc.,* **1993**, *115*, 2373.

48. Albert, K.; Gisdakis, P.; Rösch, N.; *Organometallics*, **1998**, *17*, 1608.

49. Matsubara, T.; Koga, N.; Ding, Y.; Musaev, D. G.; Morokuma, K.; *Organometallics*, **1997**, *16*, 1065.

50. Dedieu, A.; *Inorg. Chem.*, **1980**, *19*, 375.

51. Margl, P.; Ziegler, T.; Blöchl, P. E.; *J. Am. Chem. Soc.*, **1996**, *118*, 5412.

52. Haynes, A.; Mann, B. E.; Morris, G. E. Maitlis, P. M.; *J. Am. Chem. Soc.*, **1993**, *115*, 4093.

53. Bassetti, M.; Monti, D.; Haynes, A.; Pearson, J. M.; Stanbridge, I. A.; Maitlis, P. M.; *Gaz. Chim. Ital.*, **1992**, *122*, 391.

54. Adamson, G. W.; Daly, J. J.; Forster, D.; *J. Organomet. Chem.*, **1974**, *71*, C17.

55. Adams, H.; Bailey, N. A.; Mann, B. E.; Manuel, C. P.; Spencer, C. M.; Kent, A. G.; *J. Chem. Soc., Dalton Trans.*, **1988**, 489.

56. Howe, L. A.; Bunel, E. E.; *Polyhedron*, **1995**, *14*, 167.

57. Roth, J. F.; Craddock, J. H.; Hershman, A.; Paulik, F. E.; *Chem. Technol.*, **1971**, 600.

58. Forster, D.; Dekleva, T. W.; *J. Chem. Edu.*, **1986**, 63 (3), 204.

59. Watson, D. J.; *Catalysis of Organic reactions*, Marcel Dekker, New York, **1998**, p. 369.

60. Schultz, R. G.; Montgromerry, P. D.; *J. Catal.*, **1969**, *13*, 105.

61. Krzywicki, A.; Marczewski, M.; *J. Mol. Catal.*, **1979**, *6*, 431.

62. Scurrell, M. S.; Howe, R. F.; *J. Mol. Catal.*, **1980**, *7*, 535.

63. *US Patent* to Hoechst, **1987**, 4657884.

64. *US Patent* to Hoechst, **1988**, 4776987.

65. Drago, R. S.; Nyberg, E. D.; Amma, A. E.; Zombeck, A.; *Inorg. Chem.*, **1981**, *20*, 641.

66. Jarrel, M. S.; Gates, B. C.; *J. Catal.*, **1975**, *40*, 255.

67. Hjortkjaer, J.; Chen, Y.; Heinrich, B.; *Appl. Catal.*, **1991**, *67*, 269.

68. *European Patent* to Reilly, **1988**, 277824.

69. *US Patent* to Chiyoda, **1994**, 5334755.

70. *US Patent* to Chiyoda, **1994**, 5364963.

71. *US Patent* to Chiyoda, **1996**, 5576458.

72. Yoneda, N.; Minami, T.; Weiszmann, J.; Spehlmann, B.; *Science and Technology in Catalysis*, Proceedings of the Third Tokyo Conference on Advanced Catalytic Science and Technology, **1998**, p. 93.

73. Murphy, M. A.; Smith, B. L.; Torrence, G. P.; Agulio, A.; *J. Organomet. Chem.*, **1986**, *303*, 257.

74. Smith, B. L.; Torrence, G. P.; Murphy, M. A.; Agulio, A.; *J. Mol. Catal.*, **1987**, *39*, 115.

75. *Japanese Patent Koukoku* to Daicel, **1992**, 04-69136.

76. *Japanese Patent Koukoku* to Daicel, **1995**, 07-23337.

77. *Japanese Patent Koukai* to Poulenc, **1994**, 06-340573.

78. Vercauteren, C. J. E.; Clode, K. E.; Watson, D. J.; *European Patent*, **1994**, 616,997.

79. Maitlis, P. M.; Haynes, A.; Sunley, G. J.; Howard, M. J.; *J. Chem. Soc., Dalton Trans.*, **1996**, 2187.

80. Baker, M. J.; Giles, M. F.; Garland, C. S.; Rafeletos, G.; *European Patent*, **1995**, 749,948.

81. Sunley, J. G.; Giles, M. F.; Garland, C. S.; *European Patent*, **1994**, 643,034.

82. Garland, C. S.; Giles, M. F.; Poole, A. D.; Sunley, J. G.; *European Patent*, **1994**, 728,726.

83. Singleton, T. C.; Urry, W. H.; Paulik, F. E.; *European Patent*, **1982**, 55,618.

84. Paulik, F. E.; Hershman, A.; Knox, W. R.; Shultz, R. G.; Roth, J. F.; *U.S. Patent*, **1988**, 5,003,104.

85. Smith, B. L.; Torrence, G. P.; Aguilo, A.; Adler, J. S.; *U.S. Patent*, **1992**, 5,144,068.

86. Koyama, H.; Kojima, H.; *Bristish Patent*, **1987**, 2,146,637.

87. Watson, D. J.; *Proc. 17th Conf. Catal. Org. React.*, ORCS, New Orleans, 29th March-2nd april, **1998**, Marcel Dekker, New York.

88. Eby, R. T.; Singleton, T. C.; *Applied Industrial Catalysis*, Academic Press, London, **1983**, *1*, p. 275.

89. Sunley, J. G.; Ditzel, E. J.; Watt, R. J.; *European Patent*, **1998**, 849,248.

90. Baker, M. J.; Giles, M. F.; Garland, C. S.; Muskett, M. J.; *European Patent*, **1997**, 752,406.

91. Collman, J. P.; Hegedus, L. S.; Norton, J. R.; Finke, R. G.; *Principles and Applications of Organotransition Metal Chemistry*; University Science Books: Mill Valley, CA, **1987**.

92. Robinson, K. K.; Hershman, A.; Craddock, J. H.; Roth, J. F.; *J. Mol. Catal.*, **1972**, *27*, 389.

93. Dilworth, J. R.; Miller, J. R.; Wheatley, N.; Baker, M. J.; Sunley, J. G.; *J. Chem. Soc., Chem. Commun.*, **1995**, 1579.

94. Ghaffar, T.; Adams, H.; Maitlis, P. M.; Haynes, A.; Sunley, G. J.; Baker, M. J.; *Chem. Commun.*, **1998**, 1359.

95. Wegman, R. W.; Abatjoglou, A. G.; Harrison, A. M.; *J. Chem. Soc., Chem.Commun.*, **1987**, 1891 and references therein.

96. Moloy, K. G.; Wegman, R. W.; *Organometallics*, **1989**, *8*, 2883.

97. Rankin, J.; Poole, A. D.; Benyei, A. C.; Cole-Hamilton, D. J.; *Chem. Commun.*, **1997**, 1835.

98. Rankin, J.; Benyei, A. C.; Poole, A. D.; Cole-Hamilton, D. J.; *J. Chem. Soc., Dalton Trans.*, **1999**, 3771.

99. Yang, J.; Haynes, A.; Maitlis, P. M.; *Chem. Commun.*, **1999**, 179.

100. Gonsalvi, L.; Adams, H.; Sunley, G. J.; Ditzel, E.; Haynes, A.; *J. Am. Chem. Soc.*, **1999**, *121*, 11233.

101. Katti, K. V.; Santarsiero, B. D.; Pinkerton, A. A.; Cavell, R. G.; *Inorg. Chem.*, **1993**, *32*, 5919.

102. Baker, M. J.; Giles, M. F.; Orpen, A. G.; Taylor, M. J.; Watt, R. J.; *J. Chem. Soc., Chem. Commun.*, **1995**, 197.

103. Schenck, T. G.; Milne, C. R. C.; Sawyer, J. F.; Bosnich, B.; *Inorg. Chem.*, **1985**, *24*, 2338.

104. Lamprecht, G. J.; Van Zyl, G. J.; Leipoldt, J. G.; *Inorg. Chim. Acta*, **1989**, *164*, 69.

105. Menu, M. J.; Desrosiers, P.; Darguenave, M.; Darguenave, Y.; *Organometallics*, **1987**, *6*, 1822.

106. Douek, I. C.; Wilkinson, G.; *J. Chem. Soc. A*, **1969**, 2604.

107. Blagborough, T. C.; Davis, R.; Ivison, I.; *J. Organomet. Chem.*, **1994**, *467*, 85.

108. Bader, A.; Lindner, E.; *Coord. Chem. Rev.*, **1991**, *108*, 27.

109. Fleming, I.; *Frontier Orbitals and Chemical Reactions*, Wiley, Chichester, **1976**.

110. Carraz, C.-A.; Ditzel, E. J.; Orpen, A. G.; Ellis, D. D.; Pringle, P. G.; Sunley, G. J.; *Chem. Commun.*, **2000**, 1277.

111. Casey, C. P.; Paulsen, E. L.; Beuttenmueller, E. W.; Proft, B. R.; Matter, B. A.; Powell, D. R.; *J. Am. Chem. Soc.*, **1999**, *121*, 63 and references therein.

112. Brunner, H.; Stumpf, A.; *J. Organomet. Chem.*, **1993**, *459*, 139.

113. Kapoor, P. N.; Pathak; D. D., Gaur, G.; Kutty, M.; *J. Organomet. Chem.*, **1984**, *276*, 167.

114. Howard, M. J.; Sunley, G. J.; Poole, A. D.; Watt, R. J.; Sharma, B. K.; *Stud. Surf. Sci. Catal.*, **1999**, *121*, 61.

115. Katritzky, A. R.; Lan, X.; Yang, J. Z.; Denisko, O. V.; *Chem. Rev.*, **1998**, *98*, 409.

116. Guilard, R.; Kadish, K. M.; *Chem. Rev.*, **1988**, *88*, 1121.

117. van Asselt, R.; Rijnberg, E.; Elsevier, C. J.; *Organometallics*, **1994**, *13*, 706.

118. Byers, P. K.; Canty, A. J.; Skelton, B. W.; White, A. H.; *J. Chem. Soc., Chem. Commun.*, **1986**, 1722.

119. de Graaf, W.; Boersma, J.; Smeets, W. J. J.; Spek, A. L.; van Koten, G. *Organometallics*, **1989**, *8*, 2907.

120. Canty, A. J.; *Acc. Chem. Res.*, **1992**, *25*, 83.

121. Brown, D. G.; Byers, P. K.; Canty, A. J.; *Organometallics*, **1990**, *9*, 1231.

122. (a) Dehand, J.; Pfeffer, M.; *Coord. Chem. Rev.*, **1976**, *18*, 327. (b) Bruce, M. I.; *Angew. Chem.*, **1977**, *89*, 75; *Angew. Chem. Int. Ed. Engl.*, **1977**, *16*, 73.

123. Evans, D. A.; Woerpel, K. A.; Hinman, M. M.; Faul, M. M.; *J. Am. Chem. Soc.*, **1991**, *113*, 726.

124. Corey, E. J.; Imai, N.; Zhang, H.-Y.; *J. Am. Chem. Soc.*, **1991**, *113*, 728.

125. Muller, D.; Umbricht, G.; Weber, B.; Pfaltz, A.; *Helv. Chim. Acta*, **1991**, *74*, 232.

126. Mazet, C.; Gade, L.; *Organometallics*, **2001**, *100*, 79.

127. (a) Britovsek, G. J. P.; Gibson, V. C.; Kimberley, B. S.; Maddox, P. J.; Mc Tavish, S. J.; Solan, G. A.; White, A. J. P.; Williams, D. J.; *Chem. Commun.*, **1998**, 849. (b) Small, B. L.; Brookhart, M.; Bennett, A. M. A.; *J. Am. Chem. Soc.*, **1998**, *120*, 4049.

128. Wang, C.; Ziller, J. W.; Flood, T. C.; *J. Am. Chem. Soc.*, **1995**, *117*, 1647.

129. Ghosh, C. K.; Graham, W. A. G.; *J. Am. Chem. Soc.*, **1987**, *109*, 4726.

130. Ghosh, C. K.; Graham, W. A. G.; *J. Am. Chem. Soc.*, **1989**, *111*, 375.

131. Bloyce, E.; Mascetti, J.; Rest, A. J.; *J. Organomet. Chem.*, **1993**, *444*, 223.

132. Purwoko, A. A.; Lees, A. J.; *Inorg. Chem.*, **1996**, *35*, 675.

133. Wang, L.; Flood, T. C.; *J. Am. Chem. Soc.*, **1992**, *114*, 3169.

134. Wang, L.; Lu, R. S.; Bau, R.; Flood, T. C.; *J. Am. Chem. Soc.*, **1993**, *115*, 6999.

135. Haarman, H. F.; Bregman, F. R.; van Leeuwen, P. W. N. M.; Vrieze, K.; *Organometallics*, **1997**, *16*, 979.

136. Crabtree, R.; *Acc. Chem. Res.*, **1979**, *12*, 331, and references therein.

137. Inoue, M.; Kubo, M.; *Coord. Chem. Rev.*, **1976**, *21*, 1.

138. Steel, J.; *Coord. Chem. Rev.*, **1990**, *106*, 227.

139. Constable, E. C; Harverson, P.; Oberholzer, M.; *Chem. Commun.*, **1996**, 1821.

140. Corey, E. J.; Imai, N.; Zhang, H.-Y.; *J. Am. Chem. Soc.*, **1991**, *113*, 728.

141. Muller, D.; Umbricht, G; Weber, B.; Pfaltz, A.; *Helv. Chim. Acta*, **1991**, *74*, 232.

142. van Asselt, R.; Rijnberg, E.; Elsevier, C. J.; *Organometallics*, **1994**, *13*, 706.

143. Byers, P. K.; Canty, A. J.; Skelton, B. W.; White, A. H.; *J. Chem. Soc., Chem. Commun.*, **1986**, 1722.

144. de Graaf, W.; Boersma, J.; Smeets, W. J. J.; Spek, A. L.; van Koten, G.; *Organometallics*, **1989**, *8*, 2907.

145. Canty, A. J.; *Acc. Chem. Res.*, **1992**, *25*, 83.

146. Brown, D. G.; Byers, P. K.; Canty, A. J.; *Organometallics*, **1990**, *9*, 1231.

147. Katritzky, A. R.; Rachwal, S.; Hitchings, G. J.; *Tetrahedron*, **1991**, *47*, 2683.

148. Katritzky, A. R.; *Bull. Soc. Chim. Belg.*, **1992**, *101*, 409.

149. Katritzky, A. R.; Yang, Z.; Cundy, D. J.; *Aldrichimica Acta*, **1994**, *27*, 31.

150. Katritzky, A. R.; Lan, X.; *Chem. Soc. Rev.*, **1994**, 363.

151. Katritzky, A. R.; Lan, X.; Fan, W.-Q.; *Synthesis*, **1994**, 445.

152. (a) Reedijk, J.; Roelofsen, G.; Siedle, A. R.; Spek, A. L.; *Inorg. Chem.*, **1979**, *18*, 1947. (b) Himes, V. L.; Mighell, A. D.; Siedle, A. R.; *J. Am. Chem. Soc.*, **1981**, *103*, 211. (c) Boyd, P. D. W.; Martin, R. L.; *J. Chem. Soc., Dalton Trans.*, **1981**, 1069. (d) Hendriks, H. M. J.; Birker, P. J. M. W. L.; Verschoor, G. C.; Reedijk, J.; *J. Chem. Soc., Dalton Trans.*, **1982**, 623. (e) Kokoszka, Baranowski, J.; Goldstein, C.; Orsini, J.; Mighell, A. D.; Himes, V. L.;

Siedle, A. R.; *J. Am. Chem. Soc.*, **1983**, *105*, 5627. (f) Bencini, A.; Gatteschi, D.; Reedijk, J.; Zanchini, C.; *Inorg. Chem.*, **1985**, *24*, 207. (g) Handley, J.; Collison, D.; Garner, C. D.; Helliwell, M.; Docherty, R.; Lawson, J. R.; Tasker, P. A.; *Angew. Chem., Int. Ed. Engl.*, **1993**, *32*, 1036. (h) Murrie, M.; Collison, D.; Garner, C. D.; Helliwell, M.; Tasker, P.A.; Turner, S. S.; *Polyhedron*, **1998**, *17*, 3031. (i) Plakatouras, J. C.; Bakas, T.; Huffman, C. J.; Huffman, J. C.; Papaefthymiou, V.; Perlepes, S. P.*; J. Chem. Soc., Dalton Trans.*, **1994**, 2737. (j) Skorda, K.; Bakalbassis, E. G.; Mrozinski, J.; Perlepes, S. P.; Raptopoulou, C. P.; Terzis, A.; *J. Chem. Soc., Dalton Trans.*, **1995**, 2317. (k) Bakalbassis, E: G.; Diamantopoulou, E.; Perlepes, S. P.; Raptopoulou, C. P.; Tangoulis, V.; Terzis, A.; Zafiropoulos, Th. F.; *J. Chem. Soc., Chem. Commun.*, **1995**, 1347. (l) Tangoulis, V.; Raptopoulou, C. P.; Terzis, A.; Bakalbassis, E. G.; Diamantopoulou, E.; Perlepes, S. P.; *Inorg. Chem.*, **1998**, *37*, 3145.

153. Moore, D. S.; Robinson, S. D.; *Adv. Inorg. Chem.*, **1988**, *32*, 171.

154. Aleksandrov, G. G.; Babin, V. N.; Kharchenvikov, A. P.; Struchkov, Y. T.; Kochetkova, N. S.; *J. Organomet. Chem.*, **1984**, *266*, 109.

155. Mikolajczyk, M.; Kielbasinsky, P.; *Tetrahedron*, **1981**, *37*, 233.

156. Hassner, A.; Alexanian, V.; *Tetrahedron Letters*, **1978**, *19*, 4475.

157. Holmberg, K.; Hansen, B.; *Acta Chem. Scand.*, **1979**, *B33*, 410.

158. Boden, E. P.; Keck, G. E.; *J. Org. Chem.*, **1985**, *50*, 2394.

159. Rich, D. H.; Singh, J.; *Peptides*, **1979**, *1*, 241.

160. Scriven, E. F. V.; *Chem. Soc. Rev.*, **1983**, *12*, 129.

161. Katritzky, A. R.; Rachwal, S.; Caster, K. C.; Mahni, F.; Law, K. W., Rubio, O.; *J. Chem. Soc., Perkin Trans.*, **1987**, *1*, 781.

162. Katritzky, A. R.; Drewniak, M.; *Tetrahedron Letters*, **1988**, *29*, 1755.

163. de Silva, E. D.; Miao, S.; Andersen, R. J.; Schultz, L. W.; Clardy, J.; *Tetrahedron Lett.*, **1992**, *33*, 2917.

164. Nakatsuji, Y.; Bradshaw, J. S.; Tse, P.-K.; Arena, G.; Wilson, B. E.; Dalley, N. K.; Izatt, R. M.; *Chem. Commun.*, **1985**, 749.

165. (a) Grossel, M. C.; Goldspink, M. R.; Hrijac, J. A.; Weston, S. C.; *Organometallics*, **1991**, *10*, 851. (b) Hall, D. C.; Danks, I. P.; Nyburg, S. C.; Parkins, A. W.; Sharpe, N. W.; *Organometallics*, **1990**, *9*, 1602. (c) Wang, J.-T.; Yuan, Y.-F; Xu, Y.-M.; Zhang, Y.-W.; Wang, R.-J.; Wang, H.-G. J.; *J. Organomet. Chem.*, **1994**, *481*, 211. (d) Seidelmann, O.; Beyer, L.; Richter, R.; *Z. Naturforsch.*, **1995**, *50B*, 1679. (e) Seidelmann, O.; Beyer, L.; Zdobinsky, G.; Kirmse, R.; Dietze, F.; Richter, R.; *Z. Anorg. Allg. Chem.*, **1996**, *622*, 692. (f) Wen, Z.; Li, F.-Z.; Liu, Q.-W.; Huang, X.-Y.; *Jiegou Hauxue*, **1995**, *14*, 108.

166. Butler, I. R.; Cullen, W. R.; Rettig, S. J.; Trotter, J.; *Acta Crystallogr.*, **1988**, *C44*, 1666.

167. Cotton, F. A.; Reid, A. H. Jr.; *Acta Crystallogr.*, **1985**, *C41*, 686.

168. Palenik, G. J.; *Inorg. Chem.*, **1969**, *8*, 2744.

169. Luo, Y.; Barton, R. J.; Robertson, B. E.; *Acta Crystallogr.*, **1990**, *C46*, 1388.

170. Podlaha, J.; Stepnicka, P.; Ludvik, J.; Cisarova, I.; *Organometallics*, **1996**, *15*, 543.

171. Kraatz, H.-B.; Lusztyk, J.; Enright, G. D.; *Inorg. Chem.*, **1997**, *36*, 2400.

172. Sokol, V. I.; Zefirov, Y. V.; Porai-Koshits, M. A.; *Sov. J. Coord. Chem.*, **1979**, *5*, 985.

173. Blonk, H. L.; Driessen, W. L.; Reedijk, J.; *J. Chem. Soc., Dalton Trans.*, **1985** 1699.

174. Tolman, W. B.; Liu, S.; Bentsen, J. G.; Lippard, S. J.; *J. Am. Chem. Soc.*, **1991**, *113*, 152.

175. Balch, A. L.; Tulyathan, B.; *Inorg. Chem.*, **1977**, *16*, 2840.

176. Blagborough, T.C; Davis, R.; Ivison, P.; *J. Organomet. Chem.*, **1994**, *467*, 85.

177. Balch, A. L.; Hope, H.; Wood, F. E.; *J. Am. Chem. Soc.*, **1985**, *107*, 6936.

178. Breit, B.; Winde, R.; Harms, K.; *J. Chem. Soc., Perkin Trans.*, **1997**, *1*, 2681.

179. Berger, S.; Braun, S., Kalinowski, H.-O.; *NMR-Spektroskopie von Nicht metallen*, Thieme, Stuttgart, **1993**, *vol. 3*, 164.

180. Breit, B.; *Eur. J. Org. Chem.*, **1998**, 1123.

181. Li Wu, M.; Desmond, M. J.; Drago, R. S.; *Inorg. Chem.*, **1979**, *18*, 679.

182. Dunbar, K. R.; Haefner, S. C.; *Inorg. Chem.*, **1992**, *31*, 3676.

183. Ceriotti, A.; Ciani, G.; Sironi, A.; *J. Organomet. Chem.*, **1983**, *247*, 345.

184. Tolman, C. A.; *Chem. Rev.*, **1977**, *77*, 313.

185. Fernandez, E.; Ruiz, A.; Claver, C.; Castillon, S.; Polo, A.; Piniella, J. F.; Alvarez-Larena, A.; *Organometallics*, **1998**, *17*, 2857.

186. Evans, D.; Osborn, J. A.; Wilkinson, G.; *Inorg. Synth.*, **1990**, *28*, 79.

187. Hughes, R. P.; in *Comprehensive Organometallic Chemistry* (Eds.: G. Wilkinson, F. G. A. Stone, E. W. Abel), Pergamon, Oxford, **1982**, Chapter 35, pp. 296ff.

188. Moloy, K. G.; Petersen, J. L.; *J. Am. Chem. Soc.*, **1995**, *117*, 7696.

189. Harlow, R. L.; Westcott, S. A.; Thorn, D. L.; Baker, R. T.; *Inorg. Chem.*, **1971**, *17*, 393.

190. Vastag, S.; Heil, B.; Marko, L.; *J. Mol. Catal.*, **1979**, *5*, 189.

191. Moloy, K. G.; Petersen, J. L.; *J. Am. Chem. Soc.*, **1995**, *117*, 7696.

192. de Montauzon, D.; Poilblanc, R.; *J. Organomet. Chem.*, **1975**, *93*, 397.

193. Franks, S.; Hartley, F. R.; *Inorg. Chim. Acta*, **1981**, *47*, 235.

194. Strohmeier, W.; Rehder-Strirnweiss, W.; Reishig, G.; *J. Organomet. Chem.*, **1971**, *17*, 393.

195. Clarke, M. L.; Cole-Hamilton, D. J.; Slawin, A. M. Z.; Woollins, J. D.; *Chem. Comm.*, **2000**, 2065.

196. Poulton, J. T.; Folting, K.; Streib, W. E.; Caulton, K. G.; *Inorg. Chem.*, **1992**, *31*, 3190.

197. Adamson, G. W.; Daly, J. J.; Forster, D.; *J. Organomet. Chem.,* **1974**, *71*, C-17.

198. Dilworth, J. R.; Morales, D.; Zheng, Y.; *J. Chem. Soc., Dalton. Trans.*, **2000**, 3007.

199. Adams, H.; Bailey, N. A.; Mann, B. E.; Manuel, C. P.; Spencer, C. M.; Kent, A. G.; *J. Chem. Soc.*, *Dalton Trans.*, **1988**, 489.

200. (a) Wasson, J. R.; Woltermann, G. M.; Stoklosa, H. J.; *Fortschr. Chem. Forsch.* (*Top. Curr. Chem.*), **1973**, *35*, 65. (b) LeSuer, W. M.; Dunn, H. J.; *Chem. Abstr.*, **1975**, *82*, 155758v. (c) LeSuer, W. M.; Dunn, H. J.; *Chem. Abstr.*, **1975**, *83*, 205973e. (d) LeSuer, W. M.; Dunn, H. J.; *Chem. Abstr.*, **1975**, *82*, 124652b.

201. (a) Kuchen, W.; Hertel, H.; *Angew. Chem. Int. Ed. Engl.*, **1969**, *8*, 89. (b) Haiduc, I.; Sowerby, D. B.; Lu, S.-F.; *Polyhedron*, **1995**, *14*, 3389. (c) Haiduc, I.; Sowerby, D. B.; Lu, S.-F.; *Polyhedron*, **1996**, *15*, 2469.

202. (a) Harrison, P. G.; Begley, M. J., Kikabhai, T.; Killer, F.; *J. Chem. Soc., Dalton Trans.*, **1986**, 925. (b) Lin, Y.; *Lubr. Eng.*, **1995**, *51(10)*, 855. (c) Burn, A. J.; Gosney, I.; Warrens, C. P.; Wastle, J. P.; *J. Chem. Soc., Perkin Trans.*, **1995**, 2, 265. (d) Yamaguchi, E. S.; Ryason, P. R.; *Tribo Test*, **1996**, *3(2)*, 123. (e) Contarini, S.; Tripaldi, G.; Ponti, G.; Lizzit, S.; Baraldi, A.; Paolucci, G.; *Appl. Surf. Sci.*, **1997**, *108(3)*, 359. (f) Chen, B.; Song, J.; Ye, Y.; Dong, J.; *Tribologia*, **1998**, *29(2)*, 207.

203. Mehrotra, R. C.; Srivastava, G.; Chauhan, B. P. S.; *Coord. Chem. Rev.*, **1984**, *55*, 207.

204. (a) Malatesta, L.; Pizzotti, R.; *Chim. Ind.*, **1945**, *27*, 6. (b) Malatesta, L.; Pizzotti, R.; *Chim. Ind.*, **1946**, *76*, 167. (c) Shetty, P. S.; Jose, P.; Fernando, Q.; *J. Chem. Soc., Commun.*, **1968**, 788. (d) Hartung, H.; *Z. Chem.*, **1967**, *7*, 241. (e) Fackler, J. P. Jr.; Thompson, L. D. Jr.; *Inorg. Chim. Acta*, **1981**, *48*, 45.

205. Kalck, P.; Frances, J.-M.; Pfister, P.-M.; Southern, T. G.; Thorez, A.; *J. Chem. Soc., Chem. Commun.*, **1983**, 510.

206. (a) Claver, C.; Kalck, P.; Ridmy, M.; Thorez, A.; Oro, L. A.; Pinillos, M. T.; Apreda, M. C.; Cano, F. H.; Foces-Foces, C.; *J. Chem. Soc., Dalton Trans.*, **1988**, 1523. (b) Cruz-Garritz, D.; Rodriguez, B.; Torrens, H.; Leal, J.; *Transition Met. Chem.*, **1984**, *9*, 284. (c) Catala, R. M.; Cruz-Garritz, D.; Hills, A.; Hughes, D. L.; Richards, R. L.; Sosa, P.; Terreros, P.; Torrens, H.; *J.*

Organomet. Chem., **1989**, *359*, 219. (d) Claver, C.; Masdeu, A. M.; Ruiz, N.; Foces-Foces, C.; Cano, F. H.; Apreda, M. C.; Oro, L. A.; Garcia-Alejandre, J.; Torrens, H.; *J. Organomet. Chem.*, **1990**, *398*, 177. (e) Bayon, J. C.; Esteban, P.; Real, J.; Claver, C.; Ruiz, A.; *J. Chem. Soc., Chem. Commun.*, **1989**, 1056. (f) Polo, A.; Claver, C.; Castillón, S.; Ruiz, A.; Baýon, J. C.; Real, J.; Mealli, C.; Masi, D.; *Organometallics*, **1992**, *11*, 3525. (g) Polo, A.; Fernandez, E.; Claver, C.; Castillón, S.; J. Chem. Soc., *Chem. Commun.*, **1992**, 639.

207. El Amene, M.; Maisonnat, A.; Dahan, F.; Poilblanc, R.; *Nouv. J. Chim.*, **1991**, *12*, 661.

208. Cheng, C.-H.; Eisenberg, R.; *Inorg. Chem.*, **1979**, *18*, 1418.

209. Dilworth, J. R.; Wheatley, N.; *Coord. Chem. Rev.*, **2000**, *199*, 89.

210. Lee, H.-S.; Bae, J.-Y.; Kim, D.-H.; Kim, H. S.; Kim, S.-J.; Cho, S.; Ko, J.; Kang, S. O.; *Organometallics*, **2002**, *21*, 210.

211. Kennosuke, I.; Shukichi, N.; Itaru, O.; Nippon Chemical Industrial Co., Ltd. Japan, **1974**, *245*, 7417.

212. Martin, S. F.; Wagman, A. S.; Zipp, G. G.; Gratchev, M. K.; *J. Org. Chem.*, **1994**, *59*, 7957.

213. Carmalt, C. J.; Clyburne, J. A. C.; Cowley, A. H.; Lomeli, V.; McBurnett, B. G.; *Chem. Commun.*, **1998**, 243.

214. StJ. Foreman, M. R.; Slawin, A. M. Z.; Woollins, J. D.; *J. Chem. Soc., Dalton Trans.*, **1996**, 3653.

215. Aragoni, M. C.; Arca, M.; Demartin, F.; Devillanova, F. A.; Graiff, C.; Isaia, F.; Lippolis, V.; Tiripicchio, A.; Verani, G.; *Eur. J. Inorg. Chem.*, **2000**, 2239.

216. Cotton, F. A.; McCleverty, J. A.; *Inorg. Chem.*, **1964**, *3*, 1398.

217. O'Connor, C.; Gilbert, J. D.; Wilkinson, G.; *J. Chem. Soc. A*, **1969**, 84.

218. Cabeza, J. A.; Riera, V.; Villa-Garcia, M. A.; *J. Organomet. Chem.*, **1992**, *441*, 323.

219. Wood, P. T.; Woolins, J. D.; *Transition Met. Chem.*, **1987**, *12*, 403.

220. Issleib, V. K.; Hohlfeld, G.; *Z. Anorg. Allg. Chem.*, **1961**, *312*, 169.

221. DeStefano, N. J.; Johnson, D. K.; Lane, R. M.; Venanzi, L. M.; *Helv. Chim. Acta*, **1976**, *59 (8)*, 2674.

222. Kapoor, P. N.; Venanzi, L. M.; *Helv. Chim. Acta*, **1977**, *60 (277)*, 2824.

223. Hirschfeld, F. L.; Sandler, S.; Schmidt, G. M.; *J. Chem. Soc.*, **1963**, 2108.

224. Hirschfeld, F. L.; *J. Chem. Soc.*, **1963**, 2126.

225. Marty, W.; Kapoor, P. N.; Buergi, H.-B.; Fischer, E.; *Helv. Chim. Acta*, **1987**, *70*, 158.

226. Wieser, C.; Matt, D.; Fischer, J.; Harriman, A.; *J. Chem. Soc., Dalton Trans.*, **1997**, 2391.

227. Wieser-Jeunesse, C.; Matt, D.; De Cian, A.; *Angew. Chem., Int. Ed. Engl.*, **1998**, *37 (20)*, 2861.

228. Armspach, D.; Matt, D.; *Chem. Commun.*, **1999**, 1073.

229. Pryde, A. J.; Shaw, B. L.; Weeks, B.; *J. Chem. Soc., Chem. Commun.*, **1973**, 947.

230. Shaw, B. L.; *J. Am. Chem. Soc.*, **1995**, *97*, 3856.

231. March, F. C.; Mason, R.; Thomas, K. M.; Shaw, B. L.; *J. Chem. Soc., Chem. Commun.*, **1975**, 584.

232. Al-Salem, N. A.; Empsall, H. D.; Markham, R.; Shaw, B. L.; Weeks, B.; *J. Chem. Soc., Dalton Trans.*, **1979**, 1972.

233. Hill, W. E.; Minahan, D. M. A.; Taylor, J. G.; McAuliffe, C. A.; *J. Am. Chem. Soc.*, **1982**, *104*, 6001.

234. Parish, R. V.; Razzoki, S. M.; *Inorg. Chim. Acta*, **1985**, *96*, 49.

235. (A) Pignolet, L. M.; *Homogeneous Catalysis with Metal Phosphine Complexes*; Perseus Books: Cambridge, 1983. (b) McAuliffe, C. A.; *Transition Metal Complexes of Phosphorus*, Arsenic and Antimony Ligands; Wiley: New York, 1973. (c) Catalytic Aspects of Metal Phosphine Complexes; Alyea, E. C.; Meek, D. W. Eds.; ACS Advances in Chemistry Series 196; American Chemical Society: Washington, DC, 1982. (d) McAuliffe, C. A.; Levason, W.; Phosphine, Arsine, and Stibine Complexes of the Transition Elements; Elsevier Science: New York, 1978. (e) Tolman, C. A.; *Chem. Rev.*, **1977**, *77*, 313.

236. Hoots, J. E.; Rauchfuss, T. B.; Wrobleski, D. A.; *Inorg. Syn.*, **1982**, *21*, 178.

237. (a) Trost, B. M.; Van Vranken, D. L.; *Angew. Chem. Int. Ed. Engl.*, **1992**, *31*, 228. (b) Hassner, A.; Krepski, L.; Alexanian, V.; *Tetrahedron*, **1978**, *34*, 2069. (c) Hassner, A.; Alexanian, V.; *Tetrahedron Lett.*, **1978**, *46*, 4475. (d) Scriven, E. F. V.; *Chem. Soc. Rev.*, **1983**, *12*, 129. (e) Thomas, C. M.; Neels, A.; Stoeckli-Evans, H.; Süss-Fink, G.; *Eur. J. Inorg. Chem.*, **2001**, *12*, 3005.

238. Hill, W. E.; Minahan, D. M. A.; Taylor, J. G.; McAuliffe, C. A.; *J. Am. Chem. Soc.*, **1982**, *104*, 6001.

239. Pryde, A. J.; Shaw, B. L.; Weeks, B. J.; *J. Chem. Soc., Dalton Trans.*, **1976**, 322.

240. Sanger, A. R.; Tan, K. G.; *Inorg. Chim. Acta*, **1978**, *31*, L439.

241. Brunie, S.; Mazan, J.; Langlois, N.; Kagan, H. B.; *J. Organomet. Chem.*, **1976**, *114*, 225.

242. Bianchini, C.; Farnetti, E.; Glendenning, L.; Graziani, M.; Nardin, G.; Peruzzini, M.; Rocchini, E.; Zanobini, F.; *Organometallics*, **1995**, *3*, 1489.

243. (a) van den Beuken, E. K.; Meetsma, A.; Kooijman, H.; Spek, A. L.; Feringa, B. L.; *Inorg. Chim. Acta*, **1997**, *264*, 171. (b) Bürgi , H.-B.; Murray-Rust, J.; Camalli, M.; Caruso, F.; Venanzi, L. M.; *Helv. Chim. Acta*, **1989**, *72*, 1293, and references therein. (c) Bauer, E. B.; Ruwwe, J.; Martín-Alvarez, J. M.; Peters, T. B.; Bohling, J. C.; Hampel, F. A.; Szafert, S.; Liz, T.; Gladysz, J. A.; *Chem. Commun.*, **2000**, 2261. (d) Arena, C. G.; Drommi, D.; Faraone, F.; Graiff, C.; Tiripicchio, A.; *Eur. J. Inorg. Chem.*, **2001**, 247. (e) Armstrong, S. K.; Cross, R. J.; Farrugia, L. J.; Nichols, D. A.; Perry, A.; *Eur. J. Inorg. Chem.*, **2002**, 141.

244. Casey, C. P.; Paulsen, E. L.; Beuttenmueller, E. W.; Proft, B. R.; Matter, B. A.; Powell, D. R.; *J. Am. Chem. Soc.*, **1999**, *121*, 63 and references therein.

245. Cheng, C.-H.; Eisenberg, R.; *Inorg. Chem.*, **1979**, *18*, 1418.

246. Heras, J. V.; Pinilla, E.; Ovejero, P.; *J. Organomet. Chem.*, **1987**, *332*, 213.

247. Stahl, E.; *Dünnschichtchromatographie. Ein Laboratoriumshandbuch*, 2. Aufl., Springer, Berlin, **1967**.

248. Merck; *Mitteilungen zur Dünnschichtchromatographie*, **1985**.

249. Perrin, D. D.; Armarego, W. L. F.; *Purification of Laboratory Chemicals*, Pergamon Press, Oxford, **1988**.

250. Herde, J. L.; Lambert, J. C.; Senoff, C. V.; *Inorg. Synth.*, **1974**, *15*, 18.

251. McCleverty, J. A.; Wilkinson, G.; *Inorg. Synth.*, **1966**, *8*, 211.

252. Chatt, J.; Venanzi, L. M.; *J. Chem. Soc.*, **1957**, 3178.

253. Criegee, R.; Schröder, G.; *Liebigs Ann. Chem.*, **1951**, *623*, 1.

254. Stoe & Cie. *IPDS Software*. Stoe & Cie GmbH, Darmstadt, Germany, **2000**.

255. Sheldrick, G. M.; "SHELXS-97 Program for Crystal Structure Determination", *Acta Cryst.*, **1990**, *A46*, 467.

256. Sheldrick, G. M.; "SHELXL-97", Universität Göttingen, Göttingen, Germany, **1999**.

257. Spek, A. L.; "PLATON/PLUTON version Jan. 1999", *Acta Cryst.*, **1999**, *A46***,** C34.

La science est obscure - peut-être parce que la vérité est sombre.
Victor Hugo (*Faits et croyances*)

Une civilisation sans la Science, ce serait aussi absurde
qu'un poisson sans bicyclette.
Pierre Desproges (*Vivons heureux en attendant la mort*)